UNIVERSIDADE D
COIMBRA

João Pedro da Silva Pereira

Study and development of evaporators for residential-scale cogeneration systems based on organic Rankine cycles

Doctoral Thesis in Sustainable Energy Systems, supervised by Professor José Manuel Baranda Moreira da Silva Ribeiro and Professor Jorge Campos da Silva André, submitted to the Department of Mechanical Engineering, Faculty of Sciences and Technology of the University of Coimbra.

December 2021

João Pedro da Silva Pereira

Study and development of evaporators for residential-scale cogeneration systems based on organic *Rankine* cycles

Doctoral Thesis in Sustainable Energy Systems, supervised by Professor José Manuel Baranda Moreira da Silva Ribeiro and Professor Jorge Campos da Silva André, submitted to the Department of Mechanical Engineering, Faculty of Sciences and Technology of the University of Coimbra.

December 2021

UNIVERSIDADE D
COIMBRA

“Out of clutter, find simplicity.

From discord, find harmony.

In the middle of difficulty lies opportunity.”

Albert Einstein

Abstract

The environmental awareness and energy sustainability concerns have reached an unprecedented level of importance that is leading to, among other things, continuous improvements in the traditional methods of energy conversion. One of those improvements involves the use of micro-scale CHP (combined heat and power production) systems for residential applications since the potential in terms of primary energy savings and greenhouse gases reductions is enormous. Among the different technologies available for micro-CHP systems, Organic Rankine Cycles (ORC) seem the most suitable and promising option due to its simplicity and ability to retrofit current heating systems used in residential dwellings.

Therefore, this work starts by reviewing the use of ORC for micro-CHP applications considering the intrinsic requirements of the residential sector. One of those requirements is the ability to face highly variable thermal demand loads for which a short response time is necessary. Hence, the way how manufacturers and research centres are dealing with this key requirement is analysed in-depth. One of the findings is that the referred requirement is essentially dependent on the ORC-evaporator design and how the primary energy reaches the power cycle, while the remaining ORC main components (expander, pump, and condenser) play a minor role in that ability.

Being the evaporator a crucial component of the ORC based micro-CHP systems attempting to retrofit the current combi-boilers, the recommended design principles for its development are discussed. From those principles, among which is the need for organic fluid direct vaporization, emerged a hybrid (topping/bottoming) CHP configuration in which the thermal energy is produced stepwise: firstly, in the ORC-condenser and then in a post-heater, that is integrated on the ORC-evaporator, directly with the combustion gases. A physical model of this configuration was developed to determine the fraction of the CHP water heating process performed in the post-heater that maximizes the primary energy savings and ORC net power output for a wide range of CHP operating conditions. When compared to a standard CHP configuration, this solution shows benefits for the greater part of those conditions. This configuration has an additional positive side effect: the decrease of the combustion gases' temperature before they reach the organic fluid heat-exchanger section in the ORC-evaporator that, in turn, leads to a reduction of the risk of thermal degradation.

The evaluation of the risk that direct vaporization, even considering the use of this hybrid CHP configuration, strains to the organic fluid thermal degradation needs to be investigated. Limits to the fluid bulk temperatures are well known and easily controllable. Nevertheless, the relevance of the thermal boundary layer and the temperature of the heat transfer surfaces over the thermal degradation must be considered and analysed in-depth because of the significant temperature differences between the combustion gases and the organic fluid. As its experimental measure is

extremely difficult to accomplish, such determination requires the development of a detailed model of the combustion and heat transfer processes that occur in the ORC-evaporator.

The development, calibration, and validation of such a model are thoroughly described and presented. This allows a detailed evaluation of several key features of the combustion and heat transfer processes as a function of some ORC operating parameters. Among those features is the temperature of the internal surface of the tubes with which the organic fluid is in contact. This temperature, which can be used to assess the risk of thermal degradation, has proved to be highly affected by the thermal resistances and by the combustion gases temperature. Therefore, to avoid that risk, and besides the adoption of solutions like the hybrid CHP configuration to reduce the combustion gases' temperature, the operating conditions of the ORC should also be those allowing the vaporization process to start as early as possible and reducing the superheating phase to the minimum as possible.

The first insight into the effect of the heat transfer surfaces' temperature in contact with the organic fluid over its chemical integrity is also investigated. This is achieved by coupling a detailed comprehensive characterization of the system operating conditions, which comprise the determination of the heat transfer surface' temperatures (retrieved by the evaporator model), with the realization of dynamic thermal stress tests that include the experimental evaluation of the organic fluid thermal degradation. The operating conditions defined in this work lead to heat transfer surface temperatures well above the threshold found in the literature. The absence of thermal degradation in that situation may be seen as an indication that the literature threshold should not be used to impose upper bounds to the evaporator heat transfer surface temperature and that time (and not only temperature) has a significant effect on the thermal degradation of the organic fluid in real systems.

Additionally, an extensive and updated review of the most relevant works regarding thermal degradation of organic fluids is offered. From this review, a framework was developed to classify them according to the thermal stress test, the degradation evaluation method, and the determination of a limiting temperature. The output of that classification is presented together with the thermal degradation temperature value as they are related.

Keywords: Residential CHP systems; Organic Rankine cycles; ORC-evaporator,
Direct vaporization; Thermal degradation assessment.

Resumo

A consciência ambiental e as preocupações com a sustentabilidade energética atingiram uma importância sem precedentes que promove, entre outros aspetos, melhorias constantes nos métodos tradicionais de conversão de energia. Uma dessas melhorias envolve o uso de sistemas de cogeração (produção combinada de energia térmica e elétrica) em aplicações residenciais, uma vez que o potencial em termos de poupança de energia primária e diminuição das emissões de gases de efeito estufa é significativo. Entre as diferentes tecnologias disponíveis, os Ciclos Orgânicos de Rankine (ORC) destacam-se como a opção mais adequada e promissora devido à sua simplicidade e capacidade de se adequar às condições exigidas pelos sistemas residenciais.

Assim sendo, este trabalho inicia-se com a avaliação do uso da tecnologia ORC em aplicações de cogeração residenciais, tendo em consideração os requisitos intrínsecos do setor. Um desses requisitos é a capacidade de enfrentar cargas térmicas altamente variáveis para as quais é necessário um tempo de resposta reduzido. Posto isto, a forma como os fabricantes e os centros de investigação estão a lidar com essa questão é analisada em detalhe. Um dos resultados dessa análise é que esse requisito é, essencialmente, dependente do projeto do evaporador e de como a energia primária chega ao ciclo de potência, sendo que os restantes componentes principais do ORC (expansor, bomba e condensador) desempenham um papel secundário nesta tarefa.

Sendo o evaporador um componente crucial para os sistemas residenciais de cogeração baseados na tecnologia ORC, os requisitos de projeto recomendados para o seu desenvolvimento são analisados. Desses requisitos, entre os quais está a necessidade de realizar uma vaporização direta do fluido orgânico, surge uma configuração híbrida (topping/bottoming) na qual a energia térmica é produzida sequencialmente: primeiro no condensador e depois num pós-aquecedor, integrado no evaporador, diretamente com os gases de combustão. Foi desenvolvido um modelo exploratório dessa configuração para determinar qual a fração de água aquecida no pós-aquecedor, que maximiza a poupança de energia primária e a produção de energia elétrica para uma alargada gama de condições de funcionamento. Quando comparada com uma configuração padrão, esta solução apresenta benefícios para a generalidade dessas condições. Para além desses benefícios, esta solução apresenta um efeito colateral positivo: uma diminuição da temperatura dos gases de combustão antes que eles entrem em contacto com o permutador de calor do ciclo orgânico e, desta forma, reduzir do risco de ocorrer uma degradação térmica do fluido de trabalho.

Mesmo considerando a utilização da referida configuração híbrida, a avaliação do risco que a vaporização direta coloca na degradação térmica do fluido orgânico precisa de ser investigada. Os limites para as temperaturas médias do fluido de trabalho são bem caracterizados quanto à degradação térmica do fluido de trabalho e facilmente controláveis experimentalmente. No entanto,

a importância da camada limite térmica, e das temperaturas das superfícies de transferência de calor, sobre a degradação térmica deve também ser considerada e analisada em detalhe, devido às diferenças significativas de temperatura entre os gases de combustão e o fluido orgânico. Como a avaliação experimental dessas temperaturas de superfície é extremamente difícil de realizar, tal determinação exige o desenvolvimento de um modelo matemático detalhado sobre os processos de combustão e transferência de calor que ocorrem no evaporador.

O desenvolvimento, as calibrações e validações do referido modelo são, cuidadosamente, descritos e apresentados. O modelo permite realizar uma avaliação detalhada de vários fatores dos processos de combustão e transferência de calor em função de alguns parâmetros operacionais. Dentro desses parâmetros encontra-se a temperatura da superfície interna dos tubos com os quais o fluido orgânico está em contato. Essa temperatura, que pode ser utilizada para avaliar o risco de degradação térmica, é altamente afetada pelas resistências térmicas e pela temperatura dos gases de combustão. Portanto, de forma a reduzir esse risco, e para além da adoção de soluções como a configuração híbrida para reduzir a temperatura dos gases de combustão, as condições de operação do sistema devem ser aquelas que permitam que o processo de vaporização inicie o mais cedo possível e que a fase de sobreaquecimento seja reduzida ao mínimo possível.

O primeiro insight sobre o efeito da temperatura das superfícies de transferência de calor em contato com o fluido orgânico sobre a sua integridade química é também investigado. Isso é conseguido através da combinação de uma caracterização detalhada das condições de operação do sistema, que compreende a determinação das temperaturas da superfície de transferência de calor (calculadas através do modelo desenvolvido para o evaporador), com a realização de ensaios dinâmicos de stress térmico que incluem a avaliação experimental da degradação térmica do fluido orgânico. As condições de operação definidas neste trabalho levam a temperatura das superfícies de transferência de calor a atingirem valores bastante superiores aos limites encontrados na literatura. A ausência de degradação térmica nessa situação pode ser vista como uma indicação de que o valor limite apresentado na literatura não deve ser usado para impor barreiras à temperatura da superfície de transferência de calor do evaporador e que o tempo (e não apenas a temperatura) tem um efeito significativo na degradação térmica do fluido orgânico em sistemas reais.

Para além disso, é apresentada uma revisão extensa dos trabalhos mais relevantes relativos à degradação térmica de fluidos orgânicos. A partir desta revisão, foi desenvolvida uma estrutura de classificação de acordo com o tipo de ensaios de stress térmico, com a método de avaliação e com a determinação da temperatura limite. O resultado desta classificação é apresentado juntamente com o valor da temperatura de degradação térmica, uma vez que estes estão relacionados.

Palavras-chave: Sistemas de cogeração residenciais; Ciclos orgânicos de *Rankine*; Evaporador; Vaporização direta; Avaliação da degradação térmica.

Acknowledgements

I would like to express my utmost gratitude to all of those who, in some way, contributed to materializing this PhD thesis.

First of all, I would like to thank my supervisors, Prof. José Baranda Ribeiro and Prof. Jorge Campos André, for their contributions to this research work. Besides my supervisors, I would also thank Prof. Ricardo Mendes and Prof. Gilberto Vaz for their contributions and availability whenever requested. A very special mention needs to be given to Prof. José Baranda for his important and constant guidance, encouragement, commitment, patience and tolerance during this research work.

The research presented in this PhD thesis was sponsored by several research entities and private companies: the University of Coimbra itself (www.uc.pt), the Association for the Development of Industrial Aerodynamics (www.adai.pt), Sciven Lda. (www.sciven.com) and the Institute for Systems Engineering and Computers at Coimbra (www.uc.pt/en/org/inescc) This financial support is gratefully acknowledged.

I want to also express my gratitude to all of my PhD and work colleagues. Thank you for sharing your ideas, for the constant company and expertise given when requested. The working days become lighter and productive thanks to you. Great success to all of you.

In addition, a huge thanks to all of my friends that somehow ask me about my thesis and always gave me some comfort words and encouragement to go on.

Last but not least, a massive thanks to my family, especially to my mother and to my sister, for all the recommendations, support, concern and tolerance with me throughout this journey.

This page is intentionally left blank.

Contents

This page is intentionally left blank.

List of figures

List of tables

This page is intentionally left blank.

List of Acronyms

B	Natural-gas burner
CEN	European Committee for Standardization
CHP	Combined Heat and Power
CL	Compressed liquid
CODE	Cogeneration Observatory and Dissemination Europe
COP26	United Nations Climate Change Conference (2021)
CV	Control volume
DHW	Domestic hot water
EHE	Organic fluid heat-exchanger (evaporator)
EU	European Union
FID	Fluoride Ion Detector
FS	Full-Scale range
FTIR	Fourier-transform infrared spectroscopy
Geo	Geothermal
GHG	Greenhouse gas
HVAC	Heating, ventilation and air conditioning
ICE	Internal Combustion Engine
NG	Natural-gas
ORC	Organic Rankine Cycle
PH	Post-Heater (evaporator)
PI	Prediction Interval
R&D	Research and Development
RC	Rankine Cycle
SH	Superheated vapour
SL	Saturated liquid
SME	Small and medium-sized enterprises
TAN	Total Acid Number
TPES	Total primary energy supply
UK	United Kingdom
USA	United States of America
WHR	Waste heat recovery

This page is intentionally left blank.

List of Symbols

Symbol	Name	Unit
A	Area	m^2
AF	Air-to-fuel ratio	kg_{air}/kg_{NG}
CF	Calibration factor	$-$
c_p	Specific heat	$kJ/(kg.K)$
D	Diameter	m
D_h	Hydraulic diameter	m
dp	Damping factor	%
F	LMTD correction factor	$-$
f	Friction factor	$-$
FS	Full-scale range of the pressure sensor	kPa
G	Mass velocity	$kg/(s.m^2)$
H	Heat transfer coefficient	$W/(m^2.K)$
h	Specific enthalpy	kJ/kg
$\overline{h}$	Specific enthalpy	$kJ/kmol$
h_{fg}	Latent heat of vaporization	kJ/kg
j_h	*Colburn* factor	$-$
k	Thermal conductivity	$W/(m.K)$
L	Length	m
L_e	Mean beam length	m
LM	*Lockhart-Martinelli* factor	$-$
$LMTD$	Log mean temperature difference	K, ℃
M	Molar mass	$kg/kmol$
$\dot{m}$	Mass flow rate	kg/s
m'	Mass fraction	kg_i/kg_g
N	Number of samples	$-$
N_c	Number of CV per tube	$-$
n	Number of moles	$kmol$
NB_f	Nucleate boiling factor	$-$
Nu	*Nusselt* number	$-$
PES	Primary Energy Savings	%
Pr	*Prandtl* number	$-$
p	Pressure	kPa
p'	Partial pressure	kPa
$\dot{Q}$	Thermal power	kW
$\overline{q}$	Combustion energy	$kJ/kmol$
R	Thermal resistance	K/W
RA	Internal/external heat transfer area ratio	$-$

Re	*Reynolds* number	$-$
R_f	Fouling factor	$(m^2.K)/W$
$rPES$	Relative Primary Energy Savings	$-$
$r\dot{W}_{net}$	Relative ORC net power output	$-$
s	Entropy	$kJ/(kg.K)$
St	*Stanton* number	$-$
T	Temperature	K, ℃
U	Overall heat transfer coefficient	$W/(m^2.K)$
V	Volume	m^3
$\dot{V}$	Volume flow rate	m^3/s
v	Velocity	m/s
VF	View factor	$-$
$\dot{W}$	ORC power output	kW_e
X_{NB}	Nucleate boiling empirical factor	$-$
X_{tt}	*Martinelli's* parameter	$-$
x	Inverse of the temperature	k^{-1}
x_v	Quality	$-$
y	Logarithm of pressure	ln (kPa)
y_C	Molar fraction of non-condensable components	%
Z	Compressibility factor	$-$
α	Absorptivity	$-$
γ	Surface tension	N/m
δ	Molar fraction of H_2O in air	$kmol_{H_2O}/kmol_{air}$
Δ_a	Radiation correction factor	$-$
$\Delta T2$	Superheating temperature	K, ℃
Δy_x	Half-amplitude of the PI	$-$
ε	Emissivity	$-$
ϵ_r	Relative roughness	$-$
η	Efficiency	$-$
θ	Tetha	%
λ_{air}	Combustion excess of air	%
μ	Dynamic viscosity	$kg/(s.m)$
ρ	Density	kg/m^3
σ	*Stefan–Boltzmann* constant	$W/(m^2.K^4)$
σ^2	Variance	$-$
τ	Transmissivity	$-$
φ	PI Confidence level	%

List of Subscripts

Symbol	Name
$\{1 \dots 10\}$	CHP locations, undifferentiated
C	Non-condensable gases
CHE	ORC-condenser
CHP	Combined heat and power system
E	Electrical reference
EHE	Organic fluid heat-exchanger
H	Thermal reference
NG	Natural-gas
Net	Net value
ORC	Organic Rankine cycle
P	Combustion products
$P1$	ORC-pump
PH	Post-heater
R	Combustion reactants
REF	Reference value
T	ORC-expander
amb	Ambient condition
$conv$	Convection
ext	Exterior part
f	Working fluid
fc	Forced convection
ff	Free flow
fin	Fin
$flame$	Combustion flame
fr	Frontal
$fuel$	Related to the fuel used
g	Combustion gases
i	Fluid control volume number, $i \in \{1, \dots, Nc \times 14\}$
in	Inlet conditions
int	Interior part
j	Combustion gas level, $j \in \{1, 2, 3, 4\}$
l	Saturated liquid state
$loss$	Losses
max	Maximum value
nb	Nucleate boiling
np	Nucleate pool boiling
out	Outlet conditions

rad	Radiation
s	Isentropic
sat	Saturation state
sur	Surface
t	Heat-exchanger tube
v	Saturated vapour state
w	Water circuit
$wall$	Wall surface

Chapter 1 Introduction

- *"The formulation of the problem is often more essential than its solution, which may be merely a matter of mathematical or experimental skill."* (**Albert Einstein**)

1.1 Background and motivation

The last decades of worldwide social, economic and technological developments have led to an increase in the number of people requesting energy-consuming living amenities. This results in an increased rate of primary energy use much higher than what could be justified by the population growth (**Table 1-1**) [1,2]. Alongside the energy use increase rate, there has been a gradual rise in the average prices of conventional fossil fuels such as gas, oil or coal. Nowadays, these conventional fuels cover a large share of the primary energy needs (see **Fig. 1-1**) and are, by far, the biggest contributors to the world's greenhouse gas (GHG) emissions that lead, among other consequences, to climate changes and health problems [3,4]. The need to question the use of these traditional fuels, of traditional energy conversion methods and current consumption patterns, has reached an unprecedented level of importance and there are an imperative necessity to change them into low environmental impact, secure and cost-effective alternative approaches based on renewable or highly efficient energy systems [5,6].

***Table 1-1**: World energy & economic key indicators for the years 1993, 2011 and a projection for the year 2020 (data from [4]).*

	1993	**2011**	**2020**	**% growth (1993-2011)**
Population [billion]	5,5	7	8,1	27%
Gross domestic product [trillion USD]	25	70	65	180%
Total primary energy supply (TPES) [Mtoe*]	9.532	14.092	17.208	48%
Coal [Mt*]	4.474	7.520	10.108	68%
Oil [Mt*]	3.179	3.973	4.594	25%
Natural-gas [bcm*]	2.176	3.518	4.049	62%
Nuclear [TWh*]	2.106	2.386	3.761	13%
Hydro power [TWh*]	2.286	2.767	3.826	21%
Biomass [Mtoe*]	1.036	1.277	1.323	23%
Other renewables [TWh*]	44	515	1.999	1170%
Electricity production/year				
Total [TWh*]	12.607	22.202	23.000	76%
Per capita [MWh*]	2	3	3	52%
CO_2 emissions/year				
Total CO_2 [Gt*]	21	30	42	44%
Per capita [tonne CO_2]	4	4	n/a	11%

* **Mtoe** Million tonnes of oil equivalent; **Mt** Mega tonne; **Gt** Giga tonne; **bcm** Billion of cubic meters; **TWh** Tera Watt hour; **MWh** Mega Watt hour;

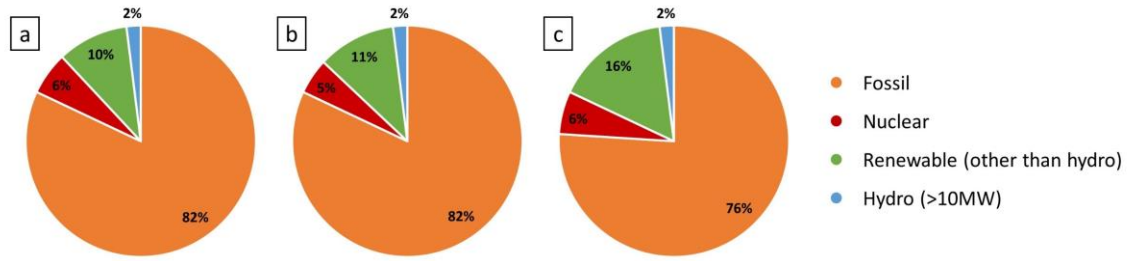

***Fig. 1-1**: World total primary energy supply per resource for the years: a) 1993, b) 2011 and c) a projection for the year 2020 (data from [4]).*

The mentioned facts enlighten all applications or technologies that, somehow, work against these major issues. One of those technologies, receiving increasingly attention from industries and research centres, is the Organic Rankine Cycle (ORC) [7]. According to Fredy Vélez et al. [8] and Bertrand F. Tchanche et al. [9] this technology presents some specific characteristics that make it suitable to be part of the solution for the aforementioned issues. Those are: i) adaptability to various heat sources, ii) proven and mature technology in medium-to-large scales, iii) simpler and reliable when compared to other technologies, iv) possibility to be built in a wide range of scales sizes, v) low investment and maintenance costs and vi) good market availability with well-known suppliers.

Often used together with ORC technology is the well-known technique of simultaneous production of heat and power, also known as CHP (Combined Heat and Power). The combined production of heat and power not only reduces the losses of the energy conversion process but also avoids the losses associated with its transportation and distribution, improving the sustainability of the whole process and contributing to the increase of grid reliability and the reduction of grid dependence [10,11]. Moreover, CHP systems not only provide significant savings over individual heating and power systems in terms of operational costs and of primary energy consumptions but also in terms of GHG emissions [12–14]. Dentice d'Accadia et al. [15], refers that the CHP has been considered as the major alternative to traditional systems in terms of significant energy savings and environmental conservation.

Both technologies (ORC and CHP) have been widely studied in the last years. Studies regarding ORC systems normally range from the development of more or less sophisticated models used to: i) estimate the economic benefits from the system operation, ii) support the system working fluid and components selection, iii) evaluate the system design, and off-design, key operation conditions or iv) develop the system control strategies; to the realization of more or less extended experimental tests. These are generally used to characterize a specific component or to validate the different options taken regarding, for example, system design configurations, component selection and control strategies [16–24]. The expander is the only ORC system's component that is frequently addressed in an isolated manner [25–30]. Usually, studies concerning CHP systems report the analysis of alternative configurations, or the comparison of different usable technologies, regarding

the energy and economic benefits [31–36]. Given its technological maturity and the individual magnitude of the energy and economic savings, the great majority of the CHP projects are generally done for steady-state operation regimes, on a medium-to-large scale. However, the potential for savings associated with micro-to-small scale and non-steady-state CHP systems (e.g. systems suitable to retrofit domestic combi-boilers) is believed to be enormous [37–41]. At this scale – micro-scale – the Rankine technology is being widely considered for CHP systems [42–44] and either due to restrictions related to dimension or with the system's response time, direct vaporization of the working fluid becomes more than an option, a demand. In those situations, to avoid high pressures and high superheating degrees that are typical of water/steam Rankine Cycles, the use of an organic fluid seems to be the reasonable option. Nevertheless, in such circumstances, the evaporator needs to be carefully engineered and, together with the expander, becomes a key component of the ORC based micro-CHP system.

1.2 Research questions

This PhD thesis is carried out with the general objective of contributing to overcoming the main obstacles that are precluding the ORC based micro-CHP systems technological breakthrough with market consequences through the identification of those obstacles and the discussion of how they can be surpassed or handled.

The achievement of that general objective involved the formulation of three main research questions and the specifications of three groups of specific assessments. In **Table 1-2**, these research questions and the respective specific assessments are presented together with the identification of the chapter where they are addressed.

***Table 1-2**: Main research questions and specific assessments.*

Main research questions	Specific assessments	Chapter
1. *What are the essential features that ORC based micro-CHP systems should present to fulfil the technological gap that is preventing the market breakthrough?*	i) Are there environmental and economic benefits in retrofitting the residential heating devices by CHP units? ii) Is the ORC technology the proper choice to fulfil the essential features of the residential-scale systems? iii) What is the current status of the ORC based micro-CHP technology and which are the main challenges that are precluding its massive implementation?	**2**
2. *What design principles should be followed to develop a suitable evaporator to achieve the market breakthrough of micro-CHP systems with ORC technology?*	i) Once direct vaporization is a known and important design principle, can it create safety or operating problems? ii) Study and development of a novel ORC-evaporator considering the identified design principles of the residential scale.	**3**
3. *What is the real risk of thermal degradation of the organic fluid associated with these direct vaporization systems? How can it be assessed and controlled?*	i) What are the common methods to evaluate the thermal degradation of organic fluids? ii) What is the role of the ORC-evaporator heat transfer surface temperatures on the thermal degradation of the organic fluid in real direct vaporization operating systems?	**4 & 5**

1.3 Contributions

The contributions/ outputs of the work performed to answer the research questions and to achieve the specific assessments are:

1. The presentation of the environmental and economic benefits obtained in the retrofit of the most common domestic heating systems (the standard or combi boilers) by CHP appliances;
2. The demonstration of the ORC technology as the proper choice for micro-scale systems, achieved by a comparative analysis between the available CHP technologies concerning the essential features of residential appliances;
3. The clarification of the importance of the evaporator and how the primary energy is transferred to the power cycle by conducting a detailed and extensive review regarding the current status of ORC based micro-CHP systems through the assessment of the works developed by the major manufacturers and research institutions.

4. The development of a new direct vaporization evaporator that follows the residential-scale design principles and the demonstration of its relevance on the operation and performance parameters of the ORC system;
5. A detailed, and experimentally validated, model of the heat transfer processes of the direct vaporization evaporator. This includes, beyond the common outputs like the power transferred or the organic fluid bulk temperature, the heat-exchanger surface temperatures used in the evaluation of the potential risk of thermal degradation of the organic fluid;
6. An exhaustive literature review regarding the common organic fluid thermal degradation assessment methods;
7. A suitable methodology to experimentally evaluate the thermal degradation of organic fluids in close-to-real operating conditions and to study the influence of the heat-exchanger surface temperatures over it.

The overwhelming part of the research present in this PhD thesis is based on the following core articles published or under review in ISI-indexed journals (abstracts and keywords of the mentioned articles are presented in **Appendix I**):

Pereira JS, Ribeiro JB, Mendes R, Vaz GC and André JC. ORC based micro-cogeneration systems for residential application – A state of the art review and current challenges. **Renewable and Sustainable Energy Reviews 2018**; 92:728–43.
DOI: 10.1016/j.rser.2018.04.039.
JCR 5-year impact factor®: 14.916; **Citations**: 43; **Readers**: 106.

Pereira JS, Ribeiro JB, Mendes R and André JC. Analysis of a hybrid (topping / bottoming) ORC based CHP configuration integrating a new evaporator design concept for residential applications. **Applied Thermal Engineering 2019**; 160:113984.
DOI: 10.1016/j.applthermaleng.2019.113984.
JCR 5-year impact factor®: 5.175; **Citations**: 6; **Readers**: 30.

Pereira JS, Almeida J, André JC, Mendes R and Ribeiro JB. Modelling and experimental validation of the heat-transfer processes of a direct vaporization micro-scale ORC-evaporator for thermal degradation risk assessment. **Energy Conversion and Management 2021**; 238:114130.
DOI: https://doi.org/10.1016/j.enconman.2021.114130.
JCR 5-year impact factor®: 8.954; **Citations**: 1; **Readers**: 3.

Pereira JS, Santos M, Mendes R, André JC and Ribeiro JB. Investigation of a direct vaporization ORC based micro-CHP system: an *in-situ* thermal degradation analysis under close-to-real operating conditions. **Applied Thermal Engineering 2021** (Submitted);

In addition, more than twenty abstracts/articles related to this PhD were published in conference proceedings, online magazines or workshops. The full list of those publications is presented in **Appendix II**.

1.4 Thesis structure

This thesis is composed of six chapters (including this introductory section and conclusions) and is structured as follows:

Chapter 2 reviews the use of ORC technology in micro-CHP applications taking into account the intrinsic requirements of the residential sector. The present research analyzes how manufacturers and research centres are dealing with those specific requirements and shows the technological gaps that are preventing its practical implementation. Additionally, this chapter also offers an analysis of the micro-CHP potential and the ORC market evolution, presenting a historical perspective of the technology, current main manufacturers, main application areas and a comparison between the use of an organic fluid and water/steam as working fluid for Rankine cycles.

Chapter 3 presents and discusses the recommended design principles for the development of evaporators for ORC based micro-CHP systems attempting to retrofit the current heating systems. One of those design principles is the direct vaporization of the organic fluid. Through the implementation of that principle, emerged a hybrid (topping/bottoming) CHP configuration in which thermal energy is produced stepwise: firstly in the ORC-condenser and then in a post-heater (that is integrated on the evaporator) directly with the combustion gases. The influence of using this new evaporator concept is evaluated regarding the primary energy savings and ORC net power output for a wide range of CHP operating conditions. The design and construction of a new direct vaporization evaporator considering the identified design principle are also presented in this chapter.

Chapter 4 describes the development of an experimentally validated heat transfer model to evaluate the combustion process and heat transfer phenomena of the direct vaporization evaporator presented in Chapter 3. Besides the general outputs (as, for example, the outlet bulk temperature or the power transferred), the inner surface temperature of the heat-exchanger is one of its main objectives, since it is virtually impossible to measure and can be used to assess the risk of organic fluid thermal degradation. Therefore, considerations about that risk may be made and limits for the operating conditions of the ORC system can be settled. The test rig used to experimentally validate the heat transfer model is also described in detail in this chapter. The experimental validation of the general outputs of the heat transfer model will be inferable for the prediction of the temperatures of the heat transfer surfaces of the evaporator since a mutual dependency is expected.

Chapter 5 analyzes the effect of the heat transfer surfaces' temperature in contact with the organic fluid over its chemical integrity. This is done by coupling a detailed comprehensive characterization of the system operating conditions, which includes the determination of the heat transfer surface temperature, with the realization of, close-to-real operating conditions, thermal stress tests that include the experimental evaluation of the organic fluid thermal degradation. In addition, an extensive up-to-date review of the most relevant works regarding the thermal degradation of organic fluids is presented. Details about the thermal stress methods, the thermal degradation detection techniques, and the ways to determine the thermal degradation temperatures are described and discussed.

This page is intentionally left blank.

Chapter 2 ORC based micro-CHP system: a state-of-the-art

- *"Research is to see what everybody else has seen, and to think what nobody else has thought."* (**Albert Szent-Györgyi**)

Summary: *This chapter not only attempts to identify the specificities of the operating conditions requested by the residential applications, and the technological gaps arising from them, but also provides an overview of the way how manufacturers and research centres of ORC based micro-CHP systems are trying to overcome the barriers that are precluding its practical implementation. Besides, a general analysis of micro-CHP specificities and its potential, in terms of energy savings and GHG emission reductions, is also presented. Since ORC is considered one of the most suitable technology for this specific application, an analysis regarding its state of maturity, through its whole power range, is made in which its main manufacturers are referenced and a trend regarding the average system size is presented.*

2.1 Micro-cogeneration potential and technologies

Micro-CHP is the designation given to the cogeneration systems that are able to fulfil thermal loads that range from those typical public/commercial buildings such as health centres, office blocks, schools, small and medium-sized enterprises (SME) and others, down to the needs of the individual household or residential dwellings. In terms of nominal electrical power, these systems range from below 1 kW_e to 50 kW_e. At medium-to-large scale (electrical power above 50 kW_e), CHP systems are a mature technology with fairly widespread use, while the micro-scale systems are still limited by several problems [45]. Nevertheless, the potential market for systems of this scale is huge [46] since one of their possible applications is the domestic hot water generation (for sanitary and space heating purposes). In fact, the Cogeneration Observatory and Dissemination Europe (CODE) performed a comparative analysis between different heating technologies currently used in buildings, especially addressing micro-CHP in order to understand its versatility and retrofitting (or add-on) ability [40]. The results of that analysis are shown in **Table 2-1**. CODE is a European project focused on the analysis and dissemination of the potential benefits and the applicable legislation of CHP systems. This analysis was done having in mind the Energy Efficiency Directive (2012/27/EU) [47].

***Table 2-1**: Features of different technologies for residential and SME/collective systems.*

TECHNOLOGY	APPLICATIONS			EXITING CONNECTIONS		FIT WITH EXISTING HEAT-EXCHANGER	EXTRA REMARKS
	Low temp. space heating	High temp. space heating	Hot tap water	Fit with gas connection	Fit with electric connection		
Condensing boiler	OK	OK	OK	OK	-	OK	Not expected efficiency improvements;
Ground source heat pump	OK	X	X	-	OK	X	Yearly balance ground source;
Air source heat pump	OK	X	X	-	OK	X	Feasible in new buildings or renewals;
Solar heat	X	X	OK	OK	-	X	Seasonal availability;
Biomass boiler	OK	OK	OK	-	-	OK	Biomass availability;
District heating	OK	OK	OK	-	-	OK	Heat network needed;
Micro-CHP	OK	OK	OK	OK	OK	OK	-

As stated by Alane and Saari [39] the most promising market for the micro-CHP systems lies in the residential sector (according to Kuhn et al. [48], in Europe this is especially true for countries like the United Kingdom, The Netherlands, Germany, France, Italy, Belgium, Denmark and Ireland). In fact, the annual dimension, in sales and stocks, of the European residential boiler market is around 8 and 100 million units, respectively; while the sales and stocks of all other sectors are around 1 and 20 million units, respectively, as shown in **Fig. 2-1**.

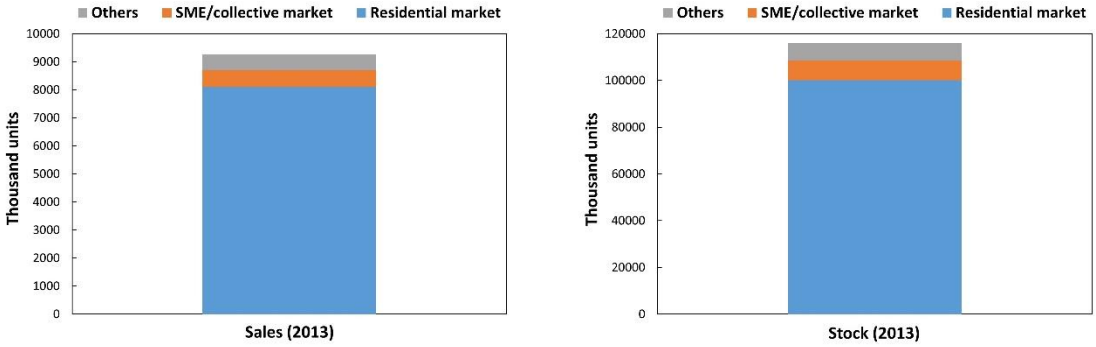

***Fig. 2-1**: Sectorial share of the European boiler market in 2013 (data from [40]).*

The enormous dimension of the European potential market of micro-CHP systems can be envisaged based on their predicted sales and stocks, for the years 2020 and 2030, shown in **Table 2-2**. On that table, the potential benefits that arise from the installation of all those micro-CHP systems in terms of primary energy savings and GHG emission reductions, for the year 2030 are also shown. The numbers presented in **Table 2-2** were taken from the references [40,47] and implicitly assume a pro-active and a strong political will regarding the promotion of the use of micro-CHP products. Currently, the European Union (EU) is supporting micro-CHP products through governmental subsidies like KWK-G [49], in Germany, or Ene.field [50], in eleven key EU state members, in order to support the accomplishment of their energy and climate targets.

***Table 2-2**: Micro-CHP predicted sales, stocks and potential primary energy savings and GHG emission reductions for the residential and SME/collective sector of the EU-27.*

Residential systems (± 1 kW_e)*		**SME/ Collective systems (± 40 kW_e)****	
Expected sales:	in 2020: 52.000 units/year; in 2030: 2.900.000 units/year;	**Expected sales:**	in 2020: 2.700 units/year; in 2030: 68.000 units/year;
Expected stock:	in 2020: 103.000 units; in 2030: 14.400.000 units; in 2040: 30.500.000 units;	**Expected stock:**	in 2020: 18.000 units; in 2030: 290.000 units; in 2040: 950.000 units;
Potential primary energy savings in 2030:			
300.000 TJ***/year;		240.000 TJ***/year;	
Potential GHG-emissions reduction in 2030:			
13 $MtCO_{2,eq}$***/year;		14 $MtCO_{2,eq}$***/year;	

* by replacement technology; ** by add-on technology; *** TJ Tera Joule; $MtCO_{2,eq}$ Mega tonne of CO_2 equivalent;

Acknowledging the great potential of micro-CHP products, considered as the "boilers of the future" [51], the European Committee for Standardization (CEN) drew up four standards, listed in **Table 2-3** in reverse chronological order, addressing the characteristics of the products and the evaluation of their efficiency. Some certification entities, as the Eurovent Certita Certification, have already used these standards to develop certification schemes for this kind of product [52].

***Table 2-3**: European Standards directly connected to micro-CHP.*

Standard No.	**Title**	**Content**
EN 15378-1: 2017	Energy performance of buildings - Heating systems and DHW in buildings. Part 1: Inspection of boilers, heating systems and DHW.	Specifies inspection procedures for the assessment of energy performance of existing boilers and heating systems (including cogeneration units).
EN 15316-4-4: 2017*	Energy performance of buildings - Method for calculation of system energy requirements and system efficiencies. Part 4-4: Heat generation systems, building- integrated cogeneration systems.	Defines a method for the performance assessment of building-integrated cogeneration units by the calculation of the electricity production, useful heat output and recoverable losses.
EN 13203-4: 2016	Gas-fired domestic appliances producing hot water. Assessment of energy consumption of gas combined heat and power appliances (micro CHP) producing hot water and electricity.	Sets out a method for assessing the energy performance of gas-fired micro CHP appliances. It defines the number of daily tapping cycles for each DHW use together with corresponding test procedures, enabling the energy performances of different gas-fired appliances to be compared and matched to the needs of the user.
EN 50465: 2015	Gas appliances - Combined heat and power appliance of nominal heat input inferior or equal to 70 kW.	Specifies the requirements and test methods for the construction, safety, fitness for purpose, rational use of energy and the marking of a micro combined heat and power appliance.

* The technical report CEN/TR 15316-6-7:2017 explains and justifies the application of this standard.

Despite the huge market and the potential benefits regarding primary energy savings and GHG emission reductions that are known to result from their widespread use (**Table 2-2**), micro-CHP systems have still not reached a sufficient state of maturity to be considered an actual valid alternative to the standard domestic heating systems as Dentice d'Accadia et al. [15] and Paepe et al. [35] demonstrated. Dentice d'Accadia et al. [15] conducted an energetic and environmental analysis of the use of a micro-CHP system in residential dwellings and small commercial buildings. Besides the obvious conclusion regarding energy savings and environmental benefits, there are still technological obstacles to its large diffusion, wherein gas and electricity prices will play a very important role to achieve a competitive micro-CHP unit that needs to be characterized by a low investment cost and easy operation. Paepe et al. [35] obtained similar conclusions after evaluating energy savings and GHG emission reductions for five different technologies of micro-CHP systems (< 5 kW_e). Paepe et al. specified that the installation of a micro-CHP system in a residential house is not financially attractive because of the high investment cost and long payback period. In addition, Qiu and Hayden [37] stated that the potential interest of this application emerges for cold climate areas where the thermal needs and consequently the system's working time are bigger.

The technologies available for micro-CHP applications can be divided into four main groups: external combustion systems (steam engines, Rankine or Stirling cycles), internal combustion systems (reciprocating spark ignition engines or gas micro-turbines), thermophotovoltaic generators and chemical conversion systems (fuel cells). All these systems are being studied and developed throughout the world in universities or research centres with the objective to reach an efficient and economically viable device capable to retrofit (or add-on) the existing heating systems [53–55].

Among the referred technologies, and excluding the chemical conversion systems, which in their actual stage of development have prohibitive costs [56–58], the Rankine technology appears as the most suitable and promising solution to convert low-grade heat into power [59] since it is the simplest and the less likely to create difficulties in retrofitting current heating systems (wall-mounted conventional or combi-boilers) in domestic dwellings [41,60–62]. According to Maghanki et al. [46], the use of Rankine based solutions for micro-CHP systems is not only the technology with better electrical efficiency, with values between 6 % and 19 % (for an approximate electric power size of 1 kW to 10 kW), but it is also the one with greater thermal efficiency, between 77 % and 90 % (for an approximate thermal power size ranging from 8 kW to 44 kW, respectively), coming up as a very good alternative to standard boilers or combi-boilers, meeting the typical residential loads. Despite all these promising technological characteristics, the investment costs were considered by several authors [15,35,38] as one of the major barriers to a widespread market introduction on the residential scale. Considering the calculations made by Bracco et al. [63] regarding the expected net revenue for a 1kW_e Rankine based CHP system, emulating the Italian energy tariffs, the operating

conditions and the energy needs of a typical dwelling (an electricity and natural-gas tariffs of 0,22 €/kWh and 0,71 €/Nm^3, respectively, an electrical and thermal efficiency of 10 % and 80 %, respectively, 2.500 h/year of operation, 20.000 kWh/year of thermal energy production, with a self-consumption of 95 %, and a self-consumption of all the electricity generated by the CHP system), evaluated in 200 €/year, it is easy to understand that the investment cost of the CHP system is crucial to have a payback period that does not obstruct its market acceptance. It is expected, however, that the continuous research efforts done in the area by manufacturers and research centres, including those done by the automotive industry [41,63], will lead to a cost-effective improved technology. Hopefully, this will contribute to reduce the investment cost and increase the net revenue of the system for which, eventually, feed-in tariff schemes and governmental subsidies, like the ones previously referred, can contribute positively.

2.2 Rankine Cycle technology

The Rankine Cycle (RC), which can be seen as a way to overcome the difficulties opposing the practical implementation of Carnot Cycle within the liquid-vapour water dome, in its basic configuration involves four main components: a pump, an evaporator, an expander and a condenser, as shown in **Fig. 2-2**-a. Its working principle may be briefly described as follows. The cycle starts with the pressurization of the working fluid in the pump leading to the evaporator, where it is heated and vaporized (and eventually superheated) by a heat flux from a suitable heat source. The pressurized vapour flows into the expander where it produces work while decreasing its temperature and pressure. The low-pressure vapour at the exit of the expander is then directed to the condenser where, losing energy to a suitable low-temperature heat sink, passes from vapour into the liquid phase. The condensed fluid is then conducted to the pump, to be pressurized again, closing the cycle. A schematic representation of the basic configuration of the RC, including the energy fluxes, is shown in **Fig. 2-2**-a. Several variations to this basic configuration have been developed over the years in order to increase the cycle efficiency - more information about these different configurations can be found in, for example, [7,64–67]. In **Fig. 2-2**-b, the four processes of an RC in a simple, superheated configuration are schematically presented in a temperature-entropy (T-s) diagram, in which the water/steam was used as the working fluid, for ideal (isentropic) compression and expansion processes.

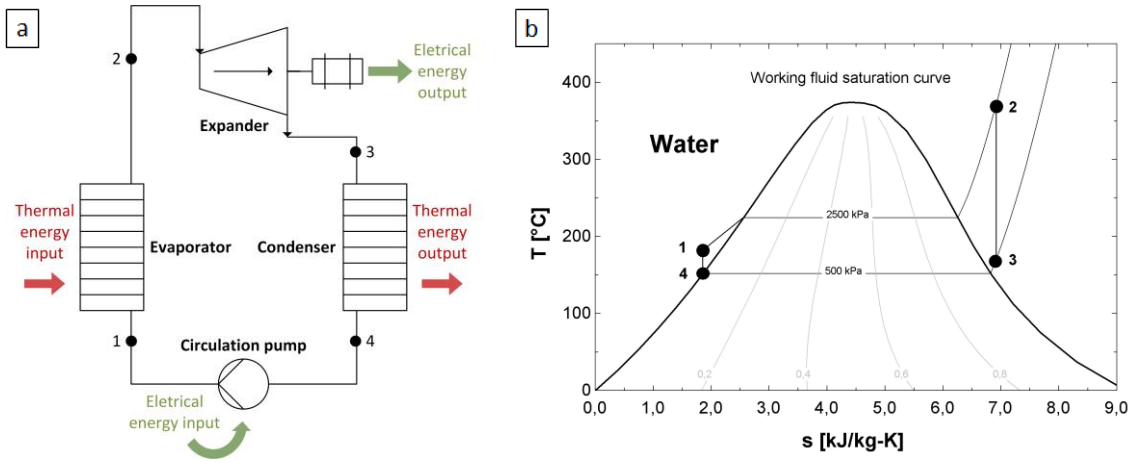

***Fig. 2-2**: Rankine cycle: a) schematic representation of the cycle components and the energy fluxes; b) schematic representation of the cycle processes in a water/steam T-s diagram.*

2.2.1 Steam versus organic Rankine cycle

Regarding the working fluid, two main alternatives are available nowadays: water/steam and, the fast-spreading, organic fluids. The T-s diagram of the saturation curves from those alternatives, where only the most common organic fluids were selected, is shown in **Fig. 2-3**.

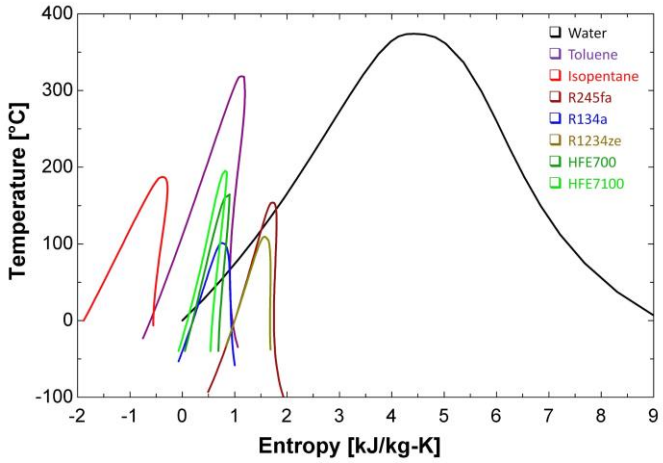

***Fig. 2-3**: T-s saturation curves for the water and the most common organic fluids used in RC.*

One of the major problems associated with the water/steam RC is the presence of high quantities of moisture in the final stage of the isentropic expansion process that not only contributes to decreasing the expander's efficiency but also to a significant reduction of its lifetime [16,68,69]. This problem, which occurs due to the markedly negative slope of the water/steam saturated vapour-line, has been solved by superheating the steam (heating it to a temperature beyond its saturation value at the working pressure) at the expander entrance so that the final stage of the expansion process occurs outside of the liquid-vapour dome, as it is schematically shown in **Fig. 2-2**-b. Organic cycles, however, may work with saturated vapour at the expander entrance once the slope of the saturated vapour-line of the working fluid is vertical or positive and, expectedly, the final stage of

the expansion process occurs outside of the liquid-vapour dome (see **Fig. 2-3**). A very important aftermath effect that results from the need of ensuring a substantial superheating degree in water/steam cycles is, for a certain heat source, the reduction of the evaporation temperature of the cycle and, consequently the reduction of the evaporator operation pressure, which will affect the pressure ratio in the expander and, eventually, preclude its practical implementation. Even if the expander specifications tolerate elevated moisture contents, allowing the practical implementation of the cycle, another problem would arise. In fact, the very high differences found for the specific volume values of vapour and liquid phases in water/steam cycles can lead to several undesired situations such as: operation instabilities due to the formation of high specific volume vapour bubbles, damage of the circuit components due to the occurrence of water hammers or liquid water entry into the expander per vapour trawl (even with a significant superheating degree). To avoid such problems, the operating pressure of water/steam cycles needs to be increased so that the difference between the specific volumes reaches acceptable values. This fact is one of the major justifications for the common use of high pressures in water/steam cycles [70,71]. However, an increase in the operating pressure has several consequences. One of the most definitive is the increase of the saturation temperature of the working fluid which makes the use of water/steam cycles impossible for some low-medium temperature heat sources like geothermal or waste heat. Two other relevant consequences are the need to guarantee safe operating conditions through extra design and manufacturing compliances (e.g. extra thickness of the under-pressure parts and extra care for manufacturing operations such as welding) and, for the typical pressure ratios involved, the need to use expensive multi-stage expansion turbines [71]. On the other hand, organic cycles, even working with relatively low operating pressures and temperatures, will still present a much smaller specific volume difference between liquid and vapour phases. When compared with the use of organic fluids, the use of water/steam in RC shows some advantageous features such as: i) lower cost, ii) higher availability, iii) much lower toxicity and flammability (water is intrinsically non-toxic and non-flammable), vi) much lower environmental impacts (lower global warming potential and null ozone-depleting potential) and, vii) much higher chemical stability (organic fluids can deteriorate when its maximum working temperature is reached) [16,72]. Water/steam cycles, except for low-temperature heat sources (e.g. geothermal, waste heat or solar), appear to be more advisable for a high-power range with a stationary working regime to reward the costs of better and more complex components and materials.

For the purpose of this study, it was important to analyze the above-mentioned characteristics of the water/steam cycles concerning the potential problems opposing their use in micro-CHP systems attempting to retrofit the actual domestic heating boilers (which represents the sector with bigger potential in micro-scale applications, see section 2.1). The two most relevant characteristics arising from the use of water as the working fluid in RC are: i) the significant

superheating degree that should be used at the turbine entrance that, due to the markedly negative slope in the saturated vapour-line, is required to avoid the condensation in the final stage of the expansion process, and ii) the important specific volume differences between liquid and vapour phases at low pressure, associated with operation instabilities, that demands high operating pressures. The potential problems arising from these features, however, may be hindered through the use of high-temperature heat sources that are normally available in domestic applications (e.g. natural-gas or biomass combustion gases). Nevertheless, the level of the operating pressure compatible with the use of water as a working fluid is non-advisable for domestic use. It is noteworthy that, besides safety questions, the elevated operating pressures also demand extra design and manufacturing compliances as well as expensive components like multi-stage expansion turbines. Given these relevant drawbacks, ORC appears to be the wisest choice to be used as prime-mover in safe, simple and reliable domestic micro-CHP systems attempting to retrofit the current standard heating systems.

2.2.2 ORC evolution, the current key manufacturers and market trends

The early beginning of the ORC technology development can be linked to the work of Sadi Carnot, in 1824, when he described the potential benefits of using other working fluids rather than steam in heat engines [73]. Just two years later, in 1826, T. Howard patented the idea of using Ether as a working fluid in a steam engine [41]. In 1859, William Rankine wrote "A Manual of the Steam Engine and Other Prime Movers" [74] where for the first time, the thermodynamic steam Rankine cycle was described [75]. In the following years, the development of ORC technology had almost stopped. The interest in ORC only rebirthed in 1890, when The Gas Engine & Power Company of New York sold about 500 Ofeldt patents [76] based on ORC engines [41]. The Ofeldt ORC engines, mainly applied to power small boats (the "naphtha launches"), used a reciprocating expander fed by a naphtha evaporator and took advantage of the U.S. law which required the presence of a qualified engineer on board if a high-pressure steam-driven engine was used to power the boats [75].

In 1907, a new relevant milestone was settled when F. Shuman successfully used a flat solar collector to vaporize Ether, at temperatures around 120 ºC, to drive a 2,6 kW_e engine [41]. About two decades later, in 1935, Prof. D'Amelio from the University of Naples, Italy, went beyond the study of the effect of the pressure ratio on the expansion process and showed, for the first time, that the use of high molecular mass fluids allows a reduction of the turbine rotational speed and the number of expansion stages [77]. In his study, Prof. D'Amelio developed an ORC system using an impulse single-stage axial turbine and Methyl Chloride as a working fluid to, among other things, keep the turbine rotor peripheral speed below 100 m/s. The evaporation and condensation temperatures were 40 ºC and 23 ºC, respectively; while the shaft power was around 4,5 kW_e [78]. Given his achievements, Prof. D'Amelio is considered one of the fathers of the modern ORCs [41].

It may be said that the commercial exploration of the ORC technology for electrical energy production started with the installation of the ORC geothermal plant, in Kiabukwa, Democratic Republic of Congo, in 1952, that used geothermal water at 91 ºC to produce a gross electrical power of 200 kW_e [41]. Throughout the rest of the 20th century, the development of ORC technology was enormous with the installations of many plants, powered by different energy sources, and the achievement of many research advances. One of those achievements, that pioneered the establishment of Ormat (currently the worldwide leader in ORC installed capacity [79]), was made at the National Physics Laboratory of Israel, in Jerusalem, between 1958 and 1961. Considering the work developed by Prof. D'Amelio, the idea to recover part of the working fluid energy content at the expander exit to be used in the evaporator preheating arose, reducing the energy supply on that component and leading to an efficiently improved version of the basic ORC configuration, currently known as a regenerative ORC [41,77].

The scientific basis that allows even further developments of the ORC technology was established in the 60s and 70s in the Politecnico di Milano, Italy, due to the work of Prof. G. Angelino and his research team, including Ennio Macchi and Mario Gaia. Together, and with the financial support of various institutions and companies, they designed and installed 14 ORC power plants with powers ranging from 3 kW_e to 500 kW_e [75,77,78]. The knowledge and experience earned with those plants were used by Ennio Macchi to find Turboden that, in close collaboration with the referred research institution, has been responsible for some of the most remarkable technological developments in the last decades like, for example, the installation of the first biomass-fueled ORC unit at Bière, Switzerland, in 1998 [41,77]. All of these developments have led, during the second half of the first decade of this century, to a rapid growth of the number of scientific/ academic papers and of the patents published in the area, as Ben-Ran Fu et al. demonstrated [80,81].

Despite all these scientific and technological developments, and of all entrepreneurship efforts to bring it to the commercial market, the level of maturity of ORC technology is not homogeneous and depends on the heat source type and system's size. The assessment of that level of maturity can be done through a worldwide ORC market analysis, including the list of the major manufacturers and of the main field of application that can be clustered, according to the cycle energy source, such as: solar, geothermal (Geo), waste heat recovery (WHR) and biomass. A list of the twenty current major, or more active, manufacturers, along with their field of application and their typical power output range, is shown in **Table 2-4**. The manufacturers listed in **Table 2-4** emerged from a cross-check analysis between scientific articles [7,8,46,71,77,79,82] and their official websites.

***Table 2-4**: Main ORC manufacturers with indication of their fields of application.*

Manufacturer	Field of application	kW_e range*	Reference
Ormat (USA)	Geo, WHR, Solar	200 – 70.000	[83]
Exergy (Italy)	Geo, Biomass, WHR, Solar	100 – 50.000	[84]
General Electric (USA)	WHR	6900 –16.000	[85]
Turboden (Italy)	Geo, Biomass, WHR, Solar	200 – 15.000	[86]
GMK (Germany)	Geo, Biomass, WHR	500 – 15.000	[87]
Cryostar (France)	Geo, WHR, Solar	500 – 15.000	[88]
TAS (USA)	Geo, WHR	500 – 15.000	[89]
BNI (USA)	Geo, WHR	15 – 6.000	[90]
Enertime (France)	Geo, Biomass, WHR, Solar	500 – 3.000	[91]
Adoratec/maxxtec (Germany)	Biomass	300 – 3.000	[92,93]
Kaishan (China)	Geo, Biomass, WHR, Solar	60 – 1.000	[94]
BEP – E-Rational (Belgium)	Geo, Biomass, WHR	55 – 800	[95]
Phoenix (Australia)	Geo, Biomass, WHR, Solar	25 – 1.000	[96]
Dürr Cyplan (Germany)	Geo, Biomass, WHR, Solar	50 – 500	[97]
Tri-o-gen (Netherlands)	Biomass, WHR	95 - 170	[98]
Zuccato Energia (Italy)	Geo, Biomass, WHR, Solar	30 - 500	[99]
Calnetix (USA)	WHR	125	[100]
Electratherm (USA)	Geo (hot springs), Biomass, WHR	35 - 110	[101]
Infinity Turbine (USA)	Geo, Biomass, WHR, Solar	10 - 100	[102]
Enogia (France)	Geo, Biomass, WHR, Solar	10 - 100	[103]

* Approximately values, based on the manufacturer reference.

The share of the worldwide ORC installed capacity attributable to each one of the major manufacturers is presented in **Fig. 2-4**. Between them, the three major manufacturers are responsible for almost 90 % of the installed capacity. The largest share, by far, owned by Ormat (65,7 %) can be justified by its focus on large-scale (>5 MW_e) binary geothermal power plants [71].

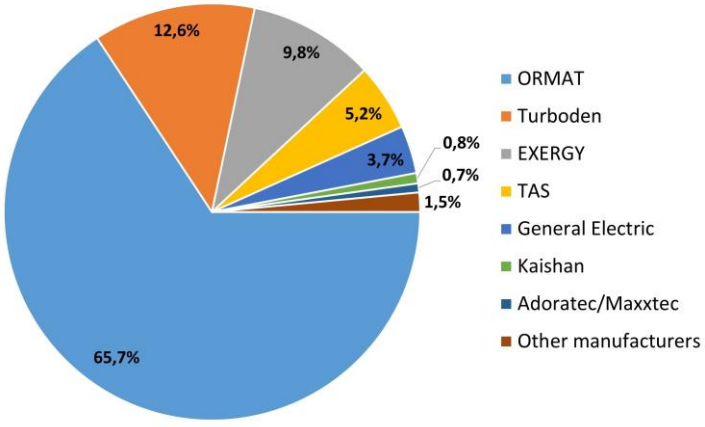

***Fig. 2-4**: Share of world ORC installed capacity per manufacturer up to 2016 (data from* [79]*).*

The evolution of the worldwide ORC cumulative installed capacity and the cumulative number of installed projects was calculated from the respective yearly values, presented in [79], and is shown in **Fig. 2-5**. From this data, it is possible to estimate the evolution of the average size of the

installed projects, shown in **Fig. 2-6**. A significant reduction of this value, of nearly one order of magnitude (from 25 MW_e to about 5 MW_e) is observed for the first decade of this century; however, in the second decade, these values appear to have stabilized.

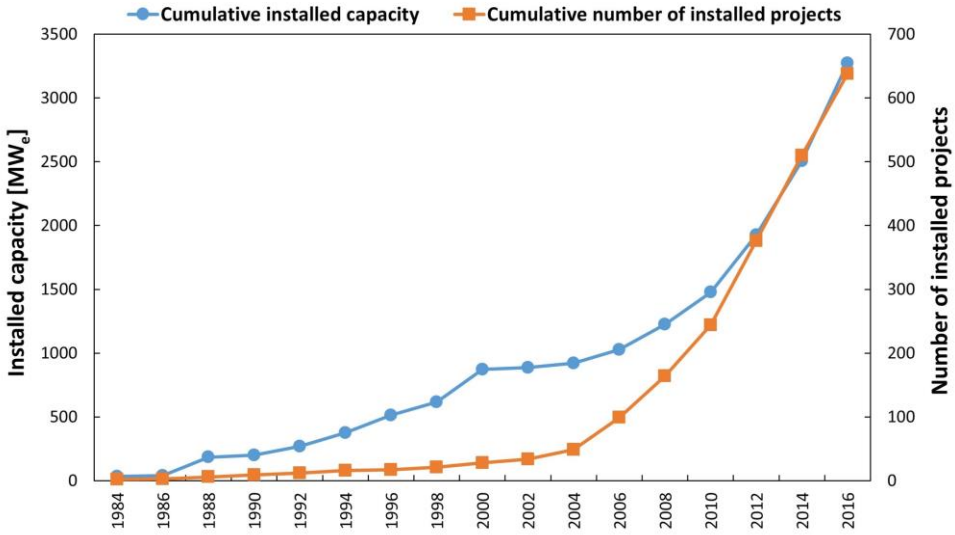

***Fig. 2-5**: Evolution of the ORC cumulative installed capacity and number of installed projects.*

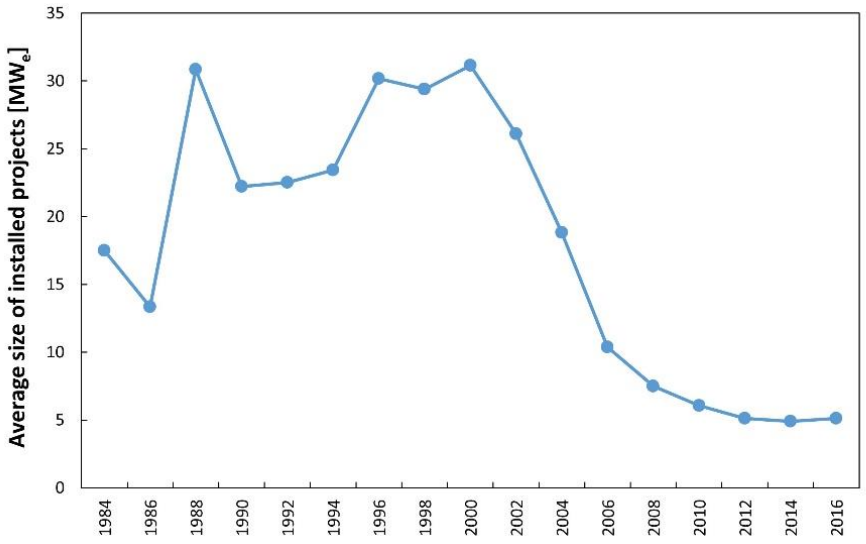

***Fig. 2-6**: Evolution of the average size of the ORC installed projects.*

The disaggregation of the worldwide ORC installed capacity and number of installed projects by field of application, up to the year 2016, is presented in **Fig. 2-7**. From the installed capacity point of view, systems for geothermal applications dominate completely, with more than 75% of the share. However, systems for biomass applications are the most numerous. It is also possible to note, whether in terms of installed capacity or terms of the number of installed projects, that the use of ORC systems for solar applications is marginal. The combination of these data made possible to estimate the average size of the projects installed up to the year 2016, per field of

application, as shown in **Fig. 2-8**. The ORC geothermal projects present, by far, the biggest average size, around 19 MW_e; while, at the other end, solar applications are found with an average size of around 400 kW_e.

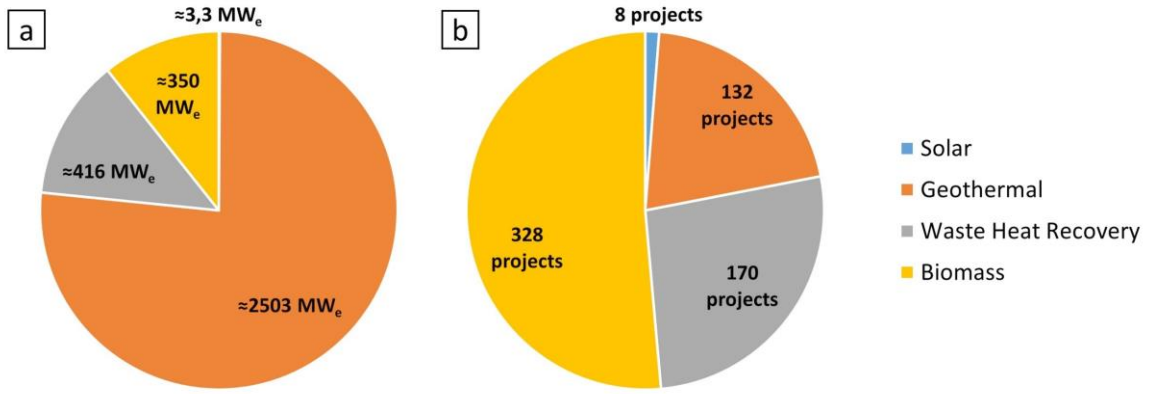

***Fig. 2-7**: Disaggregation by field of application up to the year 2016 of the worldwide ORC a) installed capacity and b) installed projects (data from* [79]*).*

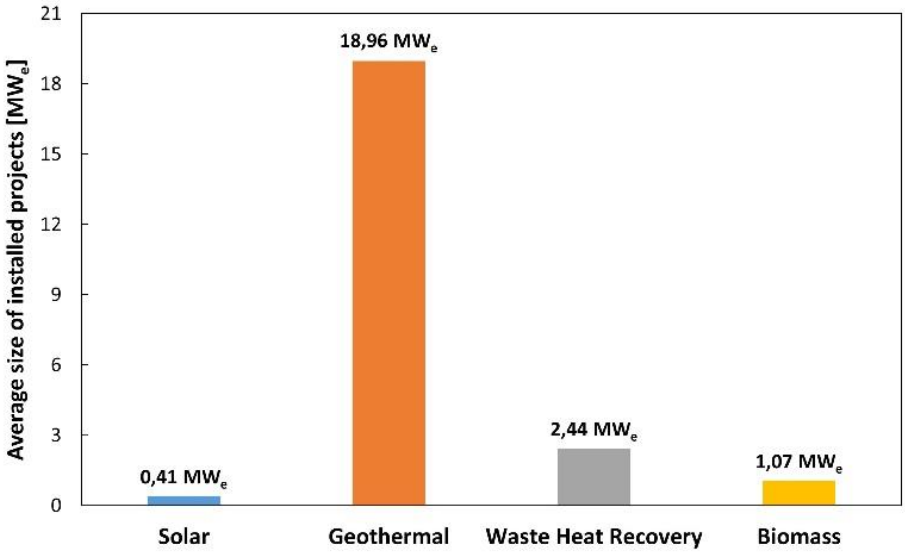

***Fig. 2-8**: Average size of ORC installed projects disaggregated by application up to 2016.*

The data presented above, namely the average size of the ORC projects, allows to state that the ORC based systems have reached the technology maturity at medium-to-large size scales with geothermal, biomass and waste heat recovery applications, but are yet to achieve that maturity at small-to-micro size scales. Nevertheless, the evolution trend regarding the size of installed projects, indicates that manufacturers are not only aware of the enormous potential of the energy-saving opportunities in micro-to-small scale applications, but also that they are willing to explore it. In fact, analyzing the size range of the systems offered by the twenty manufacturers, listed in **Table 2-4**, it is possible to see that most of them have small-scale options available in their products portfolio with six of them already offering products at the micro-scale level.

2.2.3 Overall ORC configurations for the main fields of application

Due to its intrinsic stability and easy operation, in comparison with water/steam cycles, ORC systems can be used in multiple situations, as in power generation or, either bottoming or topping, cogeneration systems with several different heat sources like solar, geothermal, biomass and fossil fuels, or even with industrial, or internal combustion engine (ICE), residual heat streams. Although sharing the essence of the thermodynamic processes, different applications require some particular specificities that can be interesting to study from the point of view of their potential use on a domestic scale.

Solar application

Well before the appearance of photovoltaic technology, solar energy was already transformed into electricity by using high-temperature steam RC in large-scale concentrated solar power plants. By the end of the last century, the number of installations based on parabolic trough solar collectors, which normally use organic working fluids, increased while its typical size decreased [104]. The specificities of the primary energy source, in which the oscillations of intensity are probably the most important, demand special design options, not in the power cycle, that is kept practically unchanged when compared to the basic configuration; but in the way how the primary energy is delivered to it. In an attempt to fade out the negative effects of the oscillations of the solar radiation intensity, the systems designed for this particular application normally use an intermediate circuit, incorporating a thermal storage tank, to transfer energy from the solar panels to the ORC power cycle. A schematic representation of these systems is presented in **Fig. 2-9**.

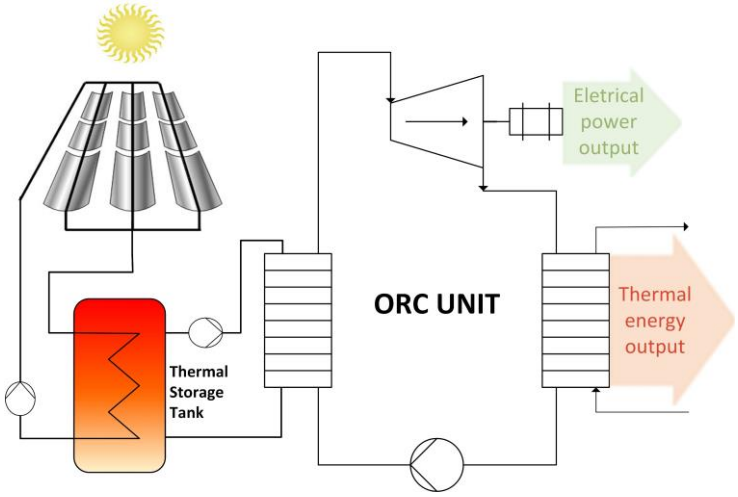

***Fig. 2-9**: Schematic representation of a solar energy fed ORC power system.*

The idea of using a thermal storage tank as a thermal inertia element seems to be very useful also for micro-CHP applications, especially those attempting to retrofit the current domestic heating systems. In fact, two of the biggest problems that these systems have to face are the highly exigent response time and the characteristic intermittence of the hot water request pattern. In such cases, the

use of a thermal inertia element on the end-user hot water side of the system would have two positive consequences: i) a reduction of the system response time, because the hot water should be available in the storage tank, and ii) an easier achievement of close-to-steady, and close-to-nominal, operating conditions of the power cycle which, in principle, should increase its overall efficiency. Nevertheless, for micro-CHP systems attempting to retrofit wall-mounted conventional or combi-boilers currently applied in residential dwellings, and besides the minor problem associated with the eventual thermal losses of these storage tanks [105], this solution may present serious constraints due to the system final dimension and weight.

Geothermal application

Geothermal energy sources are recognized as being among those with the greatest potential to help achieve the energy security, economic development and mitigation of climate changes targets [106]. Despite the relatively low temperatures at which they occur, ranging from a few Celsius degrees up to 350 ºC, the amount of energy stored in geothermal heat sources is known to be huge and, contrarily to other renewable energy sources (like solar or wind), it can be used in a continuous-controlled way [107]. Nevertheless, two problems oppose its widespread use. One of the problems is related to the location of the geothermal sources. In fact, some of the most interesting geothermal sources (with higher temperatures) are located in remote isolated places with small energy requirements [108]. The other problem is related to the economic viability of their use. According to Quoilin et al. [71], the current technological lower bound for the heat source temperature for power generation is about 80 ºC (below this value the conversion efficiency becomes too small and the geothermal power plants will not be economically feasible). In respect to the technology used, Vélez et al. [8] refer that the best way of extracting energy from geothermal heat sources with temperatures above 200 ºC, producing dry steam or a mixture of steam/brine, is to use the generated steam directly into turbines, working in open cycle with or without re-injection of fluid. However, for geothermal sources with lower temperatures, this method becomes unfeasible and the best solution is the use of an ORC module in a configuration similar to the one presented in **Fig. 2-10**.

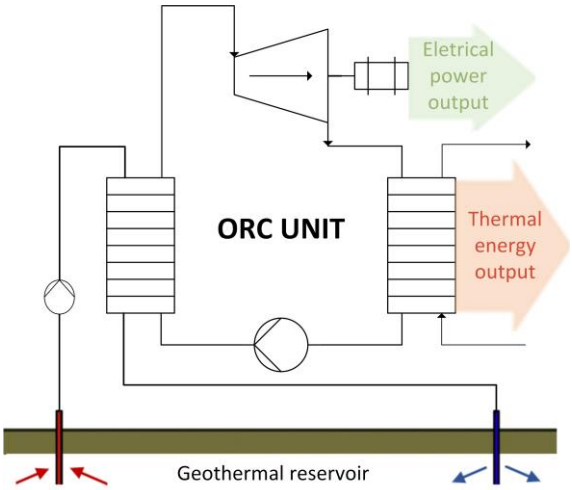

***Fig. 2-10**: Schematic representation of a geothermal energy fed ORC power system.*

In this case, and contrary to what happens in solar applications, the energy provided to the power cycle is expected to be very steady and no thermal inertia elements are needed to fade out the system oscillations. The pressurized geothermal hot water is used directly to vaporize the organic working fluid of the power cycle in a heat-exchanger, without the need of any intermediate circuits, since it is not expected that the typical temperatures of the geothermal hot-water will cause problems related to its thermal degradation. Given its simplicity, and consequently, the expected potential to reduce the system response time and its dimension and weight, this configuration seems also interesting for the domestic micro-CHP systems. Nonetheless, attention should be given to the thermal degradation of the organic working fluid when other heat sources, with higher temperatures, are directly used in the evaporator.

Biomass application

Despite the discussions around its degree of renewability, which depends on the type of biomass used and how it is cultivated and harvested, it is believed that the use of biomass as an energy source plays a key role in the mitigation of non-renewable energy consumption and the reduction of environmental impacts. Biomass, like geothermal energy, can be used in a continuous-controlled way; however, it does not have its availability geographically restricted. The production of electricity from biomass sources can be made essentially by two ways. One of them includes, as a first step, the transformation of the biomass into a fuel, like biodiesel or biogas, which is then used to produce electricity in ICE or gas turbines. The other way restricts to the combustion of the crude, or densified solid, biomass, alone or co-fired with other fuels (e.g. coal), in boilers that will act as an external heat source of an RC [109–112]. In respect to the latter, and without entering into details regarding the boiler type, is important to refer that, essentially due to economic and safety reasons, water/steam is commonly used as working fluid [42]. As stated before (see section 2.2.1), to avoid operation instabilities during the phase change in the evaporator, and/or the excess of condensation at the end of the expansion process, water/steam RC need to work at much higher pressures and

temperatures than the organic fluid-based cycles. That characteristic demands extra (compared with those necessary for ORC) design, materials, manufacturing and components specifications that are easily amortizable for medium-to-large scale power plants or cogeneration installations but possibly not for small-scale systems. For the small scale, a configuration similar to the one schematically represented in **Fig. 2-11** has generally been the option followed [61,113].

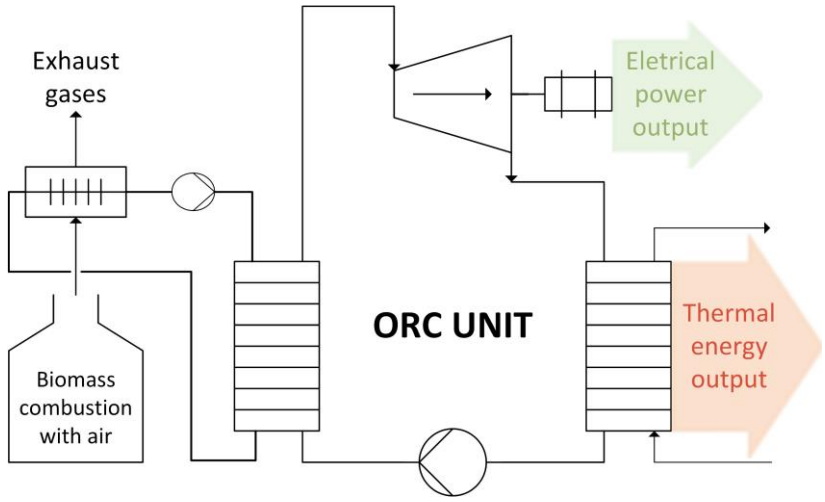

***Fig. 2-11**: Schematic representation of biomass energy fed ORC power system.*

While nothing in particular needs to be emphasized regarding the power cycle, it is important, however, to highlight the presence of an intermediate thermal circuit (generally using oil or water). The use of this intermediate circuit avoids the direct exposition of the ORC-evaporator to the high-temperature combustion gases and reduces, or eliminates, the risk of the organic working fluid thermal degradation. Additionally, this lowers the pressure design specifications of the boiler and makes the matching between the boiler and ORC operation conditions much easier [61]. However, it is reported that the existence of this intermediate circuit decreases the thermal efficiency and the ability to respond to quick load changes of the system [9]. Nevertheless, it should be noted that these kinds of systems are usually designed to work in steady-state conditions and without significant space restrictions and so, neither the response time nor the system dimension are key criteria, contrarily to what happens in a domestic application.

Waste heat recovery (WHR) application

In many areas of industry, the production processes gave origin to high/medium enthalpy gaseous (or liquid) streams that, up to some decades ago, were simply discarded into the environment. The increasing concerns related to the environmental and economic issues have led to a change in how those streams are seen, passing from strictly waste streams – with no use – to potential energy sources. Gaseous streams from continuous operating furnaces of ceramic or metallurgic industries, boilers of the standard electrical power generation industry, gas turbines, ICE and even fuel cells are good examples of situations where the waste heat can be used for electrical energy production. Since approximately 50% of the discarded heat is found in form of sensible heat

with temperatures below 230 ºC [114], ORC appears as one of the most suitable technology to convert part of it into mechanical/electrical power in, what is called, a waste heat recovery system [8,115]. The most common waste-heat-fed ORC power system configuration is identical to the one used for biomass applications, schematically represented in **Fig. 2-11**, if the biomass boiler is replaced by a hot gaseous stream discarded from industrial processes.

As well as for biomass, typical configurations of waste-heat-fed ORC power systems also present an intermediate circuit between the heat source (the waste heat stream) and the power cycle. Despite the low temperature of these gaseous streams (endorsing the use of an organic fluid as working fluid), the option for an intermediate circuit is usually made to avoid long pressurized pipes of organic fluid arising from the impossibility to install the waste heat recovery unit near the stack.

The schematic representations presented above show different ways of connecting the heat source with the ORC system. The way how this is done is affected by the existence of variations/fluctuations of the power and temperature of the energy source. To fade out those fluctuations, strategies as the one followed in solar-energy-fed ORC power systems, with an intermediate thermal circuit and including a hot water thermal storage tank, need to be followed. When high-temperature sources are employed (e.g. biomass combustion gases) an intermediate circuit is also used to reduce the risk of the organic fluid thermal degradation and simplify the match between the boiler and power cycle operating conditions. However, the implementation of the intermediate circuit appears to decrease the global efficiency as well as increase the response time of the system to quick power variations.

It is important to mention that in all of the presented configurations, specificities of the demand side or restrictions associated with the dimension and weight were not considered. In the case of micro-CHP systems attempting to retrofit the current domestic heating systems, characterized by a non-steady-state operation regime, the response time and the dimension are important design constraints and the benefits arising from the use of an intermediate circuit, as in waste heat recovery or biomass configurations, apparently do not counterbalance the cost of longer response times and bigger systems. In those cases, the exposure of the ORC-evaporator directly to the high-temperature energy source (e.g. natural-gas combustion gases) seems to be the solution to overcome the above-mentioned constraints. However, special attention must be given to the design of the ORC-evaporator and the control of the system in order to avoid the organic working fluid thermal degradation and improve the micro-CHP ability to deal with the highly sensitive operating conditions resulting from the reduction of the system thermal inertia [71]. As result, the ORC-evaporator should be seen as a key component for domestic micro-CHP applications that needs to be carefully analyzed and engineered.

2.3 ORC based micro-CHP system: an evaporator analysis

In order to understand how this subject is being addressed by the domestic micro-CHP system manufacturers and by research institutions that, all over the world, are making efforts concerning the study and the development of this kind of application, an extensive research was conducted regarding the way how the primary energy is transferred to the power cycle.

2.3.1 Systems that have reached the ready-to-market level of development

The only company that, up to the moment, developed a commercially available micro-CHP system for domestic use, was the FlowEnergy Limited. FlowEnergy, a UK based company that was formerly known as Energetix Genlec Limited, launched its natural-gas fueled ORC micro-CHP power system in the UK market on 26th January 2015 [116]. The micro-CHP system produces hot water for an exterior storage tank - as in normal boilers so the whole system can hardly be considered wall-mounted or retrofittable with combi-boilers - and uses an intermediate circuit, working with water/steam, to transfer energy from the hot combustion gases to the power cycle [117,118]. According to its patent [118], the water in the intermediate circuit is heated and vaporized in a helical-coil heat-exchanger and the organic fluid (pentane is considered the suitable choice) is vaporized in a plate-type heat-exchanger - the ORC-evaporator. The maximum allowable pressure and temperature of the intermediate circuit is 7 bar and 150 ºC, respectively. The patent does not clarify the reasons that led to the use of an intermediate circuit or the use of water/steam mixture instead of pressurized water or thermal oil. Their options may be connected to the following reasons: i) the direct exposure of the power cycle parts to the very hot combustion gases is undesired not only due to safety reasons, when the working fluid is considered flammable [9], but also due to the risk of thermal degradation in the ORC-evaporator thermal boundary layer; ii) the use of an intermediate circuit provides an additional control parameter to the system, facilitating the match between the user demands and the natural-gas burner heat input [71]; iii) the use of water/steam instead of thermal oil or pressurized water takes advantage from the high energy density and high heat transfer coefficient associated to the evaporation and condensation processes in order to reduce the size of the intermediate circuit heat-exchangers; and iv) specifically with thermal oil, the use of water/steam is not only safer from the point of view of fire risk, in case of leakage, but eventually, depending on the country legislation, less demanding in terms of circuit specifications [63]. This FlowEnergy system can produce up to 1 kW_e of electrical power, using a scroll expander connected to a generator, and a thermal power ranging from 7,4 kW to 14,1 kW [119]. Besides the referred patent targeting the entire CHP system [118], this company also protected the way to control it [120] and the working principle of the intermediate heat transfer circuit [121]. The indicative price of this system is around 3.700 € without installation or the storage tank [122].

In November 2014, an Italian company named Kaymacor started its activity by developing mini and micro scale ORC systems targeting a wide variety of applications, including the domestic-CHP, and designed to use different energy sources (e.g. biomass, solar) [123]. The company developed its own scroll expander and, according to its website, their ORC systems have simple start-up and stop procedures, operating practically without noise, with minimum maintenance requirements and presenting a good performance at partial loads which make them a good candidate to work in domestic environments [124]. Besides the scroll expander, the ORC unit uses R245fa as working fluid, a positive displacement gear-type pump and plate-type heat-exchangers for the evaporator (the hot fluid temperature must be between 80 ºC and 170 ºC) and for the condenser (the cold fluid temperature must be between 20 ºC and 90 ºC) [125]. The ORC unit must be connected to the primary energy heat source using an intermediate hot water circuit; nevertheless, the company already offers integrated solutions. Typical operation numbers for the domestic-scale CHP system are: 37 kW of thermal power input, supplied through the intermediate circuit in form of pressurized hot water at 170 ºC; 30 kW of thermal output delivered in form of hot water at 50 ºC; and 4 kW_e of net electrical power [124]. An own-developed working fluid reservoir, used by Kaymacor in their ORC power cycles, is patent protected [126]. The price of the ORC unit or any of the integrated solutions is not available.

Besides the already mentioned systems, and even if not specifically designed for CHP applications, some waste heat recovery systems are described by their manufacturers as having the ability to be coupled to natural-gas or biomass-fueled boilers and having the appropriate power size to target the domestic-scale CHP market. One of those manufacturers and one of those systems is the Spanish organization called Rank and the system Rank HT-C [127–129]. The sole operation requirements found for Rank HT-C are the existence of an intermediate heat transfer circuit, which can use thermal oil or pressurized water, between the natural-gas or biomass hot combustion gases and the power cycle, since this was originally designed to work with low-temperature heat sources [128,130]. The figures of Rank HT-C are: electrical power ranging between 2 kW_e and 50 kW_e and thermal power (in the form of hot water at 85 ºC) ranging from 50 kW to 400 kW. To produce these outputs, Rank HT-C uses an ORC regenerative configuration, R245fa as the working fluid, a volumetric-type expander (without specifying the type) and brazed plate-type heat-exchangers as evaporator and as condenser [43,131]. A solution to prevent the ORC-pump cavitation [132] and innovative cycle configurations to be used in the exploitation of low-temperature heat sources [133] are patent protected. Its indicative price appears to be around 4.500 € per kW_e [128].

Among those ORC based waste heat recovery system manufacturers claiming that their products can be adapted for micro-CHP applications is also the Norwegian company called Viking Development Group. This company developed a system named CraftEngine with a power size suitable for domestic-CHP applications. In its operating requirements, it is mentioned the need for

a vaporization temperature of the organic working fluid ranging between 80 ºC and 215 ºC, which suggests the necessity of using an intermediate heat transfer circuit if natural-gas or biomass hot combustion gases are used as heat sources [134]. The system is described as presenting an electrical power output ranging between 2 kW_e and 12 kW_e for thermal power inputs ranging from 30 kW to 150 kW. The thermal power output is not precisely defined by the manufacturer. However, it is stated that the system can reach a thermal output close to the difference between the thermal input and the electrical power output [135,136]. This particular ORC system uses a reciprocating engine from the automotive industry (low-cost solution) as an expander and standard plate-type heat-exchangers as an evaporator and as a condenser. No details are given about the pump and the working fluid used [137]. For a 12 kW_e system size, the indicative price per kW_e is around 1.700 €/kW_e, however, the company refers that this value will be higher for smaller-size units [137]. At least five topic-related patents [138–142], addressing several innovations as its own-developed ORC based heat engine fed by an external heat source and the operational and safety controls, were prepared by this company.

From the preceded analysis it seems that the key element that allows some companies to state that they can offer CHP solutions for domestic applications is their capacity to produce their own micro-scale ORC units. It can also be inferred that for this kind of application, since the most common heat-sources are natural-gas or biomass combustion gases, to avoid the direct exposition of the ORC working fluid to those hot gaseous streams, and reduce the risk of thermal degradation, an intermediate heat transfer circuit needs to be used. Not only but also, due to the use of this intermediate circuit, it is expectable that these systems have high thermal inertia and, as a consequence, longer response times which may be a problem when dealing with multiple short, and intrinsically variable, hot water demand pattern of the domestic scale. In an attempt to work around this problem, the use of a thermal storage tank, explicitly referred by FlowEnergy, and inferred from the information available in the Kaymacor webpage, is necessary.

2.3.2 Experimental products or research test rigs

In addition to the systems that have reached the ready-to-market level of development previously mentioned, ORC based micro-CHP applications are being extensively studied by companies attempting to develop their own products and by university research centres focused on studying the fundamental basis that will allow the ORC technology to evolve.

One of the companies is Cogen Microsystems, an Australian company that started to develop a steam RC based micro-CHP prototype for residential dwellings [143] (also identified in [46,58]). Its first prototype was referred by Cogen Microsystems as being able to produce up to 2,5 kW_e of electrical power and 11 kW of thermal power, operating with an overall efficiency higher than 90 %. The heat source, the working principle and the basic components are not clearly described in the

references and this never reached a commercial stage. Currently, Cogen Microsystems is trying to develop another micro-CHP prototype for residential dwellings, this time based on ORC technology and using solar energy, collected through evacuated tube collectors, as the primary energy source [144]. The company uses a specifically-built piston-type expander [145]. As it is still in the development phase, the technical information available is very sparse however, it appears that the system configuration is very close to the one presented in **Fig. 2-9**. The authors claim that their system will be capable to provide households with 1 kW_e and 8,8 kW of electrical and thermal power, respectively. The working principle [146], its control system [147] and their own-developed expanders [145,148] are patent protected.

Damgaard Solutions, a spin-off of the Czech Technical University in Prague [149], is another example of a company that is trying to develop its own ORC based micro-CHP system [150]. The company already built and tested two ORC based micro-CHP prototypes in an attempt to reach a ready-to-market product. These prototypes share some common features like a specifically-built rotary vane-type expander (more data regarding this component is given by Vodicka et al. [151]) and a modified commercial gear pump. The first prototype used a commercial biomass boiler, adapted to work with oil instead of water and capable to heat it to temperatures around 280 ºC, delivering a thermal power ranging from 16 kW to 23 kW to the ORC power cycle. The working fluid of this prototype, Isopropylbenzene, is vaporized in a plate-type heat-exchanger, the ORC-evaporator, at temperatures around 265 ºC. The electrical power produced ranges from 0,4 kW_e and 0,8 kW_e. A plate-type heat-exchanger is also used for the condenser. According to the company, this first prototype has shown to be too complex and expensive to reach the objectives initially proposed. The second prototype, also biomass-fueled, uses a specifically designed spiral-wound (3 parallel tubes) heat-exchanger, the ORC-evaporator, to vaporize the organic working fluid, Hexamethyldisiloxane (also known by MM) in this case, directly from the hot (around 600 ºC) biomass combustion gases, avoiding the use of the intermediate heat transfer oil circuit [152]. From this prototype, it is expected that a thermal input of 65 kW will retrieve an electrical output of 2 kW_e. A pilot project using this prototype is expected in the coming years [153].

The last example considered in this research is the Swiss company Eneftech Innovation SA. In spite of being closed for business since March of 2016 [154], the work developed during the twelve years of activity in the areas of micro and mini ORC systems, reach notability enough to be referenced in several scientific papers like [8,26,27,63,82,129]. The heart of its ORC systems was an own developed volumetric expander, adapted from a scroll compressor, which features are described in detail by Kane et al. [155] and by the patents [156,157]. The following information was obtained from the company website in February of 2016 [158–160] in which two products were described: i) a mini-scale ORC system – Enefcogen green – which reached the commercial phase in 2010 and presented electrical and thermal power outputs that range from 5 kW_e to 30 kW_e and from

45 kW to 255 kW, respectively, and ii) a micro-scale system – Enefcogen plus – which was never taken off from a development phase. However, the company estimated values of 5 kW_e and 33 kW for the electrical and thermal power outputs, respectively. R245fa was used as a working fluid in both systems [129]. Eneftech products were developed for low-temperature heat sources (between 120 ºC and 200 ºC) and plate-type heat-exchangers were selected for the evaporator and the condenser. The use of Eneftech products with high-temperature heat sources (e.g. biomass or natural-gas combustion gases), requires an intermediated heat transfer circuit. This ability, together with the typical values of thermal and electrical power outputs, would have made it suitable for domestic CHP applications.

The type of studies that are being done in university research centres is, normally, in comparison with the type of research/development being done in companies, not so focused on the development of practical solutions, or in the resolution of specific problems, but much more on establishing the fundamental basis for the complete understanding of the technology working principles, including the identification of the key operating parameters. The number and the variety of research works produced and published in the area of ORC based micro-CHP systems are very large and very wide not only in what refers to the specific objectives but also in the approaches followed to achieve those objectives. Since the objective of this literature review is to understand how the research groups are dealing (or not) with the specificities required for the ORC-evaporator at the micro-scale level, the works with a strong experimental component were specifically targeted in order to evaluate how the vaporization of the ORC fluid is performed. The only exceptions were the works of Algieri and Morrone [49,116] and Liu et al. [115] that, despite their theoretical nature, made some important considerations regarding the trend followed for the vaporization of the organic fluid and by this reason, were also included in the list. Given the significant amount of scientific works found, it was decided to present the most relevant ones in a tabular form (see **Table 2-5**). The works are organized in reverse chronological order and individualized by authors where, for each one, a reference to the main objective and a short description of the test rig, with special emphasis put on the solution followed for the vaporization of the ORC working fluid, are presented.

***Table 2-5**: List of the most relevant scientific researches regarding micro-CHP systems based on ORC technology.*

Author & Reference	Research summary
Bonk et al. [161] (2017)	Developed a simple micro-scale ORC test rig, easily reproducible by the scientific community, for pedagogic and research purposes. The design methodology followed by the authors includes the selection of the organic fluid, Novec 649, and of all the main components of the ORC power cycle: a 1 kW_e volumetric scroll-type expander, a piston diaphragm pump and a brazed plate-type heat-exchanger as condenser and evaporator. The vaporization of the organic fluid was made using pressurized water heated to a temperature of 140 ºC by an electrical device.

Kolasiński et al. [162] (2017)	Studied the possibility of using a rotary-vane expander, adapted from an air motor, in a domestic scale ORC system focusing on its reliability and efficiency. The test rig built to perform such studies used R123 as the working fluid and a plate-type heat-exchanger as evaporator and condenser. The type of pump was not mentioned. The heat source used for the vaporization of the organic fluid was water heated, to temperatures between 55 ºC and 85 ºC, in a natural-gas fueled boiler.
Bianchi et al. [163–165] (2017-2016)	Built a kW-scale ORC test rig using a 3 kW reciprocating engine as an expander to study the operation conditions, including the transient phase, and the performance indicators at low vaporization temperatures. Besides the expander, they used R134a as working fluid, a plate-type heat-exchanger as an evaporator, a shell-and-tube heat-exchanger as a condenser and a volumetric gear-type pump. To evaporate the organic fluid was used water heated to a temperature of 100 ºC by an electrical device.
Zywica et al. [166–168] (2015 - 2017)	Developed and characterized an ORC based micro-CHP prototype to be coupled to a biomass boiler (pellets fueled) to evolve to a commercial system. They used HFE7100 as working fluid, a four-stage radial-type turbine as an expander and a plate-type heat-exchanger as evaporator and condenser. The pump type was not identified. To vaporize the organic fluid was used thermal oil heated to a temperature of 200 ºC by the biomass combustion gases.
Eicke and Smolen [169] (2015)	Built a 1 kW_e test rig with the objective to study the performance and the technical feasibility of the micro-scale systems. The authors used R245fa as working fluid, plate-type heat-exchanger as evaporator and condenser, a slide-vane pump and a scroll-type expander. To vaporize the organic fluid was used thermal oil heated to a temperature of 130 ºC in an electrical device.
Muhammad et al. [170] (2015)	Built a kW-scale test rig to develop and characterize an ORC system to recover the waste heat from low-grade steam. The authors selected R245fa as working fluid, a scroll-type expander, a gear-type pump and a plate-type heat-exchanger as evaporator and condenser. The vaporization of the organic fluid was made using low pressure and low-temperature waste steam (3 bar and 135 ºC), from a liquefied natural-gas fueled boiler, directly in the ORC-evaporator.
Jung et al. [171] (2015)	Studied the technical feasibility and potential advantages of using a zeotropic fluid mixture (R245fa and R365mfc: 48,5% / 51,5% mole basis) in a kW-scale ORC based CHP system. For this study was used a scroll-type expander, a plunger-type pump and plate-type heat-exchanger as evaporator and condenser. To vaporize the organic fluid, the authors used thermal oil heated to a temperature of 160 ºC in a finned-tube heat-exchanger by the exhaust gases from a Capstone diesel turbine.
Galloni et al. [172] (2015)	Showed the technical considerations and the experimental methodology followed to design and characterize an ORC based micro-CHP system using low-temperature heat sources. This work aimed to assess the technical feasibility of this kind of application. They used R245fa as working fluid, a scroll-type expander, a rotary-vane pump and a plate-type heat-exchanger as evaporator and condenser. The vaporization of the organic fluid was made using water heated to a temperature of 96 ºC by a purpose-built boiler (the fuel used by the boiler was not specified).
Abadi et al. [173] (2015)	Built a micro-scale test rig to evaluate the benefits and the eventual drawbacks arising from the use of a new zeotropic mixture (R245fa 60 % / R134a 40 %) in micro-scale systems. The authors used a scroll-type expander, a plunger-type pump and a plate-type heat-exchanger as evaporator and condenser. To vaporize the organic fluid, they used water heated to temperatures between 80 ºC and 100 ºC in a boiler (the fuel used by the boiler was not specified).
Chang et al. [174,175] (2014, 2015)	Studied the influence of using a scroll-type expander in an ORC based micro-CHP system to improve the cycle performance. They used R245fa as working fluid, a plunger-type pump and a plate-type heat-exchanger as evaporator and condenser. The vaporization of the organic fluid was made with water heated to temperatures between 78 ºC and 96 ºC by an electrical device.

Algieri and Morrone [60,113] (2013, 2014)	Performed a theoretical analysis of the operating characteristics and the main performance indicators of a micro-scale ORC system for three different organic fluids: Cyclohexane, Decane, and Toluene. This research also includes an economic analysis, considering the Italian tariffs and incentives scenarios, to evaluate the economic feasibility of the system. Despite being essentially a theoretical study, the authors consider an intermediate circuit with oil to transfer the energy from the biomass combustion gases to the organic fluid.
Farrokhi et al. [44] (2013)	Presented the preliminary results of an experimental investigation of an ORC based micro-CHP system for residential buildings with the objective of studying its viability. For this study, they used Isopentane as working fluid, a rotating vane-type expander which was designed and manufactured by the authors, a diaphragm-type pump and plate-type heat-exchanger as evaporator and condenser. To vaporize the organic fluid they used water heated to temperatures between 65 ºC and 85 ºC in a natural-gas fueled boiler.
Declaye et al. [176] (2013)	Performed an experimental characterization of an oil-free air compressor modified to operate as an expander within an ORC based micro-CHP system to assess eventual improvements in the cycle efficiency. They used R245fa as working fluid, a volumetric diaphragm-type pump and a plate-type heat-exchanger as evaporator and condenser. The vaporization of the organic fluid was performed using a hot air circuit, however, no further details were given.
Bracco et al. [177] (2013)	Built a mathematical model and conducted experimental tests on a domestic-scale ORC prototype to properly simulate the system behaviour to explore and improve its performance. They used R245fa as working fluid, a scroll-type compressor adapted to work as an expander, an inverter-driven diaphragm-type pump, a plate-type heat-exchanger as a condenser and, according to the authors, an electric boiler as the evaporator. The electric boiler appears to be a series of electrical resistances externally surrounding the ORC tubes where the vaporization of the organic fluid is made.
Qiu et al. [42] (2012)	Developed a test rig to study and characterize the ORC based domestic-scale CHP behaviour in order to assess eventual improvements in the cycle efficiency. The authors selected the HFE7000 as working fluid, a rotary vane-type air compressor adapted to work as expander and plate-type heat-exchanger as evaporator and condenser. The type of the pump was not specified. To vaporize the organic fluid the authors used water heated to temperatures between 96 ºC and 102 ºC by a biomass-fueled boiler.
Liu et al. [178] (2011)	Performed a thermodynamic analysis of a 2 kW_e ORC based micro-CHP system for three different organic fluids: HFE7000, HFE7100 and n-Pentane. The main objective was to optimize the power cycle through the working fluid selection. Despite being essentially a theoretical study, the authors considered a plate-type heat-exchanger as evaporator and condenser. The type of the expander and the pump were not identified. The vaporization of the organic fluid was performed using water heated in a biomass boiler, however, no further details were given.
Pei et al. [59] (2011)	Presented the construction of a kW-scale test rig to study the behaviour of a radial-axial type turbine, developed by the authors. They used R123 as working fluid, a centrifugal-type pump and a plate-type heat-exchanger as evaporator and condenser. The vaporization of the organic fluid was made with thermal oil heated to a temperature of 106 ºC by a non-specified way.
Peterson et al. [179] (2008)	Incorporated a custom-built scroll-type expander into a regenerative ORC based micro-CHP system for a cycle performance evaluation. They used R123 as working fluid, a centrifugal-type pump, a finned-tube heat-exchanger as a condenser and a plate-type heat-exchanger as an evaporator. The vaporization of the organic fluid was made with thermal oil heated to a temperature of 182 ºC by a non-specified way.

When the author's objective is the behaviour analysis of a specific component of the ORC power cycle (usually the expander) or the comparison of the cycle performance for different working fluids, the option made regarding the way how the vaporization of the ORC working fluid is done becomes irrelevant. However, when the objective is to study the system behaviour in close-to-real situations, for which the working regime is expected to be intrinsically non-steady, as in the micro-CHP systems attempting to retrofit the current domestic heating devices, none of the options made regarding the operating conditions of the system main components is irrelevant, since some of its significant features, like response time, are strongly influenced by those options and may have a great impact on the cycle overall efficiency.

From the analysis of the works listed in **Table 2-5**, it is possible to state that two of the most important ORC components for micro-CHP systems, the pump and the condenser, are completely off the shelf products; while different kinds of expanders and working fluids have been deeply characterized and studied for this type of use [174,176,180,181]. Conversely, it is clear that the role of the evaporator, which influences the way how primary energy reaches the power cycle, the efficiency and the overall behaviour of these kinds of systems, has been vastly understudied and is yet to be identified by researchers as a crucial component. The use of an intermediate circuit, conceptually more complex and less efficient, can be justified by the absence of a market available evaporator capable of performing a direct energy exchange between the high-temperature combustion gases and the power cycle, by concerns regarding the possible thermal degradation of the organic working fluid or even by difficulties in controlling the system [71]. Nevertheless, this appears not to be the best solution for a residential application since it will promote, at least, longer response times due to its higher thermal inertia. To mitigate these longer response times, manufacturers are forced to add to the micro-CHP unit a thermal storage tank, like FlowEnergy did. The use of these storage tanks may, however, preclude the retrofitting of the wall-mounted conventional or combi-boilers currently applied in residential dwellings. To take advantage of the huge economic and environmental potential that comes from the replacement of the residential heating systems by CHP units (evaluated in section 2.1), the way how primary energy reaches the ORC-evaporator needs to be reformulated and more studies, or even the development of a new concept of the evaporator, capable to deal with all the referred restrictions, appears to be necessary.

2.4 Concluding remarks

The potential primary energy savings, GHG emissions reductions and economic benefits associated with the use of micro-scale CHP systems are huge. The biggest share of that potential is found, by far, in the residential sector and especially on those systems attempting to retrofit the current heating devices (wall-mounted conventional or combi-boilers). At this scale, and for that purpose, the Rankine based CHP systems appear to be the most suitable and promising solution due

to a set of characteristics where its simplicity deserves to be remarked. It is also clear that the organic fluids seem to be more interesting than water/steam when used as the cycle working fluid, not only because water demands higher operating pressures, to avoid the instabilities associated with the enormous specific volume variation during the liquid to vapour phase change; but also because the organic fluids, due to the shape of their saturation lines, may work with saturated vapour and avoid the high superheating degree necessary in the water/steam cycles to skip the problems associated with high moister contents in the final phase of the steam expansion in the expander.

The overview performed on the worldwide ORC market allowed the identification of the main manufacturers together with the field of application and the installed capacity of their systems. Besides, it was also possible to verify five important aspects: i) the number of patents in the area is rapidly increasing since the beginning of the second half of the first decade of this century, ii) there is a significant number of ORC systems manufacturers operating on the market, iii) the cumulative number and the cumulative installed capacity of the ORC projects are increasing at a constant rate, iv) the average size of the installed projects has been reducing, since the beginning of the century, from about 30 MW_e to 5 MW_e and v) the current smallest average size of the installed ORC systems is found for the solar application and is about 400 kW_e. All these pieces of evidence can be considered as an indicator that the ORC systems reached its technological maturity for medium-to-large scales and, due to the giant potential market and the expectable benefits in terms of primary energy savings and GHG emissions reductions, the smaller size systems are receiving increasing attention by the manufacturers and researchers working in the field.

One of the most challenging requirements that ORC based micro-CHP solutions targeted to retrofit the current heating systems in the domestic market need to show is the short response time in order to face the highly variable thermal loads that are typical of this kind of application. The accomplishment of this requirement is essentially dependent on the way how primary energy is delivered to the ORC-evaporator, while the other components of the cycle - expander, pump and condenser - have a minor role in that specific assignment.

The most common micro-CHP configuration includes an intermediate thermal circuit to transfer energy from a primary energy source to the power cycle using, in the great majority of the cases, a plate-type heat-exchanger as the ORC-evaporator. This kind of solution has, however, several drawbacks compared with the direct use of the primary energy source for the vaporization of the organic working fluid such as: a decrease of the system efficiency due to the inevitable thermal loss in the intermediate circuit, an increase of the investment cost and, most importantly, an increase of the thermal inertia. This increase of the thermal inertia affects negatively the response time of the entire system and it may affect its ability to respond accordingly to the residential thermal requests. To solve this problem, manufacturers and/or researchers are including a thermal storage tank on the end-user hot water side of the CHP system. The use of a hot water storage tank not only reduces the

system response time, because hot water is always available, but also reduces the variability of the system operating conditions since it will not operate to answer directly to the hot water end-user request but to a variation of the water temperature in the storage tank. Despite that, and besides the problem associated with the expected increase of the thermal losses, its adoption appears to be an obstacle to the objective of retrofitting the current widespread wall-mounted conventional or combi-boilers applied in residential dwellings because of the requirements regarding the system dimension and weight. It is then obvious that the ORC-evaporator, and the way how the primary energy is delivered to the power cycle, is intrinsically connected with major key issues when a residential implementation is considered and, most worryingly, these questions have passed submissive compared to the current high number of expander analysis or the organic fluid selection methodologies performed.

In order to benefit from the huge economic and environmental potential arising from the use of CHP at a micro-scale, those systems need to be able to retrofit the current residential heating devices. For the ORC based micro-CHP systems, that ability demands a reformulation of the way how primary energy is being delivered to the power cycle and more studies or even the development of specific designed ORC-evaporators, capable to deal with all the residential and organic working fluid restrictions, appears to be essential. At a time when most of the components are already accessible, studied and optimized, the development of a residential ORC based micro-CHP system still seems needed, being the evaporator and the way how primary energy is delivered to the power cycle one of the most promising and important areas for the optimization of the entire system.

This page is intentionally left blank.

Chapter 3 A direct vaporization evaporator for ORC based micro-CHP systems

- "*An experiment is a question which science poses to Nature, a measurement is the recording of Nature's answer*" (**Max Planck**)

Summary: *Recognizing the importance that the evaporator has on the technological/ commercial success of ORC based micro-CHP systems for domestic applications, and instead of avoiding the problem through the adoption of alternative restricting solutions, it seems reasonable to face the challenges associated with the development of a specifically designed ORC-evaporator capable to directly use the combustion gases to perform the vaporization of the organic fluid. In an attempt to overcome those challenges and fulfil this technological gap, which is believed to be preventing the widespread use of these systems, this chapter presents and discusses the design principles of such evaporators. In addition, a hybrid (topping/bottoming) CHP configuration, resulting from the design options taken for the ORC-evaporator, in which the useful thermal energy is produced stepwise, firstly in the ORC-condenser and then in a post-heater directly with hot combustion gases, is presented. Its benefits, in what refers to primary energy savings, cycle efficiency, net power output and risk of the organic fluid thermal degradation, are illustrated and discussed as a function of several CHP operating conditions such as the inlet and outlet water temperatures and the share of useful thermal energy that is produced in each one of the water heating steps.*

3.1 Development of a direct vaporization evaporator

It is important to start this section by remembering that the natural-gas burner and heat-exchanger set is meant to be the evaporator of a natural-gas fueled ORC based micro CHP system attempting to retrofit the actual combi-boilers for residential use. The combi-boilers are appliances that can operate in two different modes. They can be used as simple tankless gas water heaters (eventually, the water is heated up to 65 ºC, see [182]). Depending on the use given to the water in this operation mode, the demands can vary from very short, as it happens for lavatory uses, to long periods, as it happens for showers or baths. In both situations, however, the power demand is high and the predisposition of the user to wait for hot water is low. Or, the combi-boiler needs to have the capacity to heat water at relatively higher temperatures (eventually, the water is heated up to 90 ºC, see [183,184]) for space-heating. In this case, depending on climate conditions, the type of temperature control and the dwelling characteristics, the operation periods are normally much longer but at lower power levels.

3.1.1 Design principles

If the ability to retrofit the current standard combi-boilers is a key feature for the commercial success of ORC based micro-CHP systems for residential use, three of the essential characteristics of the evaporator should be: a) small dimension, b) high efficiency and c) high turn-down ratio. The dimension should be as small as possible not only because this makes it easier to fit the micro-CHP systems within the available space for the standard combi-boilers, but also because it will probably reduce its thermal inertia. The efficiency, throughout the entire power range, should be at least as high as the one (of the equivalent heat-exchanger) of standard combi-boilers. Otherwise, the eventual benefits from the CHP will be worn out by that reduction of the evaporator's efficiency. The turn-down ratio of the natural-gas burner should be as high as necessary to deal with significantly different, power demanding, operation modes. From these premises, a set of design principles are devised for the ORC-evaporator. i) The direct use of the combustion gases to heat, vaporize and, eventually, superheat the ORC working fluid (direct vaporization). This will avoid the use of an intermediate energy transfer loop with the additional heat-exchanger, pump, expansion vessel and all the necessary tubbing and insulation. One of the problems of this design principle is the increase of the risk of thermal degradation of the organic fluid in the inner thermal boundary layers of the heat-exchanger tubes. ii) The use of a counter-flow arrangement that, among other features, maximizes the extraction of energy from the combustion gases and the log mean temperature difference between the hot and cold fluid (to which an increased heat transfer rate per unit of area is associated). This results in not only a more effective but also a more compact heat-exchanger. iii) The use of a high turn-down ratio natural-gas burner to avoid the increase of flue gas losses at low partial loads and, to give the system an additional fine control degree which may be important, for example, to achieve specifically defined superheating degrees.

3.1.2 Natural-gas burner selection and heat-exchanger definition

The natural-gas burner, even with the specificities aforementioned, can be easily found on the market. A high turn-down ratio, of approximately 6 to 7, as necessary to comply with micro-CHP system needs, is easily achieved by pre-mixed gas burners. One of the market available options, with a cylindrical head shape (one of the most common), is shown in **Fig. 3-1**-a. The natural-gas burner selected has a nominal power of 35 kW and a turn-down ratio of 7. Besides these characteristics, and from the operation point of view, the burner is capable of: i) detect an instruction of the control system and start its operation in safe conditions which involve the ventilation of the combustion chamber before the opening of the natural-gas valve and ignition, ii) verify the existence of combustion/flame or, otherwise, close the natural-gas valve, iii) deliver the thermal power defined at each instant by the control system; iv) detect an instruction and switch-off the burner in safe conditions, safeguarding the accumulation of unburned gases or the formation of hot spots in the

combustion chamber or the heat-exchanger by ensuring a proper post-ventilation. The datasheet of the selected natural-gas burner, mentioning all of these characteristics, is presented in Annex A.

Contrary to the natural-gas burner, the heat-exchanger needs to be specifically designed, being the first step of that process the definition of its configuration. Given the shape of the natural-gas burner head, the heat-exchanger configuration that seems to be the most suitable may be described as a double concentric helical-coil divided into three parts: the external coil, the internal coil and a central combustion chamber (or hot gases generator) that includes the natural-gas burner head. A schematic representation of this configuration can be seen in **Fig. 3-1**-b while the technical drawings necessary for its construction and a 3D step are given in Appendix C. In this configuration, the hot combustion gases flow around the tubes of the heat-exchanger, within which is the organic fluid, in what can be described as a mixed counterflow/ crossflow arrangement. The working fluid enters into the ORC-evaporator through the heat-exchanger outer coil, where the combustion gases leave it, and exits at the point where the combustion gases pass from the central combustion chamber to the heat-exchanger inner coil. The use of high-temperature insulation material sleeves (presented in brown in **Fig. 3-1**-b) prevents the energy transfer along the radial direction from the central combustion chamber to the first (inner) and second (outer) coils in an effort to keep the counter-flow arrangement nature of the ORC-evaporator heat-exchanger as relevant as possible. The determination of the total length of the heat-exchanger coils was done using a specifically developed model (described in detail in [185]) that locally calculates the ORC working fluid and combustion gases transport properties and the respective heat transfer rates.

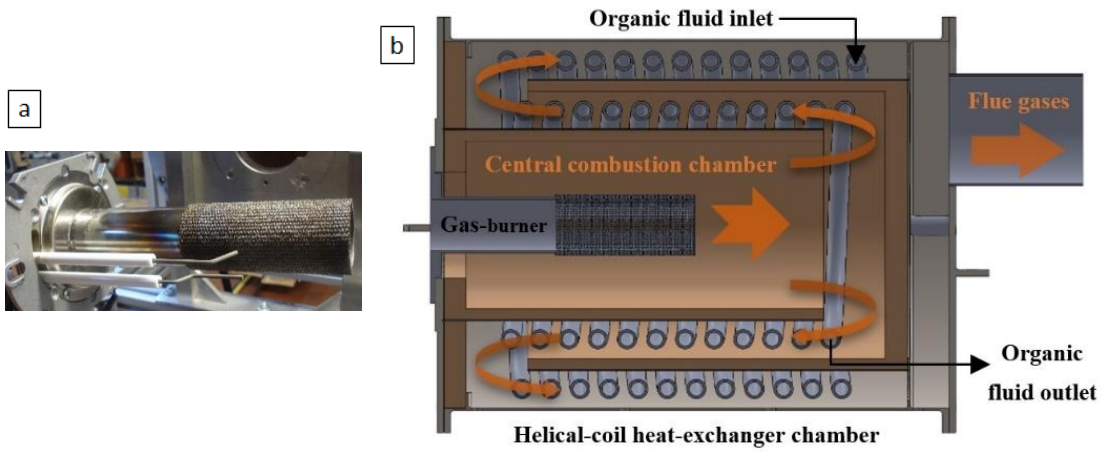

***Fig. 3-1**: Photograph of the premix burner head with the ignition spark and flame detector rod (a) and the cross-section view of a schematic representation of the ORC-evaporator (b).*

3.1.3 Preliminary tests

After the construction of the heat-exchanger, the natural-gas burner was assembled to it and the set (ORC-evaporator) was connected to a chimney for preliminary tests (during which water was used within the coils) in order to optimize the combustion conditions (e.g. excess of air) and check

safety issues. The objective was, following the burner manufacturer advice, to achieve an oxygen concentration in the flue gases between 5% and 5.5% all over the natural-gas burner power range. While performing this tuning operation and still working with the natural-gas burner at 30% of its nominal capacity, a small explosion occurred and the tests were immediately stopped.

3.1.4 Accident diagnostics

When uncoupling the natural-gas burner from the heat-exchanger, it was possible to verify the existence of a major failure in the burner head from which its tip was ripped off and where was found evident signals of metal super elongation probably due to the combined effect of overheating and explosion overpressure (see **Fig. 3-2**).

***Fig. 3-2**: Natural-gas burner head after the accident.*

The origin of the problem was discussed with the burner manufacturer and the most plausible explanation points to a localized failure due to burner head overheating, which allowed a flame backward movement into its interior causing an explosion. In order to confirm this possibility, after replacing the head, the natural-gas burner was reassembled to the inner insulation sleeve (the central combustion chamber) of the ORC-evaporator and set to work without the coils and the external covers (see **Fig. 3-3**), so that the flame characteristics and the burner head could be observed and analyzed during the combustion tuning process.

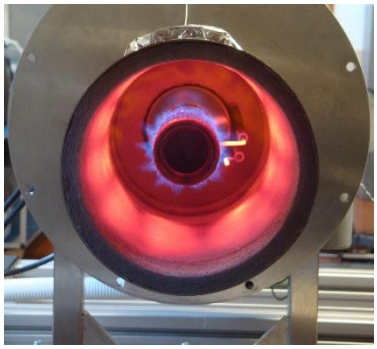

***Fig. 3-3**: Natural-gas burner head within the central combustion chamber.*

Infra-red images of the burner head operating in such conditions are shown in **Fig. 3-4**. As it can be seen, the temperature of the burner head increases with its operating power. The heat transfer mechanisms between the natural-gas burner head, the air-gas mixture and the immediate surroundings may explain this behaviour. The natural-gas burner head is heated up by the energy radiating back to its external surface from the flame (hot combustion gases) and from the inner surface of the surrounding combustion chamber while is cooled by the air-gas cold flow. It is important to note that, even if the high-power operation conditions seem more severe than the low power, none of the conditions illustrated in **Fig. 3-4** are compatible with a continuous operation of the burner head since the manufacturer established a maximum operating temperature of 600 ºC.

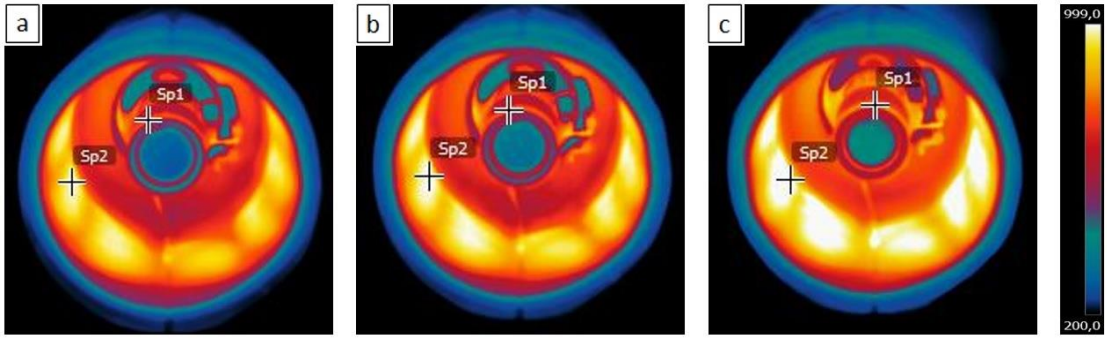

***Fig. 3-4**: Infra-red images of the natural-gas burner, operating at: a) 30% nominal power (Sp1 = 789 ºC and Sp2 = 958 ºC), b) 50% nominal power (Sp1 = 827 ºC and Sp2 > 999 ºC) and c) 70% nominal power (Sp1 = 861 ºC and Sp2 > 999 ºC).*[1]

3.1.5 ORC-evaporator redesign

It seems clear from the previous analysis that one of the ways to solve the safety issue related to the natural-gas burner head overheating is to decrease the temperature of the inner wall of the central combustion chamber. With no reason to drop off any of the initially defined design principles (see section 3.1.1), the creation of a cold wall combustion chamber appears as a fourth characteristic that should be presented by the ORC-evaporator. To achieve this specific characteristic a water-cooled baffled sleeve was considered to be used as a cold surrounding of the natural-gas burner head (instead of the current cylindrical insulation). The schematic representation of a possible ORC-evaporator design with the baffled sleeve can be seen in **Fig. 3-5**. In this solution, the water flows through the sleeve after being pre-heated in the ORC-condenser, reducing the working fluid condensing temperature in this component, which is beneficial for the cycle efficiency. Besides, this fourth specification has the additional advantage of reducing the risk of thermal degradation of the organic fluid [72,186] because it reduces the combustion gases temperature before reaching the organic fluid heat-exchanger section.

[1] Evaluated with an emissivity of 0.9. Sp1 and Sp2 refer to the maximum temperature of the natural-gas burner head and of the surrounding cylindrical wall, respectively.

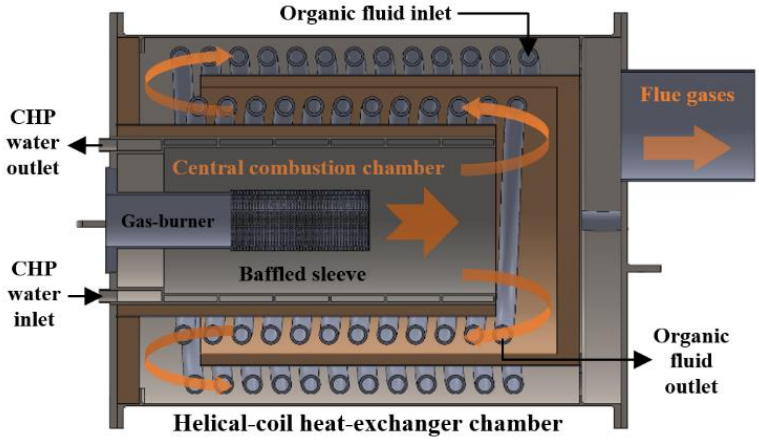

***Fig. 3-5**: Cross-section view of the schematic representation of a possible ORC-evaporator design with the water-cooled baffled sleeve.*

The practical result that comes from the use of such sleeve can be weighed by comparing the infra-red images of the natural-gas burner head operating within a cold surrounding, presented in **Fig. 3-6**, with the infra-red images presented in **Fig. 3-4** (to keep an acceptable colour range in both figures, their temperature scales are different). As can be seen in **Fig. 3-6**, the maximum temperature of the natural-gas burner head is never above 600 ºC, referred by the manufacturer as a safety limit, regardless of the operating power.

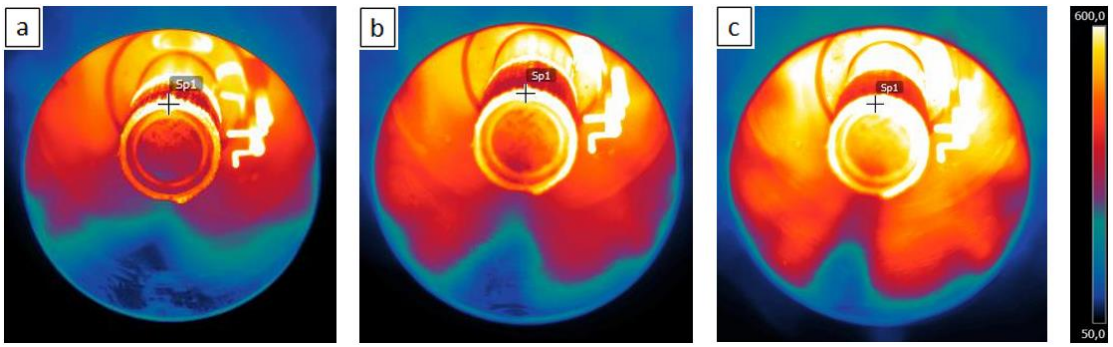

***Fig. 3-6**: Infra-red images of the natural-gas burner within a cold surrounding, operating at: a) 30% nominal power (Sp1 = 503 ºC), b) 50% nominal power (Sp1 = 528 ºC) and c) 70% nominal power (Sp1 = 548 ºC).*[2]

3.2 A hybrid CHP configuration

The schematic configuration of the micro-CHP system, derived from the integration of the new designed ORC-evaporator, is shown in **Fig. 3-7**. This can be described as a hybrid (topping/bottoming) CHP configuration since the useful thermal energy is transferred to the water stepwise - before and after the production of work in the prime mover (expander).

[2] Evaluated with an emissivity of 0.9. Sp1 refers to the maximum temperature of the natural-gas burner head.

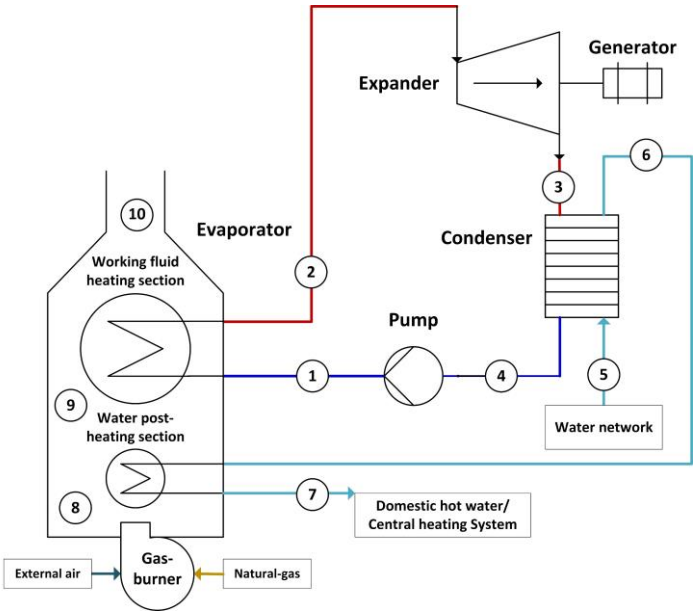

***Fig. 3-7**: Schematic diagram of the hybrid CHP configuration with the new ORC-evaporator.*

The T-s diagrams of the hybrid and standard ORC based CHP configuration, including the combustion gases and water streams, can be found in **Fig. 3-8**. For the same CHP outlet water temperature, the condensing pressure of the ORC in this hybrid configuration may be significantly lower. The well-known advantages of such a decrease of the condensing pressure are an increase of the ORC specific power (net power per unit of working fluid mass flow rate) and an increase of the cycle efficiency. However, these advantages need to be considered against an inevitable reduction of the ORC working fluid mass flow rate that can partially, or totally, hinder them.

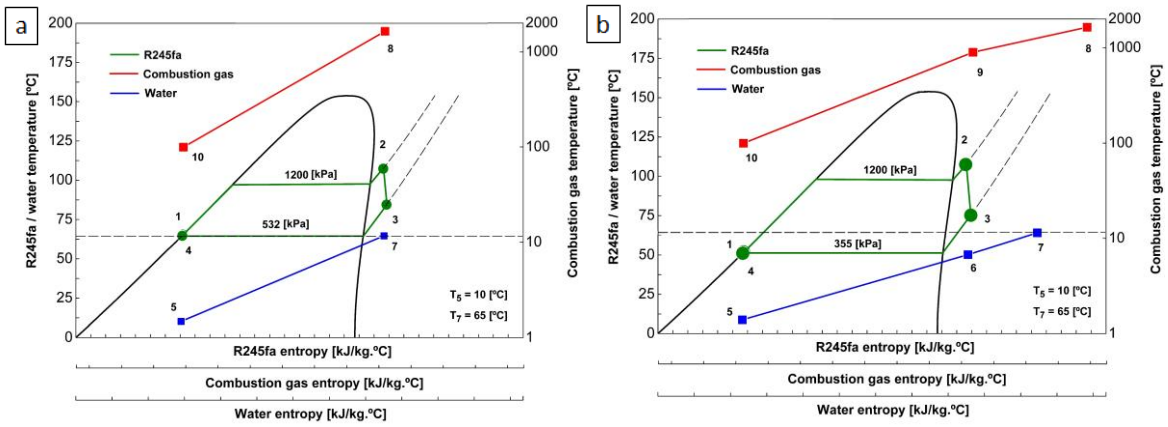

***Fig. 3-8**: T-s diagrams of R245fa ORC based CHP configurations: a) standard and b) hybrid.*

3.2.1 Hybrid CHP model, description and assumptions

In this configuration, the amount of energy transferred to the water in the post-heating section of the ORC-evaporator (see **Fig. 3-7**) is an additional design parameter that needs to be analyzed. To perform such analysis, a physical model of the CHP system, as schematically presented in **Fig. 3-7**, where all the main ORC components are considered working on their nominal

conditions, was developed using Matlab® and the *RefProp* thermodynamic database [187]. The model assumes no heat or pressure losses in the connecting pipes as well as neglects the electro-mechanical inefficiencies for both the pump motor and expander generator.

The input parameters of this model, with the values used or the intervals within they are allowed to vary (in case of a parametric analysis), are listed in **Table 3-1**. Within the list of the input parameters is the water post-heating fraction (θ), defined by the equation (3.1), that can be seen as the fraction of the water heating process that is done in the ORC-evaporator water post-heating section. A value of $\theta = 0\%$ refers to a standard CHP system in which all the water heating process occurs in the ORC-condenser, while a value of $\theta = 100\%$ refers to a situation in which there is no cogeneration or the ORC is not working.

$$\theta = \frac{T_7 - T_6}{T_7 - T_5} \times 100 \tag{3.1}$$

***Table 3-1**: Input parameters of the CHP physical model.*

Model parameter	Symbol	Units	Value
Working fluid	-	-	R245fa
Expander isentropic efficiency	η_T	%	0.75
Pump isentropic efficiency	η_{P1}	%	0.5
Condenser efficiency	η_{CHE}	%	0.98
Evaporator efficiency	η_{EHE}	%	0.9
Maximum ORC pressure	p_{max}	kPa	1200
Working fluid superheating degree	ΔT_2	°C	10
Water pressure	p_w	kPa	300
CHP inlet water temperature	T_5	°C	10 or [10,50] [a)]
CHP outlet water temperature	T_7	°C	65 or [55,85] [a)]
Water post-heating fraction	θ	%	[0,50]
End-user thermal power demand	Q_w	kW	25
Atmospheric pressure	p_{amb}	kPa	101.325
Combustion gases flame temperature	T_{flame}	°C	1540 [b)]
Combustion gases mass flow rate	$\dot{m}_g$	kg/s	0.0137 [b)]
Combustion products mass fraction	m'_{g_j} [c)]	kg_j/kg_g [c)]	[b, d)]

a) Isolated values were used to simulate a specific CHP operating condition (in accordance with the standard [182]) while the intervals were used to perform a system's parametric analysis;
b) The presented values were obtained for complete combustion of natural-gas with 30% of excess of air (according to the natural-gas burner manufacturer recommendation as shown in section 3.1.3);
c) $j = \{CO_2;\ H_2O;\ O_2;\ N_2\}$;
d) $\{m'_{g,CO_2} = 0.123;\ m'_{g,H_2O} = 0.093\ ;m'_{g,N_2} = 0.734;m'_{g,O_2} = 0.051\}$.

The way how the properties of the working fluid, the water or the combustion gases are evaluated at each of the CHP key points is presented in **Table 3-2**. To avoid problems related to the pinch-point in the ORC-condenser, the model assumes that the condensing temperature is limited (inferiorly) by the water temperature at the ORC-condenser exit (see **Table 3-2** where, for point 3, at the expander exit, the pressure is equal to the saturation value defined by the water temperature at the condenser exit, point 6). The knowledge of the enthalpy at those key points allows solving the energy balance equations as they are shown, for each of the CHP main components, in **Table 3-3** from which the CHP behaviour can be inferred and the usual performance indicators can be obtained.

***Table 3-2**: Evaluation of the thermodynamic properties at different CHP key points.*

# [a]	$\boldsymbol{p}$ $[\boldsymbol{kPa}]$	$\boldsymbol{T}$ [℃]	$\boldsymbol{h}$ $[\boldsymbol{kJ/kg}]$	$\boldsymbol{s}$ $[\boldsymbol{kJ/kg}]$	State
1_s [b]	$p_{1i} = p_{max}$	-	$h_{1i} = h(p_{1i}, s_{1s})$	$s_{1s} = s_4$	–
1	$p_1 = p_{max}$	$T_1 = T(p_1, h_1)$	$h_1 = h_4 + \left({}^{h_{1s} - h_4}/_{\eta_P}\right)$	$s_1 = s(T_1, h_1)$	CL
2	$p_2 = p_{max}$	$T_2 = T_{sat}(p_2) + \Delta T_2$	$h_2 = h(T_2, p_2)$	$s_2 = s(T_2, p_2)$	SH
3_s [b]	$p_{3i} = p_3$	-	$h_{3s} = h(p_{3s}, s_{3i})$	$s_{3s} = s_2$	–
3	$p_3 = p_{sat}(T_6)$	$T_3 = T(p_3, h_3)$	$h_3 = h_2 - \eta_T \times (h_2 - h_{3s})$	$s_3 = s(h_3, p_3)$	SH
4	$p_4 = p_3$	$T_4 = T(p_4, x_{v_4})$	$h_4 = h(T_4, p_4)$	$s_4 = s(T_4, x_{v_4})$	SL
5	$p_5 = p_w$	T_5	$h_5 = h(T_5, p_5)$	–	–
6	$p_6 = p_w$	$T_6 = T_7 - \theta \times (T_7 - T_5)$	$h_6 = h(T_6, p_6)$	–	–
7	$p_7 = p_w$	T_7	$h_7 = h(T_7, p_7)$	–	–
8	$p_8 = p_{amb}$	$T_8 = T_{flame}$	$h_8 = h(T_8, p_8)$	–	–
9	$p_9 = p_{amb}$	$T_9 = T(p_9, h_9)$	$h_9 = h_8 - \dot{Q}_{w_{PH}}/\dot{m}_g$	–	–
10	$p_{10} = p_{amb}$	$T_{10} = T(p_{10}, h_{10})$	$h_{10} = h_9 - \dot{Q}_{in}/\dot{m}_g$	–	–

[a] In accordance with Fig. 3-7;
[b] Correspond to an intermediate calculation for the isentropic thermodynamic condition.

***Table 3-3**: Power balance equations of the CHP system.*

CHP component [a)]	Stream	Power balance
Pump	ORC working fluid	$\dot{W}_{in} = \dot{m}_f \times (h_1 - h_4)$
Working fluid heating section (ORC-evaporator)	ORC working fluid	$\dot{Q}_{in} = \dot{m}_f \times (h_2 - h_1)$
	Combustion gases	$\dot{Q}_{g_f} = \left(\dot{m}_g \times (h_9 - h_{10})\right)/\eta_{EHE}$
Water post-heating section (ORC-evaporator)	Water	$\dot{Q}_{w_{PH}} = \dot{m}_w \times (h_7 - h_6)$
	Combustion gases	$\dot{Q}_{g_w} = \left(\dot{m}_g \times (h_8 - h_9)\right)/\eta_{EHE}$
Expander	ORC working fluid	$\dot{W}_{out} = \dot{m}_f \times (h_2 - h_3)$
Condenser	ORC working fluid	$\dot{Q}_{out} = \dot{Q}_{w_{CHE}}/\eta_{CHE}$
	Water	$\dot{Q}_{w_{CHE}} = \dot{m}_w \times (h_6 - h_5)$
Hybrid CHP system	Natural-gas/air mixture	$\dot{Q}_{CHP} = \dot{Q}_{g_f} + \dot{Q}_{g_w}$
	Water	$\dot{m}_w = \dot{Q}_w/(h_7 - h_5)$
	ORC working fluid	$\dot{m}_f = \dot{Q}_{out}/(h_3 - h_4)$

[a)] In accordance with Fig. 3-7.

Among these indicators are the ORC efficiency (η_{ORC}), equation (3.2), the ORC net power output ($\dot{W}_{net}$), equation (3.3), and the Primary Energy Savings (PES), defined by the EU directive [188] and calculated using equation (3.4). In this, η_{REF_H} and η_{REF_E} are harmonized efficiency reference value for separate production of heat (for this work was assumed 0.9 considering that the thermal energy produced is in the form of hot water from a natural-gas boiler manufactured before 2016 [189]) and the harmonized efficiency reference value for separate production of electricity (for this work was assumed 0.445, considering that the electrical energy is produced in a natural-gas fueled power plant built before 2012 and an aggregated correction factor that includes the climatic specificities and the grid losses for low-voltage level end-users [189]). The values of η_{CHP_H} and η_{CHP_E}, that represent the thermal and electrical efficiencies of the CHP systems, respectively, are calculated by equation (3.5). Besides that, two non-dimensional parameters, the $rPES$ and the $r\dot{W}_{net}$, that relate the values obtained for the hybrid configuration (CHP system with $\theta \neq 0\%$) with those obtained for the standard configuration (CHP system with $\theta = 0\%$), see equation (3.6), and the reduction of the combustion gases temperature associated with the energy transfer in the water post-heating section of the ORC-evaporator ($T_8 - T_9$), are also retrieved from the model.

$$\eta_{ORC} = \frac{\dot{W}_{out} - \dot{W}_{in}}{\dot{Q}_{in}} \times 100 \tag{3.2}$$

$$\dot{W}_{net} = \dot{W}_{out} - \dot{W}_{in} \tag{3.3}$$

$$PES = \left(1 - \left(\frac{1}{\left(\frac{\eta_{CHP_H}}{\eta_{REF_H}} + \frac{\eta_{CHP_E}}{\eta_{REF_E}}\right)}\right)\right) \times 100 \tag{3.4}$$

$$\eta_{CHP_H} = \frac{\dot{Q}_{w_{PH}} + \dot{Q}_{w_{CHE}}}{\dot{Q}_{CHP}}, \qquad \eta_{CHP_E} = \frac{\dot{W}_{out} - \dot{W}_{in}}{\dot{Q}_{CHP}} \tag{3.5}$$

$$rPES = \frac{PES\ (\theta)}{PES\ (\theta = 0)}, \qquad r\dot{W}_{net} = \frac{\dot{W}_{net}(\theta)}{\dot{W}_{net}(\theta = 0)} \tag{3.6}$$

3.2.2 Hybrid CHP model results

The variation's effect of the water post-heating fraction (θ) over the ORC net specific work ($\dot{W}_{net}/\dot{m}_f$), the ORC efficiency (η_{ORC}) and the ORC working fluid mass flow rate ($\dot{m}_f$) is shown in **Fig. 3-9**. As expected, mainly due to the increase of the pressure (and temperature) difference experimented by the working fluid when passing through the expander, the net specific work and the efficiency of the cycle increased with θ. However, since an increasing part of the water heating process is shifted from the ORC-condenser to the post-heating section of the ORC-evaporator, an inevitable reduction of the working fluid mass flow rate with θ is observed. The non-despicable result of these antagonistic variations is presented in **Fig. 3-10**, where the values of PES and $\dot{W}_{net}$ are shown as a function of θ. In this operating condition, the maximum positive variations of PES and $\dot{W}_{net}$ are 23% and 7% for values of θ equal to 33% and 21%, respectively. The shifting of part of the water heating process from the ORC-condenser to the post-heating section of the ORC-evaporator allows to solve a safety issue that will permit the adoption of a compact ORC-evaporator design and also induces positive effects in the CHP performance increasing not only the efficiency (an increase of PES) and economic (an increase of $\dot{W}_{net}$) figures in comparison with the standard configuration (for which $\theta = 0\%$).

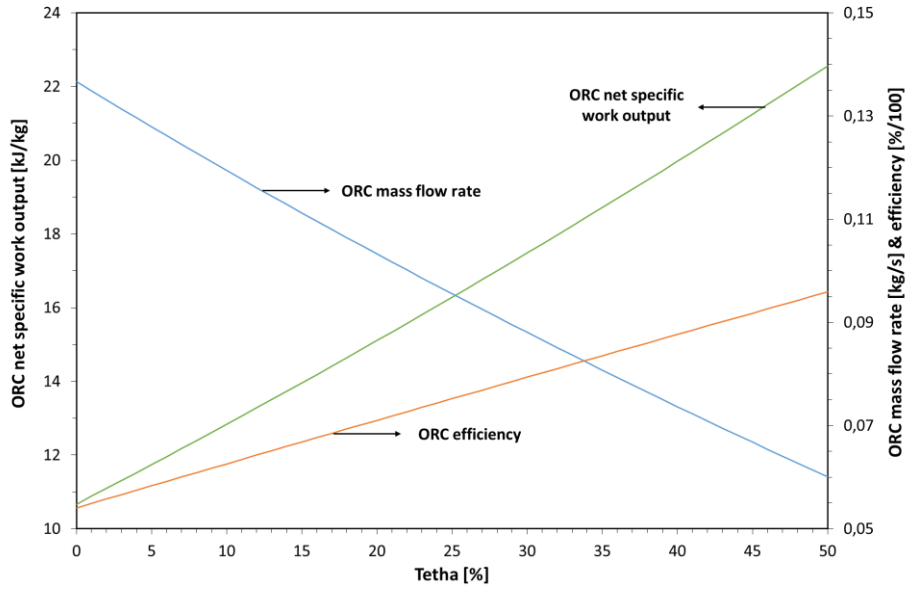

***Fig. 3-9**: ORC net specific work output, $\dot{m}_f$ and η_{ORC} as a function of θ for the conditions referred in **Table 3-1** (T_5 = 10ºC and T_7 = 65ºC).*

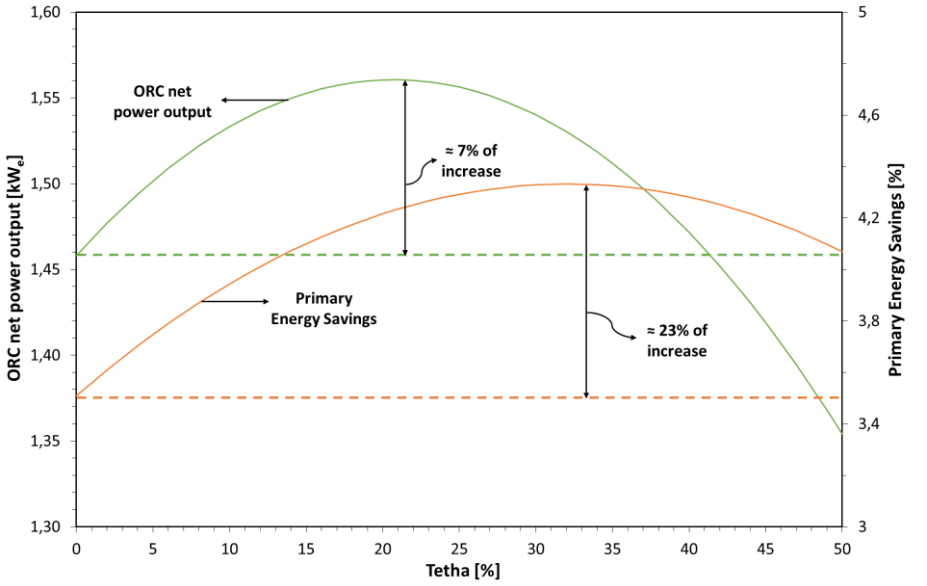

***Fig. 3-10**: PES and $\dot{W}_{net}$ as a function of θ for the conditions referred in **Table 3-1** (T_5 = 10ºC and T_7 = 65ºC).*

The values of θ for which PES and $\dot{W}_{net}$ have a maximum, designated as optimal θ_{PES} and optimal $\theta_{\dot{W}_{net}}$, are shown in **Fig. 3-11** and **Fig. 3-12**, respectively, for several CHP inlet and outlet water temperatures. The corresponding absolute (maximum) and relative values of those performance parameters are also displayed in those figures. Regardless of the performance parameter, the optimal θ increase with the CHP water inlet and outlet temperature difference. For the limit operation condition presented, in which this difference is 75 ºC, the optimal θ_{PES} can almost reach 50% while the optimal $\theta_{\dot{W}_{net}}$ is about 40%. For these values of θ, $rPES$ and $r\dot{W}_{net}$ are around 11 and 2, respectively. This means that the value of PES would be around 11 times bigger than the

value obtained in a standard CHP configuration if 50% of the water heating process is shifted from the ORC-condenser to the water post-heating section of the ORC-evaporator while the value of $\dot{W}_{net}$ would be around 2 times bigger if 40% of the water heating process is shifted. Lower values of CHP water inlet and outlet temperature difference lead, however, to situations where the optimal θ, regardless of the performance parameter, is 0. In those cases, their relative variations are equal to 1 and so there is no benefit in splitting the water heating process between the ORC-condenser and the water post-heating section of the ORC-evaporator. The values of those cases (when optimal θ is equal to 0) are neither show in **Fig. 3-11** nor in **Fig. 3-12**.

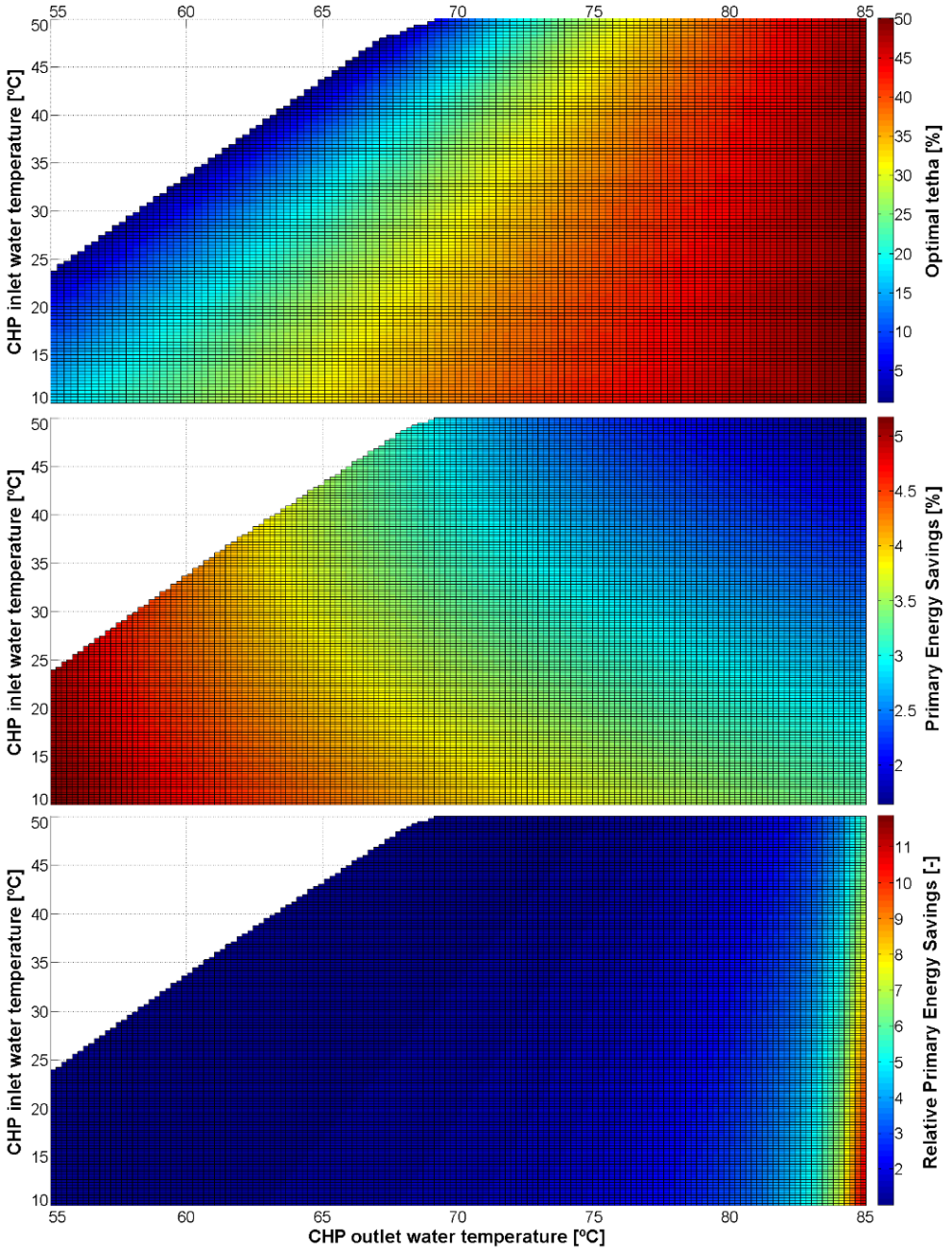

***Fig. 3-11**: Optimal θ_{PES} and corresponding (maximum) values of PES and $rPES$ for several inlet and outlet CHP temperatures.*

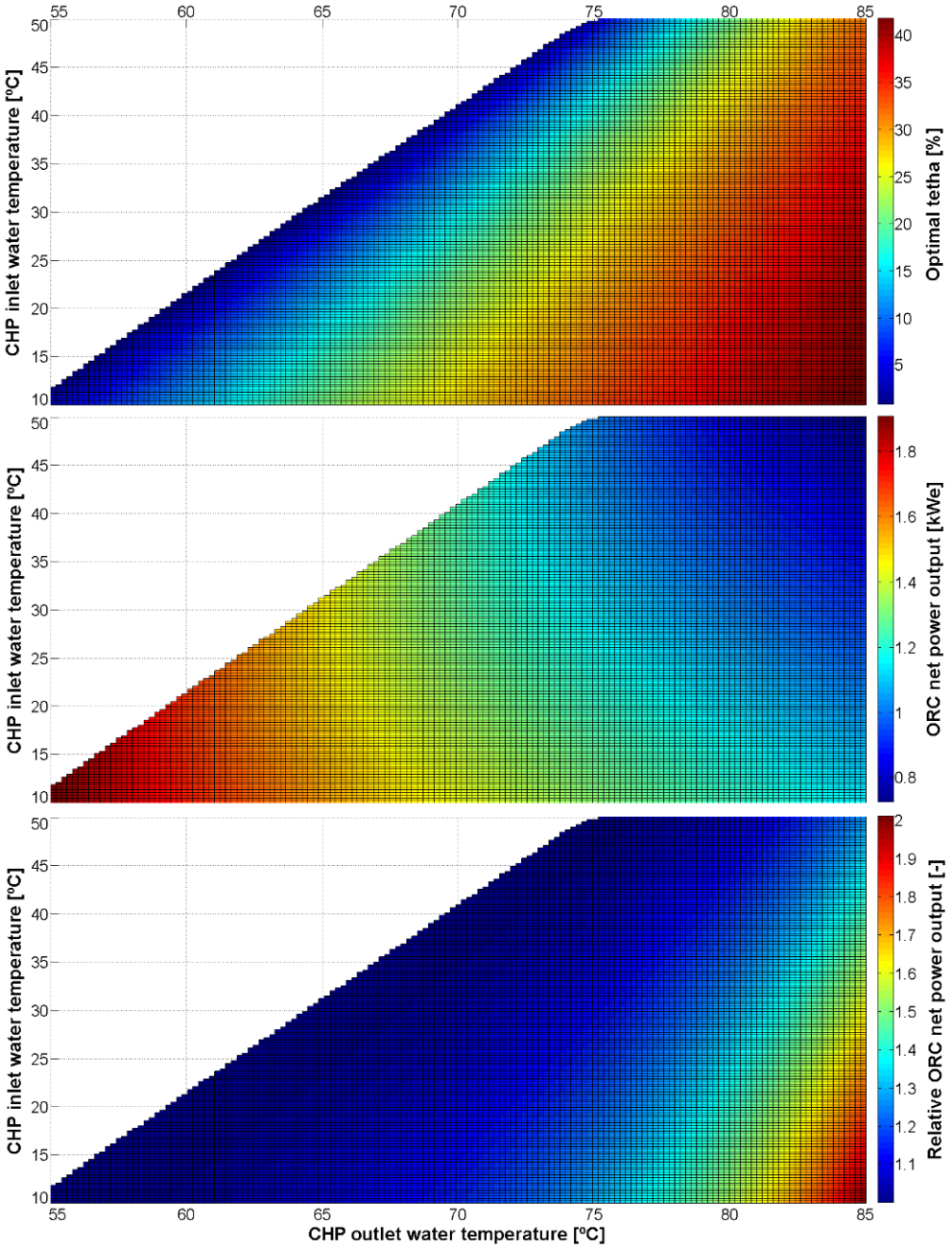

***Fig. 3-12**: Optimal $\theta_{\dot{W}_{net}}$ and corresponding (maximum) values of $\dot{W}_{net}$ and $r\dot{W}_{net}$ for several inlet and outlet CHP temperatures.*

If, attending to safety and/or control simplicity design requirements, the value of θ is fixed at, e.g. 15% for the all range of the CHP operating conditions (water inlet and outlet temperatures), the values of $rPES$ and $r\dot{W}_{net}$ will vary from about 0.89 to 6.7 and from 0.86 to 1.6 as shown in **Fig. 3-13** and in **Fig. 3-14**, respectively. Even in that situation, both of the performance parameters continue to show improvements in a significant part of the CHP operating conditions (bigger for PES than for $\dot{W}_{net}$).

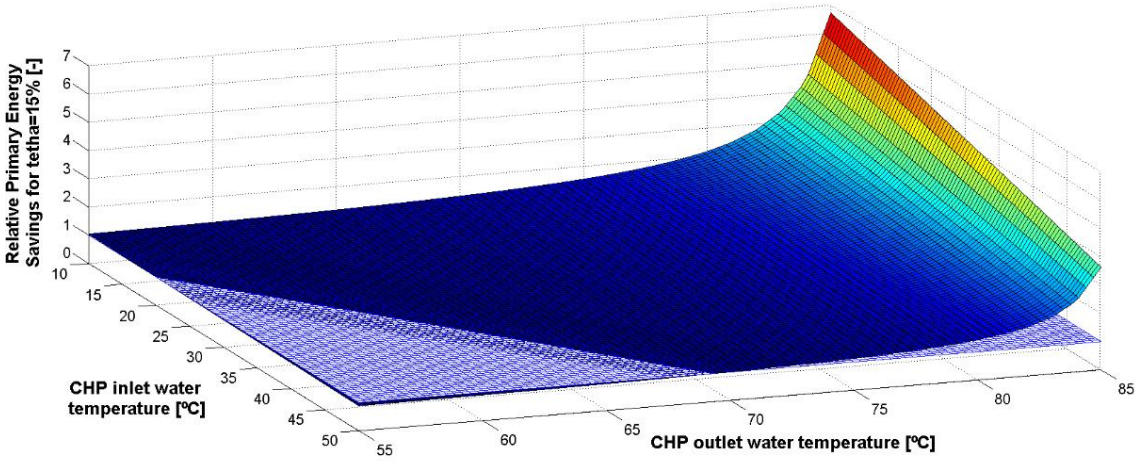

Fig. 3-13: *$rPES$ for θ = 15% and for several inlet and outlet CHP temperatures.*

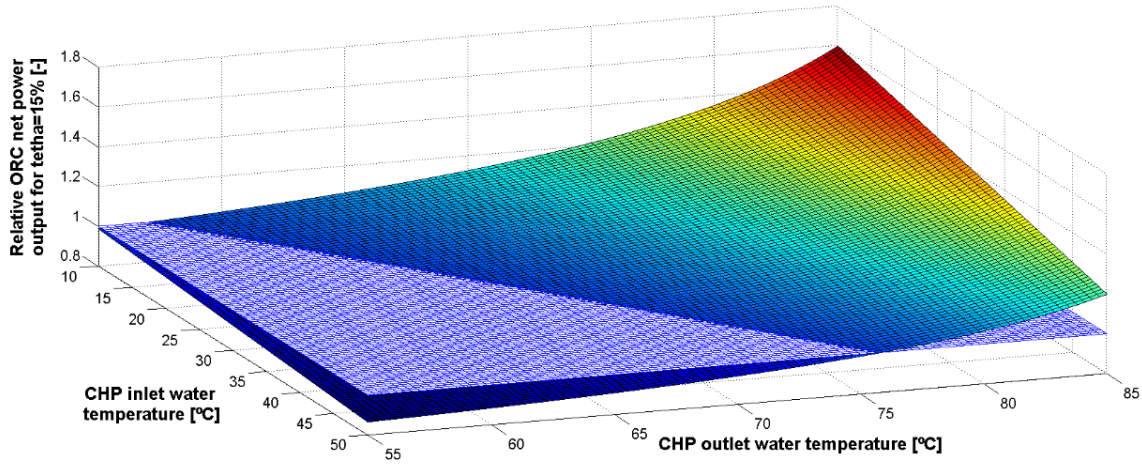

Fig. 3-14*: $r\dot{W}_{net}$ for θ = 15% and for several inlet and outlet CHP temperatures.*

Moreover, the proposed hybrid configuration presents as an additional advantage, a reduction of the risk of thermal degradation of the ORC working fluid that arises from a significant temperature reduction of the hot combustion gases on their passage through the water post-heating section of the ORC-evaporator. For the same CHP operating conditions as those used to obtain the results shown in **Fig. 3-9** and **Fig. 3-10**, the combustion gases temperature reduction for the value of θ that maximizes PES is about 420 ºC and for the value of θ that maximizes $\dot{W}_{net}$ is about 260 ºC. However, for this particular operating condition, that value can be increased without any efficiency or net power output losses regarding the standard CHP configuration ($\theta = 0\%$) to more than 500 ºC if θ is increased to around 41%, as shown in **Fig. 3-15**.

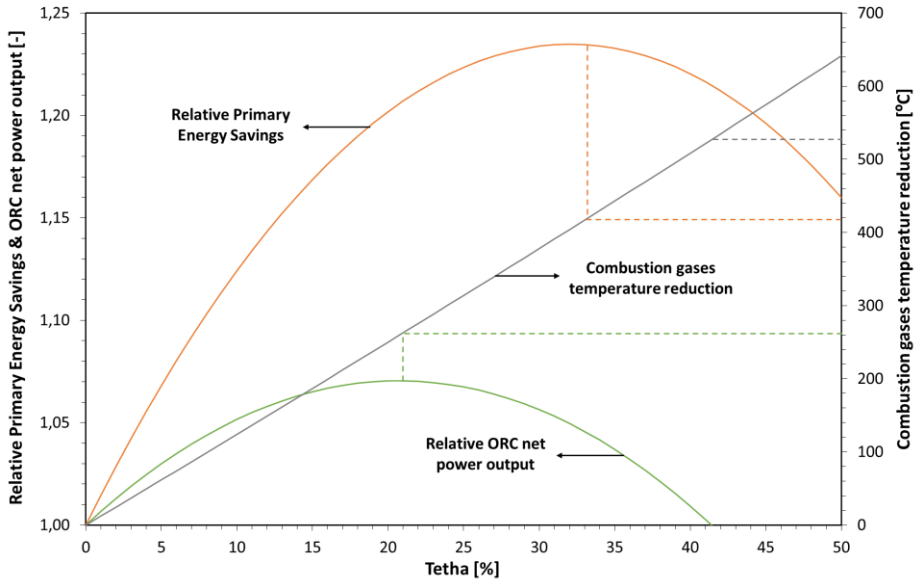

***Fig. 3-15**: $rPES$, $r\dot{W}_{net}$ and combustion gases temperature reduction as a function of θ for the conditions referred in **Table 3-1** (T_5 = 10ºC and T_7 = 65ºC).*

3.3 Concluding remarks

The development of ORC based micro-CHP systems aiming to retrofit the current combi-boilers demands for small dimension, high efficiency and high turn-down ratio evaporators. To achieve such requirements, the design principles of those ORC-evaporators should include: i) direct vaporization, ii) counter-flow arrangement and iii) pre-mixed burners. A solution of an ORC-evaporator accomplishing these specifications was presented. That solution showed important safety problems that led to a fourth design principle: iv) the need for a cold surrounding on the natural-gas burner head. This last design principle led to the development of an ORC-evaporator where part of the energy contained in the combustion gases is transferred to the water before they reach the ORC working fluid heat-exchanger. The integration of such an ORC-evaporator in the CHP system gave origin to a hybrid configuration in which the useful thermal energy transferred to the water is done stepwise: firstly, in the ORC-condenser and then in the water post-heating section of the ORC-evaporator. Such configuration, since it reduces the average temperature at the ORC-condenser, increases the cycle efficiency and the net specific work from which results, even taking into consideration the negative effect of the associated organic fluid mass flow rate reduction, for a significant part of the CHP operating conditions, an increase of the primary energy savings and the ORC net power output. Furthermore, the temperature reduction of the combustion gases in the water post-heating section of the ORC-evaporator for one of the most characteristic CHP operating condition (T_5 = 10 ºC, T_7 = 65 ºC) can be as high as 520 ºC without any losses in the primary energy savings or the ORC net power output. This temperature reduction can help prevent, in a significant way, the occurrence of one of the major concerns associated with the direct vaporization of the ORC

working fluid: the risk of thermal degradation. Therefore, the fraction of the CHP water heating process performed in the post-heater becomes a new design parameter that needs to be taken into account not only for the ORC-evaporator but to all of the CHP components which must be accordingly selected or designed. Besides, this hybrid configuration also applies to all the situations where the difference between the temperature of hot and cold sources is smaller as when water from non-pressurized biomass (or other fuels) boilers is used to power those CHP systems.

3.4 Postface

The ORC-evaporator design shown as an example in **Fig. 3-5** was not considered for the continuation of this research because it will lead to a high dimension and heavy solution (which is not advisable for the residential market). For this reason, a compact design with finned tubes was selected for both (to design a hybrid CHP configuration) heat-exchangers of the ORC-evaporator, as shown in **Fig. 3-16**. In this, the combustion gases will flow in a vertical direction from top to bottom and are produced by a premix natural-gas burner with a rectangular flat head to better suit the heat-exchangers' design. The datasheet of the natural-gas burner (model: BurnerTech VAPAC 40) and its technical drawings are shown in Annex B. A water post-heater (PH) made up of a pair of copper finned tubes is placed between the natural-gas burner and the organic fluid heat-exchanger (EHE). In its turn, the EHE is made up of stainless-steel tubes with circular copper fins.

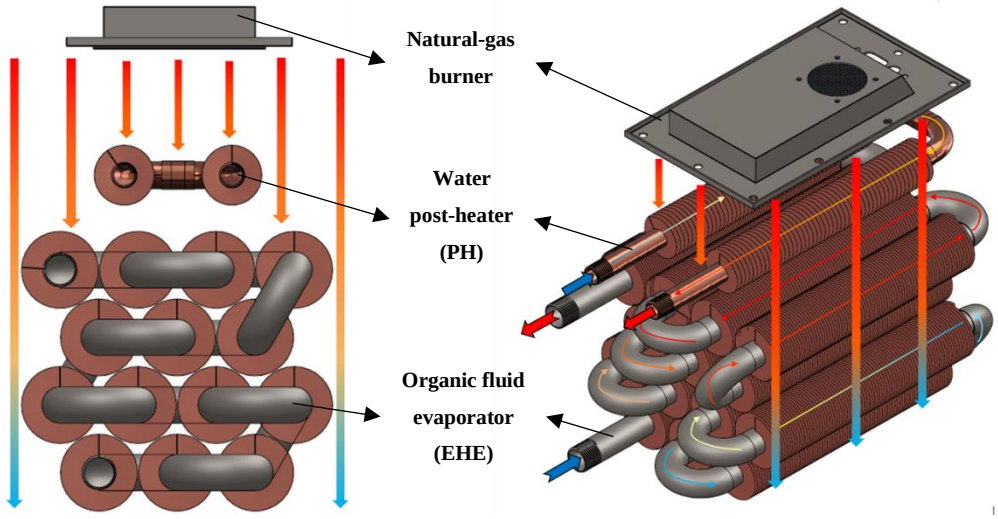

***Fig. 3-16**: Schematic representation of the two heat-exchanger sections and the natural-gas burner of the ORC-evaporator.*

The two heat-exchangers of the ORC-evaporator are essentially finned tubes welded to standard elbows. Since the EHE was designed to withstand medium pressures (≈ 15 bar), the welding process was verified through a penetrating liquid test. That test allows the identification of surface discontinuities such as cracks, pores and folds. It consists in using a penetrating liquid spray (a fluid capable to penetrate in very reduced openings) into the possible surface discontinuity - the welding

parts. After that, the excess of that penetrating liquid is removed and a revealing spray (a fluid that interacts with the penetrating liquid) is then applied to identify the surface discontinuities. Some photographs of the penetrating liquid test on the EHE welding parts are shown in **Fig. 3-17**.

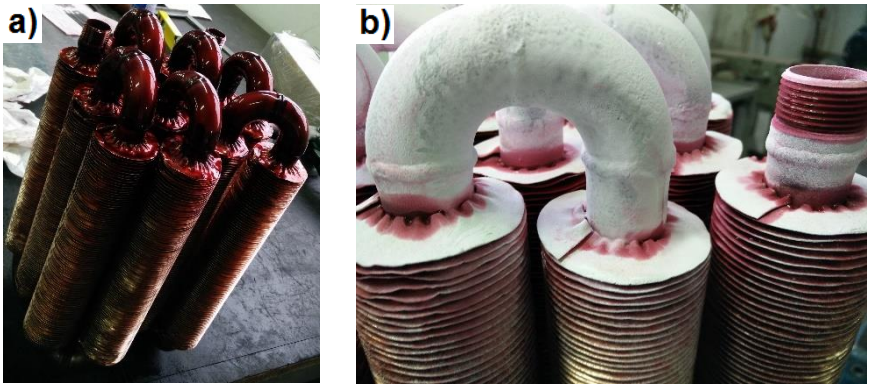

***Fig. 3-17**: Photographs of the penetrating liquid test on the EHE welding parts: a) application of the penetrating liquid and b) application of the revealing spray.*

In addition to the heat-exchangers, the ORC-evaporator has a series of metallic plates (the shell) which define the physical boundaries of the combustion gases control volumes. Its design takes into account several empirical concepts: i) a good fit to the heat-exchangers and natural-gas burner design to reduce the free flow area of the combustion gases and consequently increase the heat transfer coefficient, ii) only the part of the tubes with fins is in contact with the combustion gases flow (the elbows stay outside of the combustion gases control volumes to easily install temperature sensors in those), iii) the PH and the EHE section must be built separately to allow a possible substitution and iv) several general requests like the construction of inspection windows, ensure the safety distances (e.g. the distance between the natural-gas burner and the closest heat-exchanger), an appropriate exit for the condensation of the combustion gases and an efficient and simple insulation project. From these concepts arise the ORC-evaporator design presented in **Fig. 3-18**. Photographs of the assembly between the natural-gas burner, the heat-exchangers and some parts of the ORC-evaporator are shown in **Fig. 3-19**. A 3D step and the technical drawings produced for the construction of the ORC-evaporator are shown in Appendix D.

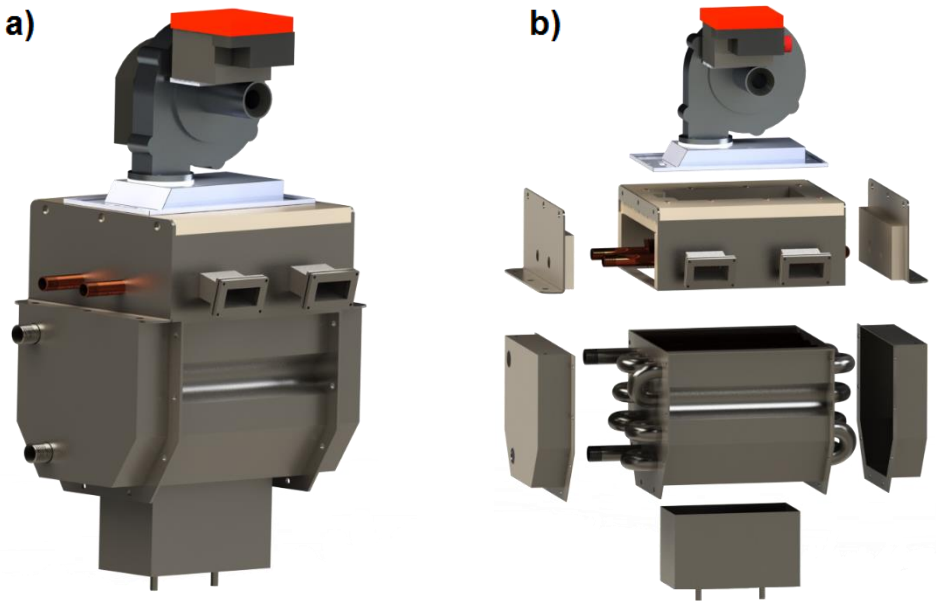

***Fig. 3-18**: Schematic representation of the ORC-evaporator: a) collapse and b) exploded view.*

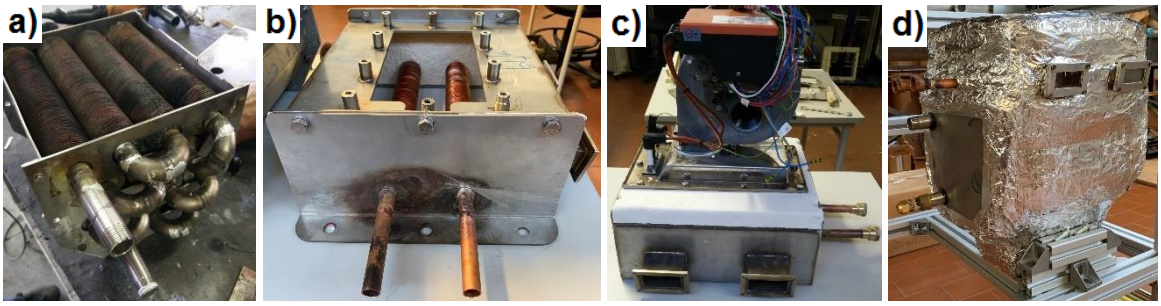

***Fig. 3-19**: Photographs of the ORC-evaporator: a) circular finned tubes and curves of the EHE; b) finned tubes and support plates of the PH; c) PH and natural-gas burner assembly with the inspection windows; d) ORC-evaporator assembly with insulation and without the natural-gas burner.*

A part of this research was inserted in a national R&D project named "HEBE - Caldeira doméstica para produção combinada de água quente e electricidade" that involves the design, construction and characterization of an ORC based micro-CHP natural-gas boiler prototype for the residential market. This project is carried out by 2 Portuguese companies (Sciven Lda and Active Space Technology SA) and 2 research institutions (the University of Coimbra and the Higher Technical Institute of Lisbon). Since this project must comply with its deadlines, the first geometric design of this new compact ORC-evaporator was made using several (unrefined) assumptions and the well-known Effectiveness - Number of Transfer Units (ε-NTU) method to quickly proceed to its physical construction. The ε-NTU methodology is not presented in this thesis because it has no interest for this investigation nor novelty. Nonetheless, a detailed heat transfer mathematical model that accurately predicts its throughout and complex behaviour (as well as presents several outputs like the temperature of the internal surface of the ORC-evaporator tubes in contact with the organic fluid which can be a very important indication regarding the risk thermal degradation) is extremely pertinent and its development is presented in the next chapter.

This page is intentionally left blank.

Chapter 4 Modelling and experimental validation of the heat transfer processes of a direct vaporization evaporator for thermal degradation risk assessment

- *"Let us dismiss the question, 'Have you proven that your model is valid?' with a quick NO. Then let us take up the more rewarding and far more challenging question: 'Have you proven that your model is useful for learning more about your system?' … "* (**James B. Mankin**)

Summary: *The development of a physical model of the combustion and heat transfer processes of the direct vaporization ORC-evaporator developed in the previous chapter, together with a thorough description of the methodology used in its calibration and experimental validation, are presented in this chapter. This model has the objective of performing a thorough evaluation of several key features of the combustion and heat transfer processes (e.g. the natural-gas burner combustion power or the organic fluid mass flow rate) as a function of some ORC operating parameters. Among those is the temperature of the internal surface of the tubes with which the organic fluid is in contact. This temperature can then be used to make considerations regarding the risk of the thermal degradation of the organic fluid.*

4.1 Framework and motivation

As justified in the previous chapters, the ORC based CHP systems appears to be the best choice to retrofit the current domestic wall-hang combi-boilers. Therefore, to deal with its extremely demanding requirements, especially in what refers to the (short) response time and (small) dimensions, it is suggested that the vaporization of the working fluid of the ORC should be done using the high-temperature combustion gases directly [190]. One of the major risks associated with this option is the thermal degradation of the organic working fluid [72,191]. The high temperature that these fluids may reach when in contact with the heat transfer surfaces can lead to the disruption of the chemical bonds of its molecules and the subsequent degradation of its physical properties. In an attempt to minimize this problem, ORC based micro-CHP systems may be reconfigured into a hybrid arrangement in which the combustions gases are firstly cooled in a combustion gases-water heat-exchanger before crossing through the organic fluid heat-exchanger as demonstrated in the previous chapter. Even so, the evaluation of the magnitude of this problem demands the calculation of the heat transfer surfaces' temperature with which the organic fluid will be in contact. That risk will be minimum if the temperature of those surfaces is kept below the one of thermal degradation. This limiting temperature, however, is normally determined by standard tests where the fluid is at rest and in thermal equilibrium with the wall of its container [186,192–195]; a quite different situation from what happens in real working conditions. Besides the bulk temperature of the organic

fluid at the exit of the evaporator (a well-known parameter since it is easy to measure and required for the evaluation of the cycle efficiency), it is also important to know the temperature of the heat transfer surfaces with which the fluid is in contact. Contrary to the organic fluid temperature, this is very difficult to measure but it can, and should, be controlled. Despite its importance, heat transfer surface temperatures are rarely measured or calculated. Since its direct measure is very difficult, as are those of any tubes' internal surface, the only option left is its estimation. That, however, is far from being trivial as it results from the mutual dependency of the internal and external heat transfer mechanisms and demands the development of an appropriate heat transfer model. The development of such a model, which is crucial for the determination of the operating conditions that should keep the risk of thermal degradation of the organic fluid at an acceptable level, however, is not yet described in the literature. This will be illustrated in the particular case of the ORC-evaporator design presented in the last chapter but the analysis will be kept as general as possible. Given the importance that the evaluation of the heat transfer surface temperatures may have on the definition of boundaries for the operating conditions, and given the scarcity of heat transfer models intended to calculate those temperatures, it is also an objective of this manuscript to contribute to the disclosure and widespread of these type of models through the presentation of the approach followed in its development, namely: disclosing the correlations used for the determination of the heat transfer coefficients and duly presenting the underlying simplifications, calibration and validation.

4.2 Evaporator heat transfer model layout

The ORC-evaporator domain to be simulated in this study comprises the natural-gas burner and the two mentioned heat-exchanger sections: the water post-heater section (PH) and the organic fluid evaporator section (EHE) as shown in **Fig. 3-16**. As the PH and the EHE heat transfer models demand, as input parameters, several combustion gases' characteristics (e.g. the combustion gases composition and mass flow rate), the thermochemical calculations of the natural-gas (NG) combustion process were also included in the overall model. Thus, the overall model includes three different sub-models: i) the natural-gas burner/combustion model, ii) the PH heat transfer model and iii) the EHE heat transfer model. These models were implemented in MatLab® while the values of the thermodynamic properties needed for the calculations were assessed from the *RefProp* database [187]. According to the physical arrangement, the models are run sequentially since the outputs of the combustion model are used as inputs for the PH heat transfer model and its outputs are used as inputs of the EHE model, as shown in **Fig. 4-1**.

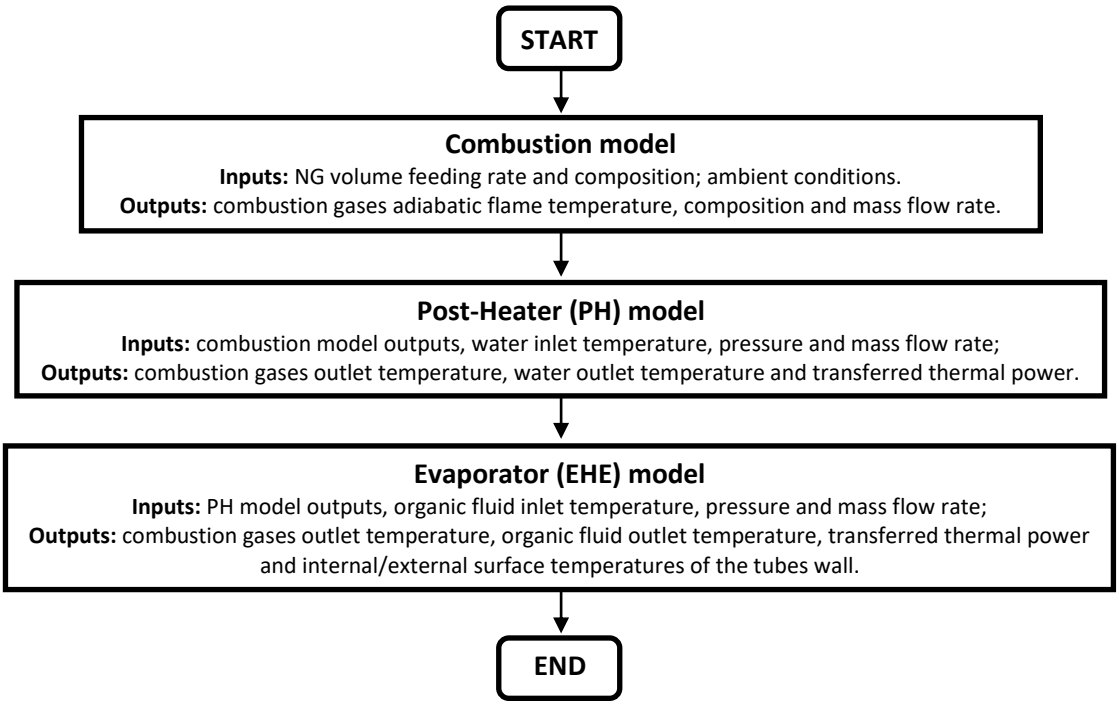

***Fig. 4-1**: General flowchart of the ORC-evaporator model with the main inputs and outputs.*

4.3 Natural-gas burner and combustion model

The objective of this model is to provide the inputs required by the subsequent calculations on the following characteristics of the combustion gases: i) the adiabatic flame temperature, ii) the mass flow rate and iii) the molar fraction of each one of its components. The combustion process to be modelled is a pre-mixed, lean, natural-gas and air mixture. Based on experimental evidence, the combustion process is admitted to be complete (CO volume fraction in the combustion products is below 5 ppm for the entire power range of the burner [7 – 35 kW]) and, for the sake of simplicity, no dissociation of the combustion products is considered. The main input variable of this model is the natural-gas volume feeding rate. Furthermore, a series of extra input variables are required: i) room air temperature and humidity; ii) natural-gas composition, temperature and pressure and iii) excess of air with what the combustion takes place. Regarding this last parameter, a previous experimental characterization of the natural-gas burner operating conditions has allowed to find the dependence between the natural-gas volume feeding rate ($\dot{V}_{NG}$) and the excess of air (λ_{air}), graphically shown in **Fig. 4-2**. This dependence is well described by a third-order polynomial equation.

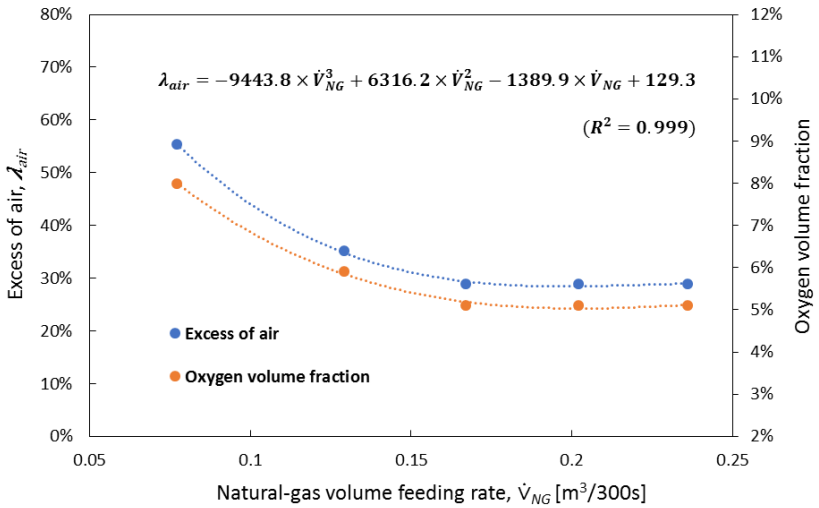

***Fig. 4-2**: Excess of air of the combustion process and oxygen volume fraction of the combustion products as a function of the natural-gas volume feeding rate.*

After knowing these values, the determination of the stoichiometric coefficients of the combustion reaction (see equation (4.3.1)) can be done using the number of atoms conservation principle for each one of the chemical species presented. In that equation, NG stands for the natural-gas chemical composition, n_x is the stoichiometric coefficient of each of the molecular species presented in the reaction, while δ is the number of water molecules per 4.76 molecules of dry air.

$$NG + n_{air}(O_2 + 3.76N_2 + \delta \times H_2O) = n_{CO_2} \times CO_2 + n_{O_2} \times O_2 + n_{N_2} \times N_2 + n_{H_2O} \times H_2O \quad (4.3.1)$$

Once the values of n_x are determined, the energy released in the combustion of a kmol of natural-gas ($\overline{q}_{NG}$) can be obtained using the equation (4.3.2) where $\overline{h}_R$ and $\overline{h}_P$ are, respectively, the combustion reactants and the combustion products' total specific enthalpy.

$$\overline{q}_{NG} = \sum n_R \times \overline{h}(T,p)_R - \sum n_P \times \overline{h}(T,p)_P \quad (4.3.2)$$

The combustion power ($\dot{Q}_g$) and the combustion gases' mass flow rate ($\dot{m}_g$) can then be calculated using equations (4.3.3) and (4.3.4), respectively. In these equations, M_{NG} is the molar mass of the natural-gas, AF is the air-to-fuel ratio of the combustion process and $\dot{m}_{NG}$ is the natural-gas mass consumption rate.

$$\dot{Q}_g = \frac{\overline{q}_{NG}}{M_{NG}} \times \dot{m}_{NG} \quad (4.3.3)$$

$$\dot{m}_g = \dot{m}_{NG} \times (1 + AF) \quad (4.3.4)$$

Finally, the adiabatic flame temperature ($T_{g_{flame}}$) is calculated by the model, which is the one that equals the combustion product's and the reactants' enthalpies (see equation (4.3.5)).

$$\left\langle T_{g_{flame}} = T_P \;\middle|\; \sum n_R \times \overline{h}(T,p)_R = \sum n_P \times \overline{h}(T,p)_P \right\rangle \quad (4.3.5)$$

4.4 Post-heater (PH) model

The Post-Heater (PH) is a cross-flow heat-exchanger placed between the natural-gas burner and the EHE (see **Fig. 3-16**). It is composed of a pair of finned tubes within which water, previously heated in the ORC-condenser, flows. The main objective of this model is the evaluation of the combustion gases' temperature decrease resulting from the energy transfer to the water and from the energy losses through the external walls. The input variables of this model are not only the outputs of the combustion model, such as the adiabatic flame temperature, the combustion gases' chemical composition and their mass flow rate but also the water temperature, mass flow rate and pressure at the PH inlet section.

To achieve the abovementioned objective, the overall heat transfer coefficient (U) must be determined. This demands the calculation of the heat transfer coefficient (h) for the water and combustion gases sides. In order to make that determination easier and since it is known that the water inside the PH tubes will remain in the liquid state and its temperature will not drastically rise, the water's physical domain was divided into two control volumes (CV) – one for each tube. For the combustion gases side, however, the physical domain was not divided and the temperature is assumed to have a uniform/ homogeneous distribution in the horizontal direction. Associated with this discretization, two internal and one external heat transfer coefficients will be determined, resulting in two values of the overall heat transfer coefficient. The CVs in which the PH domain is divided are illustrated in **Fig. 4-3**. The model considers steady-state operating conditions, no pressure losses for both fluid streams and no heat transfer by conduction in the tubes' wall along the axial direction. However, the ORC-evaporator is not an adiabatic component, so the thermal energy losses to the surroundings must be taken into account.

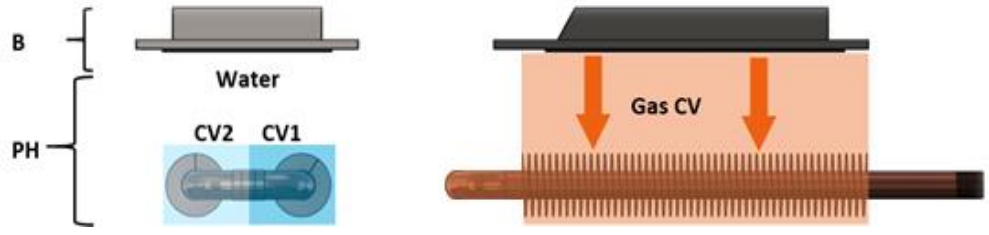

***Fig. 4-3**: 2D view of the natural-gas burner (B) and PH assembly with the CVs defined for the water and combustion gases flow.*

4.4.1 Thermal energy losses to the surroundings

Based on an exploratory experimental characterization previously conducted, which included a global energy balance made to the ORC-evaporator, the energy losses through the walls were found to be a near-constant fraction of the combustion power $\dot{Q}_g$. The average value of that fraction is 7 %. These losses, however, are not evenly distributed along the ORC-evaporator surface since the upper part of it, corresponding to the PH section, not only concentrates the non-insulated parts (e.g.: some of the natural-gas burner surfaces that need to be cooled for safety reasons, and the flame inspection windows – see **Fig. 3-19**), but also because it is where the combustion gases' higher temperatures are verified. Due to these reasons, it was empirically assumed that 75 % of those thermal losses occur in the PH section while the remaining happen in the EHE section. It was also assumed that those losses occur prior to any energy transfer from the combustion gases to the water. Consequently, the temperature of the combustion gases entering the PH ($T_{g_{PH_{in}}}$) is not the adiabatic flame temperature but the one that, accounting for those losses, verify the equation (4.4.1).

$$h(T,p)_{g_{PH_{in}}} = h(\mathrm{T},p)_{g_{flame}} - \frac{\left(\dot{Q}_g \times 0.07 \times 0.75\right)}{\dot{m}_g} \tag{4.4.1}$$

Besides the role they have in gauging the combustion gases' temperature at the inlet of the PH section, energy losses are also used to calculate the temperature of the internal surface of the PH walls ($T_{wall_{int}}$). That calculation begins considering that the external surface of the PH wall loses energy to the surroundings by convection and radiation, as shown by equation (4.4.2). In this, T_{amb} is the room air temperature, H_{amb} is the natural convection heat transfer coefficient, σ is the *Stefan-Boltzmann* constant and $T_{wall_{ext}}$, A_{ext} and $\varepsilon_{wall_{ext}}$ are temperature, area and the emissivity of the external surface of the PH walls, respectively. Equation (4.4.2) is then solved in order to $T_{wall_{ext}}$, assuming H_{amb} as 15 $[W/m^2.K]$, typical of a natural convection process, and that $\varepsilon_{wall_{ext}}$ is of 0.15 given the nature of the material of the external surface of the PH wall: polished aluminium.

$$\begin{aligned}\dot{Q}_{loss_{PH}} = {} & H_{amb} \times A_{ext} \times \left(T_{wall_{ext}} - T_{amb}\right) \\ & + A_{ext} \times \varepsilon_{wall_{ext}} \times \sigma \times \left(T^4_{wall_{ext}} - T^4_{amb}\right)\end{aligned} \tag{4.4.2}$$

Once $T_{wall_{ext}}$ is determined, *Fourier's* law is applied to the PH wall to find the temperature of the internal surface ($T_{wall_{int}}$). The wall to which *Fourier's* law is applied is a stack of three materials: 15 mm thick glass wool with a thin aluminium layer (external part), 3 mm thick of 316L stainless steel and 10 mm thick of high-density ceramic insulation (internal part).

4.4.2 External heat transfer coefficient

When convection and radiation heat transfer mechanisms play an important role in the energy transfer between the hot combustion gases and the fluid to be heated (water), a system of non-linear equations for the energy balance is expected to yield. In such circumstances, to reduce (or avoid) the convergence problems in the iterative numerical process, the radiation term of the heat transfer equation is linearized [196,197]. In those cases, the external heat transfer coefficient (H_g) is split in a radiative $H_{g_{rad}}$ and a convective $H_{g_{conv}}$ part as shown in equation (4.4.3).

$$H_g = H_{g_{rad}} + H_{g_{conv}} \tag{4.4.3}$$

For the determination of the convective heat transfer part ($H_{g_{conv}}$), a correlation developed for compact heat-exchangers was used [198], see equation (4.4.4). In this, St is the *Stanton* number, calculated using equation (4.4.5), G_g is the combustion gases' maximum mass velocity, calculated with equation (4.4.6) and c_{p_g} is the combustion gases' specific heat.

$$H_{g_{conv}} = St \times G_g \times c_{p_g} \tag{4.4.4}$$

$$St = \frac{j_h}{Pr_g^{\,2/3}} \tag{4.4.5}$$

$$G_g = \frac{\dot{m}_g}{A_{ff} \times \left(A_{ff}/A_{fr}\right)} \tag{4.4.6}$$

In the above-mentioned equations, A_{ff} and A_{fr} are the free-flow and the frontal area of the PH section, respectively, Pr_g is the *Prandtl* number and j_h is the *Colburn J factor*, obtained from Kays and London [199] as a function of the *Reynolds* number (Re_g) and taking in consideration its geometric characteristics. Re_g is calculated using equation (4.4.7), where D_h is the hydraulic diameter and μ_g the combustion gases' dynamic viscosity. All the combustion gases' properties are evaluated at film temperature (the average between the temperatures of the combustion gases (T_g) and of the external surface of the tubes ($T_{t_{ext}}$), where the first is the average between the inlet and the outlet temperatures and the second is calculated further ahead with equation (4.4.26)).

$$Re_g = G_g \times \frac{D_h}{\mu_g} \tag{4.4.7}$$

The radiative heat transfer coefficient ($H_{g_{rad}}$) is determined using equation (4.4.8) where $\dot{Q}_{rad}$ is the radiative heat transfer rate and $A_{t_{ext}}$ is the area of the external surface of the tubes.

$$H_{g_{rad}} = \frac{\dot{Q}_{rad}}{A_{t_{ext}} \times \left(T_g - T_{t_{ext}}\right)} \tag{4.4.8}$$

For the sake of simplicity, the calculation of $\dot{Q}_{rad}$ was done assuming the combustion gases as a semi-transparent/ radiative medium and all walls as black bodies. Therefore, $\dot{Q}_{rad}$ can be split into two components: one to account for the radiation from the gases ($\dot{Q}_{rad_g}$) and the other to account for the radiation from the internal surface of the walls ($\dot{Q}_{rad_{wall_{int}}}$), as shown in equation (4.4.9). Those two components can be evaluated using equations (4.4.10) and (4.4.11), respectively.

$$\dot{Q}_{rad} = \dot{Q}_{rad_g} + \dot{Q}_{rad_{wall_{int}}} \tag{4.4.9}$$

$$\dot{Q}_{rad_g} = A_{t_{ext}} \times \sigma \times \left(\varepsilon_g \times {T_g}^4 - \alpha_g \times {T_{t_{ext}}}^4\right) \tag{4.4.10}$$

$$\dot{Q}_{rad_{wall_{int}}} = \sum A_{wall_{int}} \times VF_{wall_{int}} \times \sigma \times \tau_g \times \left({T_{wall_{int}}}^4 - {T_{t_{ext}}}^4\right) \tag{4.4.11}$$

In equations (4.4.10) and (4.4.11), ε_g, α_g and τ_g are the emissivity, absorptivity and transmissivity of the combustion gases, respectively, and $A_{wall_{int}}$, $VF_{wall_{int}}$ and $T_{wall_{int}}$ are the area, the view factors and the temperature of the internal surface of the PH walls, respectively.

The evaluation of the view factors ($VF_{wall_{int}}$) was performed following the procedure described by Incropera et al. [198]. In the evaluation of the emissivity (ε_g) and the absorptivity (α_g) of the combustion gases' mixture, for which only the contributions of the water vapour and carbon dioxide were considered, equation (4.4.12) was used. In that equation, a stands for either the emissivity or the absorptivity of the index specified gas and Δ_a is a correction factor which takes in consideration the interaction between the two radiating and absorbing species.

$$a_g = a_{H_2O} + a_{CO_2} - \Delta_a, \qquad \text{where } a \equiv \varepsilon, \alpha \tag{4.4.12}$$

The terms presented in equation (4.4.12) were retrieved from Hottel [200] as a function of the H_2O and CO_2 partial pressures and of the so-called mean beam length (L_e), a parameter related with the geometric characteristics of the space occupied by the radiant gases. In this case, considering that the space has an arbitrary shape and a volume V_g, radiating to a defined surface area $A_{t_{ext}}$, the value of L_e is given by equation (4.4.13). The values of ε_g and α_g are also used to calculate the transmissivity of the combustion gases (τ_g) according to equation (4.4.14).

$$L_e = \frac{3.6 \times V_g}{A_{t_{ext}}} \tag{4.4.13}$$

$$\tau_g = 1 - (\varepsilon_g + \alpha_g) \tag{4.4.14}$$

4.4.3 Internal heat transfer coefficient

When the calculations concerning the heat transfer coefficient of the combustion gases side were completed, the model proceeded to the determination of the internal heat transfer coefficient for each one of the water CVs (H_{f_i}), using equation (4.4.15). In that equation, $D_{t_{int}}$ is the tube internal diameter, k_{f_i} the fluid's thermal conductivity and Nu_{f_i} the *Nusselt* number. The Nu_{f_i}, in this case, is determined using the *Gnielinski* correlation (see equation (4.4.16)) where Re_{f_i} and Pr_{f_i} are the *Reynolds* and *Prandtl* numbers, respectively; while f_i is a friction factor that, for smooth tubes, is given by equation (4.4.17). In these equations, the index i identifies the analysed CV.

$$H_{f_i} = Nu_{f_i} \times \frac{k_{f_i}}{D_{t_{int}}} \tag{4.4.15}$$

$$Nu_{f_i} = \frac{\left({}^{f_i}/_{8}\right) \times \left(Re_{f_i} - 1000\right) \times Pr_{f_i}}{1 + 12.7 \times \left({}^{f_i}/_{8}\right)^{1/2} \times \left({Pr_{f_i}}^{2/3} - 1\right)} \tag{4.4.16}$$

$$f_i = \left(0.79 \times \ln\left(Re_{f_i}\right) - 1.64\right)^{-2} \tag{4.4.17}$$

All the properties used in the calculation of the aforementioned parameters are evaluated at the fluid's mean temperature since the flow is clearly turbulent ($Re_f > 20000$).

4.4.4 Overall heat transfer coefficient and model features

Given the CV division established for the combustion gases and the water of the PH, two overall heat transfer coefficients (*U*) are obtained. These coefficients are calculated based on the combustion gases side to facilitate the incorporation of the fins' effect (found on the tubes' external surface). From now on, the overall heat transfer coefficient of the i^{th} CV will be represented by U_{g_i} and its calculation will be done using equation (4.4.18). In this, $R_{f_{int}}$ and $R_{f_{ext}}$ are the internal and external fouling factors, respectively, RA is the ratio between the internal and external heat transfer area, see equation (4.4.19), and the $R_{t_{g_i}}$ is the thermal resistance of the tube's wall, given by equation (4.4.20) where D_{ext} is the tube's external diameter and k_{t_i} its thermal conductivity. To complete U_{g_i} calculation it is also necessary to determine the overall fin surface efficiency ($\eta_{f,sur}$). This last parameter characterizes the behaviour of an array of fins attached to a base surface and can be calculated using equation (4.4.21), where A_{fin} is the total fin area and η_{fin} is the efficiency of each individual fin. The latter can be obtained from a general heat transfer textbook (e.g. [201]) as a function of the fin geometric parameters and the external heat transfer coefficient.

$$U_{g_i} = \frac{1}{\frac{1}{H_{f_i} \times \mathrm{RA}} + \frac{R_{f_{int}}}{\mathrm{RA}} + R_{t_{g_i}} + R_{f_{ext}} + \frac{1}{H_g \times \eta_{fin_{sur}}}} \tag{4.4.18}$$

$$RA = \frac{A_{t_{int}}}{A_{t_{ext}}} \tag{4.4.19}$$

$$R_{t_{g_i}} = \frac{D_{int} \times ln(D_{ext}/D_{int})}{2 \times k_{t_i} \times \mathrm{RA}} \tag{4.4.20}$$

$$\eta_{fin_{sur}} = 1 - \frac{A_{fin}}{A_{t_{ext}}} \times (1 - \eta_{fin}) \tag{4.4.21}$$

When the value of U_{g_i} is determined, it is possible to calculate the transferred thermal power from the combustion gases to the water in the i^{th} CV ($\dot{Q}_{f_i}$) using equation (4.4.22). In this equation, F_{PH_i} is a correction factor and $LMTD_i$ is the log mean temperature difference, given by equation (4.4.23). Since, in this specific case, the temperature variation of the fluid in the CVs is small when compared to the one of the combustion gases, the correction factor (F_{PH_i}) is made equal to 1. In the equation (4.4.23), $T_{f_{in_i}}$ and $T_{f_{out_i}}$ are the fluid temperatures at the inlet and outlet sections of the i^{th} water CV, respectively, while $T_{g_{out}}$ is the combustion gases' temperature at the exit section of its respective CV.

$$\dot{Q}_{f_i} = U_{g_i} \times A_{t_{ext}} \times F_{PH_i} \times LMTD_i \tag{4.4.22}$$

$$LMTD_i = \frac{\left(T_{g_{in}} - T_{f_{out_i}}\right) - \left(T_{g_{out}} - T_{f_{in_i}}\right)}{ln\left(\frac{T_{g_{in}} - T_{f_{out_i}}}{T_{g_{out}} - T_{f_{in_i}}}\right)} \tag{4.4.23}$$

Finally, the energy balances established for each one of the water CVs (see equation (4.4.24)) and for the combustion gases CV (see equation (4.4.25)) will allow the determination of their enthalpies, and consequentially of their temperatures, at their exit sections.

$$h(T,p)_{f_{out_i}} = \frac{\dot{Q}_{f_i}}{\dot{m}_{f_i}} + h(T,p)_{f_{in_i}} \tag{4.4.24}$$

$$h(T,p)_{g_{out}} = h(T,p)_{g_{in}} - \frac{\sum \dot{Q}_{f_i}}{\dot{m}_g} \tag{4.4.25}$$

Since it is also needed to calculate the external heat transfer coefficient and the film temperature at which some properties of the combustion gases are evaluated, the temperature of the external surface of the tubes at each one of the water CVs ($T_{t_{ext_i}}$) is determined using equation (4.4.26). For the calculation of the film temperature in the combustion gases CV, the average of $T_{t_{ext_i}}$ values is used. Additional to the calculation of $T_{t_{ext_i}}$, the temperature of the internal surface of the tube ($T_{t_{int_i}}$) is calculated using equation (4.4.27). In equations (4.4.26) and (4.4.27), $A_{t_{int_i}}$ and L_{t_i} are, respectively, the area of the internal surface and the length of each one of the water CVs while T_{f_i} is its average temperature.

$$T_{t_{ext_i}} = \dot{Q}_{f_i} \times \left(\frac{1}{H_f \times A_{t_{int}}} + \frac{R_{f_{int}}}{A_{t_{int}}} + \frac{ln(D_{ext}/D_{int})}{2 \times \pi \times L_t \times k_t} \right)_i + T_{f_i} \quad (4.4.26)$$

$$T_{t_{int_i}} = \dot{Q}_{f_i} \times \frac{1}{H_{f_i} \times A_{t_{int}}} + T_{f_i} \quad (4.4.27)$$

This physical model is solved by an iterative process since the initial values of some parameters, needed to evaluate the transport properties of the water and the combustion gases, are unknown (e.g. the combustion gases and water CVs outlet temperatures or the tubes' external surface temperature). These values start by being arbitrated and, when the iteration is complete, are updated with the results obtained. A new iteration is then performed where these values are used to obtain new results. This procedure continues until the difference between the results of two consecutive iterations is below a certain pre-defined criterion. A flowchart explaining all these procedures is shown in **Fig. 4-4**.

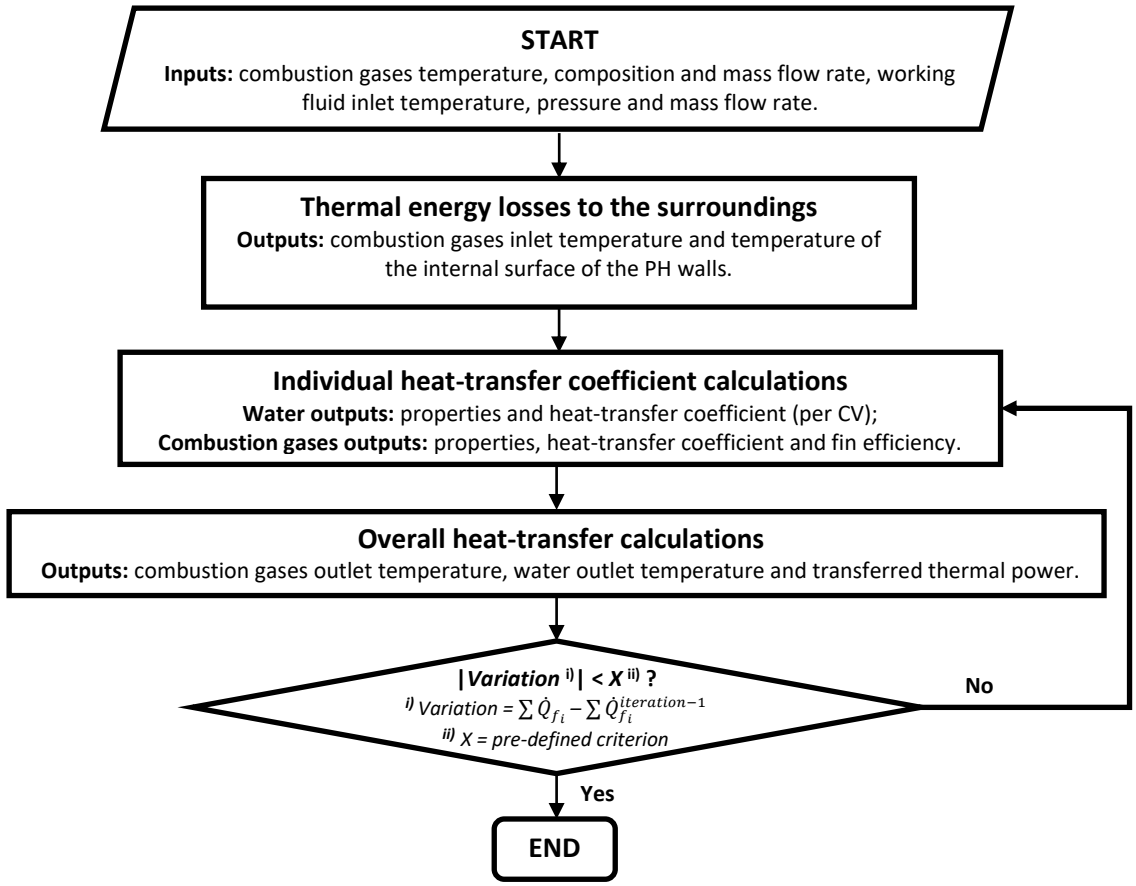

***Fig. 4-4**: Flowchart of the PH model with the main inputs and outputs.*

4.5 Organic fluid heat-exchanger (EHE) model

The EHE is a compact heat-exchanger made of stainless-steel tubes with copper fins presenting a mixed configuration regarding the interaction between the external and internal flows (combustion gases and the organic fluid, respectively), since it can be classified neither as counter-flow nor as cross-flow arrangement. **Fig. 4-5** shows a detached schematic representation of the EHE with the flow directions for both fluids.

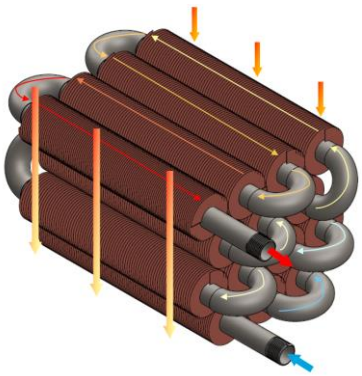

***Fig. 4-5**: Schematic representation of the (detached) EHE section.*

The EHE contains four levels of stainless-steel tubes with copper fins. Each level contains a different number of tubes, as is shown by **Fig. 4-6**. This model is expected to provide a series of important output variables, such as: i) the fluid's outlet temperature (as well as its evolution while it travels through the heat-exchanger), ii) the combustion gases' temperatures after each one of the four levels, iii) the transferred thermal power in each level and iv) the temperature of the internal surface of the heat-exchanger tubes (which will serve as a reference for the maximum fluid temperature, as previously mentioned). In a similar way to what happens with the PH, this will require a series of input variables in order to model the heat transfer process. Some of those are the outputs of the two previous models, namely: i) the combustion gases' temperature after being cooled down in the PH, ii) the combustion gases' mass flow rate and iii) the combustion gases' composition. Besides these, and regarding the organic fluid, the input parameters are: the definition of the fluid itself which, in this case, is Pentafluoropropane (also known as R-245fa) and its inlet temperature, pressure and mass flow rate.

Since the variation of the organic fluid properties is expected to be much bigger than those observed for the water in the PH section (mainly due to the vaporization process), the volume occupied by this inside the EHE tubes was split into a large number of CVs. On the other hand, the volume occupied by the combustion gases was split into as many CVs as levels of tubes.

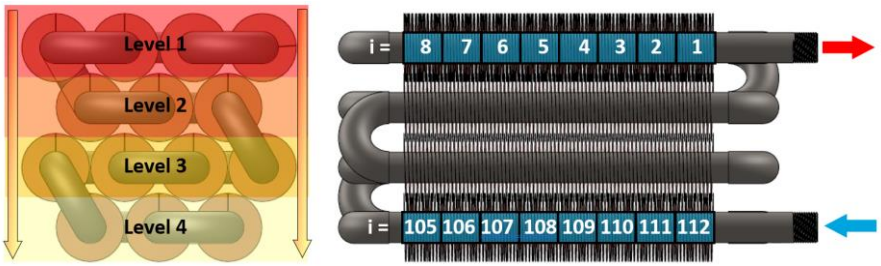

***Fig. 4-6**: 2D view of the EHE section with the discretization of the gas and organic fluid CVs.*

This model assumes steady-state operating conditions and no pressure losses of both fluid streams and does not consider heat transfer by conduction in the tubes' wall along the axial direction.

4.5.1 Thermal energy losses to the surroundings

The methodology followed in the PH regarding the thermal losses is also used in this model. Similarly, the thermal losses are used to estimate the internal surface temperature of the ORC-evaporator wall. In this evaluation, all the assumptions made in the PH are kept, except for the materials (and their thickness) considered for the wall. In this case, a 20 mm thick blanket of glass wool, with an aluminium sheet in its outside face, is used in the external part of a 3 mm thick 316L stainless steel plate. In addition, the effect of thermal losses will have a consequence on the temperature of the combustion gases. As in the PH model, these are accounted in the form of a temperature reduction at the entrance of the EHE.

4.5.2 External heat transfer coefficient

Having in consideration the geometric and flow specificities, the calculations of the heat transfer coefficient of the combustion gases side for the EHE model is performed in a similar way to what was done for the PH model. However, these calculations will now be performed four times – once per each combustion gases' level – being the outlet temperature at each level used as the inlet temperature on the following one.

4.5.3 Internal heat transfer coefficient

In the internal heat transfer coefficient calculation, depending on the fluid state, two situations can be found. A situation where the organic fluid is in a single phase (whether liquid or vapour) or a situation in which the fluid is a two-phase (liquid-vapour) state. For the first of the situations, similar to what was done with the PH model, the *Gnielinski* correlation (see equation (4.4.16)) is used. However, since the EHE tubes are no longer smooth, the friction factor (f) is now calculated using equation (4.5.1), where ε_r is the relative roughness of the tube.

$$f = \frac{1}{\left(1.8 \times \log\left(\frac{6.9}{Re_D}\right) + \left(\frac{\epsilon_r}{3.7}\right)^{1.11}\right)^2} \tag{4.5.1}$$

In the second situation (two-phase state) the method described by Coulson and Richardson [202] was adopted for the determination of the heat transfer coefficient (H_f). In this approach, H_f is given as a sum of a forced convection ($H_{f_{fc}}$) with a nucleate flow boiling ($H_{f_{nb}}$) components as shown in equation (4.5.2).

$$H_f = H_{f_{fc}} + H_{f_{nb}} \tag{4.5.2}$$

The forced convection component ($H_{f_{fc}}$) is calculated using equation (4.5.3) where $H_{f_{conv}}$ is the internal convection heat transfer coefficient determined using the methodology presented for the single phase situation and considering the organic fluid in a saturated liquid state, and LM_f is the *Lockhart-Martinelli* factor, an empirical parameter which, for a turbulent two-phase flow, is calculated using equation (4.5.4), valid if $\left[0.1 \leq \frac{1}{X_{tt}} \leq 100\right]$ [203]. In the latter, X_{tt} represents the *Martinelli's* non-dimensional parameter that may be evaluated using equation (4.5.5) where x_v is the vapour mass fraction (or the quality) of the two-phase mixture, ρ_{f_l} and ρ_{f_v} are the densities of the (saturated) liquid and vapour phases of the fluid, respectively, while μ_{f_l} and μ_{f_v} are the dynamic viscosities of the (saturated) liquid and vapour phases, respectively.

$$H_{f_{fc}} = H_{f_{conv}} \times LM_f \tag{4.5.3}$$

$$LM_f = 10^{0.0802 \times log\left(\frac{1}{X_{tt}}\right)^2 + 0.5473 \times \log\left(\frac{1}{X_{tt}}\right) + 0.4533} \tag{4.5.4}$$

$$\frac{1}{X_{tt}} = \left(\frac{x_v}{1 - x_v}\right)^{0.9} \times \left(\frac{\rho_{f_l}}{\rho_{f_v}}\right)^{0.5} \times \left(\frac{\mu_{f_v}}{\mu_{f_l}}\right)^{0.1} \tag{4.5.5}$$

The nucleate flow boiling component ($H_{f_{nb}}$) is obtained from the nucleate pool boiling coefficient (H_{np}) and an empirical factor (NB_f) which incorporates the duct flow effect, as shown in equation (4.5.6). The first of these factors is calculated using the *Forster and Zuber* correlation [204], shown in equation (4.5.7), while the second is given by equation (4.5.8).

$$H_{f_{nb}} = H_{np} \times NB_f \tag{4.5.6}$$

$$H_{np} = 0.0012 \times \frac{{k_{f_l}}^{0.79} \times {c_p}_{f_l}^{0.45} \times {\rho_{f_l}}^{0.49}}{{\gamma_{f_l}}^{0.5} \times {\mu_{f_l}}^{0.24} \times {H_{fg}}^{0.24} \times {\rho_{f_v}}^{0.24}} \times \left(T_{t_{int}} - T_{sat_f}\right)^{0.24} \times \left(p_{sat_{f_t}} - p_f\right)^{3/4} \tag{4.5.7}$$

$$NB_f = 0.146 \times log(X_{NB})^3 - 2.092 \times log(X_{NB})^2 + 9.369 \times \log(X_{NB}) - 12.459 \tag{4.5.8}$$

In equations (4.5.7) and (4.5.8), k_{f_l}, cp_{f_l} and $\gamma_{f_l}$are the thermal conductivity, the specific heat and the surface tension of the (saturated) liquid phase , respectively; h_{fg} and T_{sat_f} are the latent heat of vaporization and the saturation temperature, respectively, while $p_{sat_{f_t}}$ is the saturation pressure evaluated at the temperature of the internal surface of the tubes, p_f is the operating pressure (at which all the above mentioned properties, except $p_{sat_{f_t}}$, are evaluated) and X_{NB} is a parameter, that relates the *Reynolds* number with the *Lockhart-Martinelli* factor (LM_f), obtained using equation (4.5.9). In this, ρ_f and v_f are the density and velocity of the fluid, respectively.

$$X_{NB} = \frac{(1 - x_v) \times \rho_f \times v_f \times D_{t_{int}}}{\mu_{f_l}} \times {LM_f}^{1.25} \tag{4.5.9}$$

4.5.4 Overall heat transfer coefficient and model features

As previously mentioned, the organic fluid side is divided into a pre-defined number of CVs per tube (N_c). The identification of each one is made by the index i ($i \in \{1, 2, 3, \dots, Nc \times 14\}$). The combustion gases side is divided into four CV (or levels), being its identification made by the index j ($j \in \{1, 2, 3, 4\}$).

The heat transfer coefficients' calculations, the subsequent evaluation of the transferred thermal power and the calculation of the fluid and of the tubes' surface temperatures are completed as follows. For each level, the steps given in the aforementioned calculations are:

i) Determine the external heat transfer coefficient (H_{g_j}). The first time this value is evaluated, the arbitration of the combustion gases' temperature at the outlet section and the tubes' external surface temperature are necessary. At each iteration only one value of H_{g_j} is calculated per level.

Within the level, for increasing values of i, the following calculations are done for each one of the organic fluid CVs:

ii) Determination of the internal heat transfer coefficient (H_{f_i}) using the correlation appropriated to the organic fluid phase. The organic fluid transport properties used to determine H_{f_i} are evaluated at the operating conditions (e.g. temperature and pressure) of the CV outlet section, since the variation of those (between the inlet and outlet section) is expected to be small due to a large number of CVs per tube. The first time the value of H_{f_i} is determined for the first CV of the first level ($i = 1$), the temperature of the organic fluid at the outlet section needs to be arbitrary;

iii) Determination of the overall heat transfer coefficient (U_{g_i}). The calculation of the U_{g_i}, given the reasons pointed out in section 2.2.4, is made relative to the combustion gases side by adapting equation (4.4.18);

iv) Determination of the transferred thermal power ($\dot{Q}_{f_i}$) using, as in the PH section, the $LMTD$ and an adapted version of equation (4.4.22). Again, no correction factor is used. In this case, the justification regards a large number of CVs in which the tubes of the EHE are divided. This makes the organic fluid temperature variation between the inlet and outlet section of each one of those CVs much smaller than the combustion gases' temperature difference between the inlet and outlet sections of a level of tubes;

v) Determination of the organic fluid enthalpy at the inlet section of the CV ($h_{f_{in_i}}$) using an adapted version of equation (4.4.24) which will allow the evaluation of the temperature at that point. This temperature is made equal to the one of the organic fluid at the outlet section of the $(i+1)^{\text{th}}$ CV and will be used to evaluate its transport properties in that CV;

vi) Determination of the tubes internal ($T_{t_{int_i}}$) and external ($T_{t_{ext_i}}$) surface temperatures using adapted versions of equations (4.4.26) and (4.4.27), respectively.

After performing the aforementioned calculations for all the organic fluid CVs of a level, the enthalpy of the combustion gases at the outlet section of that level ($h_{g_{out_j}}$) is calculated using an adapted version of equation (4.4.25). This allows the determination of the combustion gases' temperature at that point ($T_{g_{out_j}}$) which will be made equal to the inlet temperature of the next level ($T_{g_{in_{j+1}}}$). Additionally, the temperature of the external surface of the tubes of that level ($T_{t_{ext_j}}$), used in the determination of film temperature at which the transport properties of the combustion gases are evaluated, is determined through an arithmetic average of the $T_{t_{ext_i}}$, as done in the PH section.

An iteration is completed when all the levels (combustion gases CVs) and all the organic fluid CVs have been run through. At each iteration, the initially arbitrated values (e.g. combustion gases' temperature at the outlet of a level), with the exception of the outlet temperature for the first ($i = 1$) organic fluid CV, are updated with the values calculated in the previous one. The values calculated in an iteration are considered reliable if the absolute difference between the calculated total transferred thermal power ($\sum \dot{Q}_{f_i}$) and the one of the previous iteration is below a certain predefined value. Here, and since the $LMTD$, used to calculate the transferred thermal power, has an asymptotic behaviour, it is worth noticing that some numerical instability may occur. In order to avoid those and help the iterative process convergence, a damping factor (dp) is used between two consecutive iterations. In practice, this is achieved by affecting the combustion gases' temperature at the outlet of each level. For this, a weighted average is calculated for each of the four values of the combustion gases' temperatures at the outlet section involving the value calculated ($T_{g_{out_j}}$) and that of the previous iteration ($T_{g_{out_j}}^{iteration-1}$), as equation (4.5.10) shows. This damping ensures that no abrupt variations occur in two consecutive iterations which may slow down the convergence process but avoids numerical instability problems.

$$T_{g_{out_j}} = T_{g_{out_j}} \times (1 - dp) + T_{g_{out_j}}^{iteration-1} \times dp \tag{4.5.10}$$

When the referred stopping criteria is met, the calculated value of the enthalpy at the inlet section of the last organic fluid CV ($i = Nc \times 14$) is compared with the real value (one of the model input parameters). If the difference between those enthalpies is below a certain pre-defined limit, the calculation process stops and the solution obtained is considered the final result. If not, the value of the outlet enthalpy of the first organic fluid CV ($i = 1$), initially arbitrated or determined in the previous iterative process, is updated by subtracting the enthalpy difference previously obtained for CV $i = (Nc \times 14)$. The reason why enthalpy is used as a comparison parameter instead of the temperature is to simplify the resolution of the iterative process even if the organic fluid leaves the EHE in a two-phase flow. This procedure can be easier understood through the visualization of the flowchart represented in **Fig. 4-7**.

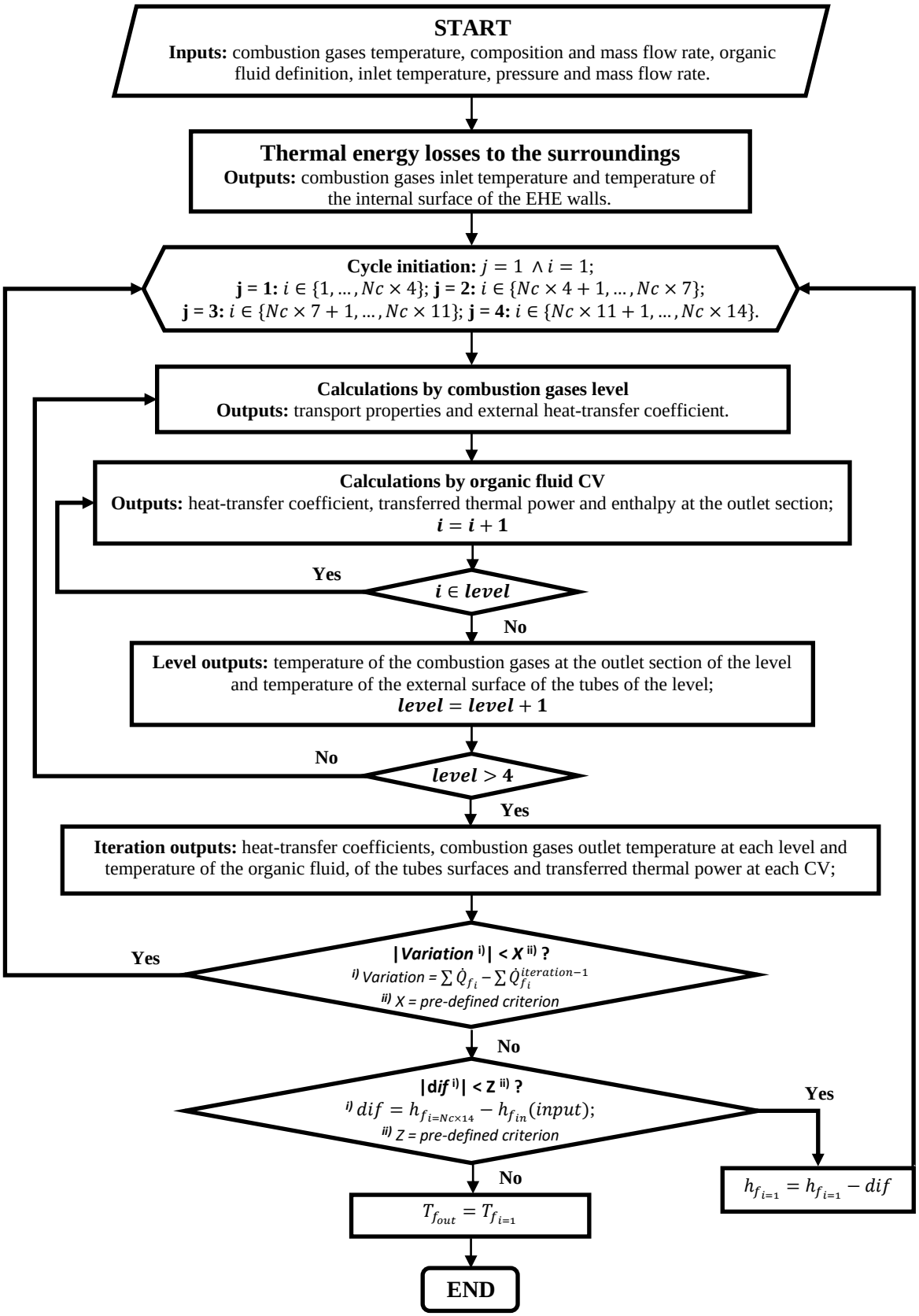

***Fig. 4-7**: Flowchart of the EHE model with the main inputs and outputs.*

4.6 Model validation, calibration and analysis

4.6.1 Experimental apparatus

In order to verify and validate the options taken and the simplification made in the development of the ORC-evaporator physical-mathematical model, a comparison needs to be done between the results retrieved with it and those obtained from the experimental tests. To perform such a task, the designed ORC-evaporator was integrated into a test rig emulating a micro-scale ORC based CHP system. A schematic diagram, including the instrumentation used to monitor and control its operation, is presented in **Fig. 4-8**.

Beyond the evaporator, the test rig includes a pump, a condenser and, instead of an expander, a needle throttling valve. The use of this valve does not affect the evaporator's behaviour if special care is taken in the condenser selection so that it will be capable to dissipate the excess of energy that otherwise would be extracted by the expander. The test rig operates as follows (see the temperature-enthalpy diagram for the hybrid solution shown in **Fig. 3-8** in what refers to the processes representation). The organic fluid (Genetron R245fa – Annex C) starts to be pressurized (process 4-1) in the pump (Fluid-o-Tech TMFR series – Annex D) after which is conducted to the evaporator (own design and manufacture) where is heated, vaporized and slightly superheated by the combustion gases (processes 1-2 and 9-10) generated in a natural-gas burner (see chapter 3) and previously cooled in the PH section of the evaporator (processes 6-7 and 8-9). Afterwards, the pressurized vapour flows through a needle throttling valve (ValSteam PRC25I – Annex E) where it is isenthalpically expanded (process 2-3). The low-pressure vapour is then directed to a brazed plate heat-exchanger (GEA WTT GBS220H – Annex F) where, losing energy to the water, condenses (processes 3-4 and 5-6). The condensed fluid is driven to the pump, to be pressurized again, closing the cycle. As mentioned in Chapter 3, the particular design of this ORC-evaporator led to a hybrid CHP configuration in which the useful thermal energy (hot water) is produced in two steps: first in the condenser (process 5-6) and afterwards in the PH section of the ORC-evaporator (process 6-7). Besides the evaporator, all of the ORC main components were selected to fulfil the operating requirements specified in **Table 3-1**. Photographs of those are shown in **Fig. 4-9**.

As there is particular interest in the characterization of the ORC-evaporator behaviour, this component is specially monitored and, in addition to the instruments presented in **Fig. 4-8**, both of its sections have a series of contact thermocouples partially embedded in the wall of the elbows. These thermocouples are kept out from the direct exposition of the combustion gases and are externally surrounded by a quasi-adiabatic media, as is shown in **Fig. 4-10**. The temperature values retrieved will be used for monitoring the heating process of the water and the heating, vaporization and superheating processes of the organic fluid that occurs in the PH and EHE sections, respectively. The main characteristics of the instruments used are presented in **Table 4-1**.

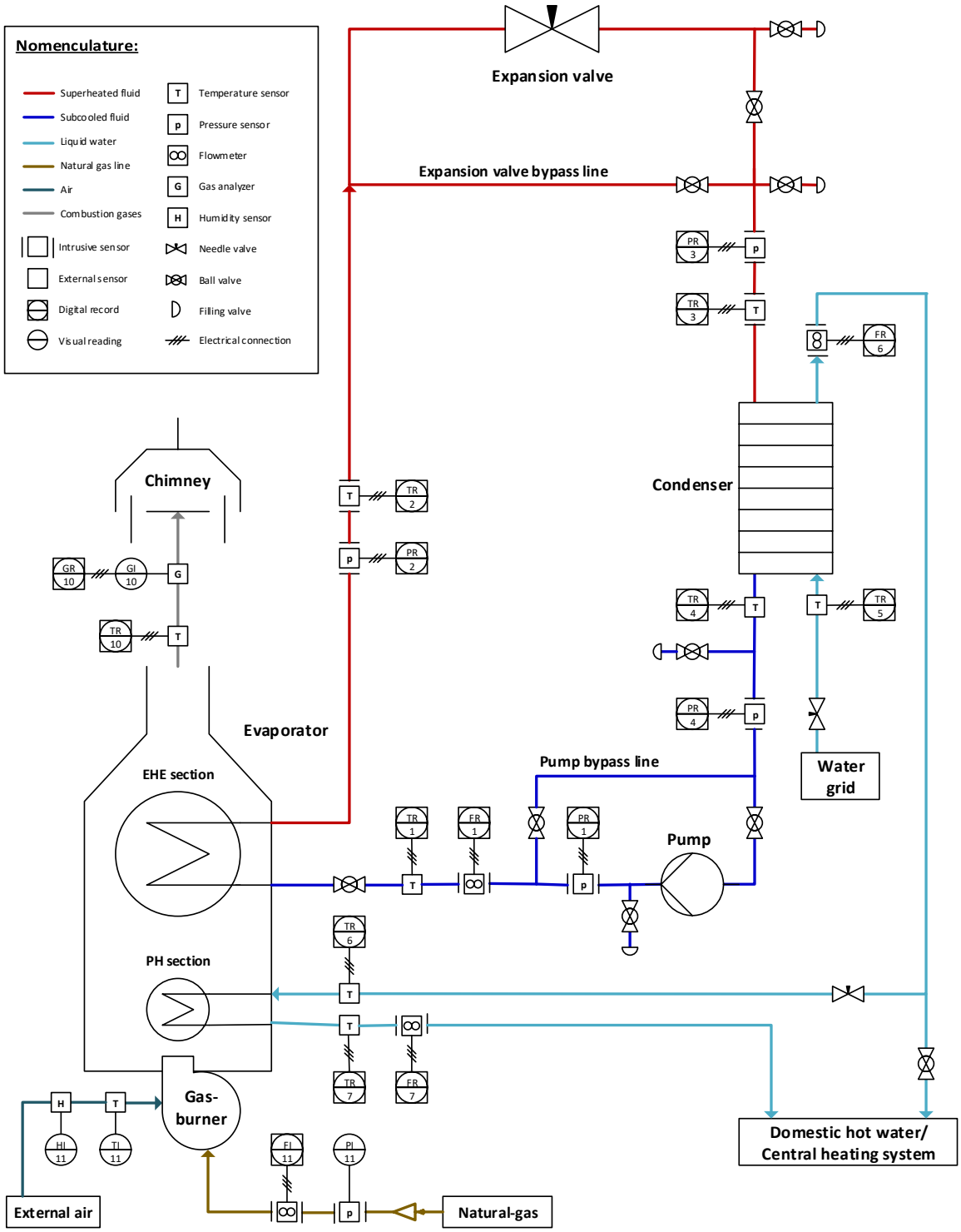

***Fig. 4-8**: Schematic diagram of the test rig used for the model calibration and validation.*

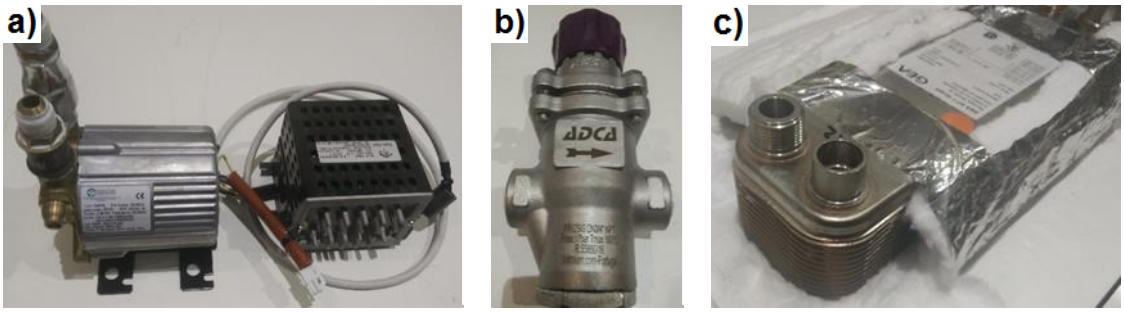

***Fig. 4-9**: Photographs of the ORC main components: a) volumetric-type pump with its electronic controller, b) needle throttling valve and c) a brazed plate-type heat-exchanger.*

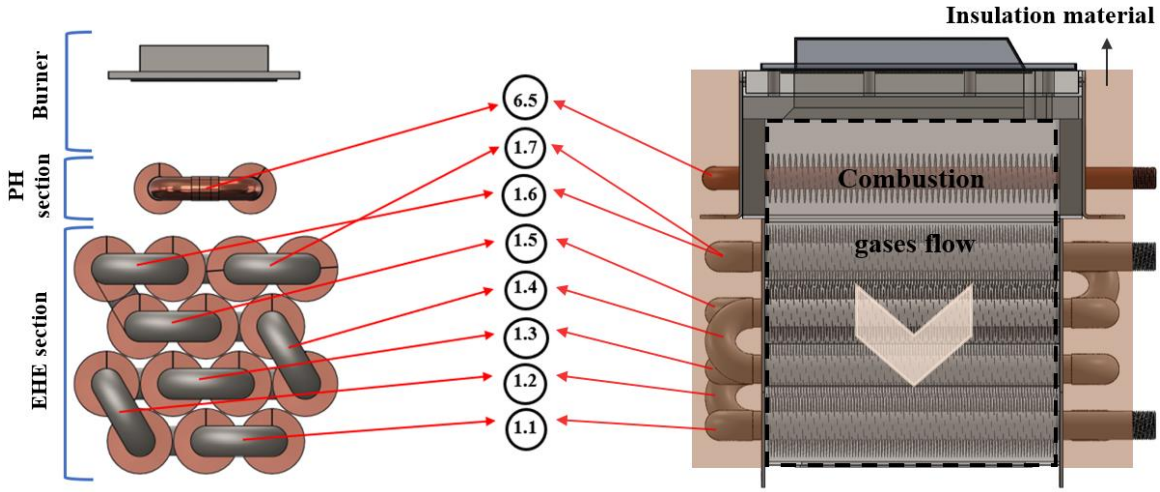

***Fig. 4-10**: Schematic representation of the ORC-evaporator with the location of the contact thermocouples alongside the PH and EHE sections.*

***Table 4-1**: Main characteristics of the instruments used in the test rig.*

Line number (see **Fig. 4-8**)	**Variant**	**Stream**	**Type**	**Range**	**Accuracy**	**Tech. data**
1	Mass flow rate	Organic fluid	Coriolis	[0 – 2.2] kg/s	0.4 %	Annex G-1.i
[1,2]	Pressure	Organic fluid	Diaphragm	[0 - 25] bar	0.25 % FS	Annex G-2.i
[3,4]	Pressure	Organic fluid	Diaphragm	[0 - 10] bar	0.05 % FS	Annex G-2.ii
[All]	Temperature	Organic fluid, PH water, comb. gases	Thermocouple type T	[-40 - 300] °C	0.75%.|T| or 1 °C	Annex G-3
[6,7]	Volumetric flow rate	PH water	Turbine	[1 - 25] L/min	2 %	Annex G-1.ii
10	Oxygen sensor	Comb. gases	Infra-red	[0 - 25] %	0.2 %	Annex G-4
11	Temperature / humidity	Ambient air	Thermistor/ polymer film	[-20 - 40] °C / [20 - 80] %	5 %	Annex G-5
11	Volumetric flow rate	Natural-gas	Diaphragm	[0 – 1.7] dm^3/s	1 %	Annex G-1.iii

The physical connection between the ORC main components (including the installation of the instruments used between those) is composed of copper tubes and brass fittings since temperatures above 150 ºC and pressures around 15 bar are expected. Wherever possible, preference has been given to welded connections as they are more reliable than threaded or clamping connections regarding the occurrence of organic fluid leakages. Between every one of the ORC main components, a section valve and a filling tap are placed to create separate sections in the test rig to perform leakages tests in small sections and, if necessary, to replace some component or the instrument without losing the organic fluid of the entire system. The operating conditions of the ORC system are automatically controlled by the natural-gas volume feeding rate (which defines the natural-gas combustion power) and by the rotational speed of the ORC-pump. The needle throttling (expansion) valve is manually controlled. . On the other hand, the water circuit of the test rig is made of PEX multilayer tubes with threaded fittings since temperatures above 90 ºC or significant pressures (atmospheric pressure - open cycle) are not expected. In this, manually operated needle valves are used to control the mass flow rate of the water. Armaflex sleeves are used to insulate the organic fluid and the water tubes. The tube sizing was selected accordingly to the fluid state and velocity for the nominal operating condition in an attempt to have low values of pressure drops, noise and prevent tube damages. From these, it was empirically defined that the value of the organic fluid velocity should not overpass 20 m/s for the vapour state and 2 m/s for the liquid state. A 3D step and the necessary drawings for the construction of the test rig are given in Appendix E-1 while a general 3D overview, with the identification of the main components, and photographs of it are presented in **Fig. 4-11** and **Fig. 4-12**, respectively.

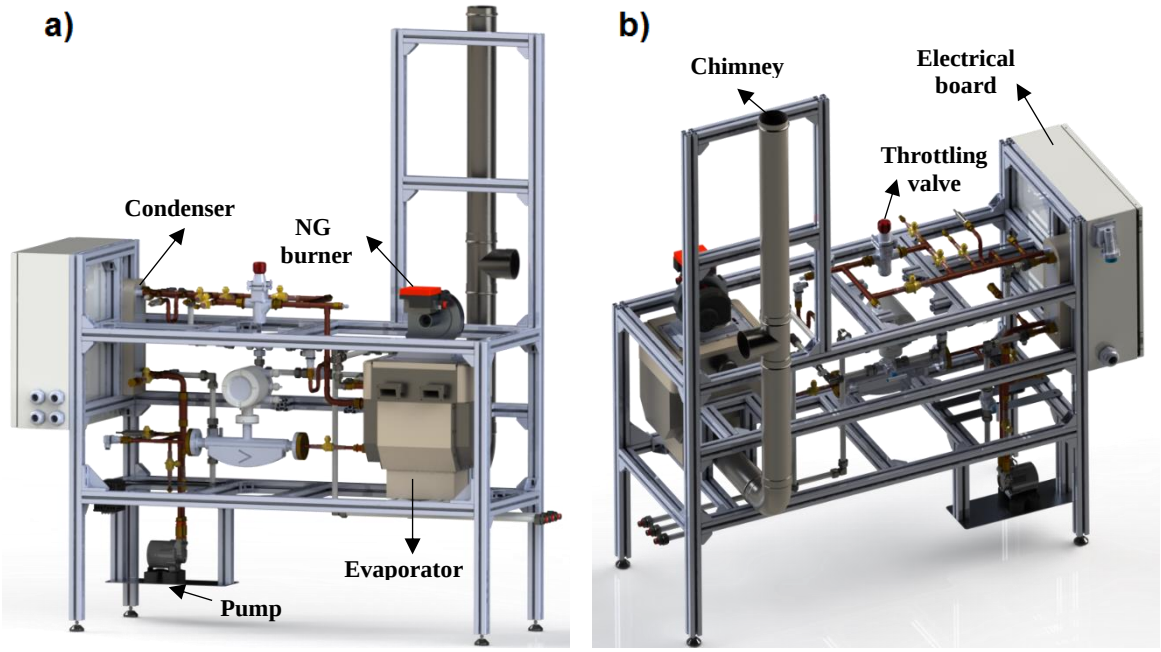

***Fig. 4-11**: 3D representation of the test rig: a) dimetric front view and b) isometric back view.*

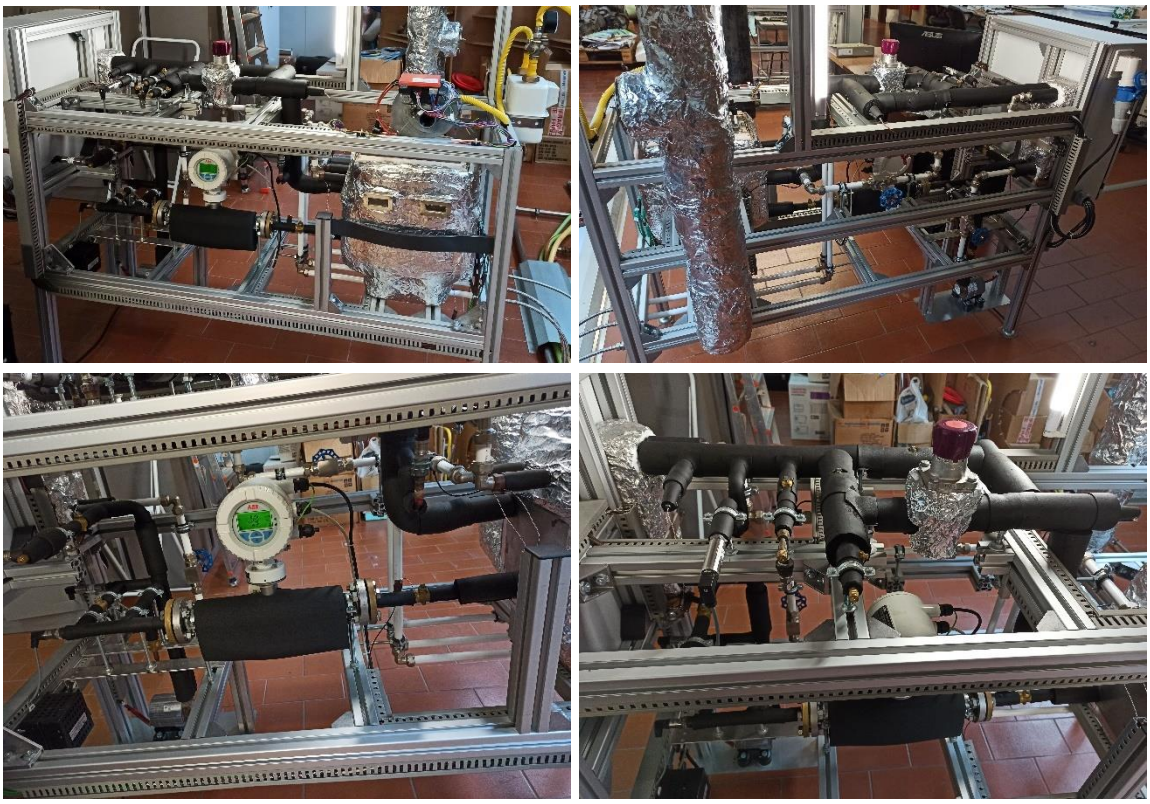

***Fig. 4-12**: Miscellaneous photographs of the test rig.*

All sensors and controllable components are cable-connected to the electrical board identified in **Fig. 4-11**. In this, all the necessary safety devices (e.g., circuit breakers, insulated plugs, emergency buttons, etc.) are installed. The acquisition of the temperature (thermocouples) signals was made through a Pico TC-08 data logger (datasheet available in Annex H-1) while the remaining ones (e.g. mass flow rates, pressure) were acquired by a NI USB 6001 (datasheet available in Annex H-2). The NI data acquisition board used is known to be a multi-purpose device because it has several analogue and digital input/output connections, a counter, a +5V power source, and other ordinary specifications. However, it cannot read current loops from, for example, the pressure sensors. Therefore, a current-voltage converter device based on high-accurate electrical resistances of 250 Ohms to convert, in this case, the 4-20 mA signal to a 1-5 V signal was used. Two current-voltage converter devices were used: one for passive and the other for active components. Additionally, due to its multi-purpose capabilities, the NI data acquisition board is also used to send the electrical signal (in both cases a 0-10 V signal) to control the natural-gas volume feeding rate and the rotation speed of the ORC-pump. These arrangements are described in detail in the electrical diagram presented in Appendix E-2. A 3D representation and photographs of the electrical board of the test rig are presented in **Fig. 4-13** and **Fig. 4-14**, respectively.

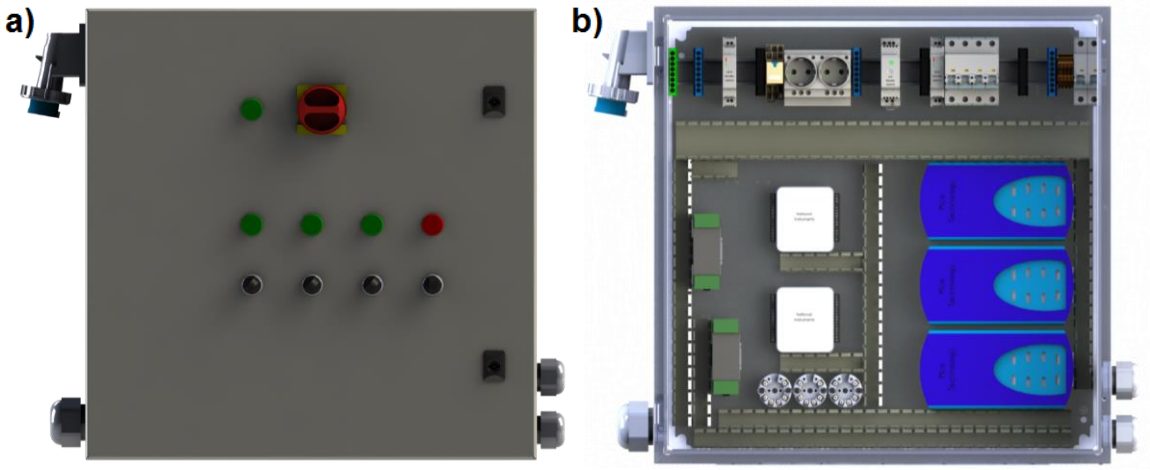

***Fig. 4-13**: 3D representation of electrical board of the test rig: a) front panel view and b) interior view in the data acquisition boards, converters and other devices.*

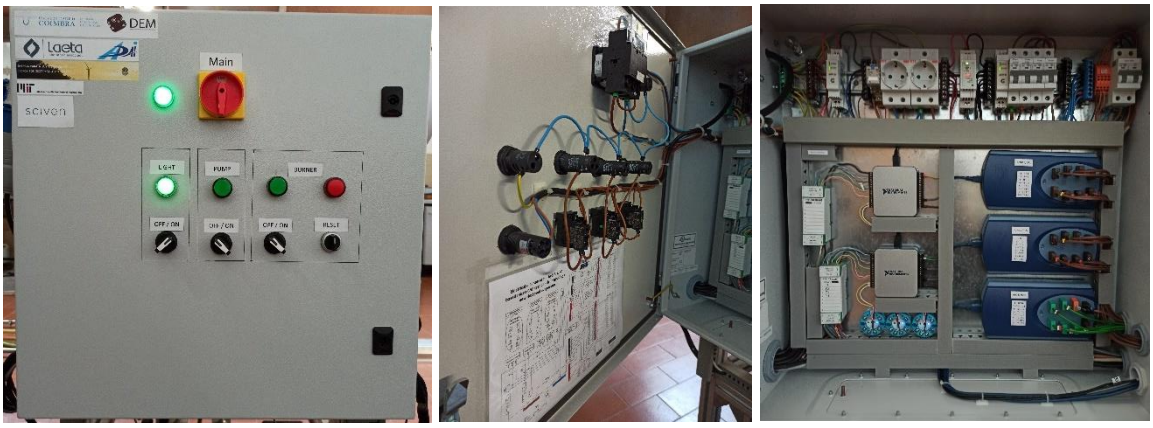

***Fig. 4-14**: Photographs of the electrical board of the test rig.*

The acquisition boards are connected through USB cables to a desktop computer that uses a LabVIEW® software-based self-developed application to record all data, process the information and control the experimental test rig in real-time. The name of the application developed is *HebeTR2_datalogger&control* and an executable file is presented in Appendix F. It is composed of three independent blocks, where two are fixed and the other one has five different tabs. The objective of these tabs is to show in more detail, and different ways (e.g., using charts or derivate parameters), some specific parts of the test rig. Images of the entire application, showing the five different tabs, are presented in **Fig. 4-15**. One of the fixed blocks is placed at the left column of the application and shows the time, start/shut-down button, alarms, and the main indicators of the test rig. The other fixed block is presented at the bottom line of the application and displays the automatic control parameters: the natural-gas volume feeding rate and the pump rotational speed. The parameters presented in both fixed blocks must always be visible to quickly alert the operator if something went wrong during the process, and he should be able to promptly assess the control parameters or even easily shut down the entire system. As for the remaining block, the operator can choose which tab, and consequently which parameters, is displayed at each moment. The first tab, named as *General*

view and presented in **Fig. 4-15-a**, shows a schematic diagram to represent how the test rig operates and where the main instruments (together with its acquired value) and valves (together with the indication if they are open or closed) are placed. The second tab, named *Power circuit* and presented in **Fig. 4-15-b**, is focused on the organic fluid circuit. It contemplates two main charts, one for pressure and another for temperature readings, to help the operator anticipate the behaviour of the system, especially in transient operating conditions. In addition, it includes the numerical indicator of each sensor and several ORC derivate parameters such as the saturation temperature, enthalpies and density at each location, the net positive suction head of the pump, the pressure ratio of the cycle, the liquid column of the organic fluid, the values of the power transferred or consumed in a specific component and the overall efficiency of the cycle. The third tab, named *Water circuit* and presented in **Fig. 4-15-c**, has a display arrangement like the *Power circuit* but, in this case, focuses on the water circuit. The fourth tab, named *Evaporator* and presented in **Fig. 4-15-d**, is specifically related to the ORC-evaporator. Two schematic pictures are presented to identify the location of the temperature sensors used. From these readings, three different charts are presented below for each independent stream: organic fluid (EHE), water (PH) and combustion gases (natural-gas-combustion). Additionally, the natural-gas and ambient conditions readings are shown as well as the percentage of the main molecules of the combustion gases and some performance parameters specifically regarding the ORC-evaporator. The fifth and last tab, named *Editor* and presented in **Fig. 4-15-e**, is not directly related to the system operating conditions but to the software programming. Here, the operator can see if, for example, some problem occurs with the Pico TC-08 datalogger boards (a most common problem since the LabView software appears to have some incompatibilities with the dataloggers), change the application recording time or even introduce the natural-gas heating value to complete some of the calculations presented in the previous tabs.

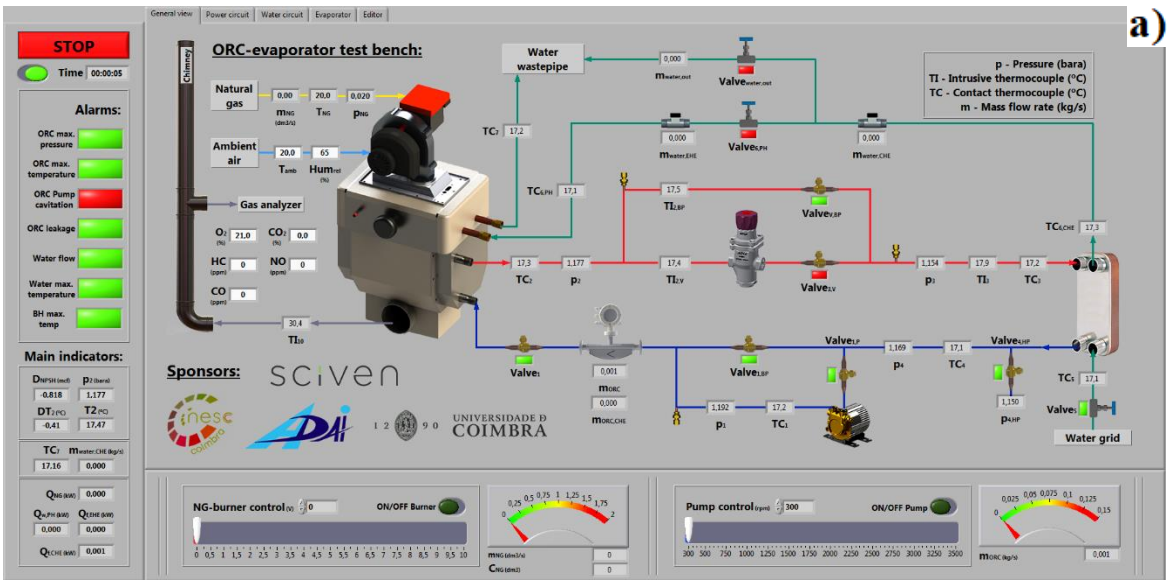

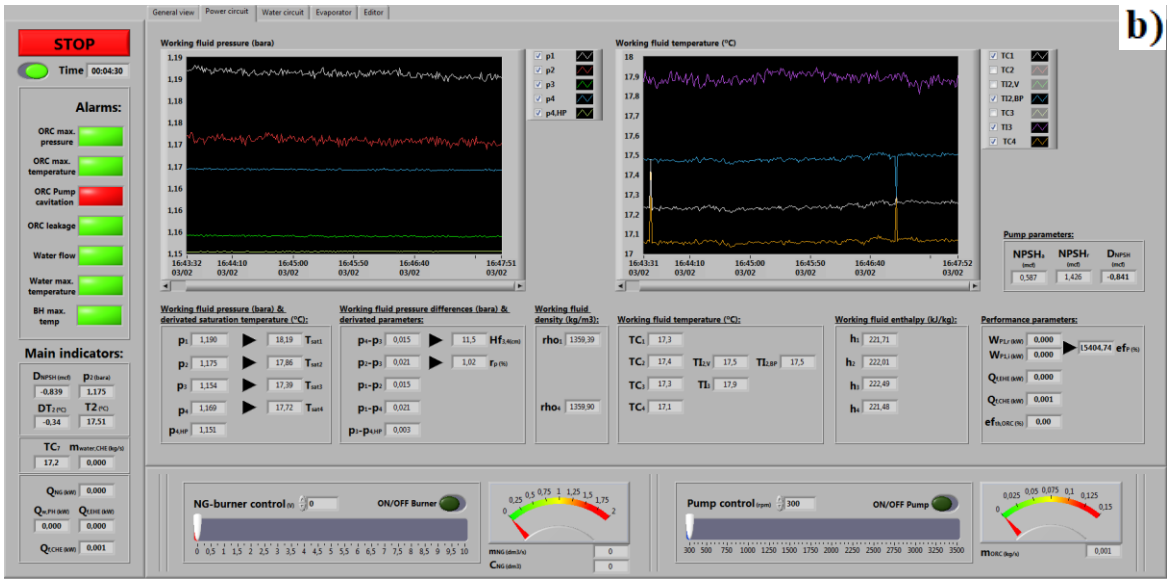
b)
STOP
Time 00:04:30
Alarms:
ORC max. pressure
ORC max. temperature
ORC Pump cavitation
ORC leakage
Water flow
Water max. temperature
BH max. temp
Main indicators:
Working fluid pressure (bara)
Working fluid temperature (°C)
Pump parameters:
Working fluid pressure (bara) & derivated saturation temperature (°C):
Working fluid pressure differences (bara) & derivated parameters:
Working fluid density (kg/m3):
Working fluid temperature (°C):
Working fluid enthalpy (kJ/kg):
Performance parameters:
NG-burner control
ON/OFF Burner
Pump control
ON/OFF Pump

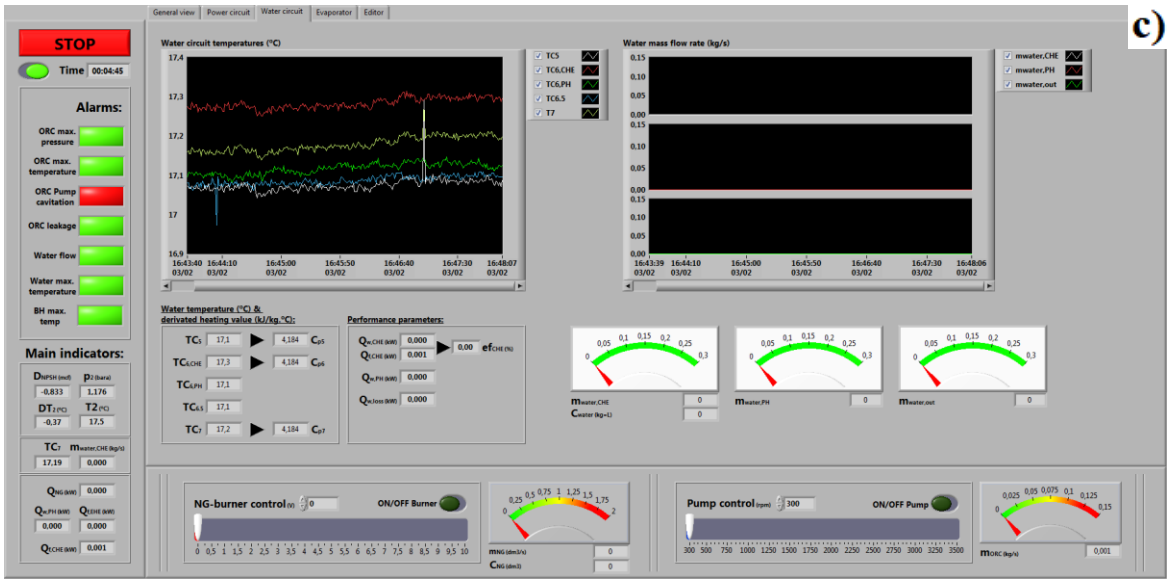
c)
STOP
Time 00:04:45
Alarms:
Main indicators:
Water circuit temperatures (°C)
Water mass flow rate (kg/s)
Water temperature (°C) & derivated heating value (kJ/kg °C):
Performance parameters:
NG-burner control
ON/OFF Burner
Pump control
ON/OFF Pump

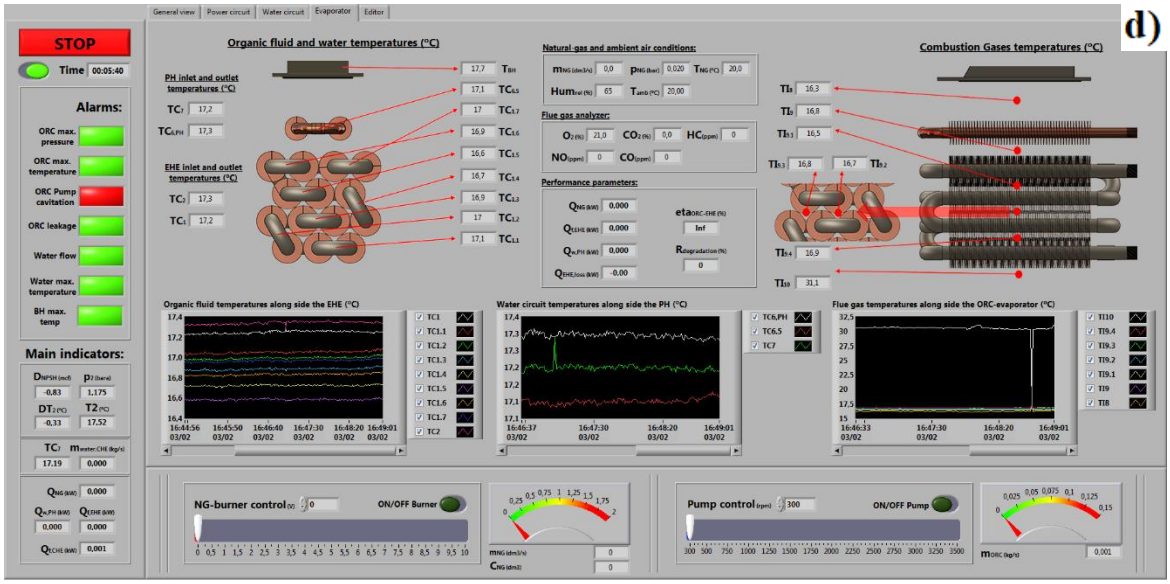
d)
STOP
Time 00:05:40
Alarms:
Main indicators:
Organic fluid and water temperatures (°C)
Natural gas and ambient air conditions:
Combustion Gases temperatures (°C)
PH inlet and outlet temperatures (°C)
EHE inlet and outlet temperatures (°C)
Flue gas analyzer:
Performance parameters:
Organic fluid temperatures along side the EHE (°C)
Water circuit temperatures along side the PH (°C)
Flue gas temperatures along side the ORC-evaporator (°C)
NG-burner control
ON/OFF Burner
Pump control
ON/OFF Pump

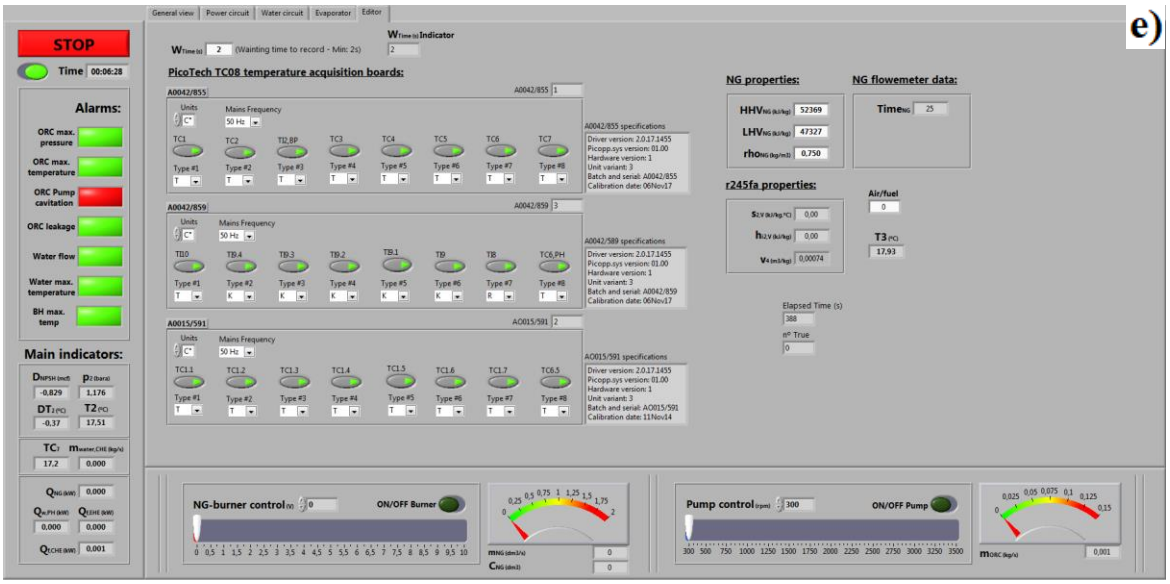

***Fig. 4-15**: Screenshots of the Labview HebeTR2_datalogger&control application: a) General view, b) Power circuit, c) Water circuit, d) Evaporator and e) Editor.*

4.6.2 Experimental tests

To allow a comparison between the experimental and the model results, for an as wider as possible range of the ORC-evaporator operation conditions, two series of experimental tests have been carried out. In the first of those series, the combustion power is gradually increased from 15% to 85% of its nominal value, with steps of approximately 15%, while the organic fluid superheating degree, at the exit of the EHE section, is kept constant at around 5 °C. This is achieved by adjusting the pump's rotational speed so that the prescribed superheating degree condition may be accomplished. The PH water's mass flow rate is also maintained approximately constant throughout this series of tests. In the second series, while keeping the combustion power set to 40% of its nominal value, the superheating degree of the organic fluid at the exit of the EHE section is, in one situation, increased from 5 ºC to 10 ºC and, in the other, set to zero (leading to a two-phase mixture state: vapour quality ≈ 0.75). As for the previous tests, this is done by adjusting the pump rotational speed and keeping the water mass flow rate fixed. Moreover, the influence of the operating pressure was also analysed in this series of tests. In order to do so, the water mass flow rate was halved and the pump rotational speed adapted to obtain a superheating degree of 5 ºC. For each of the experimental situations, the values of the operation parameters are recorded after the system stabilization that, depending on the starting condition (e.g. cold start-up or a variation from a different operating situation), can go from a few to tens of minutes. These values are recorded for about 20 minutes at an acquisition rate of 1 Hz. The arithmetic mean of these is shown in **Table 4-2**. In this table, the values of the superheating degree at the exit of the EHE section (ΔT_2), the values of the combustion power ($\dot{Q}_g$) and the values of the transferred thermal power to the water ($\dot{Q}_{PH}$) and to the organic fluid ($\dot{Q}_{EHE}$) are also shown. The superheating degree is evaluated by the difference between the saturated and the measured (at the exit of the EHE section) organic fluid

temperatures while the combustion power is calculated assuming a complete combustion and knowing the natural-gas composition and rate of consumption. The transferred thermal power to each one of the fluid streams is calculated by the product of the mass flow rate and the difference between the enthalpies evaluated at the pressure and temperature conditions at the exit and at the entrance of their respective ORC-evaporator sections. For the particular experimental situation in which a two-phase mixture occurs at the exit of the EHE section, the enthalpy cannot be determined based on the values of the temperature and pressure. In such a case, that value of enthalpy, considered equal to the one of the working fluid at the entrance of the ORC-condenser, is determined from an energy balance to that component assuming a penalty of 2% to account for energy losses.

***Table 4-2**: ORC-evaporator operating parameters (average values) in the experimental tests.*

			1st series: combustion power variation					**2nd series: combustion power fixed**		
			#1	**#2**	**#3**	**#4**	**#5**	**#6**	**#7**	**#8**
NG-burner and combustion gases	$\dot{Q}_g$	[kW]	10.193	17.152	22.137	26.777	31.283	17.152	17.152	17.152
	T_{10}	[ºC]	46.7	57.2	62.8	68.1	73.3	57.2	58.0	60.8
	$\dot{V}_{NG}^{a)}$	[dm³/s]	0.257	0.435	0.557	0.673	0.787	0.435	0.435	0.435
	T_{11}	[ºC]	26.2	26.1	26.2	26.3	26.3	25.7	25.9	25.8
	δ_{11}	[%]	63.2	63.3	63.3	63.2	63.2	63.3	63.2	63.1
	O_2	[%]	8.0	5.9	5.1	5.1	5.1	5.9	5.9	5.9
EHE section	$\dot{m}_f^{a)}$	[kg/s]	0.026	0.043	0.058	0.070	0.083	0.066	0.043	0.043
	p_f	[bara]	2.70	3.55	4.47	5.53	6.03	2.49	2.685	3.59
	T_1	[ºC]	25.5	28.1	31.9	34.0	35.0	35.4	27.6	32.6
	$T_{1.1}$	[ºC]	27.3	29.4	33.1	35.3	36.4	36.6	28.6	33.9
	$T_{1.2}$	[ºC]	30.0	32.9	36.1	38.2	39.4	38.6	32.2	36.8
	$T_{1.3}$	[ºC]	35.3	38.4	41.7	45.8	48.0	42.1	39.0	42.6
	$T_{1.4}$	[ºC]	38.6	42.1	46.2	53.7	57.6	44.2	42.9	46.5
	$T_{1.5}$	[ºC]	42.5	51.9	59.6	68.6	70.9	50.8	53.2	60.6
	$T_{1.6}$	[ºC]	42.9	51.5	59.3	67.0	70.3	51.0	52.8	60.3
	$T_{1.7}$	[ºC]	42.8	51.6	59.2	66.7	70.1	50.9	52.8	60.4
	T_2	[ºC]	46.7	55.1	64.1	71.1	74.8	49.8	62.1	67.2
	ΔT_2	[ºC]	4.4	4.1	5.3	4.7	5.2	0.0	9.9	7.4
	$\dot{Q}_{EHE}$	[kW]	5.312	8.955	12.316	14.989	17.878	9.361	9.376	9.174
PH section	$\dot{m}_w^{a)}$	[kg/s]	0.108	0.109	0.108	0.106	0.118	0.109	0.113	0.069
	T_6	[ºC]	36.4	43.8	51.1	57.4	59.5	44.8	43.6	55.1
	$T_{6.5}$	[ºC]	40.6	50.1	58.7	66.2	68.6	51.2	49.9	65.0
	T_7	[ºC]	44.0	55.5	64.7	73.0	75.6	55.9	54.5	72.1
	$\dot{Q}_{PH}$	[kW]	3.409	5.310	6.134	6.928	7.916	5.063	5.157	4.942

[a)] Control parameters.

4.6.3 Data comparison

The comparison between the experimental and the model results will be done for the water and organic fluid temperatures gathered along with the PH and EHE sections of the ORC-evaporator, respectively. Besides those temperatures, the transferred thermal power in each section will also be used to assess the match between the experimental and the model results as it allows solving the problems arising from the use of temperatures to compare the heat transfer process when a two-phase state is presented.

The temperatures' comparison may be easily accomplished through the analysis of the charts presented in **Fig. 4-16** where the calculated and the measured temperatures are plotted against each other for the PH and EHE sections. A maximum difference of 2% is found for the PH section (see **Fig. 4-16-a**). Since any calibration factor has been used, this can be considered an exceptional indication of the model's ability to describe the heat transfer process. A detailed analysis of this data identifies the intermediate sensing point ($T_{6.5}$) as the one where the maximum differences are felt. At that point, for all the operating conditions, the calculated temperatures are slightly below the measured ones, however, at the exit of this heating section (T_7) there is an excellent match between both temperatures. Such behaviour seems to indicate that the model somewhat underestimates the transferred thermal power in the first part while slightly overestimating it in the second. As for the EHE, significant differences between the measured and calculated temperatures were found. Those differences, nevertheless, are unevenly distributed along this section. They increase along the lower part of the section, up to a maximum of about 20% observed on the intermediate sensing point $T_{1.5}$, and are meaningfully reduced henceforth (see **Fig. 4-16-b**). Similarly to the intermediate points in the PH section, the calculated temperatures are below the experimentally retrieved ones and, at the exit of the section, the differences, much smaller, are either positive or negative. As such, a similar conclusion can be taken relative to the model's ability to describe the experimental results: the model underestimates the transferred thermal power at the first part while overestimating it at the second part. As a consequence, the model fails to identify the beginning of the liquid-vapour phase transition as can be clearly seen in **Fig. 4-17**. In this figure, presented as an example of what also happens for the other operating conditions, the measured and the calculated values of the temperature of the organic fluid along the EHE section for experimental test #4 are shown. It is also evident that the organic fluid is in a liquid and in a two-phase state in the underestimated and overestimated parts of the heating process, respectively.

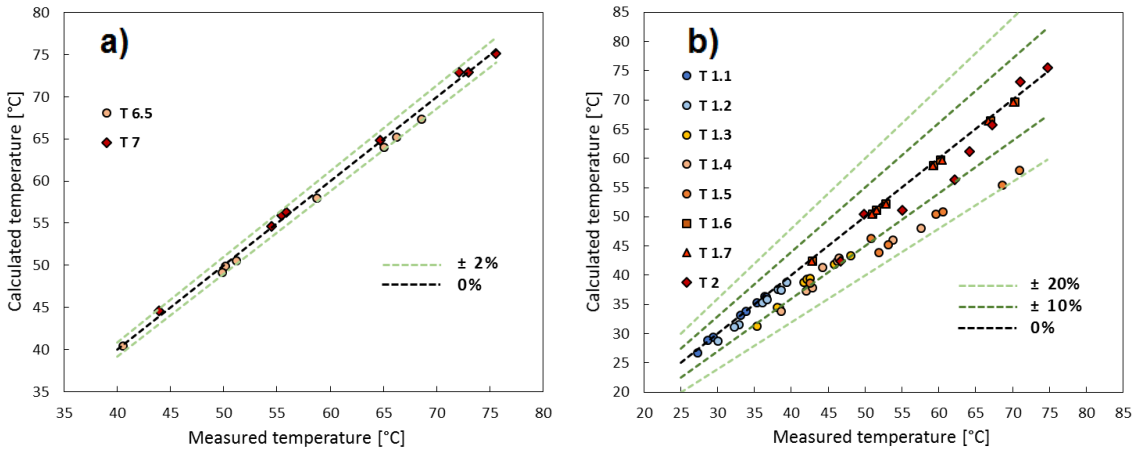

***Fig. 4-16**: Calculated versus measured temperatures for: a) water in the PH and b) organic fluid in the EHE.*

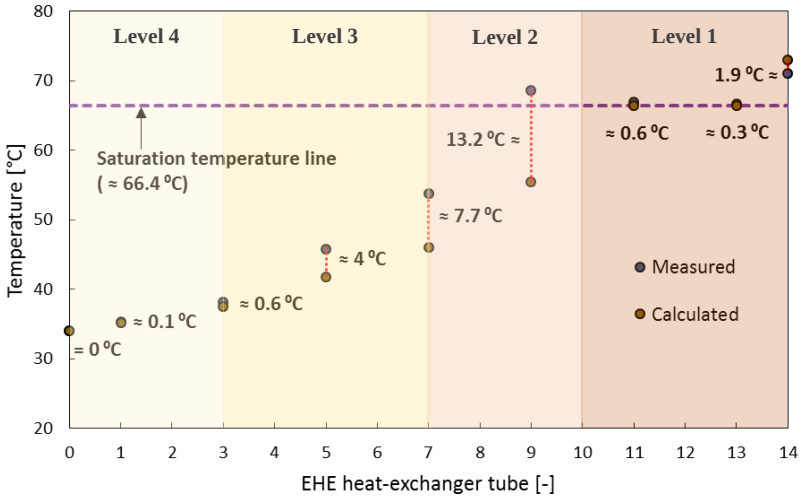

***Fig. 4-17**: Calculated and measured values of the organic fluid temperatures along the EHE section for the operating conditions of test number #4.*

The temperatures' comparison presented in **Fig. 4-16** needs to be complemented with the transferred thermal power comparison since important differences can be hindered behind small temperature variations, especially when a two-phase state is presented. Therefore, **Fig. 4-18** shows the calculated values of the transferred thermal power as a function of the experimentally determined ones for the PH (**Fig. 4-18-a**) and EHE (**Fig. 4-18-b**) sections. The data, presented for both sections, shows a good agreement (maximum difference of 5%) for all the operating conditions.

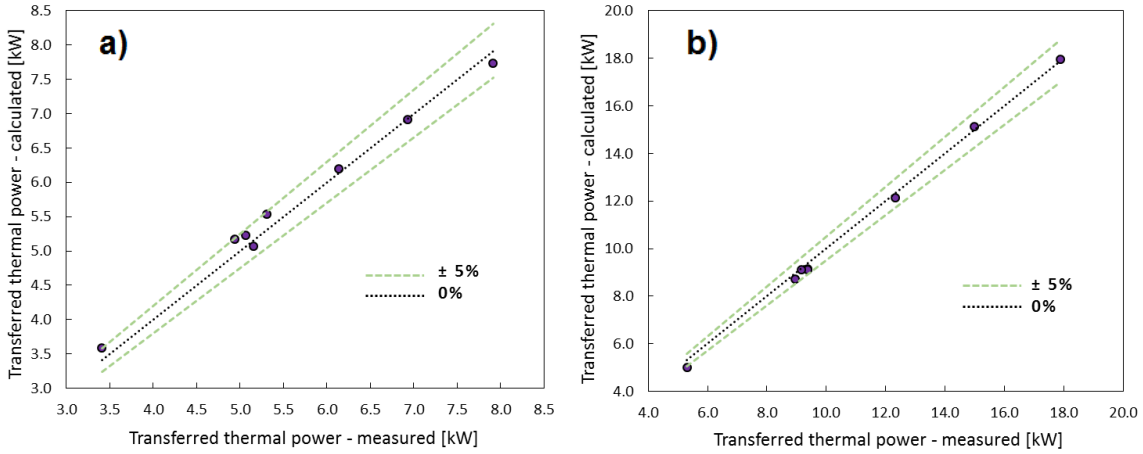

***Fig. 4-18**: Calculated versus measured transferred thermal power for: a) water in the PH and b) organic fluid in the EHE.*

Apart from the subjectivity that the above-mentioned considerations may have, it is possible to conclude that the model successfully accomplishes the calculation of the total thermal power transferred from the combustion gases to the water and the organic fluid but, somehow, fails on the evaluation of how this power is transferred to those fluids along their respective heating sections. Marginally in the PH and markedly in the EHE, it underestimates, in the initial part, and overestimates, in the final part, the thermal power transferred in each of those heating sections. The described behaviour of the model, behind which many reasons may exist, is, however, believed to be effortlessly corrected with simple semi-empirical model improvements and calibration factors.

4.6.4 Calibration process

Despite the agreement already found between the model and the experimental results, a simple calibration procedure was carried out not only for the EHE (where the biggest temperature differences are found) but also for the PH section since the heat transfer processes are sequential and the results obtained in the EHE are directly affected by the ones obtained in the PH.

In the PH section, as the heat transfer process is essentially determined by the external heat transfer coefficient (h_g), considerably smaller than the internal one, the calibration procedure involved its multiplication by a single, empirically determined, factor (CF_{PH}), so that the difference between the model and the experimental results regarding the power transferred becomes smaller than 1%. The values of CF_{PH} that make the model able to accomplish the specified match are shown in **Fig. 4-19** for each one of the operating conditions tested. The equation resulting from the linear regression of those factors (shown on **Fig. 4-19**) is used to calculate its value, as a function of the combustion power, for any other operating conditions.

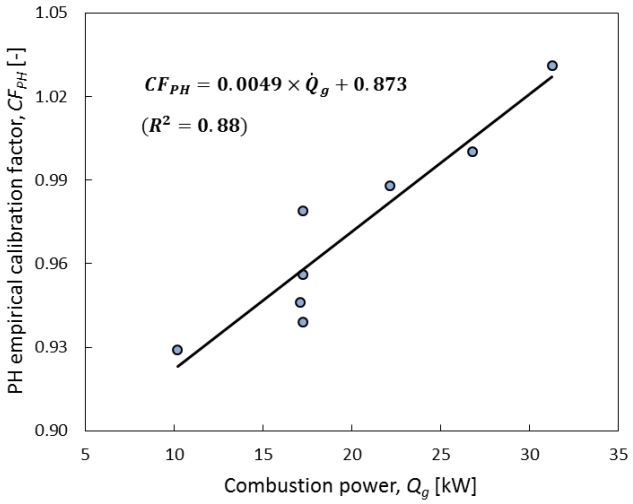

***Fig. 4-19**: Calibration factors used in the PH section as a function of the combustion power.*

The calibration of the model regarding the EHE section pretends to correct the evident underestimation and overestimation observed for the thermal power transferred between the combustion gases and the organic fluid in its initial and final parts, respectively.

In the initial part of the EHE section, the organic fluid is in the liquid state, its velocity is relatively small and, as the external (gas side) heat transfer area is large (due to the fins), the bigger thermal resistance is associated to the internal convection heat transfer coefficient. As the bulk temperature of the organic fluid is below the saturation value, the heat transfer coefficient is calculated using the usual correlations for liquids in tubes. Nevertheless, the temperature of their inner surface may be above the saturation value. In that situation, and whenever in the liquid phase, the internal convection heat transfer coefficient is multiplied by an empirical factor of 1.6, regardless of the temperature difference between the inner surface of the tubes and the saturation value. This value was empirically established to take into account the local (in the thermal boundary layer near the inner surface of the tube) vaporization of the organic fluid and the associated increase of the internal convection heat transfer coefficient from a non-boiling to a boiling (with a quality of approximately 3%) heat transfer process.

In the final part of the EHE section, the organic fluid is essentially in a two-phase condition. The internal convection heat transfer coefficient is large and the bigger thermal resistance is found associated with the external heat transfer process. The correction of the overestimation of the transferred thermal power in this part is then done by multiplying the external heat transfer coefficient (h_{g_j}) by a calibration factor smaller than one. This is made individually for levels 1 ($CF_{EHE_{j=1}}$) and 2 ($CF_{EHE_{j=2}}$) as a function of the combustion power. It is worth mentioning that these two combustion gases' levels match approximately with the part of the EHE in which the organic fluid is essentially in the two-phase state and the transferred thermal power is overestimated.

Those calibration factors, empirically determined, are shown in **Fig. 4-20** for each one of the operating conditions tested. The equations used afterwards to determine the values of those factors, for any operating condition, are also shown in that figure.

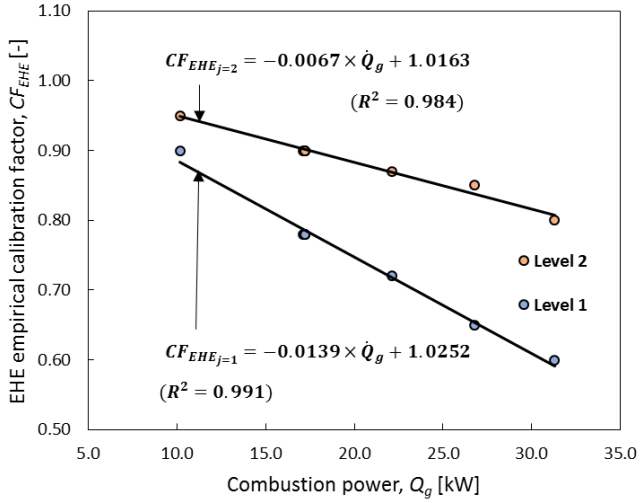

***Fig. 4-20**: Calibration factors of the EHE section as a function of the combustion power.*

The approach followed to calibrate the model was empirically, or semi-empirically, determined and no optimization strategies were considered. The values of the different calibration factors have been set based on a trial-and-error procedure attempting to minimize the differences between the calculated and the experimental values of the temperatures and the transferred thermal power along the EHE section of the ORC-evaporator.

The outcome of such a calibration procedure can be evaluated by the analysis of **Fig. 4-21** and **Fig. 4-22**. In those figures, the calculated temperatures and transferred thermal power are plotted against the experimental values for the operating conditions used in the calibration process. The data shown reveals differences between the calculated and the experimental results smaller than 2% regarding the transferred thermal power, for both sections and, concerning the temperatures, values smaller than 2% and 8% for the PH and EHE sections, respectively. This can be considered a significant improvement in comparison to what was observed for the calculations of the non-calibrated model (see **Fig. 4-16** and **Fig. 4-18**). Besides these improvements, the consequences of the model calibration are also felt in the model's ability to identify the beginning of the liquid-vapour transition. This can be clearly seen in **Fig. 4-23**, in which the measured and the calculated temperatures of the organic fluid retrieved along the EHE section are shown for the operating conditions of test number #4. The error in the identification of the beginning of the phase transition process is reduced from approximately 2 to less than 1 tube.

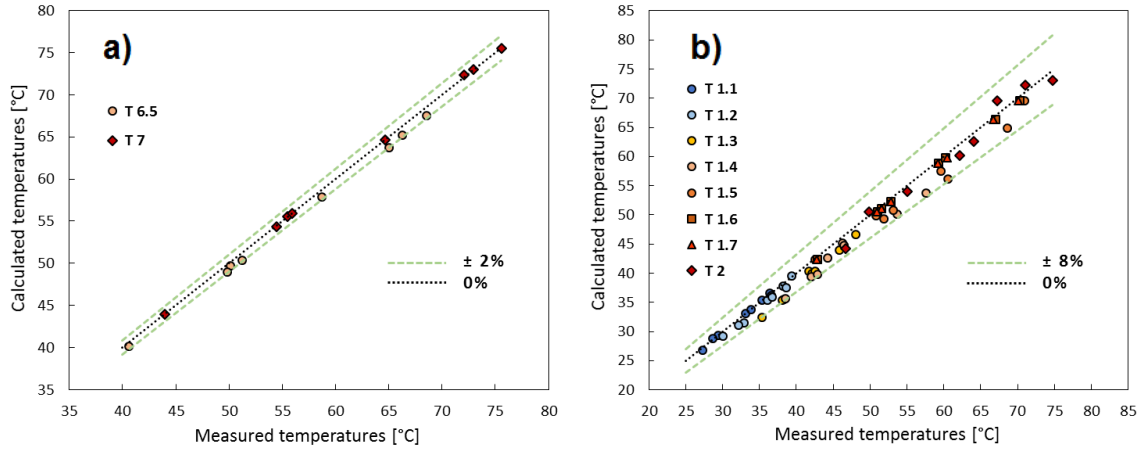

***Fig. 4-21**: Calculated (calibrated) versus measured temperatures for: a) water in the PH and b) organic fluid in the EHE.*

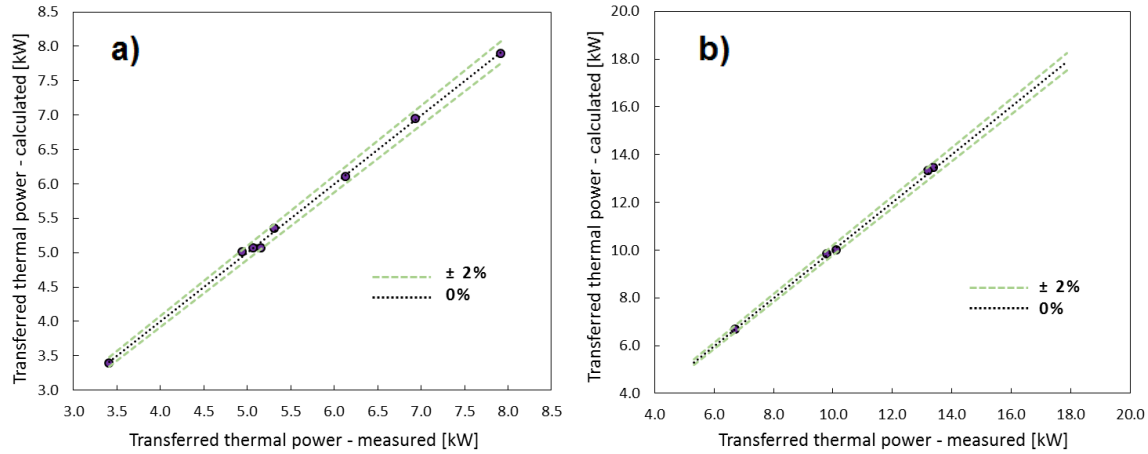

***Fig. 4-22**: Calculated (calibrated) versus measured transferred thermal power for: a) water in the PH and b) organic fluid in the EHE.*

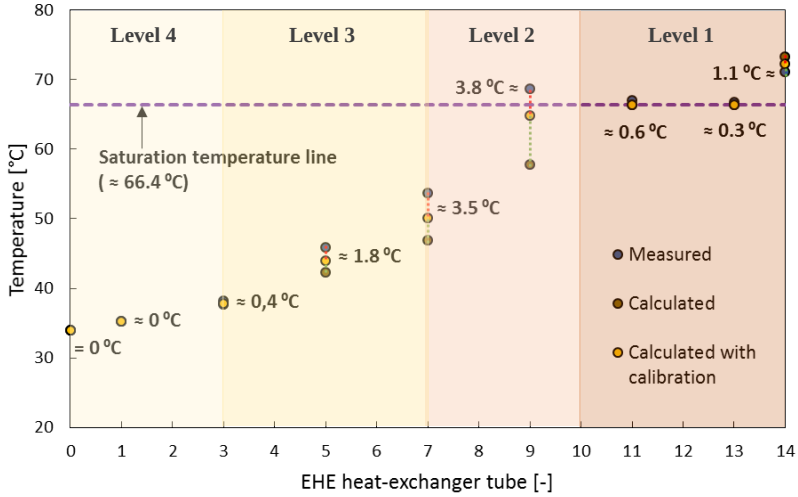

***Fig. 4-23**: Calculated (with and without calibration) and measured values of the organic fluid temperatures along the EHE section for the operating conditions of test number #4.*

4.6.5 Model validation

Following the calibration process, the model was validated by confronting the results of a new series of experimental tests. The arithmetic means of the operation parameters of those tests, obtained in a similar way to the previously described (see section 4.6.2), are presented in **Table 4-3**. This confrontation is shown, for each of the evaporator sections, in **Fig. 4-24** for the temperatures gathered along the heat-exchanger and in **Fig. 4-25** for the transferred thermal power. In addition, the experimental and the calculated temperatures along the EHE section for the operating conditions of test #11 (used as an example) are shown in **Fig. 4-26** in order to verify if the model continues to correctly detect the starting point of the organic fluid vaporization process.

***Table 4-3**: ORC-evaporator operating parameters (average values) in the calibration tests.*

			3rd series: model validation				
			#9	**#10**	**#11**	**#12**	**#13**
NG-burner and combustion gases	$\dot{Q}_g$	[kW]	12.428	17.932	17.932	23.699	23.699
	T_{10}	[ºC]	39.1	48.3	49.2	53.8	58.5
	$\dot{V}_{NG}^{a)}$	[dm³/s]	0.307	0.457	0.457	0.603	0.603
	T_{11}	[ºC]	26.0	25.9	26.0	26.1	26.2
	δ_{11}	[%]	63.0	63.3	62.6	62.9	62.8
	O_2	[%]	7.4	6.3	6.3	5.6	5.6
EHE section	$\dot{m}_f^{a)}$	[kg/s]	0.033	0.051	0.046	0.068	0.062
	p_f	[bara]	3.57	4.24	5.79	4.10	7.03
	T_1	[ºC]	26.2	34.2	32.9	40.9	38.9
	$T_{1.1}$	[ºC]	27.8	35.1	33.9	41.7	39.9
	$T_{1.2}$	[ºC]	30.6	37.8	36.9	43.5	42.2
	$T_{1.3}$	[ºC]	36.6	44.1	44.5	50.2	49.7
	$T_{1.4}$	[ºC]	39.7	46.0	47.3	53.6	53.7
	$T_{1.5}$	[ºC]	40.8	48.2	61.8	56.3	71.2
	$T_{1.6}$	[ºC]	41.0	48.7	61.3	56.6	69.8
	$T_{1.7}$	[ºC]	41.1	48.6	61.8	56.5	69.9
	T_2	[ºC]	43.9	53.6	68.1	60.6	76.8
	ΔT_2	[ºC]	3.2	5.6	4.9	4.8	5.2
	$\dot{Q}_{EHE}$	[kW]	6.703	10.116	9.791	13.382	13.179
PH section	$\dot{m}_w^{a)}$	[kg/s]	0.106	0.106	0.106	0.103	0.105
	T_6	[ºC]	36.8	43.7	43.5	51.2	50.9
	$T_{6.5}$	[ºC]	42.4	50.3	50.9	59.3	59.8
	T_7	[ºC]	45.5	55.2	55.3	65.3	65.4
	$\dot{Q}_{PH}$	[kW]	3.868	5.101	5.218	6.137	6.357

[a)] Control parameters.

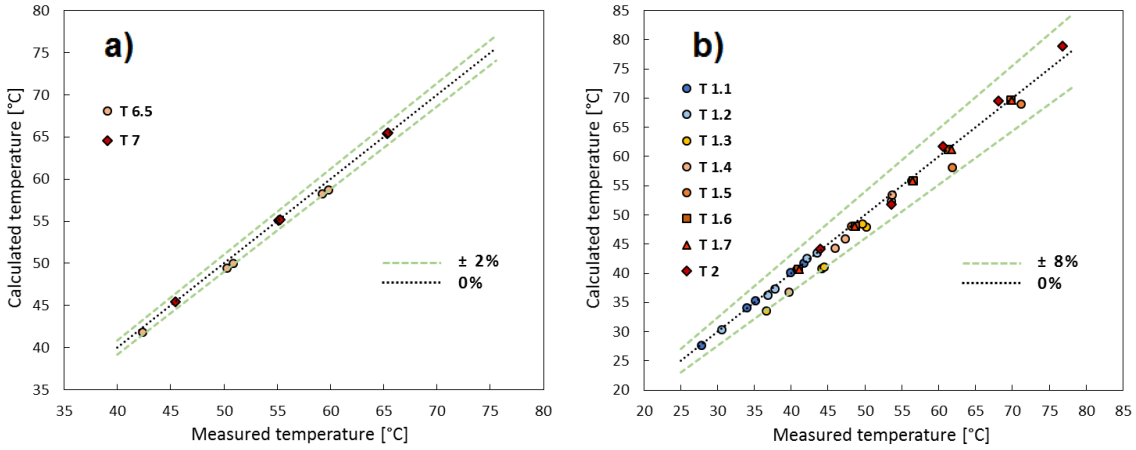

***Fig. 4-24**: Calculated versus measured temperatures for: a) water in the PH and b) organic fluid in the EHE.*

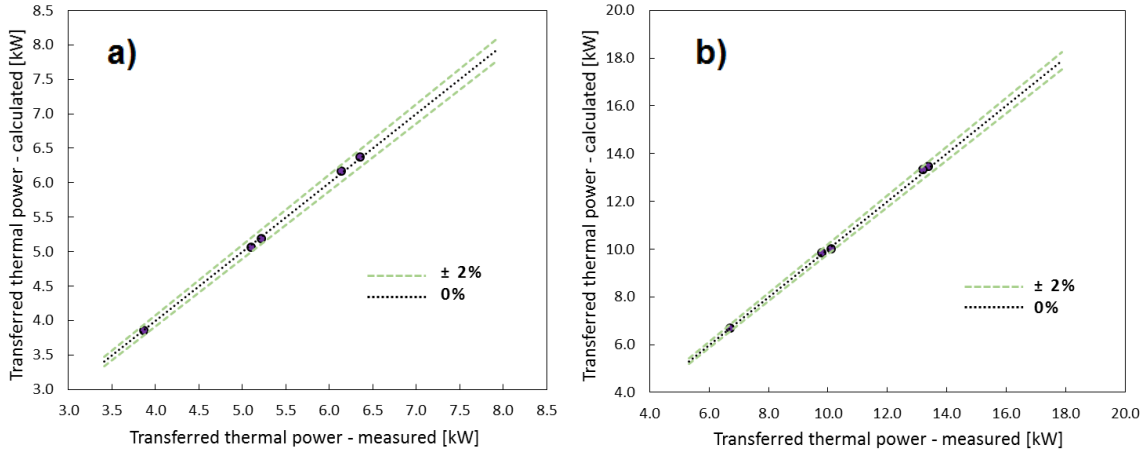

***Fig. 4-25**: Calculated versus measured transferred thermal power for: a) water in the PH and b) organic fluid in the EHE.*

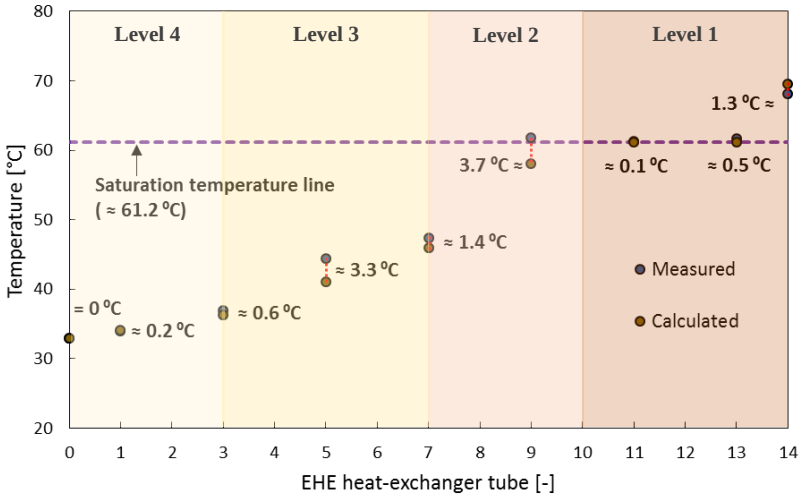

***Fig. 4-26**: Calculated and measured values of the organic fluid temperatures along the EHE section for the operating conditions of test number #11.*

The differences found between the calculated and the experimental results for this new series of tests are similar to those found between the calibrated model and the experimental results. This is proof of the model's ability to predict the ORC-evaporator behaviour within error boundaries up to 2 % for the transferred thermal power and up to 8 % for the organic fluid temperatures gathered along the heat-exchanger sections. Such ability ends up reflected in the model's capacity to predict the starting point of the organic fluid vaporization process within the ORC-evaporator tubes, as shown in **Fig. 4-26**.

4.6.6 Model exploration

It is presumed that the reliability shown by the model on the prediction of the organic fluid temperature and the transferred thermal power is inferable for the prediction of the temperatures of the inner surface of the evaporator tubes since they are mutually dependent. Thus, it will be possible to use it to identify what is and where occurs the maximum value of the inner surface temperature of the evaporator tubes, so that considerations about the risk of thermal degradation of the organic fluid may be taken into account. This temperature, together with both the outer surface and the organic fluid temperatures, are shown in **Fig. 4-27** for the operating conditions of test number #4 (see **Table 4-2**), as an example. The combustion gases' temperature values, for each of the levels in which their domain is divided, are also shown in that figure. As their behaviour (of all the mentioned temperatures) is essentially determined by the thermal resistances involved in the heat transfer process, the values of those, evaluated for each of the EHE control volumes, are shown in **Fig. 4-28** together with the cumulative transferred thermal power.

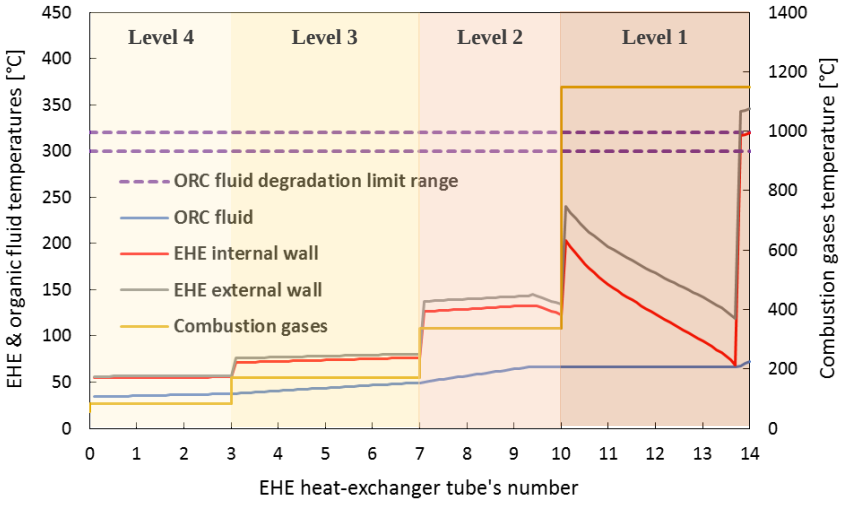

***Fig. 4-27**: Combustion gases, organic fluid (bulk) and tubes internal and external wall temperatures along the EHE tubes for the operating conditions of test number #4.*

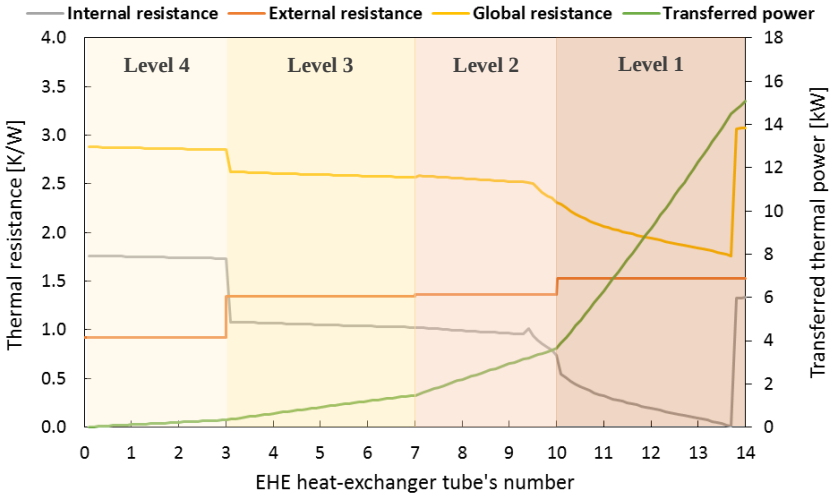

***Fig. 4-28**: Internal, external and overall thermal resistances and cumulative transferred thermal power along the EHE tubes for the operating conditions of test number #4.*

Contrary to what would be expected, given the forecasted differences between the internal and external convection heat transfer coefficients (with the first being, predictably, much higher than the second), the associated thermal resistances are comparable for all of the combustion gases' levels, except for the first (see **Fig. 4-28**). This is justifiable not only due to the differences between the heat transfer areas but also due to the existence of a non-despicable radiative component that needs to be accounted for the evaluation of the external (global) heat transfer coefficient. As a consequence, for those levels, the overall thermal resistance is equally determined by the individual behaviour of both the internal and external. For the better part of level 1, however, the thermal resistances are significantly different, with the external (much bigger than the internal) acting as the limiting one.

Regarding the external thermal resistance, a stepwise behaviour, as the one shown in **Fig. 4-28**, was expected since only one value is calculated per level. Nevertheless, the way how this parameter's values change from level to level is not intuitive, since they include the effect of the calibration process. If only the convective and radiative parts were considered, a decrease of the thermal resistance from level 4 to level 1 could be expected, as a result of the combustion gases' temperature increase. As for the convection part, the temperature increase of the combustion gases will lead to an increase of viscosity and a reduction of the *Reynolds* number. Such decrease leads to higher values of *Colburn* factors. Consequently, an increase of the convective part of the external heat transfer from which would result in the referred, but not observed, decrease of the thermal resistance. On the transition from the 4th to the 3rd level, nevertheless, the increase in thermal resistance is due to a reduction of the radiative part of the external heat transfer coefficient, an exception to the expected behaviour. This exception happens due to the considerations made in section 2.2.1 from which results in higher values of this component in the 4th level to account a non-despicable radiation thermal power transferred from the inner surface of the EHE walls to the tubes.

The effect of the reduction of this parameter (the radiative component of the external heat transfer coefficient) overlaps the one associated with the increase of the combustion gases' temperature which, in this case, is very modest. In the following level transitions (3rd to the 2nd and 2nd to the 1st), the increase of the thermal resistance is justified by the use of calibration factors in levels 2 and 1. These calibrations factors directly affect the value of the external heat transfer coefficient decreasing its value and hiding the effect of the combustion gases' temperature increase.

Contrary to what happens with the external thermal resistance, the internal can change within levels since a value of the internal heat transfer coefficient is calculated for each one of the organic fluid CVs. In this parameter, small variations are expected to arise from variations in the organic fluid mean temperature while major variations may raise from changes in the heat transfer regime (e.g. from single-phase convection to convection with phase transition – vaporization). The stepwise variation in this parameter observed from the 4th to 3rd level transition is, however, due to the use of a calibration factor to account for the local vaporization (see section 4.6.4). This is used whenever the organic fluid is in the liquid phase and the temperature of the inner surface of the wall of the tubes is above the saturation value. This happens beyond the transition from the 4th to the 3rd level and goes up to tube 9 of the 2nd level. Along with the 4th, the 3rd and part of the 2nd levels, a slight decrease of the internal thermal resistance values is observed due to the variation of the organic fluid mean temperature. At tube 9, in the 2nd level, a noticeable reduction of the internal thermal resistance is observed due to the beginning of the sustained vaporization process, coinciding with the point where the average temperature of the organic fluid reaches the saturation value. Because of that, from this point forward, along the rest of the 2nd level and during almost all the extension of the 1st one, the temperature of the organic fluid is kept constant (see **Fig. 4-27**). The sudden decrease of the internal thermal resistance in the 2nd to the 1st level transition is due to the increase of the temperature of the inner surface of the tube, which ends up affecting the fluid mean temperature as a result of the enormous increase of the combustion gases' temperature. For the remainder of this level, due to the increase of the organic fluid quality, the internal thermal resistance decreases nearly to zero. As expected, in the final part of this level, as a consequence of the end of the vaporization process, the internal thermal resistance suddenly increases. It should be noted that despite almost vanishing the internal thermal resistance, the overall value of this parameter does not follow the tendency due to the limiting action of the external one.

It is worth mentioning that the changes in the temperature difference between the combustion gases and the organic fluid, rather than the changes in the overall thermal resistance, are the main driver of the changes in the transferred thermal power, clearly shown in the variations of the slope of its cumulative value at each one of the level transitions (see **Fig. 4-28**). In fact, the significant variation observed at the end of the 2nd level (coinciding with the beginning of the vaporization process), or along the best part of the 1st, does not have visible consequences in the

slope of the cumulative transferred thermal power. Another fact that supports this finding is the unequivocal variation of the transferred thermal power observed from the 2nd to the 3rd level transition for minor variation of the overall thermal resistance. However, an exception was observed on the last tube of the 1st level where the significant increase of the overall thermal resistance, associated with the conclusion of the vaporization process, ends up having consequences on the slope of cumulative transferred thermal power.

Nevertheless, the thermal resistances seem to have a decisive influence over the values of the temperature of the internal and external surfaces of the EHE tubes. Up to tube 9, it is difficult to identify, between the combustion gases' temperatures and the thermal resistances, which is more relevant. Contrary to what is observed for the cumulative transferred thermal power, the variation of the thermal resistance at the end of the 2nd level has consequences on the temperatures of both tubes' surfaces. As expected, the decrease of the internal thermal resistance results in a reduction of not only the internal but also, due to the small conductive thermal resistance of the wall, of the external surface temperature of the tubes. This evidence is even more noticeable on the 1st level where a significant reduction of the internal thermal resistance ends up reflecting a significant reduction of the tubes' internal and external surface temperatures. Once the organic fluid vaporization process is finished, these temperatures have a sudden and huge increase as a consequence of a similar type of variation of the internal thermal resistance. Such temperature variation, apart from any fading effects, results from the non-consideration of the axial conduction heat transfer process through the tubes' walls.

From previous observations and findings, it can be said regarding the main objective of this work, the characterization of the temperature of the internal surface of the EHE tubes, that this parameter is essentially determined by the internal thermal resistance (since the external is essentially constant) and by the combustion gases' temperatures. As the non-boiling heat transfer processes, occurring when the organic fluid is either in liquid or gaseous phases, are characterized by similar values of the internal thermal resistance (see **Fig. 4-28**), the combination of these heat transfer regimes with high temperatures of the combustion gases may originate very high internal surface temperatures of the EHE tubes (see **Fig. 4-27**). Therefore, efforts should be made to avoid or, if not possible, minimize those situations. That means, reduce the superheating degree to the minimum possible value and avoid the presence of the organic fluid in a liquid phase on the 1st level of the tubes. It is also important to notice that any reduction in the temperature of the combustion gases in contact with the tubes of this 1st level, like the one induced by the PH section, will help to reduce the maximum temperature of the inner surface of the tubes' wall and with that, the risk of organic fluid thermal degradation.

4.7 Concluding remarks

The use of direct vaporization in ORC based micro-CHP systems has been disregarded due to the general idea that such an approach will lead to the thermal degradation of the organic fluid. Such an idea stems from the fact that the combustion gases' temperature is well above the one of the organic fluid thermal degradation. Even if this is an undeniable reality for a great part of the heat transfer area of the ORC-evaporator, which does not mean that the internal surface of its tubes (the one in contact with the organic fluid) is at those temperatures. The temperature of the inner surface of the ORC-evaporator tubes is neither the one of the combustion gases nor the one of the organic fluid. Instead, it is the result of the thermal balance made to the ORC-evaporator tube's wall involving the internal and external heat transfer processes. As this temperature is very difficult to measure, the only way to assess it is through modelling.

Considering all the relevant heat transfer modes, using well-established correlations for the calculation of the heat transfer coefficients in the different regimes and basic operating characteristics of the system, a model was developed to calculate the temperature of the inner surface of the tubes of an ORC-evaporator. Without any calibration factors, the model was able to predict the temperatures of the organic fluid, along the heating and vaporization process, and the transferred thermal power with differences to the experimental results under 20 and 5 %, respectively. A simple calibration procedure was able to reduce those differences to values under 8 and 2 %, respectively. Such correspondence is indicative that the essential physics of the energy transfer process in the ORC-evaporator was captured and so the calculated values of the inner surface temperature of their tubes should not be far from reality. This temperature may then be used to assess the risk of the organic fluid thermal degradation which, regardless of further detailed studies, can, from now on, be related to: i) the temperature difference between the inner surface of the tubes and the one of the thermal degradation of the organic fluid (determined by static tests) and ii) the length of the tubes along which that difference is not negative.

The inner surface temperature of the tubes was shown to be not only dependent on the combustion gases temperature, as expected, but also on the internal thermal resistance. The combination of high thermal resistances (associated with non-boiling heat transfer processes in liquid or gaseous phases) with high temperatures of the combustion gases should then be avoided. This means that the operating parameters of the ORC-evaporator must be chosen to ensure that the organic fluid vaporization process starts as earlier as possible and the superheating phase is reduced to the minimum possible. Moreover, it is also important to reduce the inlet temperature of the combustion gases through the use of ultra-lean or flameless burners or through the use of hybrid CHP configurations (as shown in this work).

This page is intentionally left blank.

Chapter 5 A thermal degradation analysis under close-to-real operating conditions

- *"Nothing in life is to be feared, it is only to be understood. Now is the time to understand more, so that we may fear less."* (**Marie Curie**)

Summary: *Continuing with the intending of demonstrating the possibility to use direct vaporization in micro ORC systems, the objective of this chapter is to give the first insight into the study of the effect of the temperature of the heat transfer surfaces in contact with the organic fluid over its chemical integrity. This will be done by coupling a detailed comprehensive characterization of the system operating conditions, including the determination of the temperature of the heat transfer surface, with the realization of, close-to-real operating conditions, endurance tests that include the experimental evaluation of the organic fluid thermal degradation. In addition, this chapter also offers an extensive up-to-date review of the most relevant works regarding the thermal degradation of organic fluids in which details about the thermal stress methods, the thermal degradation detection techniques, and the ways to determine the thermal degradation temperatures, are taken into consideration.*

5.1 Review of the thermal degradation studies

Despite the significant number of works found, it may be referred that all the thermal degradations studies share a common approach that involves: i) the thermal stress of the organic fluid, ii) its characterization to find/quantify evidence of degradation and iii) the determination of a maximum allowable working temperature. A detailed description of the methods/techniques used in each one of these phases is given below.

5.1.1 Thermal stress methods

In what refers to the way how the organic fluids are thermally stressed, two main methods are identified.

Dynamic thermal stress method

In this method, the organic fluid is thermally stressed in a situation as close as possible to the one at which it will work. To achieve that objective, the fluid is forced to circulate through a series of components which, in a more [205,206] or less [207] realistic way, attempt to emulate a real ORC system. At certain specified operating conditions, normally characterized by the organic fluid bulk temperature at the exit of the heating element, the system is left working for tens or hundreds of hours. At the end of the tests, or eventually, at predefined intervals [207], fluid samples are extracted for chemical analytic characterization.

Static thermal stress tests

Aiming the simplicity and the reproducibility (hard to achieve with the dynamic version), in this method, the organic fluid is thermally stressed within a constant volume ampoule/container kept at constant temperature for a predefined period. In its practical implementation, several variations may be found regarding the volume and the material of the container used in the tests, and the way how the heating process of the container/fluid is performed.

5.1.2 Thermal degradation characterization/detection techniques

The techniques used to characterize the organic fluid after being thermally stressed, when considering the type of information retrieved, may be classified in qualitative/indicative and analytic.

A. Qualitative/indicative technique

In this case, considerations about the thermal degradation of the organic fluid are based on changes in the appearance (e.g., colour, transparency, phase separation, etc.) of the samples. When this thermal degradation indicator is used, the thermal stress tests (always static) are performed using glass containers. Besides the subjectivity involved in the evaluation of the existence of changes in the appearance, possibly surmountable with the experience of the analyst, this technique does not provide any measurable information regarding the magnitude of that degradation, being purely qualitative. This technique is commonly used to test the organic fluid with contaminants (e.g., air or water), oil and metal strips.

B. Analytic techniques

If grouped according to the property of the organic fluid measured, the analytic techniques may be divided into those based on: 1) pressure, and 2) concentration of the degradation products. The first can be split, considering the moment when the pressure is measured, in: a) those made during the thermal stress tests and b) those made when the liquid and vapour phases of the organic fluid are in equilibrium (in absence of any stressing conditions). Considerations about the thermal degradation are made based, in the first case, on pressure deviations occurring during the stress tests; and in the second, on differences between the values measured before and after those stress tests. Bearing in mind that these considerations are being made in the scope of the thermal degradation study of organic working fluids, the second group may be classified according to the chemical analytic technique used in: c) gas or liquid chromatography with or without mass or FTIR spectroscopy, d) fluoride ion detector (FID) method and e) total acid number (TAN) test. As these are very well-known standard chemical analytic techniques no further details will be given.

5.1.3 Determination of the thermal degradation temperature

When analysed from the point of view of the reasoning behind the procedure followed, the determination of the thermal degradation temperature of the organic working fluids may be grouped in semi-empirical or in reaction kinetic based approaches.

I - Semi-empirical approach

In general terms, a succession of thermal stress tests (in the great majority of the cases, static), with an arbitrarily defined duration, is performed at increasing temperatures until an indication of the occurrence of thermal degradation is found. As the thermal stress tests are performed at discrete temperatures, the thermal degradation temperature is not precisely defined but it is considered to occur within a range upper bounded by the temperature of the test where the degradation was detected, and lower bounded by the temperature of the previous test. Considerations about the relevance of the consequences of the thermal degradation detected on the operation and the performance of the system along its lifetime are rarely done.

II - Reaction kinetic approach

The standard procedure in this approach involves i) the definition of a threshold for the thermal degradation of the organic fluid (this threshold should be understood as the maximum allowable degradation of the organic fluid so that problems on the operation or a reduction in the performance of the systems won't be observed), ii) the definition of a typical lifetime of the system and iii) the determination of the kinetic parameters of the thermal degradation reaction of the organic fluid. The thermal degradation temperature is then calculated as the one that, for an operation time equivalent to the system lifetime, will lead to a percentual value of the degradation of the organic fluid equal to the threshold. The determination of the kinetic parameters involves the evaluation of the degradation (reaction) rate constant, which means, the rate at which the organic fluid degrades. In many cases, this is done in static conditions along with experience-based established durations and temperatures, using analytic techniques to assess the way how the amount of the products of degradation change with time.

The methods/approaches previously described are summarized in **Table 5-1**. Even if some combinations are more recurrent than others, the methods or approaches from one phase can be freely combined with any of the others. Such multiplicity of combinations may reflect differently the peculiarities of the methods/approaches (which in some cases include a certain degree of arbitrariness) in the values of the degradation temperature and so considerations about these values should not be made uncoupled from the procedure followed in their determination. To allow such analysis, an extensive up-to-date review of the thermal degradation temperatures coupled with the identification of the procedure followed in its determination is offered in **Table 5-2**. To facilitate that analysis, as its consideration will introduce additional variables and complexity, studies

regarding the evaluation of the effect of the presence of contaminants (e.g., oil, water, metals) over the thermal degradation process are not presented in the table. Since they are essentially used to assess the effect of the contaminants on that process, studies resorting to qualitative/indicative and total acid number based analytic detection techniques are also not listed. However, examples of studies using those techniques can be found elsewhere [195,208–212]. **Table 5-2** is organized in alphabetic order by the organic fluid name. Besides the name, the degradation temperature, and the identification of the procedure followed in its determination, also includes the publication source and the laboratory where the research was conducted.

Table 5-1*: Methods/approaches for the thermal degradation analysis of organic working fluids.*

Thermal stress method	Thermal degradation characterization/detection technique	Thermal degradation temperature determination
Static	A. Qualitative/ indicative	I. Semi-empirical approach
	B. Analytic 1. Pressure based: a. Measured during the stress test; b. Measured before and after the stress test. 2. Concentration based: c. Gas or liquid chromatography with/ without mass or FTIR spectroscopy; d. Fluoride ion detection method; e. Total acid number test.	
Dynamic		II. Reaction kinetic approach

Table 5-2*: Thermal degradation temperatures for different organic working fluids including the methods/approaches followed.*

Working fluid	Publication	Laboratory	Methods/ approaches [1)]	Thermal degradation output
Benzene	Andersen and Bruno [213] (2005)	National Institute of Standards and Technology (USA)	Static-B2c-II	$T > 315$ °C [2)]
Biphenyl	Niggemann [205] (1969)	Aviation Division Sundstrand Corporation (USA)	Dynamic-B2c-I	$T = 370$ °C
Cyclo-pentane	Dai et al. [214] (2016)	University of Tsinghua, University of Tianjin	Static-B2c-I	$260 < T < 280$ °C
	Pasetti et al. [215] (2014)	University of Brescia	Static-B1a-I	$T > 350$ °C
			Static-B1b-I	$275 < T < 300$ °C
			Static-B1b-II	$T = 255$ °C [2)]

	Invernizzi et al. [191] (2017)	Polytechnic University of Milan, University of Brescia, ENSIC (France)	Static-B1b-I	$T \approx 350$ °C
			Static-B1b-II	$T_{td} \ll 350$ °C [2)]
	Ginosar et al. [207] (2011)	Idaho National Laboratory (USA)	Dynamic-B2c-I	$T = 300$ °C
HCFC-123	Dai et al. [216] (2018)	University of Tsinghua, University of Tianjin	Static-B2d-I	$200 < T < 220$ °C
HFC-125	Calderazzi & Colonna [217] (1997)	Polytechnic University of Milan	Static-B1b-I	$T = 396$ °C
HFC-1311	Calderazzi & Colonna [217] (1997)	Polytechnic University of Milan	Static-B1b-I	$T = 102$ °C
HFC-134a	Calderazzi & Colonna [217] (1997)	Polytechnic University of Milan	Static-B1b-I	$T = 368$ °C
	Dai et al. [216] (2018)	University of Tsinghua, University of Tianjin	Static-B2d-I	$340 < T < 360$ °C
HFC-141b	Calderazzi & Colonna [217] (1997)	Polytechnic University of Milan	Static-B1b-I	$T = 90$ °C
HFC-143a	Angelino & Invernizzi [218] (2003)	Polytechnic University of Milan, University of Brescia	Static-B1a-I	$400 < T < 450$ °C
			Static-B1b-I	$350 < T_{td} < 400$ °C
HFC-152a	Dai et al. [216] (2018)	University of Tsinghua, University of Tianjin	Static-B2d-I	$160 < T_{td} < 180$ °C
HFC-227ea	Angelino & Invernizzi [218] (2003)	Polytechnic University of Milan, University of Brescia	Static-B1a-I	$475 < T < 500$ °C
			Static-B1b-I	$425 < T < 450$ °C
HFC-236fa	Angelino & Invernizzi [218] (2003)	Polytechnic University of Milan, University of Brescia	Static-B1a-I	$400 < T < 450$ °C
			Static-B1b-I	$400 < T < 450$ °C
	Dai et al. [216] (2018)	University of Tsinghua, University of Tianjin	Static-B2d-I	$380 < T < 400$ °C
HFC-245fa	Angelino & Invernizzi [218] (2003)	Polytechnic University of Milan, University of Brescia	Static-B1a-I	$300 < T < 330$ °C
			Static-B1b-I	$300 < T < 330$ °C
	Dai et al. [216] (2018)	University of Tsinghua, University of Tianjin	Static-B2d-I	$300 < T < 320$ °C
HFC-7146	Calderazzi & Colonna [217] (1997)	Polytechnic University of Milan	Static-B1b-I	$T = 204$ °C

HFC-23	Angelino & Invernizzi [218] (2003)	Polytechnic University of Milan, University of Brescia	Static-B1a-I	$400 < T < 450$ °C
			Static-B1b-I	$400 < T < 450$ °C
HFO-1234yf	Invernizzi et al. [219] (2016)	Polytechnic University of Milan, University of Brescia, University of Bayreuth	Static-B1a-I	$T > 200$ °C
			Static-B1b-I	$T > 200$ °C
HFO-1234ze(E)	Irriyanto et al. [194,220] (2019-2020)	University of Sungkyunkwan	Static-B2c-II	$T = 180$ °C
HFO-1336mzz(Z)	Huo et al. [221] (2019)	University of Chongqing, University of Tokyo	Static-B2c,d-I	$270 < T < 310$ °C
Iso-butane	Dai et al. [214] (2016)	University of Tsinghua, University of Tianjin	Static-B2c-I	$300 < T < 320$ °C
Iso-pentane	Andersen and Bruno [213] (2005)	National Institute of Standards and Technology (USA)	Static-B2c-II	$T_{td} < 315$ °C [2)]
	Dai et al. [214] (2016)	University of Tsinghua, University of Tianjin	Static-B2c-I	$260 < T < 280$ °C
	Pasetti et al. [215] (2014)	University of Brescia	Static-B1a-I	$T > 310$ °C
			Static-B1b-I	$290 < T < 310$ °C
			Static-B1b-II	$T = 290$ °C [2)]
MDM	Keulen et al. [193,222] (2017-2018)	Polytechnic University of Milan, University of Brescia	Static-B1a-I	$T > 350$ °C
			Static-B1b-I	$250 < T < 260$ °C
			Static-B2c-I	$T \ll 350$ °C
	Erhart et al. [223] (2016)	University of Stuttgart, University of Ghent	Dynamic-B2c-I	$T < 290$ °C
MM	PreiBinger & Bruggemann [186] (2016)	University of Bayreuth	Static-B1a-I	$T > 420$ °C
			Static-B1b-I	$T < 420$ °C
			Static-B2c-I	$T < 300$ °C
	Keulen et al. [193] (2017)	Polytechnic University of Milan, University of Brescia	Static-B1a-I	$T > 340$ °C
			Static-B1b-I	$220 < T < 240$ °C
			Static-B2c-I	$T < 340$ °C

N-butane	Pasetti et al. [215] (2014)	University of Brescia	Static-B1a-I	$T > 330$ °C
			Static-B1b-I	$290 < T < 310$ °C
			Static-B1b-II	$T = 280$ °C [2)]
	Dai et al. [214] (2016)	University of Tsinghua, University of Tianjin	Static-B2c-I	$300 < T < 320$ °C
N-hexane	Dai et al. [214] (2016)	Tsinghua University, Tianjin University	Static-B2c-I	$260 < T < 280$ °C
N-pentane	Andersen and Bruno [213] (2005)	National Institute of Standards and Technology (USA)	Static-B2c-II	$T < 315$ °C [2)]
	Dai et al. [214] (2016)	University of Tsinghua, University of Tianjin	Static-B2c-I	$280 < T < 300$ °C
	Dai et al. [224] (2016)	University of Tsinghua, University of Tianjin	Static-B2c-II	$T = 280$ °C
	Invernizzi et al. [191] (2017)	Polytechnic University of Milan, University of Brescia, ENSIC (France)	Static-B1a-I	$327 < T < 376$ °C
			Static-B1b-I	$300 < T < 325$ °C
			Static-B1b-II	$T < 315$ °C [2)]
Neo-pentane	Andersen and Bruno [213] (2005)	National Institute of Standards and Technology (USA)	Static-B2c-II	$T < 315$ °C [2)]
Perfluoro-hexane	Lasala et al. [225] (2015)	Polytechnic University of Milan, University of Brescia	Static-B1a-I	$T < 450$ °C
			Static-B1b-I	$350 < T < 400$ °C
RC-1	Di Nanno et al. [206] (1983)	Thermo Electron Corporation (USA)	Dynamic-B2c-I	$T = 480$ °C
	Ragaller et al. [226] (1987)	Aviation Division Sundstrand Corporation (USA), Argonne National Laboratory (USA)	Static-B1b-I	$T < 430$ °C
Titanium tetrachloride	Invernizzi et al. [192] (2016)	Polytechnic University of Milan, University of Brescia, ENEA (Italy)	Static-B1a-I	$T < 500$ °C
			Static-B1b-I	$T < 500$ °C

Toluene	Andersen and Bruno [213] (2005)	National Institute of Standards and Technology (USA)	Static-B2c-II	$T < 315$ °C [2)]
	Cole et al. [227] (1987)	Argonne National Laboratory (USA)	Dynamic-B2c-II	$T > 360$ °C
	Invernizzi et al. [191] (2017)	Polytechnic University of Milan, University of Brescia, ENSIC (France)	Static-B1b-I	$325 < T < 350$ °C
			Static-B1b-II	$T < 300$ °C [2)]

[1)] Designation according to **Table 5-1**.
[2)] Consideration based on the values of the thermal decomposition reaction rate constant published by the author and based on a maximum degradation of 1% and a minimum system lifetime of 10 years (also contains an arbitrarily (unproven), defined multiplication factor of 10 to adapt the static data to real operating conditions, as done by Dai *et al.* [224]).

Probably due to the referred problem of the specificity of the dynamic thermal stress tests, most of the degradation temperature values available in the literature, and presented in **Table 5-2**, were obtained using the static method. The few values obtained from dynamic stress tests are either dated (with more than 30 years, see [206,227]) or, even if classified as dynamic, peculiar and detached from real ORC systems [207]. An exception occurs for the work of Erhart *et al.* [223] which uses for that assessment samples taken from real (large-scale) systems.

For the rare cases in which the thermal degradation temperature was determined using static and dynamic methods, and excluding those resorting to the analytic technique based on the pressure measurements during the stress test (due to the reasons presented below), it is possible to verify that the ones obtained with the latter method tend to be higher than those obtained with the former. Examples of this situation are found for Toluene, RC-1 and MDM (see **Table 5-2**). The reason for this finding is probably related to the time at which the organic fluid is at high temperature. In the static stress method, since the totality of the organic fluid is kept still in a container, in thermal equilibrium with the surrounding media, which is maintained at a constant temperature, that corresponds to the entire duration of the stress test. However, in the dynamic method, since the organic fluid is circulating and being sequentially (and repeatedly) vaporized and condensed, the period that the fluid is kept at the stress temperature corresponds only to a share of the test duration. Despite its greater reproducibility, as they are obtained in conditions further departed from the real ones, the degradation temperatures assessed with the static method can end up over-restricting the operating conditions of the ORC systems which may be reflected in poor performances. Therefore, taking into consideration those questions, relationships between static and dynamic methods, eventually with the development of time-temperature indicators, should be made.

When analysing **Table 5-2**, it is important to note that the values of the degradation temperature determined using pressure measurements during the thermal stress tests (B1a) are, when compared with the ones determined with other analytic techniques, higher and more dispersed (see, for example, cyclo-pentane, MDM, MM or n-pentane). Used exclusively with static methods, this

technique is based on the observation of pressure variations during the tests with the totality of the organic fluid in the vapour phase. As such, pressure variations associated with any thermal degradation will only be observed if this is accompanied by an alteration in the number of moles in that phase. As different degradation reactions (some increasing and others decreasing the number of moles, see [214]) may combine, it is not certain that a degradation phenomenon will lead to pressure variations. When this analytic technique is used, the identification of the degradation comes normally associated with a decrease of the pressure. This is associated with a reduction of the number of moles of the organic fluid in the vapour phase resulting from partial carbonization [218]. As the formation of solid carbonaceous residues is a clear sign of a high-temperature type of degradation, this may justify why the values of the thermal degradation temperature obtained with this technique are higher. In the other pressure-based analytic technique (B1b), the pressure is measured when the liquid and the vapour phases of the organic fluid are in equilibrium and, if that (the equilibrium) is maintained, the vapour pressure is kept constant. That means, up to a certain degree, the number of moles of the organic fluid in the vapour phase is independent of the existence, or not, of thermal degradation. If, as a result of the thermal degradation, there is the formation of non-condensed gases, the total number of moles in the vapour phase will increase regardless of the reaction(s) that took place. Consequently, and in comparison with the non-degraded fluid, the total (measured) pressure will increase.

Surprisingly, given the diversity of the approaches that may be followed and the degree of arbitrariness that some of them contain (evident in, for example, the absence of reasoning in the definition of the duration of the stress tests, the non-definition of a minimum precision value for the analytic techniques used to detect the products of thermal degradation or even in the empiricism used to define allowable thermal degradation thresholds at the end of a certain life-time working period), and apart the differences arising from the stress methods, different combinations of analytic techniques (excluding those based on the pressure measurement during the thermal stress test) and temperature determination approaches, retrieve similar values for the great majority of the cases in which that comparison is possible to be made. Regardless of this concordance, the importance of several of the mentioned features of the approaches used to determine the thermal degradation temperature should be clarified.

5.2 Methodology

Taking a step further the simple determination of the thermal degradation temperature and attempting to shed some light on the relevance of the thermal boundary layer on the thermal degradation process of the organic fluid, a combined experimental and modelling approach was depicted. It involves the experimental verification of the existence of thermal degradation using the pressure-based analytic technique B1b (see section 5.1) for two sets of operating parameters. These

were selected based on the evaporator heat transfer model results, within the range of the experimental test rig allowable options, to lead to working conditions for which, when compared with the literature available values, the temperature of the heat transfer surface of the evaporator in contact with the organic fluid is: i) not above that limit value allover its extension or ii) surpasses it along with an arbitrarily defined minimum evaporator heat transfer area value of 5 %. Without wanting to anticipate results, the importance of the role of the thermal boundary layer in the thermal degradation process will be proven if evidence of degradation is found in the second, but not in the first of the previously mentioned sets of the operating parameters.

The experimental verification of the existence of thermal degradation involves an original combination of dynamic thermal stress tests with one of the analytic pressure-based characterization techniques. R245fa was the organic fluid selected for this study (as also mentioned in the previous chapters) as it presents interesting performance figures for micro-power scales (< 50 kWe), it is widely used and, most importantly, it is well characterized from the thermal degradation point of view [172,185,228]. Each thermal stress test has a total duration of 80 hours.

5.2.1 Experimental apparatus

The experimental test rig used to perform the dynamic thermal stress tests is the same used for the experimental validation of the heat transfer model of the ORC-evaporator which is well described in section 4.6.1. A note, however, should be done regarding the need to add a high-accuracy pressure transducer to be used in the thermal degradation assessment. For that purpose, a diaphragm type transducer, with an absolute pressure range of 0-200 kPa and an accuracy error of 0.05% of the Full-Scale range (FS), was selected. This was connected to the ORC circuit in its upper part (where, at rest and ambient temperature, there is only gas) using a ball valve that is kept closed during the realization of the thermal stress tests since the transducer does not sustain the usual operating pressures.

5.2.2 Test operating conditions

The materialization of the experimental strategy depicted at the beginning of this section involves the realization of dynamic thermal stress tests for two different operating conditions that lead to situations at which the temperature of the EHE surface in contact with the organic fluid is: i) never above the thermal degradation value (sub-limit situation) and ii) clearly over it in a non-despicable extension of the heat transfer surface (over-limit situation). Since the temperature of the internal surface of the EHE tubes is virtually impossible to measure, the only way to determine which are the operating conditions that will lead to the desired situations is by performing a detailed simulation of the thermal behaviour of the evaporator. For that purpose, the heat transfer model developed in the previous chapter was used.

The first of the operating condition to be tested was similarly arranged to test number #5 of **Table 4-2** which results in a bulk temperature of the organic fluid at the EHE exit of 75 ºC and pressure of 6 bar. Details about the (model calculated) temperatures of the combustion gases, the organic fluid, and the heat transfer surfaces along the EHE are shown in **Fig. 5-1**. The selected operating conditions led to a maximum internal heat transfer surface temperature of 315 ºC which is slightly below the upper limit found in the literature for the R245fa thermal degradation temperature (see **Table 5-2**). This temperature, predicted to be achieved only for less than half of the length of the last of the evaporator tubes, is a consequence of a dramatic decrease of the internal heat transfer coefficient associated with the end of the phase-change process. It is worth mentioning that the decrease in the heat transfer surface temperature observed for the 10th tube marks the beginning of the evaporation process and stems from the increase of the internal heat transfer coefficient associated with that. This reduction, observed along a great part of the first level of the tubes, is due to the increase of the mass fraction of vapour of the organic fluid flow. The sudden variations of the tubes' surface temperatures observed at each level transition are due to the significant variation of the combustion gas temperature [229]. It is also important to say that these temperature variations are unparalleled by the ones of the bulk organic fluid.

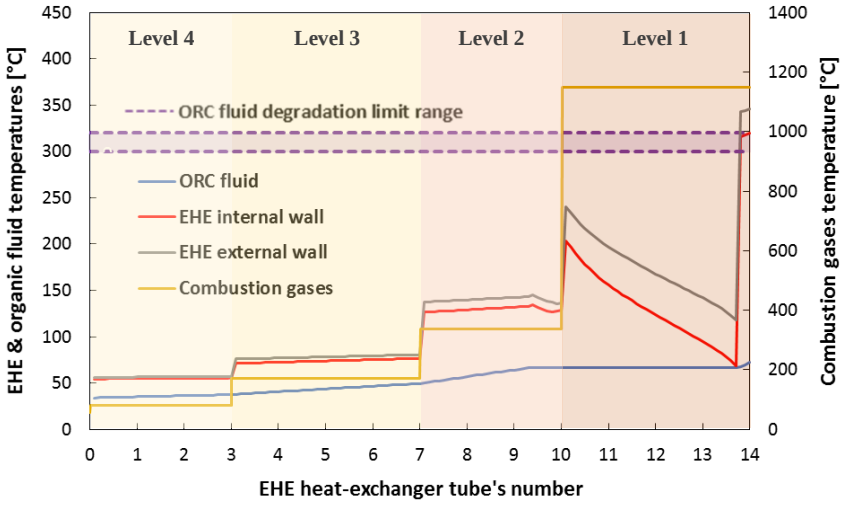

***Fig. 5-1**: Combustion gases, organic fluid (bulk) and tubes' internal and external surface temperatures along the EHE for the sub-limit situation.*

For the definition of the second operating parameters, a set of model calculations was performed. Among them, the one corresponding to a mass flow rate of 0.077 kg/s and a burner power of about 31 kW was selected as it leads to the desired situation. The resulting average working conditions are, for the organic fluid at the evaporator exit, a bulk temperature of 108 ºC and a pressure of 12 bar. Details about the temperatures of the combustion gases, the organic fluid, and the heat transfer surfaces along the EHE, resulting from model calculations, are shown in **Fig. 5-2**. The selected operating parameters led to a maximum internal heat transfer surface temperature of around 370 ºC, well above the upper value found in the literature for the R245fa for an approximated

total length of one evaporator tube (corresponding to around 7% of the total EHE heat transfer area). This situation is a consequence of the combustion gases' high temperature and the relatively low values of the internal heat transfer coefficient associated with the single-phase flow occurring at the beginning and at the end of the first EHE level. Observations and considerations regarding the tubes' internal wall and fluid bulk temperatures identical to the ones made for the first (sub-limit) situation, also apply in this case.

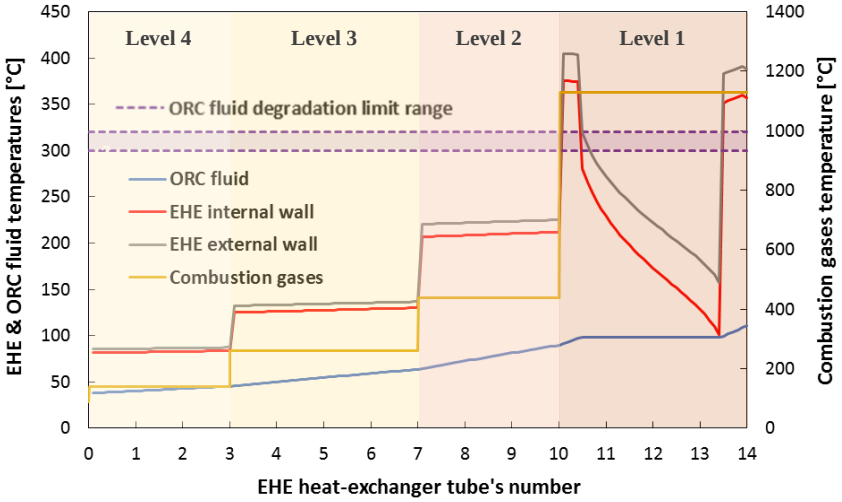

***Fig. 5-2**: Combustion gases, organic fluid (bulk) and tubes' internal and external surface temperatures along the EHE for the over-limit situation.*

5.2.3 Thermal degradation detection technique

If, as in the overwhelming majority of the cases where thermal degradation of the organic fluid occurs, there is the formation of light, low carbon number and non-condensable compounds, the total pressure of the system, when the liquid and vapour phases coexist, is expected to increase and departs from the equilibrium liquid-vapour value. In fact, for a certain temperature, assuming that the non-condensable gases resulted from the thermal degradation of the organic fluid and that the saturated vapour behaves like ideal gases (the error involved in this consideration, for the saturated vapour, is about 5% - compressibility factor Z for $T = 25$ ℃ and $p = 148\ kPa$ is 0.95), the value measured by the pressure transducer (p) is given by the equation (5.1).

$$p = p'_{v_f}(T) + \sum_i p'_{C_i} \tag{5.1}$$

Where $p'_{v_f}(T)$ is the partial pressure of the saturated vapour ($p'_{v_f}(T) = p_{sat}(T)$) and p'_{C_i} is the partial pressure of the i^{th} non-condensable compound. Assuming that the sum of the latter may be lumped in a unique value (p'_C), the equation (5.1) can be rewritten and related with their molar fraction (y_C) as shown in equation (5.2).

$$p = p'_{v_f}(T) + p'_C = p_{sat}(T) + y_C \times p \Leftrightarrow y_C = 1 - \frac{p_{sat}(T)}{p} \quad (5.2)$$

If the total pressure (p) is measured with a pressure sensor with an accuracy error of $0.25\% \times FS$ (typical value for standard diaphragm-type pressure sensors), the difference between the vapour saturation pressure $p_{sat}(T)$ and total pressure p can only be considered significant if:

$$p - p_{sat}(T) \geq 0.25\% \times FS \quad (5.3)$$

This means that the molar fraction of non-condensable components y_C will only be meaningful if:

$$y_C \geq 1 - \left(1 + \frac{0.25\% \times FS}{p_{sat}(T)}\right)^{-1} \quad (5.4)$$

Higher sensibilities, which means lower meaningful values of y_C, will be obtained for higher vapour saturation pressures, which implies higher reference (T) temperatures, and lower accuracy errors of the transducer. In the case of this work, in which a pressure transducer with an FS of 200 kPa and an accuracy error of $0.05\% \times FS$ is used, for a typical reference temperature of 25 ℃, the molar fraction y_C will only be meaningful for values higher than 0.068% (680 ppm). It is important to mention that this estimation only takes into consideration the accuracy errors of the pressure measurements. Accuracy errors associated with the temperatures and/or the combination of the accuracy errors of the pressure and temperature are expected to increase the value above which y_C may be considered significant. One could wonder if such low sensibility would not lead to higher thermal degradation temperatures in comparison with those determined by high sensibility techniques such as, for example, gas chromatography. It turns out that, normally, for these analytic techniques, arbitrarily defined thresholds (with a magnitude identical to the meaningful limit determined for the low sensibility techniques) are used in the assessment of the existence of thermal degradation, which ends up leading to similar final results [72,230].

In principle, the application of this method would only involve the measurement of the total pressure of the thermal stressed organic fluid for a situation at which its liquid and vapour phases are expected to be in equilibrium, and the comparison of that value with the one of the pure fluid (normally made available by the fluid manufacturers or taken from a thermodynamic database) for the same temperature. From a practical point of view, however, as contamination of the fluid may have occurred, due to, for example, the impossibility to achieve absolute vacuum in the container/installation, it is necessary to measure the real organic fluid pressure before the realization of the thermal stress tests (in this condition designated as virgin). Usually, this is done for more than a temperature value. After the realization of the thermal stress tests, the container/installation is brought to each one of these temperatures and the pressure of the fluid (in this condition designated

as stressed), measured again. The comparison of those two pressure values will be the basis to make considerations about the existence (or not) of thermal degradation.

In the case where, as in this work, the thermal stress tests are performed in a test rig that, when at rest, is in thermal equilibrium with the laboratory environment, it is difficult to control the temperature at which the referred pressure measurements are made. Moreover, due to the long duration of the tests (which may extend for days), the laboratory temperature may change non-despicably. This prevents a direct comparison between the pressure values measured for the virgin and stressed fluids as, most probably, they will be referred to different temperatures. If, as it is widely done for this kind of fluids [72,215], a linear relationship between the inverse of the absolute temperature and the natural logarithm of the pressure is determined by a free regression of y on x for the virgin fluid, as shown in equation (5.5), the pressure calculated with it could be compared with the one of the stressed fluid. However, when the range of temperature of the experimental points used in the determination of the referred equation is narrow, uncertainties in its slope (coefficient B) are high and significant errors may arise if extrapolations are necessary. For this reason, it may be preferable, assuming that the presence of the residual air ends up reflected in a pressure-upward shift of the $1/T - \ln(p)$ relationship, to perform a constrained regression imposing for the B coefficient a value equal to the one determined for the pure fluid using data from the *Refprop* database [187,231], for a wide temperature range, and changing the A coefficient until the differences between this constrained and the experimental free regression are minimum. The constrained regression becomes then the reference and the differences between this and the experimental free regression may be seen in **Fig. 5-3** and **Fig. 5-4** for the sub and over-limit operating situations, respectively.

$$y = A + B \times x \qquad with\ x = \ln(p) \text{ and } y = {}^{1}/_{T} \tag{5.5}$$

At this point, details about how, in practical terms, the (p, T) values used in the characterization of the virgin and stressed fluids are obtained, should be given. The pressure p is measured using the pressure transducer with the highest accuracy installed in the test rig, as previously referred in section 5.2.1. Contrary to what happened with the pressure, as all the temperature transducers (thermocouples) show the same accuracy error, the value retrieved by the thermocouple closer to the pressure transducer could be the one selected. However, as there isn't any guarantee that this is the correct one (all the thermocouples may suffer from systematic error), it was decided to combine the value of the pressure with each one of the four available temperatures. In this way, for each measurement time instant, there are four (p, T) data points sharing the same p value. For each fluid condition (virgin or stressed), the data was collected for twenty-four hours so that overnight temperature variations of the laboratory environment could be captured, widening the experimental range of (p, T).

The dispersion of the data gathered, a consequence of the conjugation of the sensors' systematic and random errors, is one of the anticipated characteristics. This, certainly also observable for the thermal stressed fluid, implies the determination of a Prediction Interval (PI) to verify if a certain (p,T) data set is significantly different from the reference relationship. The PI estimates, with a certain confidence, the range within which a future individual experimental observation will fall, given what was already observed. If the overwhelming majority of the (p,T) experimental points of the stressed fluid fall within the PI, this will mean that there aren't significant differences regarding the reference relationship and so no thermal degradation has occurred. The PI, for each value of x, is centred at the reference regression being its half-amplitude Δy_x calculated with equation (5.6) (given equations (5.7) and (5.8)), using the EXCEL™ function INV.T.2C which returns the two-tailed inverse Student's t-distribution. The limits of the PI are presented, for a prescribed confidence level of $\vartheta = 95\%$ and N =17280 experimental points, in **Fig. 5-3** and **Fig. 5-4** for the sub and over-limit situations, respectively.

$$\Delta y_x = \text{INV.T.2C}(1-\vartheta, N-2) \times \sigma_{y_x} \tag{5.6}$$

$$\sigma_{y_x}^2 = \sigma^2 \times \left(1 + \frac{1}{N} + \frac{(x-\bar{x})^2}{\sum_{i=1}^{N} {x_i}^2 - N \times \bar{x}^2}\right) \tag{5.7}$$

$$\sigma^2 = \frac{1}{N-2} \times \sum_{i=1}^{N} \left(y_i - y_{x_i}\right)^2 \text{ and } \bar{x} = \frac{1}{N} \times \sum_{i=1}^{N} x_i \tag{5.8}$$

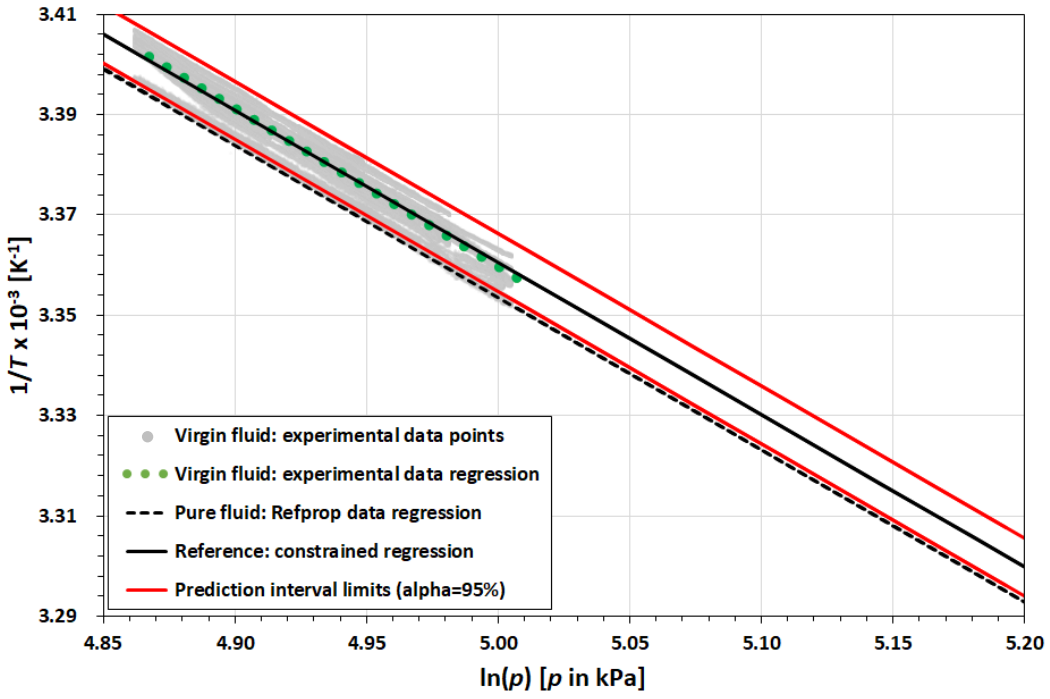

***Fig. 5-3**: Experimental (p,T) data points of the virgin fluid and regressions for the virgin, pure (RefProp data) and reference fluids together with the PI limits for the sub-limit situation.*

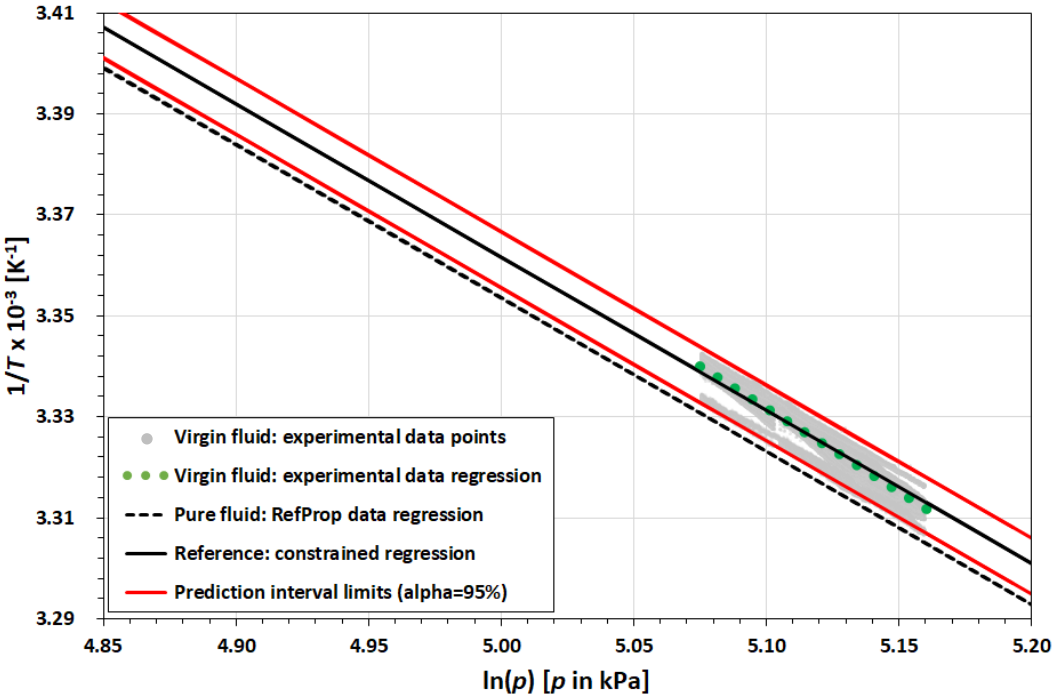

***Fig. 5-4**: Experimental (p,T) data points of the virgin fluid and regressions for the virgin, pure (RefProp data) and reference fluids together with the PI limits for the over-limit situation.*

If, in equation (5.4), the pressure sensor accuracy error $(0.25\% \times FS)$ is replaced by the half-amplitude of the PI, approximately $\pm 3\ kPa$ for both (sub and over limit) situations, the degradation products molar fraction (y_C) will only be meaningful for values greater than 2% (20,000 ppm), for a typical ambient- temperature of 25 ℃.

5.2.4 Experimental procedure

Before the initiation of any stress test, the ORC circuit was emptied and hot air was allowed to circulate, using the two drain/fill valves, to vaporize and remove any fluid residue or water eventually existing within it. The test rig is then pressurized with nitrogen (up to 15 bar) to check for possible high-pressure leakages. After that, the system is depressurized down to less than 5 mbar in an attempt to remove, as much as possible, the non-condensable gases since its presence, especially when referred to oxygen, is known to have a significant influence on the thermal degradation process [191]. The filling process of the system is performed afterwards simply allowing the organic fluid pouring by gravity (through adequate fittings and tubes) in an amount previously determined.

To capture a time-trending evolution of the organic fluid thermal degradation, the realization of the thermal stress tests was performed by breaking down the total stress time (80 hours) into four equal parts of 20 hours, involving the following steps:

1. With the test rig in thermal equilibrium with the laboratory environment, the acquisition of the (p, T) experimental data set used for the characterization of the virgin fluid is performed, continuously, for 24 hours, at a rate of 0.2 s^{-1};
2. Start-up the system and wait for its thermal stabilization (the stabilization period, less than 15 minutes, is not accounted as stress test time);
3. Keep the system working as stable as possible for the defined time (20 hours) while recording the main operating data to verify for possible deviations/fluctuations regarding the setpoint;
4. Turn off the system and wait for the re-achievement of the thermal equilibrium with the laboratory environment (takes around 12 hours). Reacquire the (p, T) experimental data set (in a similar way to what was done in the first step) to characterize the stressed fluid;
5. Repeat the steps from 2 to 4 until the completion of the total stress time predefined for the tests (80 hours).

5.3 Experimental results and discussion

For each of the experimental situations previously mentioned, two types of experimental results will be shown: i) temperature and pressure time histories of the thermal stress tests and ii) (p, T) experimental data sets for the stressed fluid at the end of each 20 hours test periods. The first will be used simply to make considerations about the system operating conditions' stability and about the match between those conditions and the ones used in the evaporator heat transfer model calculations. The second will be used to assess the existence of the organic fluid thermal degradation.

5.3.1 Thermal stress test stability

Time histories of the pressure and temperature, both measured at the EHE exit, are shown together with their average values, the saturation temperature (determined for the average pressure) and those used in the evaporator heat transfer model calculations, for the sub and over-limit situations, in **Fig. 5-5** and **Fig. 5-6**, respectively.

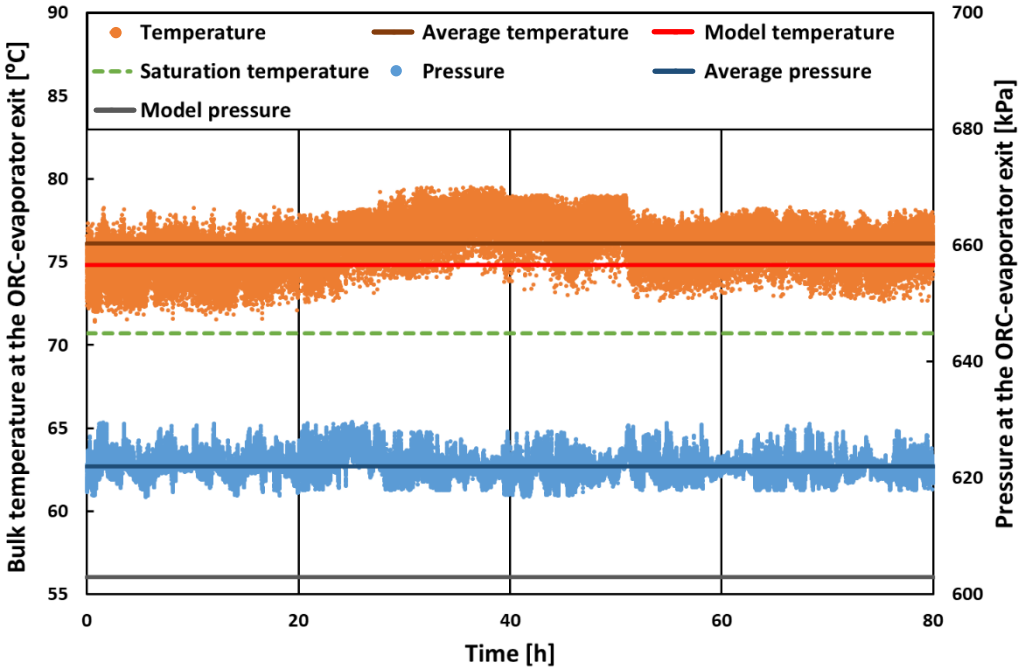

***Fig. 5-5**: Temperature and pressure time histories of the thermal stress test with their average values together with temperature and pressure used in evaporator model for the sub-limit situation.*

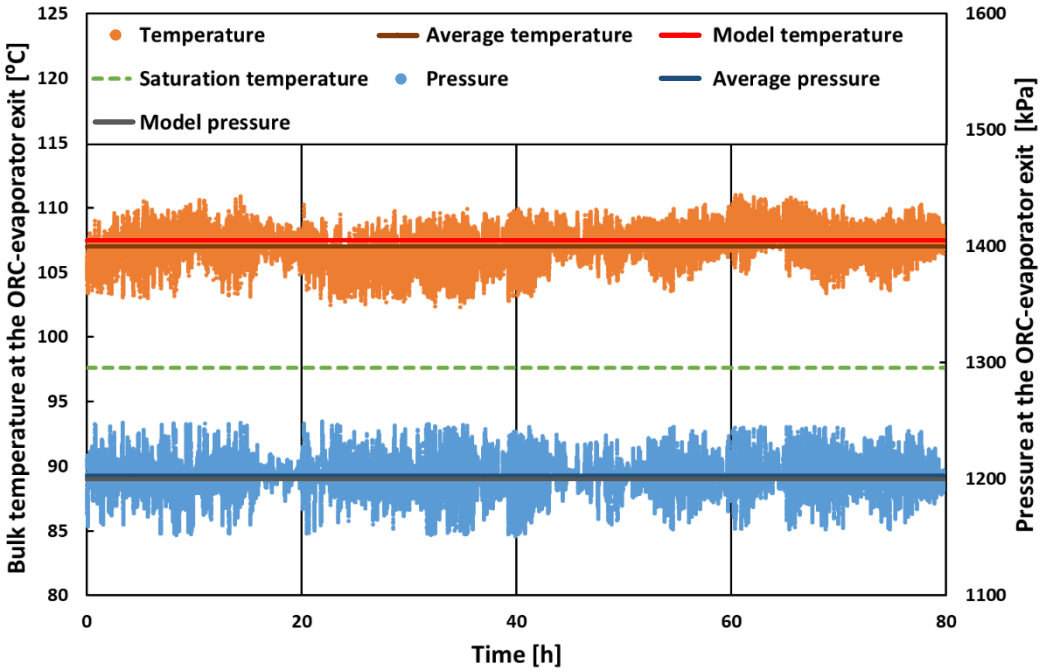

***Fig. 5-6**: Temperature and pressure time histories of the thermal stress test with their average values together with temperature and pressure used in evaporator model for the over-limit situation.*

Throughout the thermal stress tests, the average values of the temperature and pressure are kept constant and close enough to the ones used in the evaporator heat transfer model calculations, so that considerations made regarding the thermal degradation of the organic fluid, based on the information resulting from those simulations (e.g., the temperature of heat transfer surfaces), are acceptable. The oscillations observed, in both experimental situations, are due to changes in the

organic fluid temperature at the ORC-condenser exit caused by alterations in the cooling water mass flow rate arising from pressure variations of the building hydraulic grid (not controlled).

5.3.2 Thermal degradation assessment

The experimental (p, T) data sets at the end of each 20 hours test period are shown, together with the reference relationship and the PI limits, for the sub and over-limit situations in **Fig. 5-7** and **Fig. 5-8**, respectively.

It is clear for both situations and all the assessment moments that most of the data of each one of the experimental sets is within the PI limits (more than 99,9% of the points verify this condition). Therefore, it can be concluded that no degradation or, at least, no degradation with a magnitude detectable by this method, occurred. With due care, however, it may also be mentioned that it seems unjustified the idea of limiting the maximum temperature of the heat transfer surfaces to the temperature value obtained from static stress tests since levels of degradation capable of raising eventual operating problems were not detected.

Although known to be exponentially temperature-depend [232], and despite the elevated temperature value of the heat transfer surface, these results are believed to be related to the time during which the fluid is kept in the thermal boundary layer adjacent to that surface, which is small enough not to give origin to a degradation capable of raising operating problems. This does not mean a downgrade of the importance of the role of the thermal boundary layer in the organic fluid thermal degradation process. That role is still (and needs) to be understood in-depth as it can affect the system design limits, which may end up resulting in poor performances (if reflected in the maximum bulk temperature of the organic fluid) or bigger heat-exchangers (if affecting the maximum temperature of the heat transfer surface). Being time and temperature key factors affecting the thermal degradation within the boundary layer, such clarification demand for an especially depicted experimental plan centred in the establishment of correlations between those parameters and the amount of degradation of the organic fluid, and not just in the definition of limits to the operation of the system. Such an attempt, almost certainly, demands higher sensitivity analytic techniques.

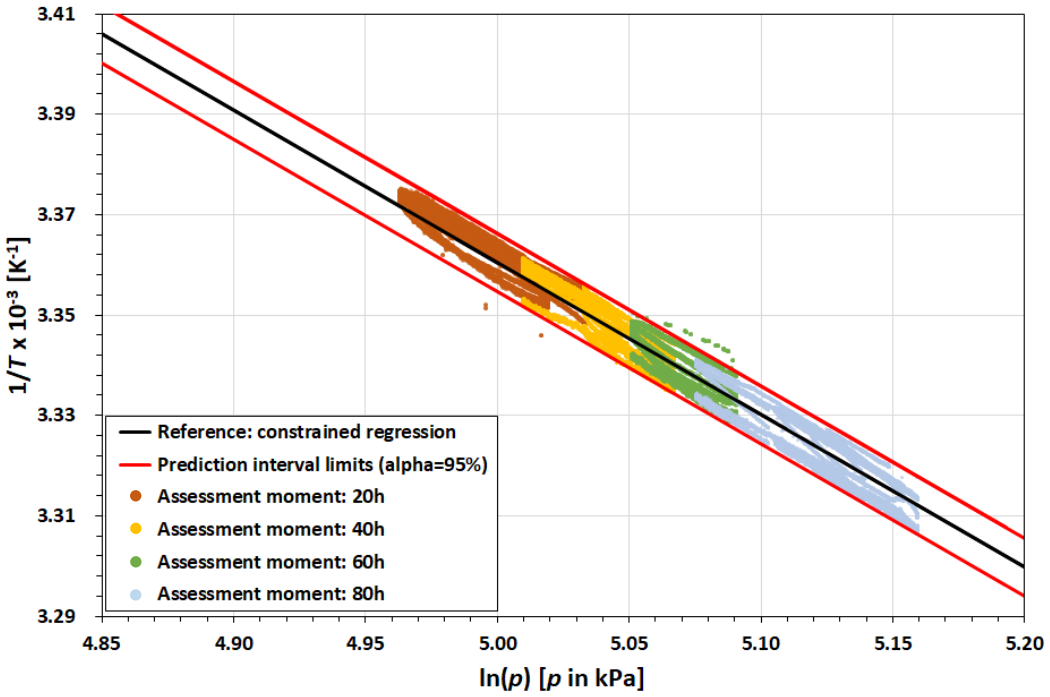

***Fig. 5-7**: Experimental (p, T) data points measured after the thermal stress assessment moments together with the reference regression and the PI limits for the sub-limit situation.*

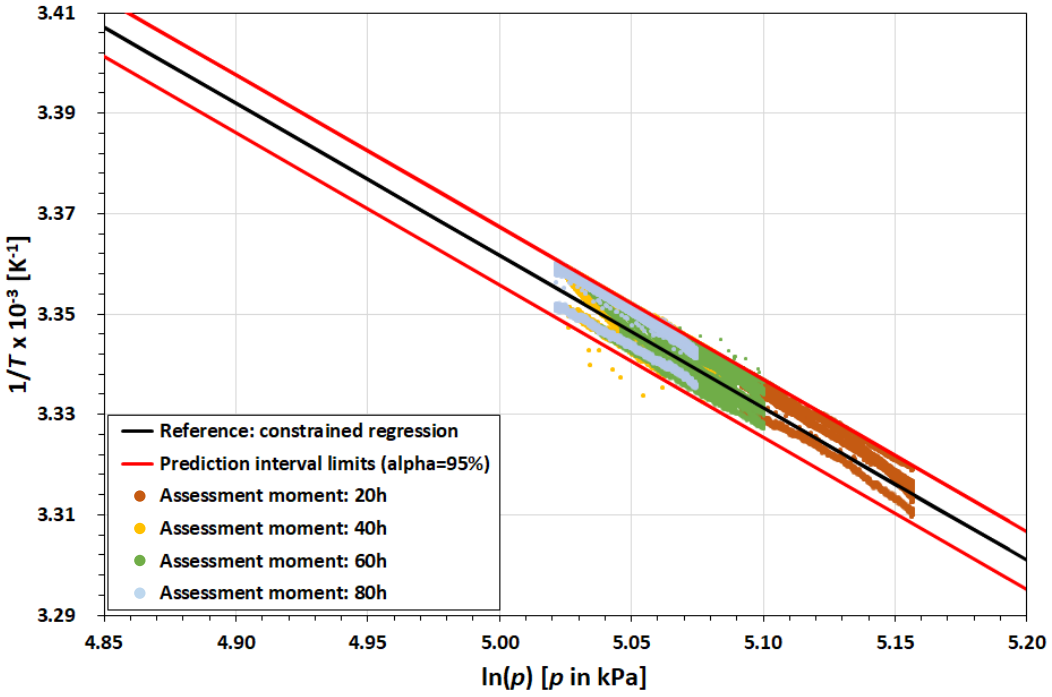

***Fig. 5-8**: Experimental (p, T) data points measured after the thermal stress assessment moments together with the reference regression and the PI limits for the over-limit situation.*

5.4 Concluding remarks

Framed by the intention of shedding light on the role of the thermal boundary layer (through the determination of the maximum temperature of the heat transfer surfaces) in the thermal degradation of the organic working fluids, this paper presents an extensive, detailed, and systematic, up-to-date review of the most relevant works in the area and proposes an experimental methodology for the evaluation of the referred role.

The forehand set of outputs of the literature review were: i) the ascertainment of the multiplicity of the approaches followed, patented not only in the way how the fluid is thermally stressed but also in how the existence of degradation is assessed and how the determination of the (degradation) temperature is performed, ii) the verification of the existence of a certain degree of arbitrariness in several of those approaches, reflected, for example, in unjustified specifications of the thermal stress time or in the definition of a degradation threshold used in the temperature determination, and iii) the perception that the degradation temperature is non-despicably affected by the approach followed in its determination. These outputs have led to the creation of a framework for the classification of the approaches followed in the determination of the thermal degradation temperature of organic fluids. The framework divides the approaches into three main steps: a) thermal stress tests, b) assessment of the degradations and c) determination of the degradation temperature. Each one of these was subdivided according to the distinctive characteristics of the procedures found during the review. The framework was used to classify the thermal degradation studies being the output of that classification shown together with the thermal degradation temperature (as they are related).

The great majority of the thermal degradation temperature values available in the literature were determined using static stress tests. The few values determined using dynamic stress tests were either dated or obtained for conditions far from those normally found in real ORC systems. For those rare cases in which the thermal degradation temperature was determined using both kinds of tests, it is possible to verify that the ones obtained with the dynamic tend to be higher than those obtained with the static. Given the intrinsic nature of these stress tests, this can be seen as an indication that the time at which the organic fluid is kept at a high temperature is a relevant parameter concerning its thermal degradation.

The methodology developed to access the relevance of the heat transfer surface temperatures over the thermal degradation of the organic fluid involved the coupling of a detailed comprehensive characterization of the system operating conditions (which includes model calculated values of that temperature) with the experimental evaluation of the thermal degradation. This evaluation was done recurring to an original combination of dynamic stress tests with the analytic pressure-based characterization technique.

Since in one of the two experimental conditions considered in this work the heat transfer surface temperature of the EHE is well above the threshold found in the literature, the absence of thermal degradation in both of those situations may be seen as: i) a clear sign that the thresholds found in the literature should not be used to impose upper bounds to the evaporator heat transfer surface temperature and ii) a second indication on the relevance of time (and not only temperature) in the thermal degradation of the organic fluid, reinforcing the literature review conclusions. The use of limits imposed on a time-temperature indicator is envisaged to better capture the real risk of the organic fluid thermal degradation. Such an indicator should also be used to extrapolate the significant amount of data existing in the literature regarding the thermal degradation temperatures obtained with static stress tests to real operating conditions.

Chapter 6 Conclusions

- *"A conclusion is the place where you get tired of thinking."* (**Arthur Bloch**)

6.1 Key findings and contributions

The development of an ORC based micro-CHP system with a direct vaporization evaporator is analyzed in-depth throughout this PhD thesis in an attempt to overpass the main obstacles that are precluding the technological breakthrough with market consequences of these types of devices. The key findings are displayed in the following paragraphs referent to the three main research questions and specific assessments formulated in Chapter 1 (**Table 1-2**).

1. ***What are the essential features that ORC based micro-CHP systems should present to fulfil the technological gap that is preventing the market breakthrough?***

    i) Are there environmental and economic benefits in retrofitting the residential heating systems by CHP units?
    ii) Is the ORC technology the proper choice to fulfil the essential features of a residential-scale CHP system?
    iii) What is the current status of the technology and which are the main challenges that are precluding its implementation?

In fact, and considering the first specific assessment, this research demonstrates that the primary energy savings, GHG emissions reductions and economic benefits obtained with the implementation of micro-scale CHP systems are effectively huge. The biggest share of that potential is found, by far, in the residential sector, especially on those systems attempting to retrofit the current wall-mounted conventional or combi-boilers. However, micro-CHP systems have still not reached a sufficient state of maturity to be considered an actual valid alternative to the standard domestic heating systems and there are still technological obstacles to its large diffusion, wherein gas and electricity prices will play a very important role to achieve a competitive micro-CHP unit that needs to be characterized by a low investment cost and easy operation.

Within the technologies available, and answering the second specific assessment, Rankine based micro-CHP systems appear as the most suitable and promising solution for this scale due to a set of typical characteristics in which its simplicity and the (thermal and electrical) efficiencies deserves to be remarked due to its suitability to the domestic scale. It is also clear that the use of organic fluids seems to be more interesting than water/steam, not only because water demands higher operating pressures but also because the organic fluids, due to the shape of their saturation

lines, may work with saturated vapour and avoid high superheating degrees necessary in the water/steam cycles due to problems associated with moister contents in the expander.

The answer to the third specific assessment involved an extensive investigation of the market and ORC research and development trends. Regarding the essential features of the residential scale, the ORC based micro-CHP system must deal with short response times to face the highly variable thermal loads that are typical of this application. This feature is essentially dependent on the way how primary energy is delivered to the ORC-evaporator, while the other components of the cycle - expander, pump and condenser - have a minor role in that specific task. The most common micro-CHP configuration includes an intermediate thermal circuit to transfer energy from the primary energy source to the power cycle using a plate-type heat-exchanger as the ORC-evaporator. This solution has, however, several drawbacks compared with the direct use of the primary energy source for the vaporization of the organic fluid such as: a decrease of the system efficiency due to the inevitable thermal loss in the intermediate circuit, an increase of the investment cost and, most importantly, an increase of the thermal inertia. This increase of the thermal inertia affects negatively the response time of the entire system and it may affect its ability to respond accordingly to the residential thermal requests.

Regarding the main research question, it is obvious that the ORC-evaporator, and the way how the primary energy is delivered to the power cycle, is intrinsically connected with major key issues when a residential implementation is considered and, most worryingly, these questions have passed submissive compared to the current high number of expander analysis or the organic fluid selection methodologies performed.

2. ***What design principles should be followed to develop a suitable evaporator to achieve the market breakthrough of micro-CHP systems with ORC technology?***

   i) Once direct vaporization is a known and important design principle, can it create safety or operating problems?
   ii) Study and development of a novel ORC-evaporator considering the identified design principles of the residential scale.

The answer to the main research question and the two specific assessments are given together since they are related.

Some of the features that an ORC based micro-CHP systems aiming to retrofit the current combi-boilers should follow are: reduced dimensions, high efficiency and high turn-down ratio evaporators. To achieve such requirements, the design principles of those ORC-evaporators should, respectively, include: i) direct vaporization, ii) counter-flow arrangement and iii) modulated pre-mixed natural-gas burners. A solution of an ORC-evaporator accomplishing these specifications was

presented. This solution showed significant safety problems created by the high temperatures involved that cause the overheating of the natural-gas burner head. From this, a fourth design principle arose: the need for a cold surrounding on the natural-gas burner head. This last design principle led to the development of an ORC-evaporator where part of the energy contained in the combustion gases is transferred to the water before they reach the ORC working fluid heat-exchanger in an attempt of creating a (water) cold surrounding to the natural-gas burner head. The integration of such an ORC-evaporator in the CHP system gave origin to a hybrid configuration in which the useful thermal energy transferred to the water is done stepwise: firstly, in the ORC-condenser and then in the water post-heating section of the ORC-evaporator. Such configuration, since it reduces the average temperature at the ORC-condenser, increases the cycle efficiency and the net specific work from which results, even taking into consideration the negative effect of the associated working fluid mass flow rate reduction, an increase of the primary energy savings and the ORC net power output for a significant part of the CHP typical operating conditions. Furthermore, the temperature reduction of the combustion gases in the water post-heating section of the ORC-evaporator for one of the most characteristic CHP operating conditions can be as high as 520 ºC without any losses in the primary energy savings nor the ORC net power output. This temperature reduction can help prevent, in a significant way, the occurrence of one of the major concerns associated with the direct vaporization of the ORC working fluid: the thermal degradation.

3. What is the real risk of thermal degradation of the organic fluid associated with these direct vaporization systems? How can it be assessed and controlled?

i) What are the common methods to evaluate the thermal degradation of organic fluids?
ii) What is the role of the ORC-evaporator heat transfer surface temperatures on the thermal degradation of the organic fluid in real direct vaporization operating systems?

Concerning the first specific assessment, an extensive, detailed and systematic up-to-date review of the most relevant works in the area was presented. The forehand set of outputs of the literature review were: i) the ascertainment of the multiplicity of the approaches followed, patented not only in the way how the fluid is thermally stressed but also in how the existence of degradation is assessed and how the determination of the (degradation) temperature is performed, ii) the verification of the existence of a certain degree of arbitrariness in several of those approaches, and iii) the perception that the degradation temperature is non-despicably affected by the approach followed in its determination. These outputs have led to the creation of a framework for the classification of the approaches followed in the determination of the thermal degradation temperature of organic fluids. The framework divides the approaches into three main steps: a) thermal stress tests, b) assessment of the thermal degradation and c) determination of the degradation

temperature. The framework was used to classify the thermal degradation studies being the output of that classification shown together with the thermal degradation temperature (as they are related).

The great majority of the thermal degradation temperature values available in the literature were determined using static stress tests. The few values determined using dynamic stress tests were either dated or obtained for conditions far from those normally found in real ORC systems. For those rare cases in which the thermal degradation temperature was determined using both kinds of tests, it is possible to verify that the ones obtained with the dynamic tend to be higher than those obtained with the static. Given the intrinsic nature of these stress tests, this can be seen as an indication that the time at which the organic fluid is kept at a high temperature is a relevant parameter concerning its thermal degradation.

To answer both the main research question and the second specific assessment, a methodology to access the relevance of the heat transfer surface temperatures over the thermal degradation of the organic fluid, which involves the combination of a detailed comprehensive characterization of the system operating conditions with the experimental evaluation of the thermal degradation, was presented.

Regarding the characterization of the system operating conditions, and being the determination of the temperature of the heat transfer surfaces a vital parameter, a detailed heat transfer model considering all the relevant heat transfer modes was developed since its experimental measurement is practically impossible to accomplish. Without the use of any calibration factors, the developed model was able to predict the temperatures of the organic fluid, along the heating and vaporization process, and the transferred thermal power with differences to the experimental results under 20 and 5 %, respectively. A simple calibration procedure was able to reduce those differences to values under 8 and 2 %, respectively. Such correspondence is indicative that the essential physics of the energy transfer process in the ORC-evaporator was captured and so the calculated values of the inner surface temperature of their tubes should not be far from reality. The inner surface temperature of the tubes was shown to be not only dependent on the combustion gases temperature, as expected, but also on the internal thermal resistance. The combination of high thermal resistances (associated with non-boiling heat transfer processes in liquid or gaseous phases) with high temperatures of the combustion gases should then be avoided. This means that the operating parameters of the ORC-evaporator must be chosen to ensure that the organic fluid vaporization process starts as earlier as possible and the superheating phase is reduced to the minimum possible. Moreover, it is also important to reduce the inlet temperature of the combustion gases through the use of ultra-lean or flameless burners or through the use of hybrid CHP configurations.

For the experimental evaluation of the thermal degradation, an original combination of dynamic thermal stress tests with the analytic pressure-based characterization technique is used.

Since in one of the two experimental conditions considered in this work the heat transfer surface temperature of the EHE is well above the threshold found in the literature, the absence of thermal degradation in both of those situations may be seen as: i) a clear sign that the thresholds found in the literature should not be used to impose upper bounds to the evaporator heat transfer surface temperature and ii) a second indication on the relevance of time (and not only temperature) in the thermal degradation of the organic fluid, reinforcing the literature review conclusions.

Such a combined methodology is believed to (re)open doors for the direct vaporization of the organic fluid to several ORC based micro-CHP systems from which important benefits regarding the efficiency, response time, size and cost are expected.

6.2 Future perspectives

Time and the need to evolve are two unavoidable aspects. Just 4 years ago, the retrofit of the conventional and combi-boilers by micro-scale CHP systems appeared inevitable since it provided significant primary energy savings, GHG emissions reduction and economic benefits, as demonstrated in chapter 2 of this PhD thesis. However, and despite those benefits, the scenario is not so clear nowadays because of the ongoing energy transition (which aims for total electrification of the economy and the exclusion of any technology that runs on fossil fuels) and the very ambitious (short term) environmental thresholds defined in the 2021 United Nations Climate Change Conference (COP26), in Glasgow [233,234]. Moreover, and since the ORC based micro-CHP system studied in this PhD thesis runs on natural-gas (an attempt to facilitate the retrofit of the current residential heating devices), we could be led to think that such technology has no future and no further investigations or efforts should be made to achieve the desired technological breakthrough with market consequences. Nevertheless, this is not so straightforward because the conventional and combi-boilers technology corresponds to, by far, the larger sectoral share of installed units of hot water production appliances in Europe (as shown in section 2.1) and a total dependency on the electrical grid (and on the power generation sector) does not seem to be a smart strategy due to, among other things, the absence of competing solutions (powered by other fuels) that could lead to a lack of control in the electricity prices. The switch from gas to electricity in hot water production for sanitary and space heating purposes, and still adding other emerging electricity-demanding technologies (e.g., the electrical vehicles), will require, at least, huge investments to improve the grid capacity and maintain its reliability. Considering all of these aspects and taking advantage of the grid of natural-gas that is already installed, solutions like mixing hydrogen with natural-gas (to burn less fossil fuel) or using the current fashionable renewable gases (e.g., biomethane, synthetic natural-gas or biogas) appears to be a very reasonable option that will, in its turn, keep the residential CHP systems in orbit. In addition, these CHP systems can also be used as a transition technology as they will contribute to the decentralization of electrical energy production, safeguarding the grid and

giving time to increase its capacity. Meanwhile, and since the deadline for the total electrification is aimed for the year 2050 [235], which is still 30 years from now, at least two hot water producing appliances renewal cycles (considering 15 years as an average lifetime of the system) will take place. Therefore, an attempt to overpass the main obstacles that are precluding the technological breakthrough of ORC based micro-CHP systems still appears to be interesting. Furthermore, this is also endorsed by the fact that the ORC technology can be (and has already been) combined with other (nowadays) state-supported applications as concentrated solar or *Carnot* batteries (for energy storage). Embraced by these perspectives, the work developed in this PhD thesis can, and should, be continued. That continuation must include, at least, developments in four different aspects of the system: i) operation, ii) reliability, iii) efficiency and iv) cost. The specification of those aspects is described below.

i) Operation:

- The response time is an important feature of residential systems, as mentioned throughout this thesis. That feature is associated with the total thermal inertia of the system and so, the way how primary energy reaches the power cycle (e.g., avoiding the intermediate oil circuit) is extremely relevant. To evaluate this relevance, the development of a mathematical, experimentally validated, model capable to study the transient state of the system should be made. A parametric analysis of that model should also be performed to understand which are the most influential parameters for the response time of the system. Additionally, the control of the CHP should also consider the information retrieved by this transient state model to minimize, for example, start-up times.
- The test rig developed for the purpose of this PhD thesis uses a needle throttling valve to simulate the behaviour of the expander. This valve should be replaced by an actual expander (and generator), suitable for this (residential) power scale. This procedure is needed i) to verify if any operational questions arise with the installation of the expander, ii) to assess its influence on the system's control (mainly because of the transient operating conditions) and iii) to experimentally verify the outputs of the simplified model, presented in Chapter 3, developed for the hybrid CHP configuration (with this inclusion, the developed model should also be improved to consider an off-design approach).

ii) Reliability:

The main questions regarding the reliability of the ORC systems arise from the definition of the operating conditions because, except for the direct vaporization evaporator, the components are already deeply studied and characterized, as mentioned in Chapter 2. Therefore, future work regarding the reliability of the system is exclusively focused on the thermal degradation of the organic fluid. This PhD thesis shows a first insight regarding the influence of the heat transfer surfaces over the thermal degradation of the organic under close-to-real operating conditions (by developing a combined model and experimental approach for its evaluation), but there is still a significant amount of research to do in this field.

- Starting by the specific situation of the work developed in chapter 5, where the organic fluid was submitted to an elevated heat transfer surface temperature (around 50 ºC above the literature limit) and no thermal degradation was detected, the experimental approach should be improved to include a higher sensibility detection method like, for example, a gas chromatograph. The method used in this work has a sensibility of around 20000 ppm, which is significantly high and, therefore, the thermal degradation temperature obtained will be related to that sensibility.
- Leaving aside the specific situation of this work and approaching a more general research question, an accurate methodology capable to extrapolate the results obtained from the static methods to close-to-real operating conditions should be developed. In this way, the huge number of results available in the literature regarding static thermal tests becomes viable for real situations. This methodology should comprise, besides the organic fluid temperature, the influence of time during which the organic is at that temperature. The data necessary for the development of this methodology can, in part, be obtained from: i) experimental data published in the literature regarding the concentration of the decomposition products dependence on time and temperature for static and dynamic situations and ii) by the realization of dynamic stress tests in test rigs very well characterized, like the one presented in this PhD thesis, to compare the results obtained with the ones available in the literature for static situations.

iii) Efficiency:

- One of the biggest advantages of these CHP systems, in comparison with the current heating appliances, is the electricity production and, in that way, improve the quality of the energy generated. This aspect can be quantified by performing an exergetic analysis of the systems which is important to understand the maximum useful work that can be extracted from them. This analysis should then be made for the current heating systems, and for the standard and hybrid configuration of the ORC based micro-CHP system to complement the conclusions obtained from the energetic analysis performed in Chapter 3 of the present PhD thesis. This exergetic analysis can also serve to evaluate the potential of using different cycles (e.g., Kalina or organic Rankine triangle cycles) in CHP residential systems.

iv) Cost:

- As stated in chapter 2, the acquisition cost is one of the major issues that can determine the technology market acceptance. Therefore, an analysis regarding the cost of the ORC based micro-CHP system, including this new direct vaporization evaporator, should be made to understand its potential of being introduced in the residential market. This analysis should be made taking into consideration the comparison with the indirect vaporization configuration and with the standard heating devices (that are characterized for low acquisition costs). As the direct vaporization system is still in the development stage, this analysis will be exploratory. However, it is still relevant to show the influence of the design options made over the final cost of the micro-CHP system and, in that way, help guide the development of these systems by keeping them controlled regarding the cost.

References

[1] Hogerwaard J, Dincer I, Zamfirescu C. Analysis and assessment of a new organic Rankine based heat engine system with/without cogeneration. Energy 2013;62:300–10. doi:10.1016/j.energy.2013.09.002.

[2] Utama NA, Fathoni AM, Kristianto MA, McLellan BC. The End of Fossil Fuel Era: Supply-demand Measures through Energy Efficiency. Procedia Environ Sci 2014;20:40–5. doi:10.1016/j.proenv.2014.03.007.

[3] Atilgan B, Azapagic A. Life cycle environmental impacts of electricity from fossil fuels in Turkey. J Clean Prod 2015;106:555–64. doi:10.1016/j.jclepro.2014.07.046.

[4] World Energy Council - Conseil mondial de l'énergie. World Energy Resources - 2013 Survey. 2013.

[5] Gaventa J, Mabey N, Dixson- S, Jackson HS-, Acke D. EU Energy Union Assessment 2015: towards a resilient energy union with a forward-looking climate policy. 2015.

[6] European Climate Foundation. Roadmap 2050 : A Practical Guide to a Prosperous, Low-carbon Europe. 2010. doi:10.2833/10759.

[7] Tchanche BF, Pétrissans M, Papadakis G. Heat resources and organic Rankine cycle machines. Renew Sustain Energy Rev 2014;39:1185–99. doi:10.1016/j.rser.2014.07.139.

[8] Vélez F, Segovia JJ, Martín MC, Antolín G, Chejne F, Quijano A. A technical, economical and market review of organic Rankine cycles for the conversion of low-grade heat for power generation. Renew Sustain Energy Rev 2012;16:4175–89. doi:10.1016/j.rser.2012.03.022.

[9] Tchanche BF, Lambrinos G, Frangoudakis A, Papadakis G. Low-grade heat conversion into power using organic Rankine cycles - A review of various applications. Renew Sustain Energy Rev 2011;15:3963–79. doi:10.1016/j.rser.2011.07.024.

[10] Ghadimi P, Kara S, Kornfeld B. The optimal selection of on-site CHP systems through integrated sizing and operational strategy. Appl Energy 2014;126:38–46. doi:10.1016/j.apenergy.2014.03.085.

[11] Streckiene G, Martinaitis V, Andersen AN, Katz J. Feasibility of CHP-plants with thermal stores in the German spot market. Appl Energy 2009;86:2308–16. doi:10.1016/j.apenergy.2009.03.023.

[12] Knizley A, Mago PJ, Tobermann J, Warren HR. Performance characterization of a power generation unit-organic Rankine cycle system based on the efficiencies of the system components. Energy Convers Manag 2015;105:480–7. doi:10.1016/j.enconman.2015.08.010.

[13] Badami M, Casetti A, Campanile P, Anzioso F. Performance of an innovative 120 kWe natural gas cogeneration system. Energy 2007;32:823–33. doi:10.1016/j.energy.2006.06.006.

[14] Bianchi M, Branchini L, De Pascale A, Peretto A. Application of environmental performance assessment of CHP systems with local and global approaches. Appl Energy 2014;130:774–82. doi:10.1016/j.apenergy.2014.04.017.

[15] Dentice d'Accadia M, Sasso M, Sibilio S, Vanoli L. Micro-combined heat and power in residential and light commercial applications. Appl Therm Eng 2003;23:1247–59. doi:10.1016/S1359-4311(03)00030-9.

[16] Bao J, Zhao L. A review of working fluid and expander selections for organic Rankine cycle. Renew Sustain Energy Rev 2013;24:325–42. doi:10.1016/j.rser.2013.03.040.

[17] Xu J, Yu C. Critical temperature criterion for selection of working fluids for subcritical pressure Organic Rankine cycles. Energy 2014;74:719–33. doi:10.1016/j.energy.2014.07.038.

[18] Qiu G. Selection of working fluids for micro-CHP systems with ORC. Renew Energy 2012;48:565–70. doi:10.1016/j.renene.2012.06.006.

[19] Desai NB, Bandyopadhyay S. Thermo-economic analysis and selection of working fluid for solar organic Rankine cycle. Appl Therm Eng 2016;95:471–81. doi:10.1016/j.applthermaleng.2015.11.018.

[20] Li J, Alvi JZ, Pei G, Ji J, Li P, Fu H. Effect of working fluids on the performance of a novel direct vapor generation solar organic Rankine cycle system. Appl Therm Eng 2016;98:786–97. doi:10.1016/j.applthermaleng.2015.12.146.

[21] Zhang J, Zhou Y, Wang R, Xu J, Fang F. Modeling and constrained multivariable predictive control for ORC (Organic Rankine Cycle) based waste heat energy conversion systems. Energy 2014;66:128–38. doi:10.1016/j.energy.2014.01.068.

[22] Dickes R, Dumont O, Daccord R, Quoilin S, Lemort V. Modelling of organic Rankine cycle power systems in off-design conditions: An experimentally-validated comparative study. Energy 2017;123:710–27. doi:10.1016/j.energy.2017.01.130.

References

[23] Astolfi M, Lasala S, Macchi E. Selection maps for ORC and CO2 systems for low-medium temperature heat sources. Energy Procedia 2017;129:971–8. doi:10.1016/j.egypro.2017.09.217.

[24] Rahbar K, Mahmoud S, Al-Dadah RK, Moazami N, Mirhadizadeh SA. Review of organic Rankine cycle for small-scale applications. Energy Convers Manag 2017;134:135–55. doi:10.1016/j.enconman.2016.12.023.

[25] Alanne K, Saari K, Kuosa M, Jokisalo J, Martin AR. Thermo-economic analysis of a micro-cogeneration system based on a rotary steam engine (RSE). Appl Therm Eng 2012;44:11–20. doi:10.1016/j.applthermaleng.2012.03.026.

[26] Qiu G, Liu H, Riffat S. Expanders for micro-CHP systems with organic Rankine cycle. Appl Therm Eng 2011;31:3301–7. doi:10.1016/j.applthermaleng.2011.06.008.

[27] Song P, Wei M, Shi L, Danish SN, Ma C. A review of scroll expanders for organic rankine cycle systems. Appl Therm Eng 2015;75:54–64. doi:10.1016/j.applthermaleng.2014.05.094.

[28] Ziviani D, Suman A, Lecompte S, De Paepe M, Van Den Broek M, Spina PR, et al. Comparison of a single-screw and a scroll expander under part-load conditions for low-grade heat recovery ORC systems. Energy Procedia 2014;61:117–20. doi:10.1016/j.egypro.2014.11.920.

[29] Quoilin S, Lemort V, Lebrun J. Experimental study and modeling of an Organic Rankine Cycle using scroll expander. Appl Energy 2010;87:1260–8. doi:10.1016/j.apenergy.2009.06.026.

[30] Imran M, Usman M, Park BS, Lee DH. Volumetric expanders for low grade heat and waste heat recovery applications. Renew Sustain Energy Rev 2016;57:1090–109. doi:10.1016/j.rser.2015.12.139.

[31] Caliano M, Bianco N, Graditi G, Mongibello L. Economic optimization of a residential micro-CHP system considering different operation strategies. Appl Therm Eng 2016;101:592–600. doi:10.1016/j.applthermaleng.2015.11.024.

[32] Di Somma M, Yan B, Bianco N, Graditi G, Luh PB, Mongibello L, et al. Operation optimization of a distributed energy system considering energy costs and exergy efficiency. Energy Convers Manag 2015;103:739–51. doi:10.1016/j.enconman.2015.07.009.

[33] Wang H, Yin W, Abdollahi E, Lahdelma R, Jiao W. Modelling and optimization of CHP based district heating system with renewable energy production and energy storage. Appl Energy 2015;159:401–21. doi:10.1016/j.apenergy.2015.09.020.

[34] Zhai H, An Q, Shi L, Lemort V, Quoilin S. Categorization and analysis of heat sources for organic Rankine cycle systems. Renew Sustain Energy Rev 2016;64:790–805. doi:10.1016/j.rser.2016.06.076.

[35] De Paepe M, D'Herdt P, Mertens D. Micro-CHP systems for residential applications. Energy Convers Manag 2006;47:3435–46. doi:10.1016/j.enconman.2005.12.024.

[36] Hawkes AD. Techno-economic assessment of small and micro combined heat and power (CHP) systems. Small Micro Comb. Heat Power Syst. Adv. Des. Performance, Mater. Appl., 2011, p. 17–41. doi:10.1533/9780857092755.1.17.

[37] Hawkes AD, Leach MA. Cost-effective operating strategy for residential micro-combined heat and power. Energy 2007;32:711–23. doi:10.1016/j.energy.2006.06.001.

[38] Qiu K, Hayden ACS. Integrated thermoelectric and organic Rankine cycles for micro-CHP systems. Appl Energy 2012;97:667–72. doi:10.1016/j.apenergy.2011.12.072.

[39] Alanne K, Saari A. Sustainable small-scale CHP technologies for buildings: The basis for multi-perspective decision-making. Renew Sustain Energy Rev 2004;8:401–31. doi:10.1016/j.rser.2003.12.005.

[40] CODE 2 - Cogeneration Observatory and Dissemination Europe. Micro-CHP potential analysis - European level report 2014.

[41] Colonna P, Casati E, Trapp C, Mathijssen T, Larjola J, Turunen-Saaresti T, et al. Organic Rankine Cycle Power Systems: From the Concept to Current Technology, Applications, and an Outlook to the Future. J Eng Gas Turbines Power 2015;137:100801. doi:10.1115/1.4029884.

[42] Qiu G, Shao Y, Li J, Liu H, Riffat SB. Experimental investigation of a biomass-fired ORC-based micro-CHP for domestic applications. Fuel 2012;96:374–82. doi:10.1016/j.fuel.2012.01.028.

[43] Peris B, Navarro-Esbrí J, Molés F, Martí JP, Mota-Babiloni A. Experimental characterization of an Organic Rankine Cycle (ORC) for micro-scale CHP applications. Appl Therm Eng 2015;79:1–8. doi:10.1016/j.applthermaleng.2015.01.020.

[44] Farrokhi M, Noie SH, Akbarzadeh AA. Preliminary experimental investigation of a natural gas-fired ORC-based micro-CHP system for residential buildings. Appl Therm Eng 2014;69:221–9. doi:10.1016/j.applthermaleng.2013.11.060.

[45] Bianchi M, De Pascale A, Spina PR. Guidelines for residential micro-CHP systems design. Appl Energy 2012;97:673–85. doi:10.1016/j.apenergy.2011.11.023.

References

[46] Maghanki MM, Ghobadian B, Najafi G, Galogah RJ. Micro combined heat and power (MCHP) technologies and applications. Renew Sustain Energy Rev 2013;28:510–24. doi:10.1016/j.rser.2013.07.053.

[47] Cogeneration Observatory and Dissemination Europe. Code 2 2015. http://www.code2-project.eu/ (accessed February 5, 2016).

[48] Kuhn V, Klemeš J, Bulatov I. MicroCHP: Overview of selected technologies, products and field test results. Appl Therm Eng 2008;28:2039–48. doi:10.1016/j.applthermaleng.2008.02.003.

[49] BHKW project. BHKW-Infozentrum - Informationsportal über BHKW und KWK. https://www.bhkw-infozentrum.de/ (accessed February 5, 2016).

[50] European Union ene.field project. Ene.field. http://enefield.eu/ (accessed February 5, 2016).

[51] Miraton A. Performance and Product Quality Certification for micro-Combined Heat and Power Units. REHVA J 2018:73–5.

[52] Eurovent Certita Certification. NF micro-Combined Heat and Power | Certita. https://www.eurovent-certification.comen/certita-mark/nf-micro-combined-heat-and-power-1 (accessed March 12, 2018).

[53] Fubara TC, Cecelja F, Yang A. Modelling and selection of micro-CHP systems for domestic energy supply: The dimension of network-wide primary energy consumption. Appl Energy 2014;114:327–34. doi:10.1016/j.apenergy.2013.09.069.

[54] Thomas B. Benchmark testing of Micro-CHP units. Appl Therm Eng 2008;28:2049–54. doi:10.1016/j.applthermaleng.2008.03.010.

[55] Pehnt M, Praetorius B, Schumacher K, Fischer C, Schneider L, Voß J-P. Micro cogeneration : towards decentralised energy systems. 2005.

[56] Staffell I, Green R, Kendall K. Cost targets for domestic fuel cell CHP. J Power Sources 2008;181:339–49. doi:10.1016/j.jpowsour.2007.11.068.

[57] Staffell I, Green R. The cost of domestic fuel cell micro-CHP systems. Int J Hydrogen Energy 2013;38:1088–102. doi:10.1016/j.ijhydene.2012.10.090.

[58] Barbieri ES, Spina PR, Venturini M. Analysis of innovative micro-CHP systems to meet household energy demands. Appl Energy 2012;97:723–33. doi:10.1016/j.apenergy.2011.11.081.

[59] Pei G, Li J, Li Y, Wang D, Ji J. Construction and dynamic test of a small-scale organic rankine cycle. Energy 2011;36:3215–23. doi:10.1016/j.energy.2011.03.010.

[60] Algieri A, Morrone P. Energetic analysis of biomass-fired ORC systems for micro-scale combined heat and power (CHP) generation. A possible application to the Italian residential sector. Appl Therm Eng 2014;71:751–9. doi:10.1016/j.applthermaleng.2013.11.024.

[61] Dong L, Liu H, Riffat S. Development of small-scale and micro-scale biomass-fuelled CHP systems - A literature review. Appl Therm Eng 2009;29:2119–26. doi:10.1016/j.applthermaleng.2008.12.004.

[62] Ziviani D, Beyene A, Venturini M. Advances and challenges in ORC systems modeling for low grade thermal energy recovery. Appl Energy 2014;121:79–95. doi:10.1016/j.apenergy.2014.01.074.

[63] Bracco R, Micheli D, Petrella R, Reini M, Taccani R, Toniato G. Micro-Organic Rankine Cycle systems for domestic cogeneration. Elsevier Ltd; 2016. doi:10.1016/B978-0-08-100510-1.00018-1.

[64] Lecompte S, Huisseune H, van den Broek M, De Paepe M. Review of organic Rankine cycle (ORC) architectures for waste heat recovery. Renew Sustain Energy Rev 2015;47:448–61. doi:10.1016/j.energy.2015.04.094.

[65] Astolfi M. Technical options for organic rankine cycle systems. Org Rank Cycle Power Syst Technol Appl 2016:67–89. doi:10.1016/B978-0-08-100510-1.00003-X.

[66] Moran MJ, Shapiro HN, Boettner DD, Bailey MB. Fundamentals of Engineering Thermodynamics. 8th Edit. 2014.

[67] Çengel YA, Boles MA. Thermodynamics: An Engineering Approach. vol. 5th editio. 2006.

[68] Banaszkiewicz M, Rehmus-Forc A. Stress corrosion cracking of a 60MW steam turbine rotor. Eng Fail Anal 2015;51:55–68. doi:10.1016/j.engfailanal.2015.02.015.

[69] Schuster A, Karellas S, Kakaras E, Spliethoff H. Energetic and economic investigation of Organic Rankine Cycle applications. Appl Therm Eng 2009;29:1809–17. doi:10.1016/j.applthermaleng.2008.08.016.

[70] Yu C, Xu J, Sun Y. Transcritical pressure Organic Rankine Cycle (ORC) analysis based on the integrated-average temperature difference in evaporators. Appl Therm Eng 2015;88:2–13. doi:10.1016/j.applthermaleng.2014.11.031.

[71] Quoilin S, Broek M Van Den, Declaye S, Dewallef P, Lemort V. Techno-economic survey of organic rankine cycle (ORC) systems. Renew Sustain Energy Rev 2013;22:168–86. doi:10.1016/j.rser.2013.01.028.

[72] Invernizzi CM, Bonalumi D. Thermal stability of organic fluids for Organic Rankine Cycle systems. Elsevier Ltd; 2016. doi:10.1016/B978-0-08-100510-1.00005-3.

References

[73] Carnot S. Réflexions sur le puissance motrice du feu, et sur les machines propes á dèveloper cette puissance 1824.

[74] Rankine WJM. A Manual of the Steam Engine and Other Prime Movers 1859:616.

[75] Knowledge Center on Organic Rankine Cycle technology. History. https://www.kcorc.org/en/science-technology/history/ (accessed October 3, 2017).

[76] Ofeldt FW. United States Patent: 611792 A 1898. https://patents.google.com/patent/US611792A/en (accessed October 3, 2017).

[77] Bronicki LY. History of organic rankine cycle systems. Elsevier Ltd; 2016. doi:10.1016/B978-0-08-100510-1.00002-8.

[78] Invernizzi CM. Closed Power Cycles. vol. 11. London: Springer London; 2013. doi:10.1007/978-1-4471-5140-1.

[79] Tartière T. ORC Market : A World Overview. https://orc-world-map.org/analysis.html (accessed October 12, 2017).

[80] Fu BR, Hsu SW, Liu CH, Liu YC. Statistical analysis of patent data relating to the organic Rankine cycle. Renew Sustain Energy Rev 2014;39:986–94. doi:10.1016/j.rser.2014.07.070.

[81] Fu BR, Hsu SW, Liu CH. Trends in patent applications relating to Organic Rankine Cycle. Procedia Eng 2014;79:249–57. doi:10.1016/j.proeng.2014.06.339.

[82] Obi JB. State of art on ORC applications for waste heat recovery and micro-cogeneration for installations up to 100kWe. Energy Procedia 2015;82:994–1001. doi:10.1016/j.egypro.2015.11.857.

[83] Ormat Technologies Inc. Home | Organic Rankine Cycle. https://www.ormat.com/en/home/a/main/ (accessed January 25, 2016).

[84] Exergy S.p.A. Organic Rankine Cycle with the radial outflow turbine. https://www.exergy-orc.com/ (accessed April 5, 2016).

[85] General Electric Company (GE). Power Generation: Generators and Gas Turbines. https://www.ge.com/gas-power (accessed April 6, 2016).

[86] Turboden srl. Organic Rankine Cycle Turbogenerators for Clean Electric Energy Production. https://www.turboden.com/ (accessed January 25, 2016).

[87] INTEC GMK GmbH. Home - GMK - Gesellschaft für Motoren und Kraftanlagen mbH. http://www.gmk.info/home.html (accessed January 25, 2016).

[88] Cryostar SAS. Cryogenic equipment by Cryostar. https://cryostar.com/ (accessed January 25, 2016).

[89] TAS Energy. Efficient Modular Systems. https://www.tas.com/ (accessed April 5, 2016).

[90] Barber-Nichols Inc. Design & Manufacture of Specialty Turbomachinery. https://www.barber-nichols.com/ (accessed January 25, 2016).

[91] Enertime SA. Innovation and new energies. https://www.enertime.com/en (accessed January 25, 2016).

[92] Adoratec GmbH. Engineering for a clean Environment. http://www.adoratec.com/companyprofilnav.html (accessed January 25, 2016).

[93] Maxxtec GmbH. The thermal oil system specialist for heat recovery, heat transfer or electricity power generation. http://www.maxxtec.com/en/ (accessed January 25, 2016).

[94] Zhejiang Kaishan Compressor Co. Engineering the future. http://www.kaishancomp.com/en/ (accessed April 6, 2016).

[95] E-Rational. Home - Value for Heat. http://www.e-rational.net/home (accessed October 2, 2017).

[96] Phoenix Thermal Energy Conversion. A division of the Fusion Power Systems. http://www.phoenixorc.com.au/phoenix-ups-system (accessed February 25, 2016).

[97] Dürr Cyplan Lts. Homepage. http://www.durr-cyplan.com/ (accessed October 2, 2017).

[98] Triogen NL. Generate power from heat. http://www.triogen.nl/ (accessed January 25, 2016).

[99] Zuccato Energia Srl. Home. http://zuccatoenergia.it (accessed October 2, 2017).

[100] Calnetix Technologies LLC. Magnetic Bearings, Motor Generators, Power Electronics, Energy Efficiency, Savings, Consumption, Reduce Harmful Emissions, Medical, Food, Marine, Composite Rotor Sleeving Technology. https://www.calnetix.com/ (accessed January 25, 2017).

[101] ElectraTherm Inc. ElectraTherm. https://electratherm.com/ (accessed January 25, 2016).

[102] Infinity Turbine LLC. The Radial Outflow Turbine Generator - ORC Turbine. http://www.infinityturbine.com/ (accessed February 25, 2016).

[103] ENOGIA. The Small Turbine ORC Company. https://enogia.com/en/home/ (accessed February 25, 2016).

[104] Villarini M, Bocci E, Moneti M, Di Carlo A, Micangeli A. State of art of small scale solar powered ORC systems: A review of the different typologies and technology perspectives. Energy Procedia 2014;45:257–67. doi:10.1016/j.egypro.2014.01.028.

[105] Manescu R. Heat Exchanger Versus Storage Tank for Hot Tap Water Preparation in District Heating Systems. Procedia Technol 2016;22:720–5. doi:10.1016/j.protcy.2016.01.030.

References

[106] International Energy Agency. Technology Roadmap - Geothermal Heat and Power. 2011. doi:10.1787/9789264118485-en.

[107] Stathis Michaelides EE. Future directions and cycles for electricity production from geothermal resources. Energy Convers Manag 2015;107:3–9. doi:10.1016/j.enconman.2015.07.057.

[108] Gabbrielli R. A novel design approach for small scale low enthalpy binary geothermal power plants. Energy Convers Manag 2012;64:263–72. doi:10.1016/j.enconman.2012.04.017.

[109] Verma M, Loha C, Sinha AN, Chatterjee PK. Drying of biomass for utilising in co-firing with coal and its impact on environment – A review. Renew Sustain Energy Rev 2017;71:732–41. doi:10.1016/j.rser.2016.12.101.

[110] Bhuiyan AA, Blicblau AS, Islam AKMS, Naser J. A review on thermo-chemical characteristics of coal/biomass co-firing in industrial furnace. J Energy Inst 2018;91:1–18. doi:10.1016/j.joei.2016.10.006.

[111] Roni MS, Chowdhury S, Mamun S, Marufuzzaman M, Lein W, Johnson S. Biomass co-firing technology with policies, challenges, and opportunities: A global review. Renew Sustain Energy Rev 2017;78:1089–101. doi:10.1016/j.rser.2017.05.023.

[112] Zhou Y, Zhang Z, Zhang Y, Wang Y, Yu Y, Ji F, et al. A comprehensive review on densified solid biofuel industry in China. Renew Sustain Energy Rev 2016;54:1412–28. doi:10.1016/j.rser.2015.09.096.

[113] Algieri A, Morrone P. Techno-economic analysis of biomass-fired ORC systems for single-family combined heat and power (CHP) applications. Energy Procedia 2014;45:1285–94. doi:10.1016/j.egypro.2014.01.134.

[114] Zhou N, Wang X, Chen Z, Wang Z. Experimental study on Organic Rankine Cycle for waste heat recovery from low-temperature flue gas. Energy 2013;55:216–25. doi:10.1016/j.energy.2013.03.047.

[115] Nguyen TQ, Slawnwhite JD, Boulama KG. Power generation from residual industrial heat. Energy Convers Manag 2010;51:2220–9. doi:10.1016/j.enconman.2010.03.016.

[116] Flowgroup plc. Why we are different. http://flowgroup.uk.com/why-we-aredifferent/ (accessed February 5, 2016).

[117] Automated Home. The 'Flow Energy' Boiler that heats & makes electricity too. https://www.automatedhome.co.uk/carbon-footprint/exclusive-the-flow-energy-boiler-that-heats-makes-electricity-too.html (accessed November 14, 2017).

[118] Bannister JJ, Barker GM, Henshaw I, Whitechurch T, Bright NS. Heating System - Modular. US 2013/0219894 A1, 2013.

[119] Flow Energy Limited. Tech Spec - Flow Boiler Technical Specifications. http://www.flowenergy.uk.com/flow-boiler-tech-zone/tech-spec/ (accessed February 5, 2016).

[120] Bannister JJ, Bannister TN, Bright NS, Henshaw IJ. ORC Heat Engine. US 9399930 B2, 2016.

[121] Benstead R, Redford SJ. Closed Cycle Heat Transfer Device and Method. US 8141362 B2, 2012.

[122] Flow Energy Limited. Flow Finance. http://www.flowenergy.uk.com/flow-boiler-packages/flow-finance/ (accessed February 5, 2016).

[123] Kaymacor Srl. Home. https://www.kaymacor.com/en (accessed October 3, 2017).

[124] Kaymacor Srl. Products. https://www.kaymacor.com/en/products/ (accessed October 3, 2017).

[125] Taccani R, Obi JB, De Lucia M, Micheli D, Toniato G. Development and Experimental Characterization of a Small Scale Solar Powered Organic Rankine Cycle (ORC). Energy Procedia 2016;101:504–11. doi:10.1016/j.egypro.2016.11.064.

[126] FLORIS MGF. A Reservoir for the Reception of a Condensed Working Fluid of an Organic Rankine Cycle System. EP 3091203 A1, 2016.

[127] RANK. Organic Rankine Cycle (ORC) Modules. https://www.rank-orc.com/ (accessed February 16, 2016).

[128] Navarro-Esbrí J, Peris B, Collado R, Molés F. Micro-generation and micro combined heat and power generation using “free” low temperature heat sources through Organic Rankine Cycles. Renew Energy Power Qual J 2013;11.

[129] Peris B, Navarro-Esbrí J, Molés F, Mota-Babiloni A. Experimental study of an ORC (organic Rankine cycle) for low grade waste heat recovery in a ceramic industry. Energy 2015;85:534–42. doi:10.1016/j.energy.2015.03.065.

[130] Peris B, Navarro-Esbrí J, Molés F, Collado R, Mota-Babiloni A. Performance evaluation of an Organic Rankine Cycle (ORC) for power applications from low grade heat sources. Appl Therm Eng 2015;75:763–9. doi:10.1016/j.applthermaleng.2014.10.034.

References

[131] Peris B, Navarro-Esbrí J, Molés F, González M, Mota-Babiloni A. Experimental characterization of an ORC (organic Rankine cycle) for power and CHP (combined heat and power) applications from low grade heat sources. Energy 2015;82:269–76. doi:10.1016/j.energy.2015.01.037.

[132] Puig RC, PIQUER MG, MATA JPM, Esbrí JN. System efficient anti-cavitation pump power cycle rankine organic. ES 2586425 R1, 2017.

[133] Esbrí JN, Puig RC. Revalue System Heat Sources of Low Temperature. ES 2383805 B1, 2013.

[134] Viking Development Group. CraftEngine - providing renewable energy at a low cost. http://www.vdg.no/index.php?Menuid=16 (accessed August 5, 2016).

[135] Viking Development Group. FAQ. http://www.vdg.no/index.php?Menuid=35&expand=35 (accessed August 5, 2016).

[136] Viking Development Group. CraftEngine - Electricity production from renewable heat sources. https://www.youtube.com/watch?V=OXkrHdP5Zfs (accessed August 5, 2016).

[137] Viking Heat Engines AS. CraftEngine - General presentation 2014. doi:10.3917/jie.015.0003.

[138] Risla HN. Thermodynamic Cycle and Heat Engine. US 8590302 B2, 2013.

[139] Risla HN, Schlüter C, Becker M, Mück A. External Heat Engine Device. US 9874175 B2, 2018.

[140] Risla HN. Device and Method for Operational and Safety Control of a Heat Engine. US 2017/0139001 A1, 2016.

[141] Risla HN. Device and Method for Energy Supply for a Thermal Power Station System for a Building or a Vessel. US 2017/0139001 A1, 2013.

[142] Risla HN. Inlet Valve Arrangement and Method for External-Heat Engine. US 2017/0211509 A1, 2017.

[143] Cogen Microsystems Pty Ltd. Home Heating Systems that Generate Electricity. http://www.cogenmicro.com/index.php?Select= (accessed February 11, 2016).

[144] Cogen Microsystems Pty Ltd. Power, Heating and Cooling Produced in your Home. http://www.cogenmicro.com/index.php?Select=24 (accessed February 11, 2016).

[145] Loo P Van De, Schultz NL. Expander for a Heat Engine. US 2016/0047243 A1, 2015.

[146] Loo P Van De, Barduca DR. Heat Engine. US 2010/0300097 A1, 2010.

[147] Loo P van de. Control System for a Cogeneration Unit. US 6838781 B2, 2005.

[148] Loo P Van De. Reciprocating Engine and Inlet System Therefor. US 7188474 B2, 2007.

[149] Damgaard Solutions. Research and development. http://www.damgaardsolutions.com/en/damgaard-hlavni-stranka/vyzkum-a-vyvoj/ (accessed September 28, 2017).

[150] Damgaard Solutions. WAVE, Inspired by Rankine - YouTube. https://www.youtube.com/watch?V=rPPmeXqTasg (accessed September 28, 2017).

[151] Vodicka V, Guillaume L, Mascuch J, Lemort V. Testing and Modeling a Vane Expander Used in an Orc Working With Hexamethyldisiloxane (MM). Proc 3rd Int Semin ORC Power Syst 2015:1–10.

[152] Damgaard Solutions. Technology. http://www.damgaardsolutions.com/en/technologie (accessed September 28, 2017).

[153] Mascuch J, Novotny V, Vodicka V, Zeleny Z. Towards development of 1-10 kW pilot ORC units operating with hexamethyldisiloxane and using rotary vane expander. Energy Procedia 2017;129:826–33. doi:10.1016/j.egypro.2017.09.196.

[154] Confédération Suisse. Registre du commerce: mutations - Eneftech Innovation SA. 2016.

[155] Kane M, Cretegny D, Merminod A. Scroll device for compression or expansion. WO 2009050126 A4, 2009.

[156] Kane M, Cretegny D. Lubrication of a turbine in a Rankine cycle. EP 2 662 539 A1, 2013.

[157] Kane M, Cretegny D, Merminod A. Scroll Device Integrating a Feed Pump. US 2017/0139001 A1, 2010.

[158] Eneftech Innovation SA. Home. http://www.eneftech.com/en/home.php (accessed February 16, 2016).

[159] Eneftech Innovation SA. Enefcogen plus. http://www.eneftech.com/en/enefcogen_plus.php (accessed February 16, 2016).

[160] Eneftech Innovation SA. Enefcogen green. http://www.eneftech.com/en/enefcogen_green.php (accessed February 16, 2016).

[161] Bonk CD, Laux C, Rödder M, Neef M. Design of a 1 KW Organic Rankine Cycle for Teaching and Research Issues. Energy Procedia 2017;129:931–8. doi:10.1016/j.egypro.2017.09.117.

[162] Kolasiński P, Błasiak P, Rak J. Experimental investigation on multi-vane expander operating conditions in domestic CHP ORC system. Energy Procedia 2017;129:323–30. doi:10.1016/j.egypro.2017.09.201.

References

[163] Bianchi M, Branchini L, De Pascale A, Orlandini V, Ottaviano S, Peretto A, et al. Experimental Investigation with Steady-State Detection in a Micro-ORC Test Bench. Energy Procedia 2017;126:469–76. doi:10.1016/j.egypro.2017.08.222.

[164] Bianchi M, Branchini L, De Pascale A, Orlandini V, Ottaviano S, Pinelli M, et al. Experimental Performance of a Micro-ORC Energy System for Low Grade Heat Recovery. Energy Procedia 2017;129:899–906. doi:10.1016/j.egypro.2017.09.096.

[165] Ancona MA, Bianchi M, Branchini L, De Pascale A, Melino F, Orlandini V, et al. A Micro-ORC Energy System: Preliminary Performance and Test Bench Development. Energy Procedia 2016;101:814–21. doi:10.1016/j.egypro.2016.11.103.

[166] Zywica G, Kicinski J, Kaczmarczyk TZ, Ihnatowicz E, Turzynski T, Bykuc S. Prototype of the domestic CHP ORC system: construction and experimental research. Proc 3rd Int Semin ORC Power Syst 2015:Paper ID: 58, Page 1-9.

[167] Kicinski J, Zywica G. Prototype of the domestic CHP ORC energy system. Bull Polish Acad Sci Tech Sci 2016;64:417–24. doi:10.1515/bpasts-2016-0047.

[168] Zywica G, Kaczmarczyk TZ, Ihnatowicz E, Turzyński T. Experimental investigation of the domestic CHP ORC system in transient operating conditions. Energy Procedia 2017;129:637–43. doi:10.1016/j.egypro.2017.09.123.

[169] Eicke A, Smole S. ORC-Demonstration-Plant With 1 kW Scroll Expander – Concept, Design and Operational Experiences. Proc 3rd Int Semin ORC Power Syst 2015;Paper ID:1–8.

[170] Muhammad U, Imran M, Lee DH, Park BS. Design and experimental investigation of a 1 kW organic Rankine cycle system using R245fa as working fluid for low-grade waste heat recovery from steam. Energy Convers Manag 2015;103:1089–100. doi:10.1016/j.enconman.2015.07.045.

[171] Jung H-C, Taylor L, Krumdieck S. An experimental and modelling study of a 1 kW organic Rankine cycle unit with mixture working fluid. Energy 2015;81:601–14. doi:10.1016/j.energy.2015.01.003.

[172] Galloni E, Fontana G, Staccone S. Design and experimental analysis of a mini ORC (organic Rankine cycle) power plant based on R245fa working fluid. Energy 2015;90:768–75. doi:10.1016/j.energy.2015.07.104.

[173] Bamorovat Abadi G, Yun E, Kim KC. Experimental study of a 1 kw organic Rankine cycle with a zeotropic mixture of R245fa/R134a. Energy 2015;93:2363–73. doi:10.1016/j.energy.2015.10.092.

[174] Chang J-C, Hung T-C, He Y-L, Zhang W. Experimental study on low-temperature organic Rankine cycle utilizing scroll type expander. Appl Energy 2015;155:150–9. doi:10.1016/j.apenergy.2015.05.118.

[175] Chang J, Chang C, Hung T, Lin J. Experimental study and CFD approach for scroll type expander used in low-temperature organic Rankine cycle. Appl Therm Eng 2014;73:1444–52. doi:10.1016/j.applthermaleng.2014.08.050.

[176] Declaye S, Quoilin S, Guillaume L, Lemort V. Experimental study on an open-drive scroll expander integrated into an ORC (Organic Rankine Cycle) system with R245fa as working fluid. Energy 2013;55:173–83. doi:10.1016/j.energy.2013.04.003.

[177] Bracco R, Clemente S, Micheli D, Reini M. Experimental tests and modelization of a domestic-scale ORC (Organic Rankine Cycle). Energy 2013;58:107–16. doi:10.1016/j.energy.2012.12.016.

[178] Liu H, Shao Y, Li J. A biomass-fired micro-scale CHP system with organic Rankine cycle (ORC) - Thermodynamic modelling studies. Biomass and Bioenergy 2011;35:3985–94. doi:10.1016/j.biombioe.2011.06.025.

[179] Peterson RB, Wang H, Herron T. Performance of a small-scale regenerative Rankine power cycle employing a scroll expander. Proc Inst Mech Eng Part A J Power Energy 2008;222:271–82. doi:10.1243/09576509JPE546.

[180] Cambi M, Tascioni R, Cioccolanti L, Bocci E. Converting a commercial scroll compressor into an expander: Experimental and analytical performance evaluation. Energy Procedia 2017;129:363–70. doi:10.1016/j.egypro.2017.09.234.

[181] Clemente S, Micheli D, Reini M, Taccani R. Energy efficiency analysis of Organic Rankine Cycles with scroll expanders for cogenerative applications. Appl Energy 2012;97:792–801. doi:10.1016/j.apenergy.2012.01.029.

[182] European Committee for Standardization. EN 13203: Gas-fired domestic appliances producing hot water. 2016.

[183] BDR Thermea Group. Baxi 100 Combi, Cupboard Fit Gas Boiler. https://www.baxi.co.uk/boilers/our-boilers/baxi-100-combi (accessed October 30, 2018).

[184] Ariston Thermo Group. CLAS HE evo | Combi Gas Boiler. http://www.ariston.com/uk/Wall-Hung_Boilers_Combi/clas_he_evo (accessed October 30, 2018).

[185] Santos M, André J, Francisco S, Mendes R, Ribeiro J. Off-design modelling of an organic Rankine cycle micro-CHP: Modular framework, calibration and validation. Appl Therm Eng 2018;137:848–67. doi:10.1016/j.applthermaleng.2018.04.009.

References

[186] Preißinger M, Brüggemann D. Thermal stability of hexamethyldisiloxane (MM) for high-temperature Organic Rankine Cycle (ORC). Energies 2016;9. doi:10.3390/en9030183.

[187] Lemmon, E.W., Huber, M.L., McLinden MO. NIST Reference Fluid Thermodynamic and Transport Properties (REFPROP) - Version 9.1. Natl Inst Stand Technol 2013.

[188] European Parliament, European Council. Directive 2012/27/EU. Off J Eur Union 2012;L315/1:1–56. doi:10.3000/19770677.L_2012.315.eng.

[189] European Commision. COMMISSION DELEGATED REGULATION (EU) 2015/2402 of 12 October 2015 reviewing harmonised efficiency reference values for separate production of electricity and heat in application of Directive 2012/27/EU of the European Parliament and of the Council and rep. Off J Eur Union 2015;L 333/54:54–61.

[190] Pereira JS, Ribeiro JB, Mendes R, Vaz GC, André JC. ORC based micro-cogeneration systems for residential application – A state of the art review and current challenges. Renew Sustain Energy Rev 2018;92:728–43. doi:10.1016/j.rser.2018.04.039.

[191] Invernizzi CM, Iora P, Manzolini G, Lasala S. Thermal stability of n-pentane, cyclo-pentane and toluene as working fluids in organic Rankine engines. Appl Therm Eng 2017;121:172–9. doi:10.1016/j.applthermaleng.2017.04.038.

[192] Invernizzi CM, Iora P, Bonalumi D, Macchi E, Roberto R, Caldera M. Titanium tetrachloride as novel working fluid for high temperature Rankine Cycles: Thermodynamic analysis and experimental assessment of the thermal stability. Appl Therm Eng 2016;107:21–7. doi:10.1016/j.applthermaleng.2016.06.136.

[193] Keulen L, Gallarini S, Landolina C, Spinelli A, Iora P, Invernizzi C, et al. Thermal stability of hexamethyldisiloxane and octamethyltrisiloxane. Energy 2018;165:868–76. doi:10.1016/j.energy.2018.08.057.

[194] Irriyanto MZ, Lim HS, Choi BS, Lee M, Myint AA, Kim J. Thermal stability study of HFO-1234ze(E) for supercritical organic Rankine cycle: Chemical kinetic model approach through decomposition experiments. J Ind Eng Chem 2020;90:244–50. doi:10.1016/j.jiec.2020.07.018.

[195] Huo E, Li Q, Liu C, Huang Z, Xin L. Experimental and theoretical studies on the thermal stability and decomposition mechanism of HFO-1336mzz(Z) with POE lubricant. J Anal Appl Pyrolysis 2020;147:104795. doi:10.1016/j.jaap.2020.104795.

[196] Shen ZF, Smith TF, Hix P. Linearization of the radiation terms for improved convergence by use of the zone method. Numer Heat Transf 1983;6:377–82. doi:10.1080/01495728308963094.

[197] Marín E. Linear relationships in heat transfer. Latin-American J Phys Educ 2009;3:3.

[198] Incropera FP, DeWitt DP, Bergman TL, Lavine AS. Fundamentals of Heat and Mass Transfer 6th Edition. 2007. doi:10.1016/j.applthermaleng.2011.03.022.

[199] W. M. Kays, A. L. London. Compact Heat Exchangers. Third edition, Krieger Pub Co; 1997, p. 335.

[200] Hottel HC. Heat Transmission. 3rd ed. NY, USA: McGraw-Hill Book Company; 1954.

[201] Holman JP. Heat Transfer. 9th ed. New York, USA: McGraw-Hill Book Company; 2002.

[202] J. M. Coulson, J. F. Richardson. Tecnologia Química VI. VI. 1988.

[203] Lockhart; RWMRC. Proposed correlation of data for isothermal two-phase, two-component flow in pipes. Chem Eng Prog 1949;45:10.

[204] Forster HK, Zuber N. Dynamics of vapor bubbles and boiling heat transfer. AIChE J 1955;1:531–5. doi:10.1002/aic.690010425.

[205] Niggeman RE. Quarterly progress report No. 12 - Organic Rankine Cycle Technology Program. 1969.

[206] Di Nanno LR, Koplow MD, DiBella FA. Status Report for an RC-1 Organic Rankine Bottoming Cycle for an Adiabatic Diesel Engine. Proc - Soc Automot Eng 1983:155–67.

[207] Ginosar DM, Petkovic LM, Guillen DP. Thermal Stability of Cyclopentane as an Organic Rankine Cycle Working Fluid. Energy and Fuels 2011;25:4138–44. doi:10.1021/ef200639r.

[208] Rohatgi ND, Clark RW, Hurst DR. Material compatibility & lubricants research for low GWP refrigerants – Phase I: thermal and chemical stability of low GWP refrigerants with lubricants. Sylva, NC: 2012. doi:10.1057/978-1-349-95988-4_24.

[209] ASHRAE Standard 97-2007 (RA 2017). Sealed Glass Tube Method to Test the Chemical Stability of Materials for Use within Refrigerant Systems. Atlanta, GA: 2017.

[210] Minor B, Kontomaris K, Hydutsky B. Nonflammable low GWP working fluid for organic Rankine cycles. ASME Turbo Expo 2014 Turbine Tech. Conf. Expo., 2014, p. 8.

[211] Kontomaris K, Leck TJ. Low GWP refrigerants for centrifugal chillers. ASHRAE Annu. Conf., ASHRAE Annulal Conference; 2009, p. 24.

[212] Kontomaris K. HFO-1336mzz-Z: High Temperature Chemical Stability and Use as A Working Fluid in Organic Rankine Cycles. Int Refrig Air Cond Conf 2014:10.

[213] Andersen WC, Bruno TJ. Rapid Screening of Fluids for Chemical Stability in Organic Rankine Cycle Applications. Ind Eng Chem Res 2005;44:5560–6. doi:10.1021/ie050351s.

References

[214] Dai X, Shi L, An Q, Qian W. Screening of hydrocarbons as supercritical ORCs working fluids by thermal stability. Energy Convers Manag 2016;126:632–7. doi:10.1016/j.enconman.2016.08.024.

[215] Pasetti M, Invernizzi CM, Iora P. Thermal stability of working fluids for organic Rankine cycles: An improved survey method and experimental results for cyclopentane, isopentane and n-butane. Appl Therm Eng 2014;73:762–72. doi:10.1016/j.applthermaleng.2014.08.017.

[216] Dai X, Shi L, An Q, Qian W. Thermal stability of some hydrofluorocarbons as supercritical ORCs working fluids. Appl Therm Eng 2018;128:1095–101. doi:10.1016/j.applthermaleng.2017.09.046.

[217] Calderazzi L, di Paliano PC. Thermal stability of R-134a, R-141b, R-13I1, R-7146, R-125 associated with stainless steel as a containing material. Int J Refrig 1997;20:381–9. doi:10.1016/S0140-7007(97)00043-1.

[218] Angelino G, Invernizzi C. Experimental investigation on the thermal stability of some new zero ODP refrigerants. Int J Refrig 2003;26:51–8. doi:10.1016/S0140-7007(02)00023-3.

[219] Invernizzi CM, Iora P, Preißinger M, Manzolini G. HFOs as substitute for R-134a as working fluids in ORC power plants : A thermodynamic assessment and thermal stability analysis. Appl Therm Eng 2016;103:790–7. doi:10.1016/j.applthermaleng.2016.04.101.

[220] Irriyanto MZ, Lim HS, Choi BS, Myint AA, Kim J. Thermal stability and decomposition behavior of HFO-1234ze(E) as a working fluid in the supercritical organic Rankine cycle. J Supercrit Fluids 2019;154:104602. doi:10.1016/j.supflu.2019.104602.

[221] Huo E, Liu C, Xin L, Li X, Xu X, Li Q, et al. Thermal stability and decomposition mechanism of HFO-1336mzz(Z) as an environmental friendly working fluid: Experimental and theoretical study. Int J Energy Res 2019;43:4630–43. doi:10.1002/er.4599.

[222] Keulen L, Landolina C, Spinelli A, Iora P, Invernizzi C, Lietti L, et al. Design and commissioning of a thermal stability test-rig for mixtures as working fluids for ORC applications. Energy Procedia 2017;129:176–83. doi:10.1016/j.egypro.2017.09.102.

[223] Erhart TG, Gölz J, Eicker U, Van Den Broek M. Working fluid stability in large-scale organic rankine cycle-units using siloxanes - Long-term experiences and fluid recycling. Energies 2016;9:1–16. doi:10.3390/en9060422.

[224] Dai X, Shi L, An Q, Qian W. Chemical kinetics method for evaluating the thermal stability of Organic Rankine Cycle working fluids. Appl Therm Eng 2016;100:708–13. doi:10.1016/j.applthermaleng.2016.02.091.

[225] Lasala S, Invernizzi C, Iora P, Chiesa P, Macchi E. Thermal Stability Analysis of Perfluorohexane. Energy Procedia 2015;75:1575–82. doi:10.1016/j.egypro.2015.07.358.

[226] Ragaller D, Sibert L, Cole RL, Demirgian JC, Allen JW. Degradation of the Organic Rankine-Cycle Fluid RC-1. In: American Institute of Aeronautics and Astronautics, editor. 22nd Intersoc. Energy Convers. Eng. Conf., Reston, Virginia: American Institute of Aeronautics and Astronautics; 1987. doi:10.2514/6.1987-9074.

[227] Cole RL, Demirgian JC, Allen JW. Predicting Toluene Degradation in Organic Rankine-Cycle Engines 1987:1402–7. doi:10.2514/6.1987-9075.

[228] Chang JC, Hung TC, He YL, Zhang W. Experimental study on low-temperature organic Rankine cycle utilizing scroll type expander. Appl Energy 2015;155:150–9. doi:10.1016/j.apenergy.2015.05.118.

[229] Pereira JS, Almeida J, André JC, Mendes R, Ribeiro JB. Modelling and experimental validation of the heat-transfer processes of a direct vaporization micro-scale ORC-evaporator for thermal degradation risk assessment. Energy Convers Manag 2021;238:114130. doi:10.1016/j.enconman.2021.114130.

[230] Dai X, Shi L, Qian W. Review of the Working Fluid Thermal Stability for Organic Rankine Cycles. J Therm Sci 2019;28:597–607. doi:10.1007/s11630-019-1119-3.

[231] Lemmon EW, Span R. Short fundamental equations of state for 20 industrial fluids. vol. 51. 2006. doi:10.1021/je050186n.

[232] Johns IB, Mcelhill EA, Smith JO. Thermal stability of organic compounds. Ind Eng Chem Prod Res Dev 1962;1:2–6. doi:10.1021/i360001a001.

[233] UNFCCC. Glasgow Climate Pact Advance unedited version Decision. Cop26 2019:1–8.

[234] UNFCCC. COP26 - United Nations Climate Change Conference 2021. https://unfccc.int/ (accessed December 2, 2021).

[235] European Commission. The European Green Deal. Eur Comm 2019;53:24. doi:10.1017/CBO9781107415324.004.

Appendices

Appendix A: Core publications (abstracts)

ORC based micro-cogeneration systems for residential application – a state of the art review and current challenges

João S. Pereira [a,*], José B. Ribeiro [a,*], Ricardo Mendes [a], Gilberto C. Vaz [b], Jorge C. André [a].

[a] ADAI-LAETA, Department of Mechanical Engineering - University of Coimbra, Portugal.

[b] ISEC, Polytechnic Institute of Coimbra - Department of Mechanical Engineering, Portugal.

[*] **Corresponding author:** joao.pereira@dem.uc.pt (JS Pereira),

Abstract

The environmental awareness and sustainability concerns have reached an unprecedented level of importance that is leading to, among other things, constant improvements in the traditional methods of energy conversion. One of those improvements involves the use of micro-CHP (combined heat and power production) systems for residential applications since the potential in terms of primary energy savings and GHG (greenhouse gases) reductions is considered to be enormous. Among the different technologies available for micro-CHP systems, ORC based ones seem the most suitable and promising option due to its simplicity and its ability to retrofit current heating systems used in residential dwellings.

This work reviews the use of ORC for micro-CHP applications taking into account the intrinsic requirements of the residential sector. One of those requirements is the ability to face highly variable thermal demand loads for which a short response time is necessary to ensure. The present research analyzes how manufacturers and the researcher centers are dealing with this key requirement. One of the findings of this work is that the referred requirement is essentially dependent on the ORC-evaporator design and how the primary energy reaches the power cycle, while the remaining ORC main components (expander, pump and condenser) play a minor role on that ability. Additionally, this research also offers an analysis of the micro-CHP potential and of the ORC market evolution, presenting a historical perspective of the technology, current main manufacturers, main application areas and a comparison between the use of an organic fluid and water/steam as working fluid for Rankine cycles.

Keywords: Low-carbon & efficient energy systems; Organic Rankine Cycle (ORC); Micro-Cogeneration; ORC-evaporator.

Analysis of a hybrid (topping/bottoming) ORC based CHP configuration integrating a new evaporator design concept for residential applications

João S. Pereira [a,*], José B. Ribeiro [a], Ricardo Mendes [a], Jorge C. André [a].

[a] ADAI-LAETA, Department of Mechanical Engineering – University of Coimbra, Portugal.

[*] **Corresponding author:** joao.pereira@dem.uc.pt (JS Pereira).

Abstract

The recommended design principles for the development of evaporators for ORC based micro-CHP systems attempting to retrofit the current combi-boilers are presented and discussed in this paper. From those principles, among which is the need of organic fluid direct vaporization, emerged a hybrid (topping/bottoming) CHP configuration in which the thermal energy is produced stepwise: firstly in the ORC-condenser and then in a post-heater, that is integrated on the ORC-evaporator, directly with the combustion gases. A model of this configuration was developed to determine the fraction of the CHP water heating process performed in the post-heater that maximizes the primary energy savings and ORC net power output for a wide range of CHP operating conditions. When compared to a standard CHP configuration, this solution show benefits for the greater part of those conditions. Besides solving the safety issue posed by the ORC-evaporator requirements and the performance benefits shown, this configuration has an additional positive side effect: the decrease of the combustion gases' temperature before they reach the organic working fluid heat-exchanger section in the ORC-evaporator that leads to a reduction of the risk of the working fluid thermal degradation.

Keywords: Organic Rankine Cycle (ORC); Residential scale; Hybrid CHP configuration; ORC-evaporator; Direct vaporization arrangement.

Appendices

Modelling and experimental validation of the heat transfer processes of a direct vaporization micro-scale ORC-evaporator for thermal degradation risk assessment

João S. Pereira [a,b*], João Almeida [a], Ricardo Mendes [a], Jorge C. André [a], José B. Ribeiro [a].

[a] University of Coimbra, ADAI-LAETA, Department of Mechanical Engineering, Portugal.

[b] Sciven, Lda. IPN Incubadora, Coimbra, Portugal.

[*] **Corresponding author:** joao.pereira@dem.uc.pt (JS Pereira).

Abstract

Demanding size and response time requirements imposed to ORC based micro-CHP systems, attempting to retrofit wall-hang domestic combi-boilers, suggests that the vaporization of the organic fluid should be done directly by the combustion gases. The evaluation of the risk that this option may put to the organic fluid thermal degradation requires the determination of the temperature of the heat transfer surfaces with which the organic fluid is in contact. As its experimental measure is extremely difficult to accomplish, such determination requires the development of a detailed physical model of the combustion and heat transfer processes in the ORC-evaporator.

The development, calibration and validation of such model is presented in this paper. This model will allow a detailed evaluation of several key features of the combustion and heat transfer processes as a function of some ORC operating parameters. Among those features is the temperature of the internal surface of the tubes with which the organic fluid is in contact. This temperature, which can be used to assess the risk of the thermal degradation of the organic fluid, has shown to be highly affected by the thermal resistances and by the combustion gases temperature. To reduce that risk, the operating conditions of the ORC should be those allowing the vaporization process to start as early as possible and reducing the superheating phase to the minimum possible.

Keywords: Organic Rankine Cycle; Heat transfer model, ORC-evaporator, Direct vaporization arrangement, Thermal degradation risk assessment.

Appendix B: Full list of publications

Articles in international journals

Published:

Pereira JS, Ribeiro JB, Mendes R, Vaz GC and André JC. Development of a direct concept helical-coil evaporator for an ORC based micro-CHP system. Energy Procedia 2017;129:474–8.
DOI: 10.1016/j.egypro.2017.09.162.

JCR Impact Factor® (2017): -

Pereira JS, Ribeiro JB, Mendes R, Vaz GC and André JC. ORC based micro-cogeneration systems for residential application – A state of the art review and current challenges. Renewable and Sustainable Energy Reviews 2018; 92:728–43.
DOI: 10.1016/j.rser.2018.04.039.

JCR Impact Factor® (2018): 10.565

Pereira JS, Ribeiro JB, Mendes R and André JC. Analysis of a hybrid (topping / bottoming) ORC based CHP configuration integrating a new evaporator design concept for residential applications. Applied Thermal Engineering 2019; 160:113984.
DOI: 10.1016/j.applthermaleng.2019.113984.

JCR Impact Factor® (2019): 4.725

Pereira JS, Almeida J, André JC, Mendes R and Ribeiro JB. Modelling and experimental validation of the heat transfer processes of a direct vaporization micro-scale ORC-evaporator for thermal degradation risk assessment. Energy Conversion and Management 2021; 238:114130.
DOI: https://doi.org/10.1016/j.enconman.2021.114130.

JCR Impact Factor® (2021): 8.208

Submitted to ISI-indexed journal:

Pereira JS, Santos M, Mendes R, André JC and Ribeiro JB. Investigation of a direct vaporization ORC based micro-CHP system: an *in-situ* thermal degradation analysis under close-to-real operating conditions. Submitted to the **Applied Thermal Engineering Journal** (Impact Factor®: 5.295) in December 2021.

Appendices

Papers and oral communications in proceedings of national/international conferences

1. Pereira JS, Ribeiro JB, Mendes R and André JC. Investigation of a topping/bottoming ORC based CHP configuration using a new evaporator concept for residential applications. 6th International Seminar on Organic Rankine Cycle Power Systems 2021. University of Munich, Germany.
2. Pereira JS, Pereira JB and Ribeiro JB. Generation and Cogeneration technologies for residential applications – a state of the art review and current challenges. International Conference on Construction, Energy, Environment & Sustainability (CEES) 2021. ITECONS, Portugal.
3. Pereira JS, Ribeiro JB, Mendes R and André JC. Energy analysis of a topping/bottoming ORC based CHP configuration using a new evaporator concept for residential applications. 15th International Conference on Heat Transfer, Fluid Mechanics and Thermodynamics (HEFAT) and Editorial Board of Applied Thermal Engineering (ATE) 2021. Virtual Conference.
4. Pereira JS, Ribeiro JB, Almeida JP, Mendes R and André JC. Evaporator heat transfer model and thermal degradation analysis of r245fa used in a direct vaporization ORC based micro-CHP system. 4th Energy for Sustainability International Conference: Designing a Sustainable future 2019. Politecnico di Torino, Italy.
5. Pereira JS, Ribeiro JB, Mendes R and André JC. Investigation of a topping/bottoming ORC based CHP configuration integrating a new evaporator concept for residential applications. 4th Energy for Sustainability International Conference: Designing a Sustainable future 2019. Politecnico di Torino, Italy.
6. Pereira JS, Ribeiro JB, Mendes R and André JC. Dual-purpose heat–exchanger for direct vaporization and condenser water post-heating in ORC based micro–CHP systems for residential applications. The Engine ORC Consortium 2018 (EORCC). IFP Energies Nouvelles Research and Training Centre, France.
7. Pereira JS, Ribeiro JB, Mendes R, Vaz GC and André JC. Development of a direct concept helical-coil evaporator for an ORC based micro-CHP system. 4th International Seminar on Organic Rankine Cycle Power Systems 2017. Politecnico di Milano, Italy.
8. Pereira JS, Ribeiro JB, Mendes R and André JC. Design, modelling, construction and experimental characterization of a gas-fired heat-exchanger set for a μ-CHP system based on an ORC. 13th International workshop on environment and alternative energy: Increasing Space Mission Ground Infrastructure Resiliency through Sustainability 2015. European Space Astronomy Centre (ESA - ESAC), Spain.
9. Pereira JS, Ribeiro JB, Mendes R and André JC. Experimental features of a direct helical-coil evaporator for a micro-cogeneration system based on an organic Rankine cycle. 2nd International Conference on Energy and Environment: bringing together Engineering and Economics 2015. University of Minho, Portugal.

10. Pereira JS, Ribeiro JB, Mendes R and André JC. Experimental features of a direct helical-coil evaporator for an ORC based μ-CHP system. 2nd Energy for Sustainability: Sustainable Cities: Designing for People and the Planet 2015. University of Coimbra, Portugal.
11. Pereira JS, Ribeiro JB, Mendes R and André JC. Experimental features of an Organic Rankine Cycle based micro-CHP system for domestic boilers. ICERE - International Conference on Environment and Renewable Energy 2015. Grand Hotel Wien, Austria.

Posters in national and international conferences, fairs or workshops

1. Pereira JS, Ribeiro JB, Mendes R and André JC. Development and validation of the heat transfer processes of a direct vaporization ORC-evaporator for thermal degradation risk analysis. 6th International Seminar on Organic Rankine Cycle Power Systems 2021. University of Munich, Germany.
2. Pereira JS, Ribeiro JB and André JC. Design, modelling, construction and characterization of a gas-fired heat-exchanger set for a Micro-CHP system based on ORC. XIII EfS Meeting - Students and Companies 2020. ITECONS, Portugal.
3. Pereira JS, Ribeiro JB and André JC. Design, modelling, construction and characterization of a gas-fired heat-exchanger set for a Micro-CHP system based on ORC. XII EfS Meeting - Students and Companies 2019. University of Coimbra, Portugal.
4. Pereira JS, Ribeiro JB and André JC. Design, modelling, construction and characterization of a gas-fired heat-exchanger set for a Micro-CHP system based on ORC technology. XI EfS Meeting - Students and Companies 2018. University of Coimbra, Portugal.
5. Pereira JS, Ribeiro JB and André JC. Design, modelling, construction and characterization of a gas-fired heat-exchanger set for a Micro-CHP system based on an ORC. X EfS Meeting - Students and Companies 2017. University of Coimbra, Portugal.
6. Pereira JS, Ribeiro JB, Mendes R and André JC. Design, Modelling, Construction and Experimental Characterization of a Compact Gas-Fired Heat-Exchanger Set for a Micro-CHP System Based on an Organic Rankine Cycle. MIT Portugal Annual Conference 2016: 10 years engineering a better future. University of Minho, Portugal.
7. Pereira JS, Ribeiro JB and André JC. Design, modelling, construction and characterization of a gas-fired heat-exchanger set for a Micro-CHP system based on an ORC. IX EfS Meeting - Students and Companies 2015. ITECONS, Portugal.
8. Pereira JS, Ribeiro JB, Mendes R and André JC. Experimental features of an Organic Rankine Cycle based micro-CHP system for domestic boilers. ICERE - International Conference on Environment and Renewable Energy 2015. Grand Hotel Wien, Austria.

9. Pereira JS, Ribeiro JB, Mendes R and André JC. Design, modelling, construction and experimental characterization of a gas-fired heat-exchanger set for a μ-CHP system based on an ORC. 13th International workshop on environment and alternative energy: Increasing Space Mission Ground Infrastructure Resiliency through Sustainability 2015. European Space Astronomy Centre (ESA - ESAC), Spain.
10. Pereira JS, Ribeiro JB and André JC. Design, modelling, construction and testing of a compact evaporator for a μCHP ORC based system. VIII EfS Meeting - Students and Companies 2014. University of Coimbra, Portugal.
11. Pereira JS, Ribeiro JB and André JC. Design and characterization of a Burner-HE for a μCHP system test bench. VII EfS Meeting - Students and Companies 2013. ITECONS, Portugal.

Online magazines

1. Pereira JS. ORC technology for residential applications. Science Trends 2018, ISSN: 2639-1538. **DOI**: 10.31988/SCITRENDS.41658.

The remaining appendices are described and organized as presented below. The corresponding documents are digitally available through the following link (open access):

https://drive.google.com/drive/folders/1eDUlybMEOITwkSgx4QSkNKLYIWThhrLU?usp=sharing

Appendix C: Helical-coil ORC-evaporator design

Appendix D: Hybrid ORC-evaporator design

Appendix E: Test rig design

1 – 3D drawings

2 – Electrical scheme

Appendix F: HebeTR2_datalogger&control LabView program

This page is intentionally left blank.

Annexes

All of the annexes are described and organized as presented below. The corresponding documents are digitally available through the following link (open access):

https://drive.google.com/drive/folders/1OeRIopamB75AzcLGbbt3qyQqUqFlz0wX?usp=sharing

Annex A: Natural-gas burner Riello RX35

Annex B: Natural-gas burner BurnerTech VAPAC 40

Annex C: Organic Fluid r245fa

Annex D: Pump Fluid-o-Tech TMFR

Annex E: Needle throttling valve Valsteam PRC25I

Annex F: Condenser GEA WTT GBS220H

Annex G: Instruments

1 – Flow rate sensor

i) Organic fluid stream
ii) Water stream
iii) Natural-gas stream

2 - Pressure transducers

i) RS sensors
ii) Omega sensors

3 - Temperature sensors

4 - Oxygen sensor

5 – Hygrometer

Annex H: Data acquisition boards

1 - Pico TC-08 datalogger

2 - National Instruments USB-6001

This page is intentionally left blank.